



HAL
open science

Evoked EMG-based torque prediction for muscle fatigue tracking and closed-loop torque control in FES

Qin Zhang

► **To cite this version:**

Qin Zhang. Evoked EMG-based torque prediction for muscle fatigue tracking and closed-loop torque control in FES. Biotechnology. Université Montpellier II - Sciences et Techniques du Languedoc, 2011. English. NNT: . tel-00820474

HAL Id: tel-00820474

<https://theses.hal.science/tel-00820474>

Submitted on 5 May 2013

HAL is a multi-disciplinary open access archive for the deposit and dissemination of scientific research documents, whether they are published or not. The documents may come from teaching and research institutions in France or abroad, or from public or private research centers.

L'archive ouverte pluridisciplinaire **HAL**, est destinée au dépôt et à la diffusion de documents scientifiques de niveau recherche, publiés ou non, émanant des établissements d'enseignement et de recherche français ou étrangers, des laboratoires publics ou privés.

ACADÉMIE DE MONTPELLIER
UNIVERSITÉ MONTPELLIER II
- SCIENCES ET TECHNIQUES DU LANGUEDOC -

THÈSE

pour obtenir le grade de

DOCTEUR DE L'UNIVERSITÉ MONTPELLIER II

Discipline : Génie Informatique, Automatique et Traitement du Signal

Formation Doctorale : Systèmes Automatiques et Microélectronique

École Doctorale : Information, Structures et Systèmes

présentée et soutenue publiquement

par

Qin Zhang

le 13 Décembre 2011

**Estimation du couple généré par un muscle sous SEF à la base de
l'EMG évoquée pour le suivi de la fatigue et le contrôle du couple en
boucle fermée**

**Evoked EMG-based torque prediction for muscle fatigue tracking and closed-loop
torque control in FES**

JURY :

Jean-Pierre Richard	Professeur, Ecole Centrale de Lille	Rapporteur
Guy Carrault	Professeur, IUT de Rennes - Université de Rennes I	Rapporteur
Philippe Fraisse	Professeur, Université de Montpellier	Directeur de thèse
Mitsuhiro Hayashibe	Chargé de recherche, INRIA, Sophia-Antipolis	Co-Directeur de thèse
André Crosnier	Professeur, Université de Montpellier	Examineur
Gentiane Venture	Professeur associé, Tokyo University of Agric. and Tech.	Examineur
Charles Fattal	Docteur en médecine, Centre Neurologique PROPARGA	Examineur
David Guiraud	Directeur de recherche, INRIA, Sophia-Antipolis	Examineur

This work was completed in DEMAR project team, LIRMM/INRIA, France

CONTENTS

List of Figures	vii
List of Tables	ix
List of Acronyms	xi
General Introduction	1
1 FES-Induced Muscle Fatigue and Its Compensation	3
1.1 Introduction	4
1.2 Motor Control of the Lower Limbs	4
1.2.1 Nervous System	4
1.2.2 Skeletal Muscle	7
1.2.3 Lower Limb and Ankle Motion	8
1.2.4 Impairment of Motor Function	10
1.3 FES and Induced Muscle Fatigue	12
1.3.1 FES Principle	12
1.3.2 FES-Induced Muscle Fatigue	14
1.3.3 EMG and Its Application for Muscle Fatigue Analysis	16
1.4 The State of the Art	17
1.4.1 Reducing or Delaying Muscle Fatigue with FES	17
1.4.2 Identifying and Predicting Muscle Fatigue with FES	19
1.4.3 Current FES Control Strategies	21
1.5 Conclusion	23
2 Modeling of FES-Induced Torque Based on Evoked EMG	25
2.1 Introduction	26
2.1.1 Problem Formulation	26
2.1.2 Previous Work	26
2.1.3 Discussion	28
2.2 Modeling of the Electrically Stimulated Muscle	28
2.2.1 Model Structure	29
2.2.2 Model Identification	31
2.3 Experimental Description and Signal Processing	33
2.3.1 Experiment Design	34
2.3.2 Data Collection	35
2.3.3 Experimental Protocol	35
2.3.4 Signal Processing	36
2.4 Results in Surface FES	37
2.4.1 Muscle Fatigue and Recovery Characteristics	37
2.4.2 Model Identification and Prediction	39
2.4.3 Comparative Analysis to Improve Torque Prediction	41
2.5 Model Validation in Implanted FES	44
2.5.1 Muscle Fatigue in Implanted FES	45

2.5.2	Muscle Model Validation in Implanted FES	46
2.6	Discussion and Perspectives	47
2.7	Conclusion	49
3	Adaptive Torque Prediction and Fatigue Tracking from FES-Evoked EMG	51
3.1	Introduction	52
3.2	Previous Works	52
3.3	Online Torque Prediction during Muscle Fatigue	54
3.3.1	State-Space Representation and Filter Configuration	54
3.3.2	Kalman Filter with Forgetting Factor	56
3.3.3	Filter Configuration	58
3.4	Results of Time-Variant Torque Prediction	59
3.4.1	Time-Variant Parameter Tracking in Simulation	59
3.4.2	Fatigue Tracking Based on Experimental Data	62
3.4.2.1	Fatigue Dynamics	63
3.4.2.2	Torque Prediction Performance	64
3.4.2.3	Adaptive Performance for Internal and External Disturbances	65
3.4.2.4	Discussion on Filter Predictive Performance	68
3.4.3	Robust Fatigue Tracking	70
3.4.4	Discussion	74
3.5	Conclusion	75
4	EMG Feedback Predictive Torque Control in FES	77
4.1	Control System for Movement Induced by FES	78
4.2	Previous Works	80
4.3	Muscle Excitation and Contraction Model	81
4.4	Controller Design	83
4.4.1	Nonlinear Generalized Predictive Control	83
4.4.2	Closed-Loop Implementation of the Dual Predictive Controller	85
4.5	Evaluation of Predictive Performance for Drop Foot Correction	87
4.5.1	Experimental Validation of Predictive Torque Control	88
4.5.2	Simulation Results on Predictive Control Performance	96
4.6	Discussion	97
4.7	Conclusions	100
	General Conclusion	103
	Concluding remarks	103
	Perspectives	104
	Appendix	105
A	FES Experiment Description	107
A.1	Fundamental Concepts in FES	107
A.2	Experiment Description of Implanted FES	107
A.2.1	Experimental design	107

A.2.2	Data collection	108
A.2.3	Experimental protocol	108
A.2.4	Data Processing	110
B	State-Space and Kalman Filter	113
B.1	State-Space of Polynomial Hammerstein Model	113
B.2	Results of Model Identification and Torque Prediction	115
C	EMG Feedback Predictive Control	123
C.1	Generalized Predictive Control	123
C.2	Results of Control Performance	124
	List of Publications	129
	Bibliography	131

LIST OF FIGURES

1.1	Central nervous system and neurons	5
1.2	Structure of skeletal muscle	6
1.3	Motor units	8
1.4	Muscles and nerves of lower limb	9
1.5	Gait phase	10
1.6	Motor lesion and injury sites map hemiplegia and tetra/paraplegia	11
1.7	Neuroprosthesis systems	13
1.8	Typical FES system	13
1.9	Different FES interfaces	14
1.10	Different EMG recording interfaces	15
1.11	EMG raw signals of voluntary and FES-induced muscle contraction	17
1.12	Sliding mode FES controller	22
1.13	Neuro-Sliding-Mode control strategy for FES control of knee joint control	23
2.1	Hammerstein model structure.	29
2.2	Multi-Hammerstein model structure.	31
2.3	Identification scheme of muscle contraction model.	33
2.4	Experimental set-up for electrical stimulation and EMG, torque acquisition.	34
2.5	Schematic representation of the experimental sessions.	36
2.6	An example of the processed eEMG and torque of surface FES.	38
2.7	An example of the relationship of eEMG and torque in intermittent stimulation.	38
2.8	Demonstration of FES-induced muscle fatigue in subject S3.	39
2.9	The changes in torque and eEMG in surface intermittent FES.	40
2.10	Criterion of fit for determining appropriate model complexity.	40
2.11	The measured and predicted torque obtained by the eEMG-to-torque model	42
2.12	The measured and predicted torque obtained by the eEMG-to-torque model	43
2.13	The correlation between torque and eEMG in implanted continuous FES	46
2.14	The correlation between torque and eEMG in implanted continuous FES	47
2.15	The measured and predicted torque in implanted FES	48
3.1	Input and output data sets for model identification in simulation study	60
3.2	Convergence and tracking of both static and time-variant parameters	61
3.3	The estimated torque and identification error in subject S5 with surface FES	62
3.4	The estimated torque and identification error in the implanted subject	63
3.5	The changes in muscle contraction dynamics due to fatigue	64
3.6	Illustration of torque estimation based on eEMG information	65
3.7	Prediction errors in subject S3	66
3.8	Adaptive performance of the filter in subject S3	67
3.9	Adaptive performance of the filter in the implanted subject	68
3.10	Adaptive performance of the filter in the subject S3	69
3.11	Adaptive performance of the filter in the implanted subject	69
3.12	Robust fatigue tracking based on eEMG and KF in subject S3	71
3.13	Robust fatigue tracking based on eEMG and KF in subject S1	72

3.14 Robust fatigue tracking based on eEMG and KF in implanted FES	73
4.1 Organization of traditional functional electrical stimulation control systems	79
4.2 Model structure of stimulated muscle for model identification	82
4.3 Diagram illustrating the EMG-feedback predictive control strategy	84
4.4 A single nonlinear generalized predictive controller based on a PHM model	84
4.5 Diagram illustrating the dual predictive control strategy	86
4.6 Relationship among stimulation pulse width, MAV of eEMG, and torque	88
4.7 Evaluation of EFPC to obtain randomly changed torque in subject OR	91
4.8 Evaluation of EFPC to obtain gradually increased torque in subject HG	92
4.9 Evaluation of EFPC to obtain gradually increased torque in subject ZQ	93
4.10 Robustness of the proposed EFPC to obtain randomly changed torque	94
4.11 Robustness of the proposed EFPC to obtain gradually increased torque	95
4.12 The effects of weighting factors and constraints on control performance	96
4.13 Muscle fatigue compensation in subject2	98
4.14 Stimulation pattern created by EFPC for designed torque trajectory	98
4.15 Stimulation pattern created by EFPC for obtaining different torque levels	99
4.16 FES system for real-time fatigue compensation and torque tracking.	105
A.1 Common stimulus output waveform	107
A.2 The stimulation parameters which can be modulated	108
A.3 Stimulation train and stimulation envelope	109
A.4 Implant position and experimental set-up illustration.	109
A.5 Removal of radio signal from the eEMG signal.	110
A.6 Torque and eEMG respond to stimulation in implanted subject	111
B.1 Estimated torque and model parameters in subject S4.	116
B.2 Estimated torque and model parameters in subject S5.	117
B.3 Estimated torque and model parameters in implanted subject.	118
B.4 Fatigue tracking based on muscle eEMG-to-torque model and KF in subject S2.	119
B.5 Fatigue tracking based on eEMG-to-torque model and KF in subject S4.	120
B.6 Fatigue tracking based on eEMG-to-torque model and KF in subject S5.	121
C.1 Control performance of the EFPC with gradually increased stimulation	125
C.2 Control performance of the EFPC with gradually increased stimulation	126
C.3 Control performance of the EFPC with constant stimulation strategy	127
C.4 Simulation of fatigue compensation performance of the EFPC.	128
C.5 The performance of the EFPC in generating stimulation pattern for natural trajectory.	128

LIST OF TABLES

2.1	Patient configurations	34
2.2	Stimulation parameters	35
2.3	Summary of the prediction error	44
3.1	NRMS error of estimation	61
3.2	Prediction performance with experimental data	65
3.3	Computational time of different prediction horizons	67
4.1	Stimulation parameters for drop foot correction	88
4.2	Coefficient initialization for online identification of the muscle models	89
4.3	The selection of penalty weights in a dual NGPC controller	90
4.4	Configuration of the dual predictive controller	90
4.5	Summary of the control errors	90
A.1	Stimulation parameters	108

List of Acronyms

ARX	Autoregressive with External Input
ASIA	American Spinal Injury Association
EFPC	EMG-Feedback Predictive Control
CNS	Central Nervous System
EMG	Electromyography
eEMG	evoked Electromyography
FES	Functional Electrical Stimulation
GPC	Generalized Predictive Control
GM	Gastrocnemius
KF	Kalman Filter
LS	Least Squares
MUAP	Motor Unit Action Potential
MAV	Mean Absolute Value
MDF	Median Frequency
MDL	Rissanen's Minimum Description Length
NGPC	Nonlinear Generalized Predictive Control
NRMS	Normalized Root Mean Squares
NPE	Normalized Peak Error
OLS	Ordinary Least Squares
PNS	Peripheral Nervous System
PW	Pulse Width
PHM	Polynomial Hammerstein Model
RF	Radio Frequency
RMS	Root Mean Squares
SCI	Spinal Cord Injury
SNR	Signal to Noise Ratio
TA	Tibialis Anterior

General Introduction

Functional Electrical Stimulation (FES) is one of the solutions to improve lost motor functions in persons with Spinal Cord Injury (SCI) or cerebral injury. The electrical currents artificially generate action potentials on the axons of the alpha motor neurons to induce muscle contraction in place of the Central Nervous System (CNS). To date, FES has been used in a wide range of rehabilitation applications, including the FES-aided support of standing, walking, grasping/releasing, drop foot correction, tremor compensation, and bladder/bowel management.

Apart from the ability to improve functional movements, this technique has numerous other benefits for patients, including preventing muscle atrophy, reducing muscle spasms, increasing blood circulation and facilitating muscle reeducation. Yet, despite its many potential advantages, FES has not achieved widespread clinical use thus far because of its limitations, such as rapid muscle fatigue and imprecise force/torque control. In this context, an FES control system should deliver an appropriate stimulation pattern to paralyzed muscle and control the muscle force or joint torque compensating for the variations in muscle responses to the stimulations.

In the current FES systems, some researchers have presented their efforts to develop a closed-loop control of FES. Most of them have focused on joint angle control without consideration of muscle state changes. However, the joint angle may be affected not only by muscle contraction, but also by unexpected external disturbances. Moreover, it is appropriate to confirm the muscle state induced by FES to control the actual muscle contraction state as well as the joint torque. Therefore, this thesis aims to develop an advanced FES closed-loop control method which is based on evoked Electromyography (eEMG) feedback to achieve more accurate, safe, and robust stimulation control.

In the domain of lower limb FES systems, muscle state changes (muscle fatigue) are a major cause of degraded performance. However, the inadequacy of torque/force sensors is another problem with this rehabilitation technique. In order to track muscle state changes and perform accurate torque control, the joint torque must therefore be estimated. This motivated us to develop a torque estimation method from biosignals that can be measured or well estimated. Although some works have attempted to use eEMG to predict torque production [Erfanian et al., 1998], day-to-day differences are still considerable and have to be manually adjusted. In addition, these works did not consider the effects of different muscle fatigue levels and subject-specific differences on torque prediction accuracy. In this thesis, one focus is on the techniques for identifying muscle models in order to estimate the time-variant joint torque on the basis of muscle activity information. The other focus is the development of a closed-loop control framework for FES-elicited joint torque to allow for compensation of the physiological muscle changes. From a practical point of view, a measurement of muscle activity is preferred as the feedback signal, as it directly provides the information on muscle response to the stimulation.

In this thesis, two primary contributions are made to achieve the purposes described above :

1. An online torque estimation method is proposed for FES-elicited torque prediction and muscle fatigue tracking under isometric condition. The muscle contraction dynamics are modeled by a Polynomial Hammerstein Model (PHM) to represent joint torque from muscle activity [Zhang et al., 2010] [Hayashibe et al., 2011b]. Kalman Filter (KF) with forgetting factor is proposed to estimate the time-variant muscle contraction dynamics. The estimation technique allows for the compensation of the subject-specific, protocol-specific changes and fatigue level-related variations. In order to evaluate its performance,

experimental and simulation studies are conducted. The results demonstrate good tracking performance of muscle variations and robustness to external disturbances and sensing failure [Zhang et al., 2011b] [Zhang et al., 2011a].

2. On the basis of the good predictive performance of the proposed estimation method, a new control strategy, EMG-Feedback Predictive Control (EFPC), is proposed to explicitly control the joint torque [Hayashibe et al., 2011a]. Both the muscle excitation and contraction dynamics are modeled by PHM. The main idea is to use the eEMG signal in a dual-purpose : correlating stimulation to muscle electrical behavior in the muscle excitation process and correlating muscle electrical behavior to muscle mechanical behavior in the muscle contraction process. The performance of this controller is assessed by simulation and experiments for FES-induced drop foot correction. The proposed control framework provides promising results in terms of controllability and robustness. The great computational power also makes it feasible for real-time implementation.

This thesis is organized as follows :

In the first chapter, the basic and necessary neurological principles are presented, as well as a brief review of the musculoskeletal system and motor-function impairment of the lower limbs. Muscle fatigue induced by voluntary contraction and FES are compared, highlighting the influence of muscle fatigue in an FES system. In order to analyze muscle fatigue, an eEMG technique is introduced and the relevant works related to fatigue reduction and prediction are described in detail. In addition, the FES control strategies, especially those involving fatigue compensation features, are presented and discussed.

In the second chapter, a predictive torque model is presented and driven by eEMG signals recorded from stimulated muscle. Two fatigue experiments in different stimulation conditions are conducted to investigate muscle fatigue features and then to identify and validate the muscle contraction model.

In the third chapter, adaptive torque prediction is explored under time-variant muscle dynamics. The proposed muscle model identification and torque prediction method are described in detail, and incorporated into a muscle fatigue tracking task. Its performance is assessed with simulation and experimental studies on SCI patients.

In the fourth chapter, a closed-loop control framework is developed to control joint torque based on eEMG. In the underlying predictive strategy, a dual PHM structure is proposed to catch muscle excitation and contraction dynamics. The prediction method proposed in the third chapter is integrated to the torque tracking scheme along with an FES controller. We evaluate the FES control performance with both simulation and experimental studies for FES application to drop foot correction.

A conclusion is given to summarize the contributions of this thesis and to project the future perspectives for more accurate, safe, and robust FES systems.

Following the conclusion, readers can find some additional aspects related to this work in the Appendix. For example, the experiment of implanted FES and the algorithms of KF and EFPC used throughout this work are all provided. We also present some additional results from chapter 3 and chapter 4 here.

CHAPTER 1

FES-Induced Muscle Fatigue and Its Compensation

Contents

1.1 Introduction	4
1.2 Motor Control of the Lower Limbs	4
1.2.1 Nervous System	4
1.2.2 Skeletal Muscle	7
1.2.3 Lower Limb and Ankle Motion	8
1.2.4 Impairment of Motor Function	10
1.3 FES and Induced Muscle Fatigue	12
1.3.1 FES Principle	12
1.3.2 FES-Induced Muscle Fatigue	14
1.3.3 EMG and Its Application for Muscle Fatigue Analysis	16
1.4 The State of the Art	17
1.4.1 Reducing or Delaying Muscle Fatigue with FES	17
1.4.2 Identifying and Predicting Muscle Fatigue with FES	19
1.4.3 Current FES Control Strategies	21
1.5 Conclusion	23

1.1 Introduction

The main objective of this thesis is to investigate the feasibility of eEMG in a model-based FES control system for compensation of muscle state variations (such as muscle fatigue). This is a challenging and meaningful goal that should improve the performance of the present FES system.

It has been estimated that at least 90 million people currently suffer from SCI worldwide [Ragnarsdottir, 2001], and 15 million people suffer stroke each year [WHO, 2007]. FES is an active solution to improve the motor deficits of hemiplegics who suffer from cerebral injuries (such as stroke) and the para/quadruplegics who suffer from SCI. Whatever the specific causes of these injuries, the pathway from the brain that drives and regulates muscle contractions is interrupted. The patients lose all or part of their functional movements as a result. Therefore, restoration or improvement of the motor function is significant for such patients to improve the quality of their lives. To date, FES has been widely used in clinical applications and research, such as assisted standing [Solomonow et al., 2000] [Kobetic et al., 2009], walking [Hardin et al., 2007], grasping/releasing [Mangold et al., 2005], drop foot correction [Breen et al., 2006], tremor suppression [Bó and Poignet, 2010] and bladder/bowel management [Johnston et al., 2005] [Lafor t et al., 2011]. For the application of FES, the accuracy of the induced movement and the safety to the patient are both critical.

In this chapter, a brief introduction of the fundamental knowledge on the neural and musculoskeletal systems, which some engineers are not familiar with, is given. Next, the FES technique, FES-induced muscle fatigue, and its analysis are introduced. Last, an overview of the strategies to reduce, identify or predict FES-induced muscle fatigue and to control electrical stimulation are presented and discussed.

1.2 Motor Control of the Lower Limbs

Humans are able to perform accurate, goal-oriented movements—from simple to complex—and easily compensate unexpected perturbations, during which various and elaborate information processing systems are involved in the nervous system. In this section, the neurological basis for motor control and the primary organization and control of skeletal muscles are described. Because the focus is lower limb movement, the relevant musculoskeletal structure, properties and impairments are also introduced in this section. The main sources referred to in this chapter are included in [Kandel et al., 2000], [Brodal, 2010] and [Winters and Crago, 2000].

1.2.1 Nervous System

The nervous system is a specialized system of cells, tissues, and organs. It controls the body's responses to internal and external stimuli and coordinates the actions of different body parts. Anatomically, the nervous system is divided into the CNS, consisting of brain and spinal cord, and the Peripheral Nervous System (PNS), which connects the CNS with various receptors and effectors.

The nervous system is built up of numerous nerve cells (or neurons), the main functional units, and glial cells, which are non-neuronal and primarily support and protect the neurons. A

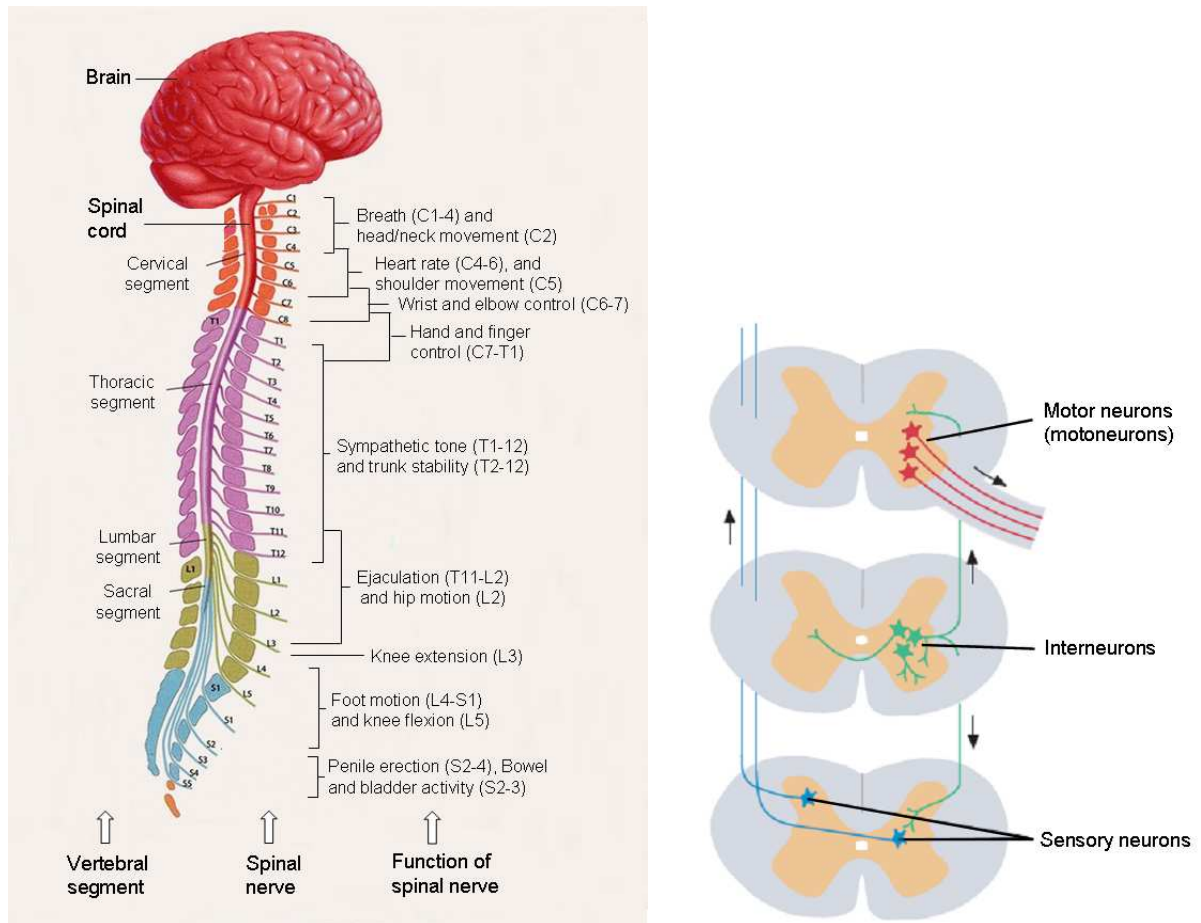


FIGURE 1.1 – Left : Central nervous system and the functions of spinal nerves. Right : Three main types of neurons in the spinal cord. Motor neurons transmit signals from the CNS efferent to effectors, while sensory neurons bring signals from receptors afferent to the CNS [Brodal, 2010].

typical neuron consists of the cell body (or soma), dendrites, and the axon. In the spinal cord, there are three main types of neurons classified according to where their axons terminate. They have the same structures yet different functions as depicted in Fig. 1.1. Motor neurons, with their cell body mainly located in the ventral horn, send their axons efferent from the CNS to the effectors that carry out the response. The interneurons connect neurons in the cord. Sensory neurons, with their cell body mainly located in the dorsal horn, transmit impulses afferent from various receptors to the CNS. The gaps between these three types of neurons, namely synapses, serve as junctions passing signals between individual target neurons.

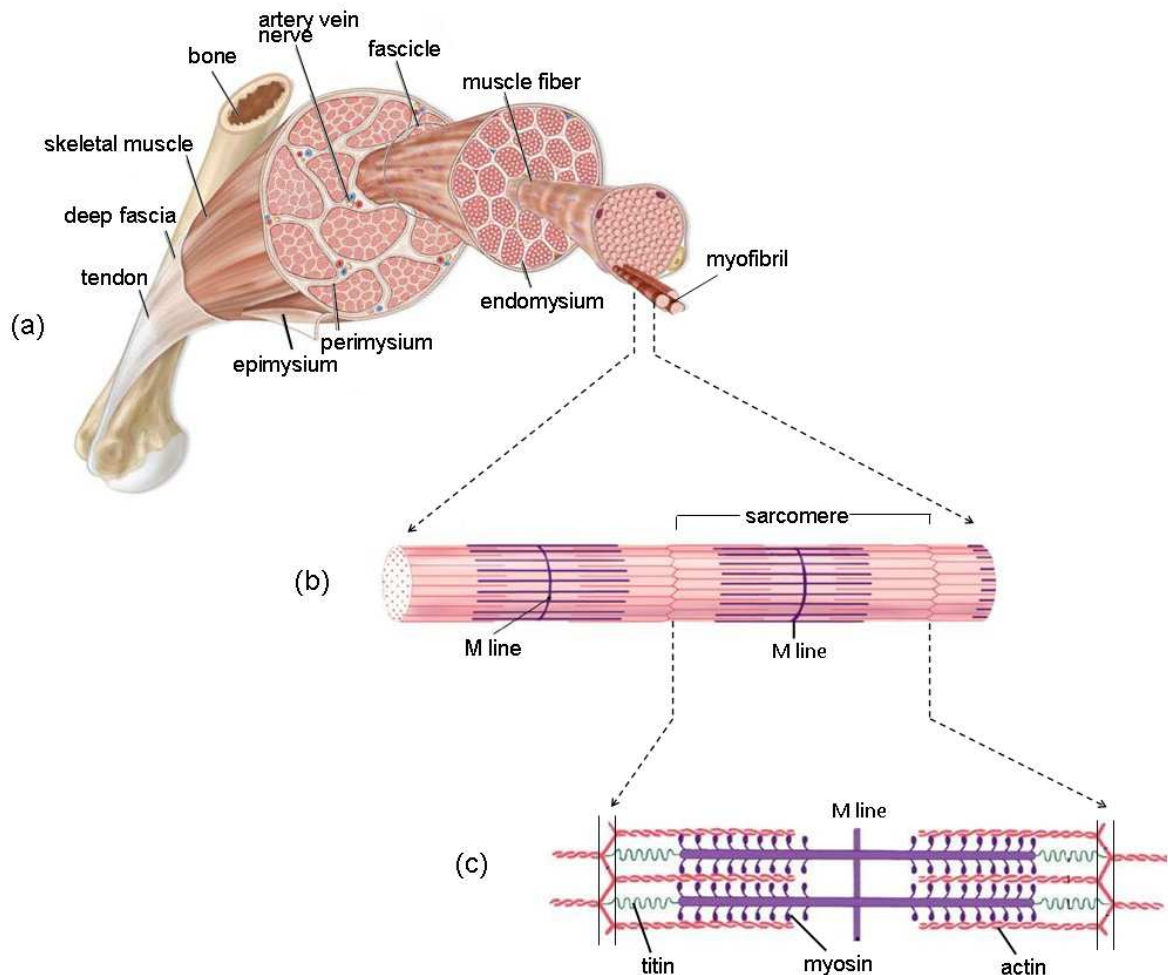


FIGURE 1.2 – (a) Skeletal muscle is composed of numerous muscle fibers ; (b) Sarcomere, a basic unit of muscle contraction, is primarily composed of actin and myosin ; (c) Cross-bridge between actin and myosin in a sarcomere results in muscle contraction.

Although all the motor neurons activate skeletal muscles, not all of them contribute to voluntary skeletal muscle contraction. Alpha motor neurons activate extrafusal muscle fibers throughout the extrafusal muscle fibers and control voluntary muscle activity. Gamma motor neurons do not contribute to the muscle force supplement provided by the extrafusal fibers ;

instead, they activate the intrafusal muscle fibers within the muscle spindles and feedback the muscle states (e.g., muscle length, position).

1.2.2 Skeletal Muscle

The skeletal muscles maintain posture, stabilize joints and provide skeletal movements. Voluntary contractions of skeletal muscles occur as a result of conscious control of the CNS, differing from smooth and cardiac muscles which are under unconscious control. Thus, the nervous system and muscular system are closely interconnected and well coordinated. Here we focus on the skeletal muscle—its structure, property and how it works.

Muscle Structure and Properties

Skeletal muscles are primarily attached to the bones by tendons and made up of numerous muscle fibers, which are bundled into fascicles along the axis of the muscle. The muscle fibers are long and cylindrical, composed of myofibrils which are arranged in parallel. These myofibrils consist of sarcomeres—basic contraction units—in series. Within each sarcomere, there are two types of myofilaments organized in a regular pattern, the thin actin filaments and the thick myosin filaments. Fig. 1.2 illustrates the structure of skeletal muscles.

In a single muscle, the numerous muscle fibers are distinct in terms of functional properties, peak force, contraction velocity, resistance to fatigue, oxidative and glycolytic capacities, and actino-myosin ATPase activities. Nonetheless, based on observations of their contractile properties (muscle strength, contraction velocity and fatigability), muscle fibers can be divided into three types. Type I fibers, oxidative fibers, contract slowly and have high fatigue resistance. The force produced by Type I fibers rises and falls slowly, but can be kept consistent for long periods. They are mainly used for maintaining posture and sports like long-distance running. Type IIb fibers, contrary to Type I, are glycolytic fibers and respond to the action potential quite fast. They can produce high force, but they tend to fatigue easily and need a long time to recover. This type of muscle fiber is needed to generate instantaneous or vigorous motion, such as jumping or sprinting. Type IIa fibers use both oxidative and glycolytic processes for metabolism. Compared with the other two fiber types, Type IIa fibers are intermediate in terms of contraction speed, force productivity and fatigability. Single muscles may be composed of three fiber types in different proportions, which results in compound muscle contractile properties in the different muscles. For instance, if we compare Soleus with Gastrocnemius (GM) in the Triceps surae muscle group, Soleus is a relatively slow muscle, while GM is a fast and fatigable muscle, as they contain different amounts of muscle fibers I and IIb.

Whatever the muscle fiber type, each muscle fiber is exclusively innervated by a single motor neuron; in contrast, a motor neuron can activate a number of muscle fibers with the same muscle fiber type. The group composed of a motor neuron and all the muscle fibers it innervates is known as a motor unit, as shown in Fig. 1.3. According to the muscle fiber type, the motor unit can be correspondingly classified into three types: slow-twitch fatigue-resistant (Type I fiber), fast-twitch fatigue-resistant (Type IIa fiber), and fast-twitch fatigable (Type IIb fiber).

The complex and efficient movement of humans depends on the suitable recruitment of muscles. The overall force produced in a single muscle is limited and depends on the number and size of the activated motor units and their individual firing rates. As a result, the synthetical force

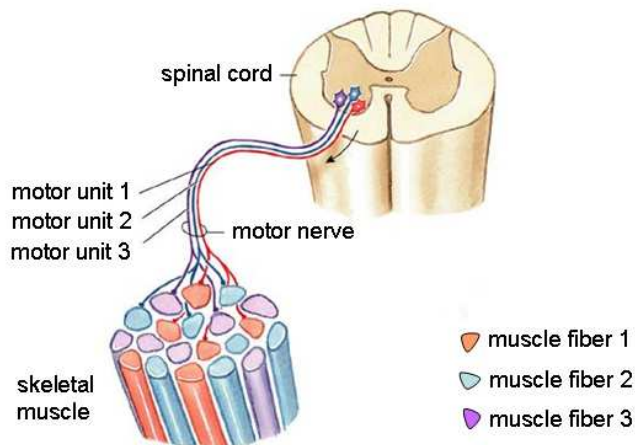


FIGURE 1.3 – The motor unit is composed of a motor neuron and the muscle fibers it innervates. Corresponding to three muscle fiber types, the motor units also have three types with different fatigability [2007 Pearson Education, Inc.].

is a spatial and temporal combination of the forces induced by all the recruited muscle fibers. In addition, skeletal muscle has mixed biochemical responses under all contractile conditions due to its heterogeneous nature [Binder-Macleod and Snyder-Mackler, 1993]. Therefore, the CNS must optimally activate suitable muscle and further muscle fibers to induce the desired motion and preserve energy supply.

Muscle Contraction

Skeletal muscles contract only when they are activated by neural signals. The muscles transform the neural signals into mechanical outputs, such as muscle force or length. The muscle contractile mechanism is complex and basically summarized by the "sliding filament" theory [Huxley, 1957]. At the molecular level, muscle contraction is generated through the "cross-bridge" cycling between actin and myosin in a sarcomere. Here, we briefly explain the development of the neuromuscular system. The brain sends a neural signal, in the form of a neural action potential, which then propagates along the motor neuron axons. When the neural action potential reaches the neuromuscular junction, the depolarization produced in the nerve end plate and then in the postsynaptic receptors on the muscle gives rise to a muscle action potential. When the muscle action potential propagates along the membrane and along the T-tubules, calcium is released across the entire sarcomere. Calcium release makes the active site of the thin actin bind with the myosin head (or cross-bridge), and then pulls the actin sliding along the myosin toward the center of the sarcomere. At the same time, the cross-bridge rotates, allowing for the attachment to a new active site at a shorter length. When a new neural action potential arrives, this process is repeated, resulting in progressive myofibril contraction. The entire muscle fiber and then the entire muscle consequently contract. If no action potential arrives, the cross-bridge cycle is terminated due to the decrease in calcium release. The muscle relaxes and returns to the rest state as a result.

1.2.3 Lower Limb and Ankle Motion

The human lower limbs play an important role in locomotion, such as standing, walking, jumping, running and similar activities. Compared with the upper limbs, which mainly serve as organs of manipulation, the lower limbs serve for locomotion, emphasizing stability rather than

mobility. Various joints within the entire lower limb allow for stable locomotion at variant speed and over uneven ground. The lower limb is divided by the hip joint, knee joint and ankle joint into four parts : buttock, thigh, leg and foot. As this work concentrates on motion control of the ankle, a special emphasis is put on the foot and leg, as well as the muscles and nerves involved, as shown in Fig. 1.4.

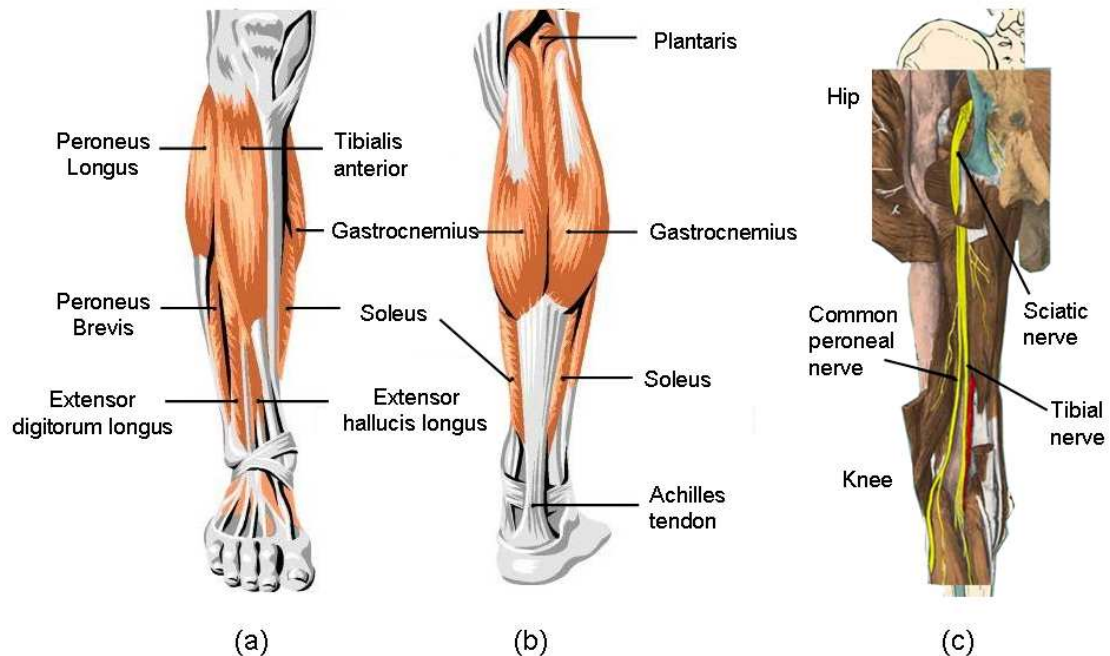


FIGURE 1.4 – Anterior (a) and posterior (b) muscles of the lower limb [<http://knol.google.com/k/shin-pain>]; (c) Nerves activating the muscles of lower (posterior) [<http://home.comcast.net/~wnor/postthigh.htm>].

The ankle joint is a hinge-type joint and relatively simple in terms of the number of muscles involved in the actuation. It permits several movements such as dorsiflexion, plantarflexion, eversion and inversion [Mackenzie, 2004]. Dorsiflexion and plantarflexion provide the primary range of motion at the ankle.

Ankle dorsiflexion — moving the toes toward the shin — helps with our ability to place the ankle in a stable position and also gives more power upon contact with the ground. This movement is brought by all the muscles whose tendons pass into the foot anterior to the ankle joint, including the Tibialis Anterior (TA), Extensor hallucis longus and Extensor digitorum longus. All these muscles are innervated by the common peroneal nerve, which comprises the nerve fibers deriving from the L4-L5-S1-S2 levels of spinal segments.

Ankle plantarflexion — pointing the toes away from the shin and toward the ground — helps to release tension, which in turn helps to move more easily and absorb the shock of contact with the ground. Plantarflexion is brought by all the muscles whose tendons attach to the calcaneus (e.g., Soleus, GM) and whose tendons pass into the foot posterior to the ankle joint (e.g., TA, Flexor digitorum longus, Peroneus longus and brevis). The GM and Soleus are generally grouped as Triceps surae muscle with the two heads of the GM attaching to the femur

above the knee, and another head (Soleus) attaching to the tibia. The Triceps surae muscle is innervated by the tibial nerve arising from L4-L5-S1-S2 nerves.

Ankle motion plays an important role during gait. A gait cycle starts when the heel contacts the ground and ends when that heel contacts the ground again. The ankle alternately plantarflexes and then dorsiflexes twice during a single gait cycle [O’Keeffe et al., 2003]. Each gait cycle consists of a stance phase and a swing phase as shown in Fig. 1.5. The stance phase begins from the initial heel strike and ends with the lift of the toe at the beginning of swing phase. It accounts for approximately 70% of the duty cycle. During the swing phase, the foot is off the ground. It accounts for approximately 30% of the duty cycle.



FIGURE 1.5 – One gait cycle consists of a stance phase and a swing phase, and the ankle alternately plantarflexes and then dorsiflexes twice.

1.2.4 Impairment of Motor Function

The impairment of motor function is often the result of SCI, cerebral injury, multiple sclerosis or other neurological disorders. In order to help understand the underlying principle of FES, the nature of motor neuron lesions is briefly introduced, which will be helpful in understanding how FES contributes to restoring lost motor functions.

Fig. 1.6 illustrates the pathways of lower motor neurons and upper motor neurons. Lower motor neurons are the neurons that directly serve for the effectors (such as skeletal muscles). They are either from the cranial nerve in the brain stem or from motor nerves in the spinal cord. On the contrary, the upper motor neurons originating from the motor cortex or the brain stem are not directly responsible for stimulating effectors, but connect the brain to the appropriate level in the spinal cord. From this spinal segment, the nerve signals propagate to the effectors by means of lower motor neurons. Accordingly, motor neuron lesion is usually divided into upper motor neuron lesion and lower motor neuron lesion with respect to different injury sites and resultant symptoms. An upper motor neuron lesion is usually accompanied by innervated and paralyzed muscle, while a lower motor neuron lesion results in denervated and paralyzed muscle.

SCI refers to any damage to the spinal cord from trauma, loss of normal blood supply, compression from tumor or inflammation. SCI severity is roughly qualified as "complete" or "incomplete" and classified according to the American Spinal Injury Association (ASIA) scale. Higher level injuries imply greater functional deficits and impairment of personal mobility [R.J. et al., 1996]. The meanings of the five classifications are no motor or sensory function

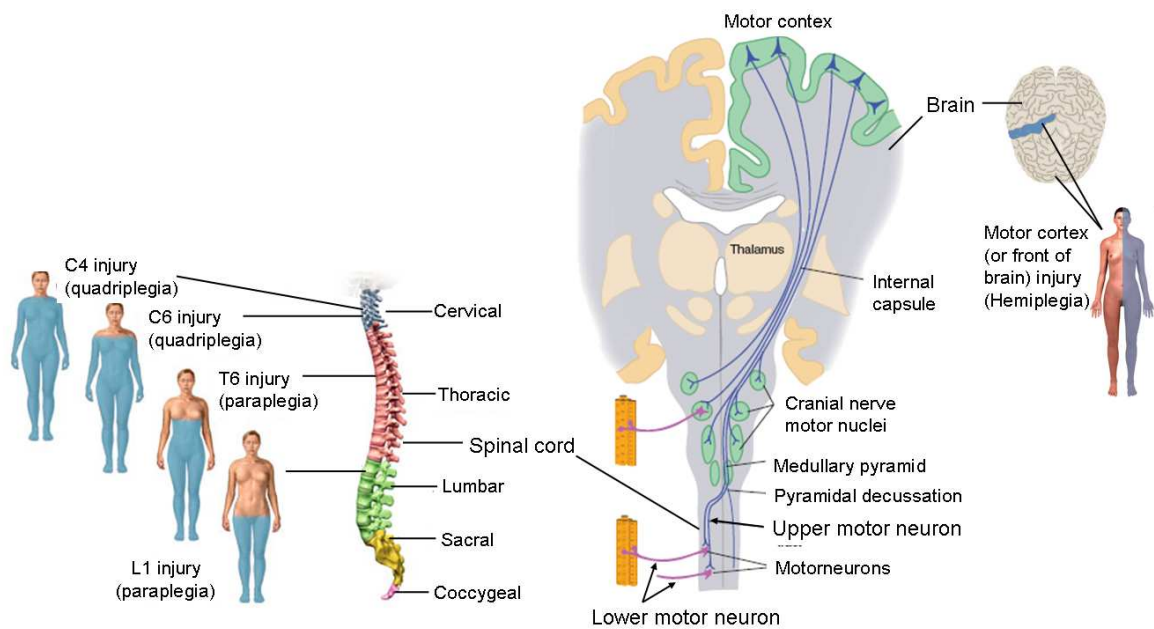


FIGURE 1.6 – Middle : Lower motor neurons (purple) directly serve for the effectors (such as skeletal muscles). They are either from the cranial nerve in the brain stem or from motor nerves in the spinal cord. On the contrary, the upper motor neurons (blue) originating from the motor cortex or the brain stem are not directly responsible for stimulating effectors, but connect the brain to the appropriate level in the spinal cord. From this spinal segment, the nerve signals propagate to the effectors by means of lower motor neurons. Modified from [Brodal, 2010]. Left : SCI refers to any injury within the spinal cord, leading to quadri/paraplegia at different levels. Right : Hemiplegia is caused by various injuries, such as traumatic injury to the brain, resulting in the opposite side of the body being affected.

(ASIA A), only sensory function remaining (ASIA B), some sensory and motor preservation (ASIA C), useful motor function (ASIA D) and normal function (ASIA E). Injuries at different sites in the cerebral column lead to complete paralysis in all the upper and lower limbs (quadriplegia) or in the lower limbs only (paraplegia), as shown in Fig. 1.6. Hemiplegia can be caused by various injuries, such as traumatic injury to the brain resulting in the opposite side of body being affected (Fig. 1.6).

1.3 FES and Induced Muscle Fatigue

In order to improve movement in hemiplegics or para/quadruplegics, several treatments have been proposed, such as an assistant brace, exoskeleton (orthotic device) [Colombo, 2000] [Rosen and Arcan, 2001] [Tsukahara et al., 2011], FES [O'Halloran et al., 2003] [Johnston et al., 2003] [Johnston et al., 2005] [Guiraud et al., 2006] [Hardin et al., 2007], and a hybrid neuroprosthesis incorporating FES with an external exoskeleton [Yukawa et al., 1996] [Kobetic et al., 2009]. Some examples of neuroprosthesis systems are illustrated in Fig. 1.7. FES is used to remedy some of the shortcomings of mechanical orthotic devices [Kralj, 1973]. In comparison with a passive external exoskeleton, FES is an active technique for regaining functional motion, and it has advantages in terms of no power consuming problem, the use of a natural exoskeletal system and levers (human body), and avoidance of the "learned disuse" of the paralyzed muscle. Apart from the ability to improve motor function, FES has various benefits such as preventing muscle atrophy, reducing muscle spasm, increasing blood circulation and facilitating muscle reeducation.

1.3.1 FES Principle

FES delivers electrical currents to activate the paralyzed muscles in order to stabilize the body from collapse and provide power to move. However, not every patient can benefit from this technique because it requires intact lower motor neurons (see Fig. 1.6). In this case, the underlying neurophysiological principle of FES is the generation of action potentials in the uninjured lower motor neuron activated by external electrical stimuli. For patients with lower motor lesions, although FES is not able to improve their mobility as it does for patients with upper motor neuron lesion, it is still helpful to reduce muscle atrophy and enhance muscle contractility [Kern et al., 2010].

FES was first put forward for surface stimulation in the lower extremities of patients by [Liberson et al., 1961] to correct the drop foot condition. With the development of high-level techniques, such as microprocessors, microelectronics, manufacturing and control theory, more advanced systems have been developed, such as implantable FES systems for lower extremity applications in paraplegic patients [R.J. et al., 1996] [Johnston et al., 2003] [Guiraud et al., 2006] and hemiplegic patients [O'Halloran et al., 2003].

A traditional FES system consists of a stimulator, electrodes and a control unit. The control unit determines the electrical stimulation pattern to achieve the desired movement. The stimulator generates and delivers the stimulus to the muscle of interest through the electrodes, as shown in Fig. 1.8. The FES system can be surface, needle, or implanted, depending on the application. Surface stimulation may be affected by day-to-day variations but it is convenient to

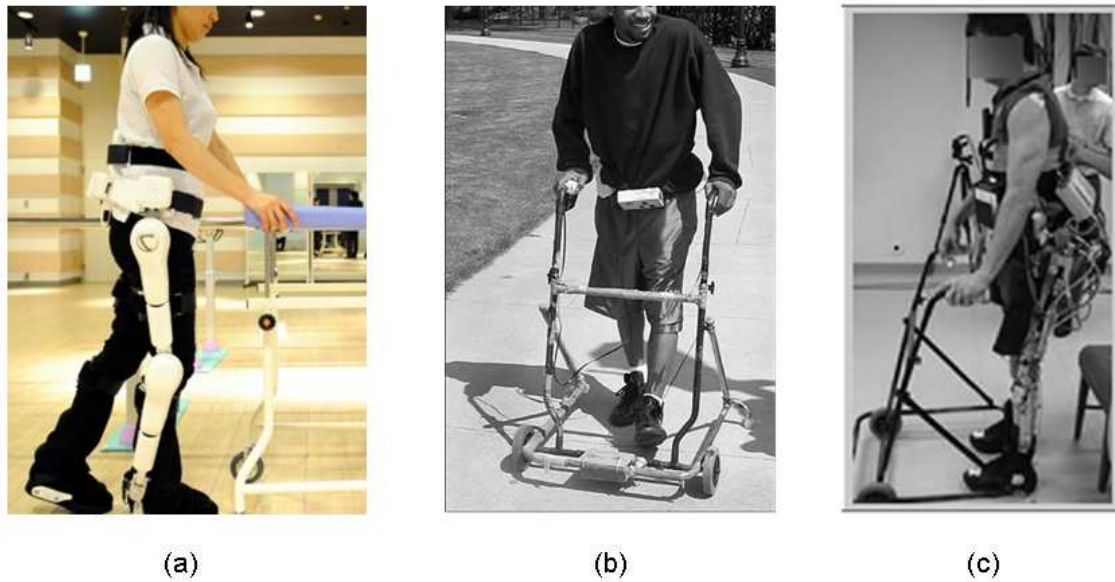


FIGURE 1.7 – (a) The Hybrid Assistive Limb (HAL) is under research for applications in SCI [Tsukahara et al., 2011]; (b) The implanted FES system [Hardin et al., 2007], including implanted 8-channel receiver stimulator, intramuscular electrodes, connector, and external components—control unit, coupling coil and finger switch. A customized stimulation pattern is applied to an incomplete cervical patient for gait training. The stimulation is triggered by a finger switch; (c) A hybrid neuroprosthesis combining an orthotic device with electrical stimulation [Kobetic et al., 2009]. The knee mechanism locks during stance to prevent collapse and unlocks during swing, while the FES system consisting of 16-channel stimulation via intramuscular electrodes, moves the ankle in the sagittal plane.

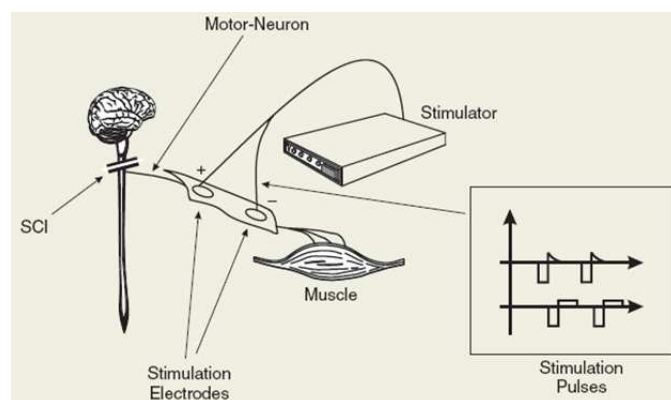


FIGURE 1.8 – A typical FES system consists of a stimulator, electrodes and a control unit. The control unit determines the pattern of electrical stimulus for desired movement. The stimulator generates and delivers the stimulus to the muscle of interest through the electrodes [Milos, 2001].

implement and remove. The implanted FES can cover the daily variation problem, but a surgical operation is required and infection is still a potential problem [Jaeger, 1994]. Therefore, when implanted FES is not available, surface FES is still useful, and currently the most commonly used in the community and in labs. With surface FES, the stimulation electrodes can be placed on the muscle, activating a single muscle, or near the motor nerve, thus allowing the activation of multiple muscles. Note that, if the electrodes are placed on the motor nerve, the parallel sensory nerve tends to be activated simultaneously, which can be observed as H-reflex in a myoelectrical recording.

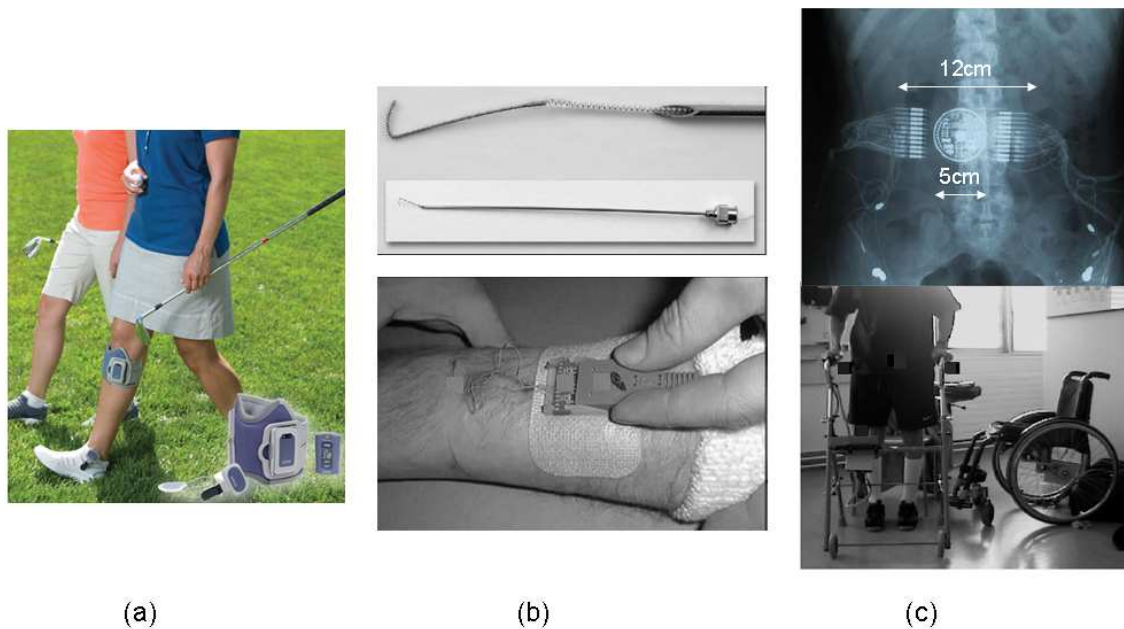


FIGURE 1.9 – Different FES interfaces. (a) Surface FES system for drop foot correction [NESS L300, CA, US], which mainly consists of an RF foot sensor for detecting heel off and heel contact, an RF control unit, and an RF controlled stimulation unit; (b) Needle FES system for restoring upper limb functions [Knutson et al., 2002]. The percutaneous intramuscular electrodes are fine wires with a diameter of approximately $200\ \mu\text{m}$ anchored inside the target muscles. The external stimulator is connected to the lead (a diameter of approximately $580\ \mu\text{m}$) exiting through the skin by a connector block; (c) Implanted electrodes and overall system [Guiraud et al., 2006] for restoring lower limb movement. This FES system has 16 channels for inducing muscle contraction either by epimysial electrodes or neural electrodes to support standing or walking.

1.3.2 FES-Induced Muscle Fatigue

Muscle fatigue has been defined as "a failure to maintain the required or expected force" from a repeatedly activated muscle [Edwards, 1981]. In voluntary contraction, a variety of biological and motivational factors contribute to muscle fatigue [Gandevia et al., 1995], such as reduced motor drive by the CNS, failure of peripheral electrical transmission, and failure of the muscular contractile mechanism. Although the action potential activated by artificial stimulation is not distinguishable from the action potential activated by natural stimulation [Riener, 1999],

the rate of muscle fatigue during FES is much greater than that seen during natural contractions [Binder-Macleod and Snyder-Mackler, 1993]. The exact reason for this fast fatigue phenomenon is complex and is not yet fully understood. The possible reasons can be summarized as : (1) the inverse size principle, according to which the artificial stimulation recruits the motor neurons from the largest to the smallest [Hamada et al., 2004], and the larger the motor neuron, the more fatigable the muscle fiber ; (2) motor units are activated in synchronized manner with artificial stimulation, which is different from the asynchronous activation during natural contraction ; and (3) the constant order of recruitment, with fast fatigable motor units activated first, then slow fatigue-resistant motor units. These opposite features of FES activation compared with natural contraction have motivated a number of researchers to find the optimal stimulation

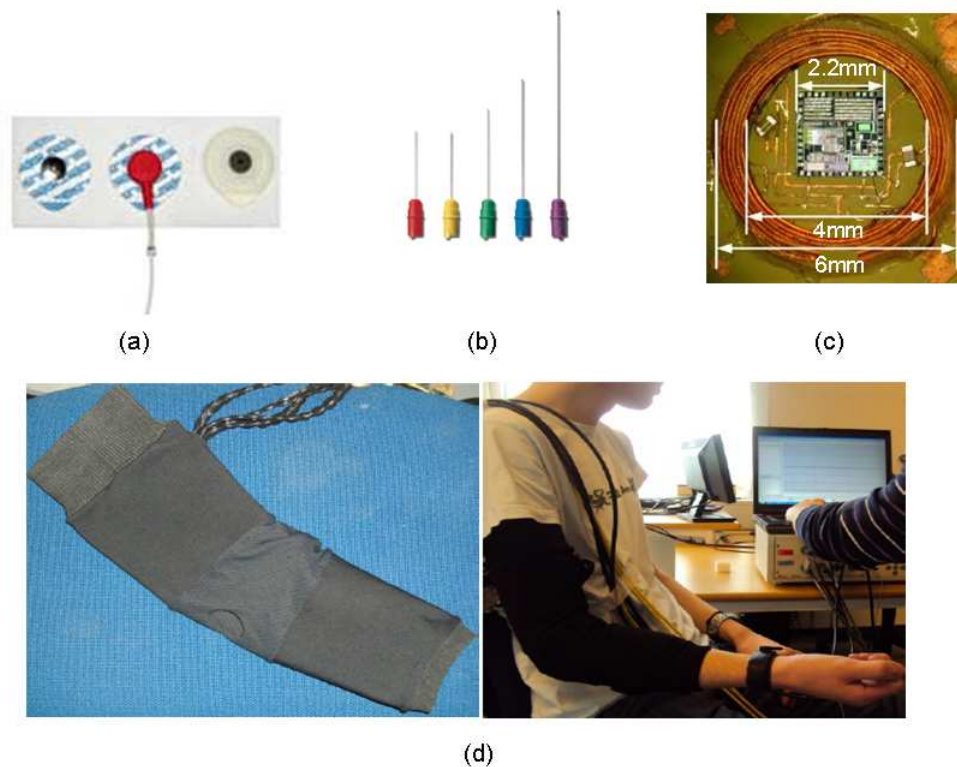


FIGURE 1.10 – Different EMG recording interfaces. (a) Surface EMG electrodes [MediTr100, The Mind People]. (b) Fine-wire EMG recording system [TECA, CareFusion]. (c) The wireless implantable EMG sensing microsystem consists of two epimysial EMG electrodes, a custom-designed application-specific integrated circuit, and an RF telemetry coil [Farnsworth et al., 2008]. (d) High-density EMG E-Textile System contains 100 electrodes arranged in 4 grids of 5×5 electrodes [Farina et al., 2010].

strategy, as similar to CNS as possible to improve FES performance. Another factor relating to fast fatigue with FES is that the fatigue resistance of the paralyzed muscle decreases after injury [Pelletier and Hicks, 2011].

For an able-bodied person, fatigue can be perceived and compensated by various strategies so that motor function is prolonged. However, for a paraplegic individual with little or even no sensory feedback, fatigue is not detected until the desired movement fails. Therefore, how

to detect fatigue before the failure of movement and how force changes with fatigue are both meaningful issues. The ability to detect the muscle state and compensate the muscle changes are both significant for the future FES system.

1.3.3 EMG and Its Application for Muscle Fatigue Analysis

When muscles contract, they exhibit both electrical and mechanical behaviors. The mechanical behavior can be estimated by muscle force/length, or joint torque/angle. The electrical behavior can be assessed by recording the electrical signals within the muscle, which is referred to as Electromyography (EMG). The EMG signal has been popularly applied in areas like ergonomics and occupational biomechanics for kinesiological or diagnostic purposes. The main applications include determining the activation onset and levels of a muscle, estimating the force produced by muscle, monitoring the rate of muscle fatigue, and analysis of Motor Unit Action Potential (MUAP)s.

The EMG system can be classified according to the interface, such as surface, intramuscular (needle or fine-wire), and implanted [Farnsworth et al., 2008] [Madeleine et al., 2006], with the recording channel varying from single to high-density, as shown in Fig. 1.10. A typical EMG recording system contains recording electrodes, an amplifier, an A/D converter and wires. The recording electrodes pick up electrical signals underneath them and send them to the amplifier. As the electrical signal is very small, an amplifier gain is selected to amplify the signals. Usually, the amplifier also involves signal processes such as filtering.

In all EMG interfaces, the commonly used surface EMG provides a noninvasive measurement of muscle electrical activities and can be easily implemented in practice. However, when using surface EMG, we should pay more attention to the recording artifacts, which may come from different sources. Accordingly, various measures should be taken to eliminate or reduce them. For instance, environmental artifacts from the surrounding electrical equipments can be removed by a notch filter. Movement artifacts from dynamic movement can be avoided by firmly adhering the electrodes on the muscle and fastening the wire cables. As some muscles are narrow and close to other muscles, the EMG signal may be affected by crosstalk, which is recorded from other muscles we are not interested in. Through careful placement and sufficient interelectrode distance, it can be minimized to some extent [Solomonow et al., 1995]. In addition, some filters (software or hardware) can be used to remove the residual artifacts.

Compared with surface EMG, needle and implanted EMG provide more stable and reliable measurements, but their invasive nature limits their applications. Thus, if needle and implanted EMG are not available, surface EMG is still useful. In particular, the occurrence of multiple-channel and even high-density surface EMG has enhanced the application of surface EMG. High-density surface EMG produces a spatially filtered EMG channel that can have sufficient resolution to identify individual MUAPs. It is especially applied to observe the conduction velocity of MUAPs to better understand and analyze the mechanism of muscle fatigue [Farina and Merletti, 2000] [Merletti et al., 2008] [Holobar et al., 2009]. Recently, several active research works have attempted to identify the optimal spatial filters, electrode array configurations and signal decomposition methods through high-density surface EMG [He et al., 2009] [Zhou et al., 2011].

The EMG signal is a summation of the recruited MUAPs. Typical EMG signals from volun-

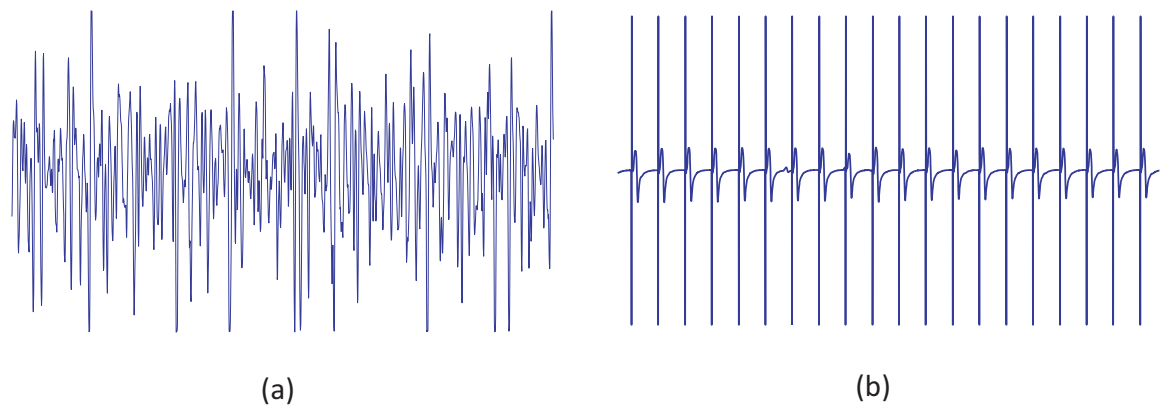


FIGURE 1.11 – (a) Voluntary EMG signals represent asynchronous muscle activity ; and (b) FES-evoked EMG signals consist of artifacts and Mwave. The Mwave is the summation of recruited MUAPs. It represents synchronous muscle activity compared with voluntary muscle contraction.

tary contraction and from FES-evoked muscle contraction are shown in Fig. 1.11. The active motor units during voluntary contraction have different firing frequencies and behave asynchronously, showing the so-called interference pattern. In contrast, the motor units with electrical stimulation have synchronous activity, showing the so-called Mwave in the EMG signal. When processing the FES-evoked EMG signals, one has to deal with stimulation artifacts, which appear at the onset of each stimulation impulse and are quite larger than Mwave. In order to retrieve the signal of interest, Mwave, suitable techniques should be employed to remove the stimulation artifacts first. As seen from Fig. 1.11, the EMG signal is a complex spiky signal that is difficult to interpret. Fortunately, a variety of signal processing techniques make it easier to understand. The various techniques generally represent either time-domain or frequency domain properties of EMG signals, as described in [Cifrek et al., 2009].

1.4 The State of the Art

Two major issues associated with the electrical stimulation of muscle are the force production capacity and the force maintenance capacity against various perturbations. Thus, when FES is applied for rehabilitation purposes, special attention should be paid to the design of appropriate stimulation protocols for the desired trajectory and the control of the stimulation allowing for reactions to the variations of muscle (such as muscle fatigue and reflex).

1.4.1 Reducing or Delaying Muscle Fatigue with FES

When electrical current is delivered to the paralyzed muscle, the produced muscle force can be modified by modulating the stimulation parameters. Thus, appropriate stimulation parameters are important considerations in the design of an FES protocol. The parameters that can be changed include pulse amplitude, pulse width and stimulation frequency. Roughly, the pulse amplitude determines the spatial extent of a stimulation field, while pulse width determines the percentage of recruitment within that field [Tyler and Dlihan, 1995]. Stimulation frequency affects the fusion of muscle force from different muscle fibers. Increasing any stimulation para-

meter will theoretically increase the muscle force, but may result in faster muscle fatigue. During voluntary contractions, the CNS optimally modulates both the number of motor units (recruitment) and the activation frequency (firing rate) to generate targeted muscle force and preserve energy supply [Chou et al., 2008]. Relatively, most FES systems only modify pulse amplitude or pulse width, with the frequency being fixed at a minimum level, inducing fused force.

Many researchers have been inspired by the natural CNS control scheme to explore more physiological muscle activation protocols in order to maximize muscle strength while at the same time prolonging muscle endurance in FES. The main ideas are grouped into three directions as follows.

- Electrode selectivity has attracted some attention as it allows small muscle fibers to be stimulated first to reduce muscle fatigue from fast muscle fiber recruitment. For instance, by means of a current block, unidirectional action potentials are generated in smaller nerve fibers with the larger fibers blocked [Bhadra and Kilgore, 2004] [Wang et al., 2008] [Tai et al., 2009], which is of great benefit for attenuating muscle fatigue in neuroprostheses. In [Popović and Popović, 2009], an optimal surface electrode configuration from multi-pad electrodes was developed for selective stimulation of finger extension and flexion. Their idea arose from the hypothesis that the superposition of several electrodes would achieve asynchronous stimulation, similar to natural activation. In another work [Wise et al., 2001], adjustable distributed stimulation of motor nerves was proposed for prolonged stimulation with less fatigue. The intervals between multi-channel stimuli are controlled by computer and allow the generation of equal tension at all channels, which can help to establish a smooth force over a wide range.
- Assuming that an optimal stimulation protocol can allow for more natural and physiological stimulation to reduce muscle fatigue with FES, different stimulation protocols were evaluated. Based on the experiments of stimulating the sciatic nerve of cats, combining the modulation of amplitude and pulse width was suggested to augment the functional performance [Tyler and Dlihan, 1995], and shorter pulse width was found to be able to generate a larger range of stimulation amplitude dynamics [Grill, 1996]. In [Szlavik and de Bruin, 1999], the authors also reported that longer pulse width resulted in more recruitment of larger nerve fibers, which implies that more muscle fatigue is generated with longer pulse width. In another work [Chou et al., 2008], a combination of stimulation amplitude modulation and stimulation frequency modulation was suggested to maintain quadriceps femoris muscle force, which is superior to solely modulating one of them. Comparably, if the frequency and amplitude are kept constant, the lowest frequency and longest pulse width can minimize muscle fatigue [Kesar and Binder-Macleod, 2006]. In their following work [Kesar et al., 2008], they further compared frequency modulation with pulse width modulation, and they suggested modulating frequency to improve muscle performance. Random modulation of FES parameters was also assumed to be able to reduce muscle fatigue but finally proved to be ineffective regarding the muscle fatigue rate of isometric contraction in SCI subjects [Graham et al., 2006]. A similar finding was reported in [Thomas and E.Butler, 2003], who observed that the variations in stimulation frequency, pulse pattern, and pulse number had little influence on thenar muscle fatigue in both SCI subjects and healthy subjects.
- Evolutional current wave form has been considered to be helpful in improving stimu-

lation performance. During surface FES, the synchronous recruitment in which all the muscle fibers are activated simultaneously causes more rapid fatigue in the paralyzed limb. A possible means to reduce fatigue is by using intermittent stimulation, in which fatigue and recovery occur in sequence [Levin and Mizrahi, 1999] [Duan et al., 1999]. High frequency electrical stimulation was suggested in an intermittent stimulation protocol to reduce fatigue [Matsunaga et al., 1999]. This work was tested on healthy and paraplegic subjects. In addition, the use of N-lets or catch-like stimulation was proposed to maximize muscle performance and delay fatigue [Karu et al., 1995] [Routh and Durfee, 2003] [Shimada et al., 2006]. However, an opposite result was reported in [Routh and Durfee, 2003], who showed that doublet stimulation generated fewer cycles in a cycling task compared with conventional singlet stimulation of quadriceps muscle in healthy subjects.

From these previous works, we find that the main idea to reduce muscle fatigue in FES is based on the hypothesis that the muscle will generate higher force and less fatigue if it can be activated in a more natural and physiological manner. Although various protocols have been proposed, no consensus has been reached to date. Possible reasons are that muscle fatigue is complex, multi-factorial and task-specific [Russ et al., 2002], which complicates the comparison among studies, and that insufficient experimentation has led to incomplete understanding of the muscle fatigue mechanism. As a result, it is difficult to find a generally effective solution to reduce fatigue in FES. However, I still believe that all of these ideas can contribute to improving muscle contraction endurance in some specific situations. Probably, a combination of several methods will contribute to the overall performance.

1.4.2 Identifying and Predicting Muscle Fatigue with FES

Muscle fatigue is not easy to effectively reduce despite the attempts to address this problem, as outlined above. Another meaningful study is how to detect fatigue and predict force production when muscle has been fatigued by stimulation. First, objective fatigue monitoring is especially important in paraplegic patients, who suffer from a lack of sensory feedback from their paralyzed muscles, because it can be used to readjust stimulation to prevent failure. Second, force prediction is essential if the muscle force has to be used as feedback in closed-loop stimulation. Thus, for these purposes, a fatigue model can be useful to predict the force production that accounts for muscle fatigue and also the recovery during intermittent stimulation.

Various fatigue models have been established, based on physiological and mathematical interpretation or fitting from experimental measurements. A biomechanical model was developed to predict the shank motion induced by FES [Riener et al., 1996]. Individual model parameters were identified by specific experiments. A four-parameter nonlinear equation was proposed to extract fatigue indices for predicting torque decrease in paraplegic subjects during an isometric sustained contraction [Rabischong and Chavet, 1997]. A five-element musculotendon model was developed to predict the force generation capacity of the activated muscle, and a fatigue recovery function, based on the metabolic profile, was introduced into this model [Mizrahi et al., 1997b]. In [Cai et al., 2010], a Wiener-Hammerstein model was proposed to predict FES-induced muscle force in unfatigued and fatigued muscle, and this work was verified by stimulating Soleus in SCI patients. A computer model of activation dynamics was developed

to interpret FES-induced muscle fatigue in [Lim et al., 2000]. It represented the reduction in muscle force and fatigue recovery from intermittent stimulation.

Some researchers have attempted to predict force/torque variations with fatigue based on eEMG. An exponential function was proposed to predict force of the FES-activated quadriceps muscles from eEMG Peak-to-Peak (PTP) [Mizrahi et al., 1994]. PTP was suggested as a fatigue index during constant cycling speed in [Chen and Yu, 1997]. The authors proposed a hyperbolic modeling of PTP to dynamic cycling numbers under intermittent FES. A high correlation between EMG Mean Absolute Value (MAV) and knee torque was found under continuous stimulation in paraplegic subjects [Erfanian et al., 1996]. In their following work [Erfanian et al., 1998], they proposed a predictive model of muscle force production under an isometric percutaneous continuous FES system. After comparing the performance of force prediction from stimulation and from EMG, they suggested using measured EMG signals instead of stimulation signals to predict muscle torque. A metabolic model was presented to predict the force decline and recovery from EMG signals under intermittent condition [Levin and Mizrahi, 1999]. Second Phase Area (SPA) and Root Mean Squares (RMS) were suggested to monitor activation over a long fatigue period during isometric continuous stimulation in [Heasman et al., 2000].

All of these works suggest that EMG could be used to monitor the muscle fatigue during electrical stimulation. However, as [Mizrahi and Isakov, 1994] pointed out, the EMG-to-force relationship could be affected by different recruitment levels and muscle recovery in time-domain analysis. Next, some alternative EMG methods have been investigated for muscle fatigue modeling, or to predict FES-elicited force throughout the entire range of measurement.

Decreases in time-domain parameters (integrated sEMG, MAV, PTP and RMS) and frequency-domain parameters (Power Spectral Density (PSD), Mean Frequency (MNF) and Median Frequency (MDF)) with decreased force due to muscle fatigue were observed in [Tepavac and Schwirtlich, 1997]. They suggested combining time-domain parameters and frequency-domain parameters to track muscle fatigue. A simple combination was implemented to validate this proposal and showed some improvement in force prediction, but the accuracy was still far from the requirements for practical use. In [Mizrahi et al., 1997a], the authors reported that both MDF and Total Spectral Power (TSP) decreased with fatigue and were fit by an exponential function over time. However, when muscle fatigue increased, an extremely low correlation was found between force and MDF in one of the subjects. In another work [Chesler and Durfee, 1997], the authors attempted to track fatigue from RMS and MNF. Unfortunately, the results demonstrated that it is difficult to reliably track fatigue for practical FES applications.

From these previous works, we can conclude that muscle fatigue estimation and force prediction are important if they are used in closed-loop control of FES. For these purposes, the primary ideas include developing a fatigue model and estimating fatigue from muscle activity. However, the fatigue properties vary at different fatigue levels and recovery processes, which complicates the identification of a fatigue model. Moreover, the fatigue model cannot work when the desired stimulation pattern is unknown in advance. The time-variant EMG-to-force relationship also challenges the identification method and the reliability of force prediction from EMG information.

1.4.3 Current FES Control Strategies

In the current FES rehabilitation system, open-loop control is predominantly used, while closed-loop control is primarily carried out in research. Open-loop control provides an empirically predefined stimulation pattern to the paralyzed muscle. Due to the lack of feedback on the real muscle output, the stimulation cannot be adjusted when it is not suitable for eliciting the intended motion. Thus, some of the present open-loop FES systems require manual adjustment of the stimulation by pushing buttons or choosing different programs. Others provide additional support such as a brace or crutch to avoid failure and enhance stability.

First, although open-loop control does not enable adaptive adjustment of stimulation in reaction to unwanted variations, it can still work when the accuracy of the force is not seriously required or the muscle variations are not prominent. In this case, identifying the appropriate stimulation pattern is crucial to improve FES performance in terms of generating more natural or more complex trajectories. To generate a more natural gait profile, an optimal stimulation envelope was investigated in [O’Keeffe et al., 2003]. They proposed a method to optimize the classic trapezoidal stimulation envelope by comparing the produced muscle activity with the natural EMG signals of TA muscle from able-bodied persons. The stimulation pattern was designed by using user-customized model-based control of walking in a simulation work [Dosen and Popovic, 2006]. In this work, the model was a multi-segment structure with each muscle modeled by a three-compartment multiplicative model, and optimization was achieved by minimizing the tracking error of the joint angles and muscle activations levels. A transfer function to convert the EMG signal recorded from able-bodied subjects into appropriate stimulation signals was proposed [Johnson and Fuglevand, 2011]. This transfer function can modulate muscle output through both frequency and pulse width modulation.

Second, closed-loop control of FES has attracted increasingly more attention, but to accomplish different tasks, different strategies have been designed and evaluated in simulations and in experiments on able-bodied persons or patients. Afferent neural activity from muscle spindle fibers was proposed as feedback for controlling ankle angle, which requires the preservation of sensory nerves [Yoshida and Horch, 1996], and this system was tested on animals. In [Graupe and Kordylewski, 1997], the authors proposed using upper-limb EMG signals to trigger the stimulation of the lower limbs by applying an artificial neural network. A closed-loop self-adaptive fuzzy logic controller based on reinforcement learning was developed to minimize upper-limb forces and the terminal velocity of the knee joint for FES standing up in a computer simulation [Davoodi and Andrews, 1998]. A nonlinear, physiologically based model was developed for describing the dynamic behavior of the knee joint and muscles [Ferrarin et al., 2001]. Four different control strategies (open-loop, feedback-PID, a combination of both, and an adaptive feed-forward control) were tested through simulation and experiments on two paraplegic subjects. The three nonadaptive control approaches showed satisfactory results, and the adaptive controller showed more robust and reasonable adaptation speed. The EMG signal recorded from the normal leg was proposed for triggering stimulation of the paralyzed leg in hemiplegia [Yu et al., 2002]. In order to overcome the errors from subject-specific variations, a feed-forward artificial neural network was introduced to this process. An artificial neural network (ANN) system was developed for compensating muscle fatigue during FES by maintaining a constant joint angle in able-bodied subjects [Winslow et al., 2003]. In this work, the

ANN system was created using the entire Mwave (including time- and frequency-domain information) as the input and a discrete fatigue compensation control signal, indicating when to increase the stimulation current, as the output. The performance of these ANN systems demonstrated the feasibility of using surface EMG feedback in a FES control system. A complex physio-mathematical muscle model was developed based on macroscopic Hill and microscopic Huxley concepts [Mohammed et al., 2007]. Its control was designed based on a higher order sliding mode to achieve the prediction of the needed stimulation pattern (amplitude and pulse width). This controller was mathematically computed and shown to provide satisfactory stability and tracking errors.

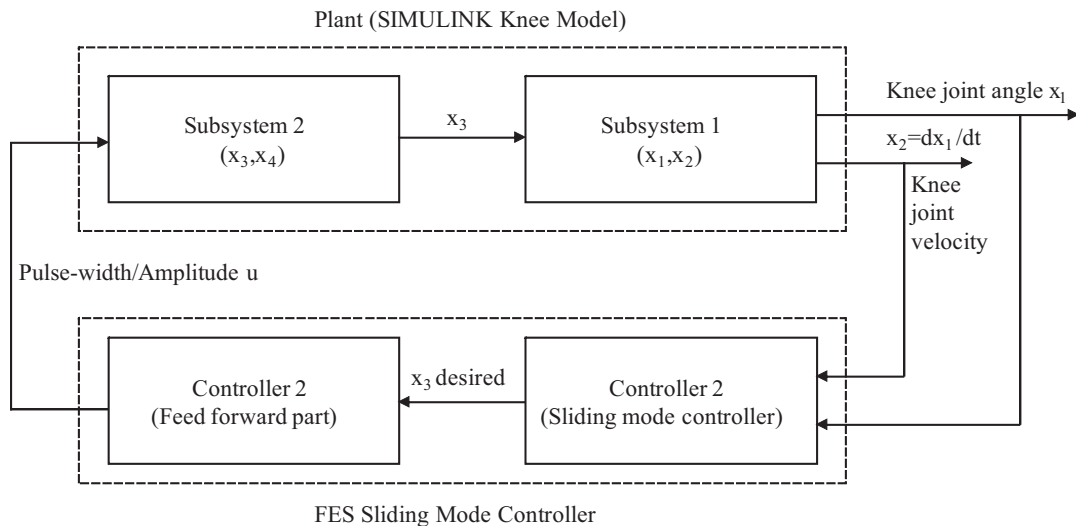


FIGURE 1.12 – Sliding mode FES controller proposed in [Jezernik et al., 2004] to control knee joint movement.

Most closed-loop control strategies aimed to control the onset of stimulation according to the user's intention, or in adaption to walking speed. The closed-loop controls with adaptivity to subject-specific variations, muscle property changes, and reflex or other external disturbances have not been widely researched. In the latter scope, two works are cited here because of their improvement in FES feedback/closed-loop control. As shown in Fig. 1.12, a sliding mode controller was developed to control knee joint angle [Jezernik et al., 2004]. In order to reduce chattering, they proposed to replace the continuous term by a discontinuous one in the control law. However, the finite-time convergence of the sliding variable could not be guaranteed. Moreover, this approach did not investigate the performance of the controller facing muscle-state changes.

In another work [Ajoudani and Erfanian, 2009], a control strategy based on the synergistic combination of neural networks with sliding-mode control (neuro-SMC) was developed for controlling FES as illustrated in Fig. 1.13. The result in paraplegic and able-bodied patients showed that the controller was able to provide more accurate tracking control with fast convergence compared with a neural network alone or sliding model control alone. However, chattering still occurred, especially when it was used to compensate muscle fatigue or external disturbances.

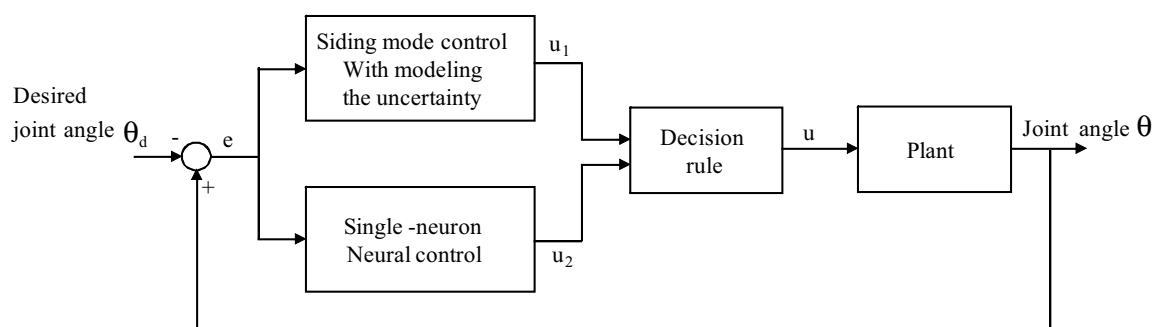


FIGURE 1.13 – Neuro-Sliding-Mode control strategy for FES control of knee joint movement [Ajoudani and Erfanian, 2009].

From these works, we find that knee angle control has been widely investigated. Most studies have focused on adaptive control without attending to the muscle states. Furthermore, how to achieve good tracking performance with less fluctuation, in order to guarantee patient safety is still a challenging problem for FES control. Last, after widely investigating the current FES control strategies, Zhang et al. predicted that the future FES control would have three properties : learning from natural motor control strategy, adaptivity to unexpected disturbances, and predictive behavior before stimulation [Zhang et al., 2007]. Coinciding with their suggestions, this thesis aims to evaluate an EFPC strategy in order to adaptively modulate the stimulation pattern compensating the effect of variations in FES.

1.5 Conclusion

In this chapter, some fundamentals about the neuromuscular system, motor control and motor impairment, which engineers from other fields may be unfamiliar with, have been introduced. FES and its limitation in terms of fast muscle fatigue and the corresponding control problems are discussed. We conclude that, first, FES is a promising technique to help hemiplegic, para/quadriplegic patients to improve their motor functions. Second, the muscle fatigue induced by electrical stimulation occurs much faster than voluntary contraction ; hopefully, this can be reduced or delayed by modulating stimulation parameters or selective stimulation. Third, if force accuracy is not seriously required, or the muscle fatigue is not significant, open-loop control of FES can still work, but a suitable and optimal stimulation pattern is required to perform the intended motion. Last, if the motion is complex or the muscle fatigue is prominent, adaptive and predictive closed-loop control is desired, allowing for compensation of the unexpected perturbations and assuring muscle safety.

CHAPTER 2

Modeling of FES-Induced Torque Based on Evoked EMG

Contents

2.1 Introduction	26
2.1.1 Problem Formulation	26
2.1.2 Previous Work	26
2.1.3 Discussion	28
2.2 Modeling of the Electrically Stimulated Muscle	28
2.2.1 Model Structure	29
2.2.2 Model Identification	31
2.3 Experimental Description and Signal Processing	33
2.3.1 Experiment Design	34
2.3.2 Data Collection	35
2.3.3 Experimental Protocol	35
2.3.4 Signal Processing	36
2.4 Results in Surface FES	37
2.4.1 Muscle Fatigue and Recovery Characteristics	37
2.4.2 Model Identification and Prediction	39
2.4.3 Comparative Analysis to Improve Torque Prediction	41
2.5 Model Validation in Implanted FES	44
2.5.1 Muscle Fatigue in Implanted FES	45
2.5.2 Muscle Model Validation in Implanted FES	46
2.6 Discussion and Perspectives	47
2.7 Conclusion	49

2.1 Introduction

For patients with SCI or cerebral injury, FES is a potential solution to enhance functional movements. When electrical currents are delivered to the relevant motor nerve, action potentials are generated in the alpha motor axon in the place of the CNS. Although these action potentials are not distinguished from the natural action potentials, the muscle fatigues faster when activated by FES than by the CNS. The direct result of fast muscle fatigue is rapid muscle force decline and ultimately the distortion or failure of the intended movement. Therefore, the prediction of force variations with muscle fatigue is important for adaptive FES control. The idea of predicting muscle force/torque to improve the FES control performance has motivated several works. The solutions vary from developing mathematical or experimental fatigue models to estimating fatigue from muscle activity. Although a general effective method of force/torque prediction is still an open problem, a suitable muscle force/torque model is basically required. This chapter aims to develop and validate a predictive joint torque model that will be used for the subsequent design of a predictive torque control framework in FES.

2.1.1 Problem Formulation

Muscle fatigue is a complex phenomenon, and it is often a combination of excitation, contractile and ischemic fatigue [Erfanian et al., 1994]. Its behavior tends to be distinct in response to various factors in FES. For instance, with the same stimulation level, different stimulation patterns (e.g., high frequency or low frequency stimulations), different muscle fiber types (e.g., fast or slow muscles), and different muscle contraction conditions (e.g., dynamic or static contractions), produce different muscle fatigue behaviors. Muscle fatigue is hence considered as a protocol-specific, muscle-specific, task-specific, and even subject-specific phenomenon. In addition, most SCI patients have lost their sensory functions as well as motor functions; that is, they cannot perceive muscle fatigue as FES proceeds. Generally, the patients or therapists manually adjust the stimulation pattern when they observe fatigue from the decay of motion performances in practice. Apart from muscle fatigue, reflexes also affect the induced torque level. These are unwanted in the FES system, even though the withdrawal reflex is used to actuate some motion restoration. In this context, accurate muscle force/torque information is important for FES control that adapts to the muscle variations and external disturbances (such as environmental contact).

However, existing force/torque sensors are not suitable for daily use to provide force/torque feedback in the FES control. Some works have attempted to tailor force/torque sensors for human use, such as an implanted force sensor [Hoffer, 1988], or a knee rehabilitation orthosis that also serves as a torque sensor [Nikitzuk et al., 2009], but they are not yet available for practical use. Although this hardware-related problem will not be dealt with in this work, it has motivated us to develop a method for estimating muscle mechanical output from natural sensors that allow for measurement or accurate estimation (such as EMG).

2.1.2 Previous Work

A muscle model is basically required in a model-based FES controller, and it may vary in structure from a physiological to a black-box model. Both these model structures have been

widely investigated in research, with discriminating advantages and drawbacks. Generally, a suitable model structure is chosen depending on what the user intends to do with the model. The physiological muscle model is developed on the basis of physiological knowledge or principles. The black-box model has a generic mathematic formation that has nothing to do with physiological meaning, but its ease of use or simplicity makes it popular in practical control systems.

Physiological Muscle Model

In a physiological muscle mechanical model, the muscle mechanical output is often modeled in response to electrical stimulation, which is strongly nonlinear and time-variant. The muscle output depends on spatial and temporal muscle fiber recruitment, muscle length, and the velocity of muscle contraction [Vallery, 2009]. If the model parameters have physiological meaning, the model provides insight into muscle behavior and the effects of model parameters on certain behavior, and it is helpful for clinical diagnosis. Specific procedures are required to identify the individual parameters. The two problems are that, first, a number of parameters complicate the identification process and, second, some parameters cannot be retrieved from experiments; that is, they are not identifiable [Ljung, 1991]. In addition, the parameters identified from specific conditions are likely to poorly predict the synthetic movement. Furthermore, the muscle property variations require re-identification of the model, which is difficult to carry out in practice.

In order to take muscle fatigue into account for muscle force/torque control, various fatigue models have been proposed as a supplement to the physiological muscle model. For instance, a muscle fatigue model [Riener et al., 1996] [Ding et al., 2000] and a fatigue recovery model [Mizrahi et al., 1997a] have been proposed to predict joint torque or muscle force variations with muscle fatigue. The fatigue models work when the stimulation scheme can be predetermined. However, the stimulation pattern is unknown in advance in most cases and, if unexpected events occur during stimulation, the fatigue model no longer works. For muscle force/torque control, another solution is to take advantage of the muscle activity represented by the EMG signal. In the course of stimulation, a change in muscle force is accompanied by a change in the EMG signal, such that it is logical to associate the electrical muscle activity with mechanical muscle activity. For example, the eEMG signal and muscle force were fit by an exponential function [Mizrahi et al., 1994]. In [Tepavac and Schwirtlich, 1997], a combination of integrated eEMG and median frequency demonstrated some improvement in force prediction during muscle fatigue, and the force decay was fit by an exponential function with this combined eEMG parameter. In these works, a fixed relationship between eEMG and muscle force/torque during continuous stimulation was assumed.

Black-Box Muscle Model

In comparison with the physiological muscle model, if one does not intend to interpret the physiological mechanism or go through the troubles of physiological modeling, black-box model is a promising alternative structure, allowing the prediction of muscle output for controller design. The Hammerstein cascade, comprising a nonlinearity followed by a linear subsystem, is one of the most popular black-box model structures [Bernotas et al., 1986]

[Chia et al., 1991] [Erfanian et al., 1998] [Le et al., 2010], owing to its identifiability and controllability. In [Bernotas et al., 1986] and [Chia et al., 1991], stimulation Pulse Width (PW) and muscle output torque were correlated by a Hammerstein model. In the experimental protocols on animals or paraplegic patients, special considerations were taken to minimize muscle fatigue, such as low amplitude, low frequency, and sufficient rest between adjacent stimulation trains. This means the authors did not intend to investigate the fatigue phenomenon. By comparing the torque prediction performance, using the eEMG signal from stimulated muscle instead of the stimulation signal was suggested to predict joint torque generation in [Erfanian et al., 1998]. This work was validated in a percutaneous continuous stimulation protocol on two paraplegic patients. They assumed that the relationship between eEMG and torque was constant. In order to compensate day-to-day variances in EMG pickup, an auto-calibration gain, which was defined by the ratio of steady-state gain on the reference day to steady-state gain on the tested day, was introduced. The steady-state gains were computed from the identified model of the muscle excitation process (stimulus-to-eEMG) to catch any change in the relationship between neural stimulation and eEMG. The torque prediction with fixed contraction model and auto-calibration was tested in a 200-s continuous stimulation. The result showed significant increases in prediction accuracy and repeatability to estimate torque without a torque sensor. However, they did not take into account the different muscle fatigue levels and muscle recovery processes that are quite noticeable in prolonged or intermittent FES systems.

2.1.3 Discussion

On the basis of pioneering work [Erfanian et al., 1998], this work takes advantage of the eEMG signal from the stimulated muscle for torque prediction and the subsequent torque control. A Hammerstein with eEMG as the model input is adopted to correlate with the joint torque under isometric condition. In this context, the first problem is how eEMG relates to the torque generation that alters with muscle fatigue during different stimulation conditions. If a fixed relationship exists, the eEMG information can be directly applied to indicate fatigue and identify fatigue levels. If this relationship varies with subjects or stimulation conditions, another problem is subsequently exposed, which is the need to determine whether this model can cover these variations. Based on these considerations, this work introduces a muscle model which would be useful for different purposes, such as the prediction of torque decline with muscle fatigue, and the design of model-based controllers for muscle fatigue compensation.

In this chapter, the muscle model structure and model identification are described. The variations in the eEMG signals with fatigue in the time-domain and frequency-domain are presented. The eEMG-to-torque model is verified using experimental data from an implanted continuous and a surface intermittent stimulation protocol. Last, the main benefits and challenges of using this model for EMG-feedback torque control in an FES system are discussed.

2.2 Modeling of the Electrically Stimulated Muscle

In the design of a model-based controller of FES, a suitable model which is able to catch the system behavior, especially predicting the future changes of a time-variant system is essential for improving control performance. In an FES system, the stimulation conditions are based on

the requirements for completing a certain task and involve various processes. With regard to the muscle contraction condition, isometric contraction, where the muscle tension increases with constant muscle length and static joint, explicitly occurs in specific tasks, such as standing, sitting and maintaining posture. Moreover, as controlled dynamic motion is usually slow and smooth in a patient, quasi-isometric behavior is dominant, allowing for ignoring the effects of inertia and velocity [Le et al., 2010]. In addition, since this preliminary work aims to investigate a pure excitation-contraction process in a stimulated muscle, the isometric condition is preferred to avoid complex dynamic properties such as the muscle force-length-velocity relationship. Thus, isometric muscle contraction is the concern of this work.

For an electrically stimulated muscle under isometric condition, excitation and contraction processes are involved, from delivering current impulses to obtaining joint movement. As described above, the Hammerstein model is a popular structure to model muscle with fixed length, so it was chosen to represent the muscle contraction dynamics here. In biomechanical systems modeling, it has been used to model the stretch reflex EMG signal [Dempsey and Westwick, 2004], and it has been shown to extend to dynamic conditions [Farahat and Herr, 2005], which is essential for developing stable adaptive controllers for future dynamic movement production.

2.2.1 Model Structure

A Hammerstein structure consists of a memoryless nonlinearity followed by a time-variant linear subsystem. It has been popularly applied to model the muscle contraction system in isometric condition because its nonlinearity represents the motor unit recruitment characteristics, and all the muscle dynamics are assumed to be linear [Riener, 1999]. These components are shown in Fig. 2.1. The nonlinearity has been parameterized by polynomial function [Erfanian et al., 1998] and cubic spline [Dempsey and Westwick, 2004]. The linear dynamics can be modeled as either a finite impulse response (FIR), Autoregressive with External Input (ARX) or output error (OE) model [Ljung, 1999] [Ikharia and Westwick, 2006].

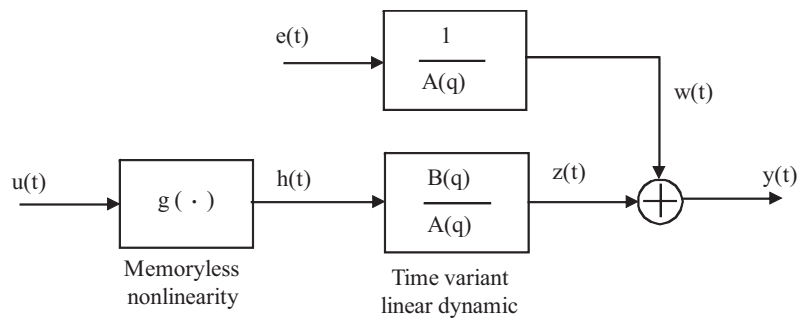


FIGURE 2.1 – Hammerstein model structure.

To model muscle electrical-mechanical behavior, the eEMG signal from stimulated muscle and the isometric torque are considered as system input $u(t)$ and output $y(t)$, respectively, as [Erfanian et al., 1998] proposed. The memoryless nonlinear function maps the system input $u(t)$, to the intermediate variable $h(t)$, which represents the activation level of the stimulated muscle. It is traditionally modeled by an n th-order polynomial of $u(t)$

[Dempsey and Westwick, 2004] as follows :

$$h(t) = g(u(t)) = \sum_{i=1}^n \gamma_i u^i(t) \quad (2.1)$$

where n is the polynomial order.

The linear time-variant system is described by an ARX, which has been shown experimentally to yield good prediction of output torque/force in isometric situation [Bernotas et al., 1986]. It can be described as :

$$A(q)y(t) = B(q)h(t) + e(t) \quad (2.2)$$

where $A(q)$ and $B(q)$ are polynomials in the backward shift operator, q^{-1} , given by,

$$\begin{aligned} A(q) &= 1 + a_1 q^{-1} + a_2 q^{-2} + \dots + a_l q^{-l} \\ B(q) &= b_1 q^{-1} + b_2 q^{-2} + \dots + b_m q^{-m} \end{aligned} \quad (2.3)$$

where q^{-1} makes $q^{-1}y(t) = y(t-1)$, with l and m being the maximum time delay for the numerator and denominator dynamics, respectively. Term $e(t)$ is zero mean and Gaussian white noise, which corrupts system (model) output and is statistically independent of $h(t)$. Note that the $h(t)$ is the output of the nonlinear element, and the input of the linear element as seen in Fig. 2.1. Dividing both sides of (2.2) by $A(q)$ produces

$$y(t) = \frac{B(q)}{A(q)}h(t) + \frac{1}{A(q)}e(t) \quad (2.4)$$

The linear model and noise model thus have the same poles, with transfer function $B(q)/A(q)$ and $1/A(q)$, respectively, as shown in Fig. 2.1. Next, substituting (2.1) and (2.3) into (2.2), the PHM is parameterized by

$$\begin{aligned} y(t) &= f(u(t-i), y(t-i), \theta) \\ &= \sum_{i=1}^l a_i y(t-i) + \sum_{i=1}^m \sum_{j=1}^n \mu_{ij} (u(t-i))^j \end{aligned} \quad (2.5)$$

coefficient $\mu_{ij} = b_i \gamma_j$. The stimulated muscle model has $l + m \times n$ unknown parameters in all, which are contained in parameter vector θ . If we care about how torque and eEMG change with fatigue, we can observe the changes of parameters in $\theta = [\theta_t \ \theta_e]$, where $\theta_t = [a_1 \ a_2 \ \dots \ a_l]$ are the coefficients of the past system output and $\theta_e = [\mu_{11} \ \mu_{12} \ \dots \ \mu_{21} \ \dots \ \mu_{mn}]$ are the coefficients of the past system input.

The structure in (2.5) implies that the current output $\hat{y}(t)$ is predicted as a weighted sum of past output values plus past input values. The value of past torque $y(t-i)$ has two versions — past measured torque $y_m(t-i)$ and past predicted torque $\hat{y}_p(t-i)$. When model identification is performed, the past measured torque is preferred, as the measurement represents the model output. For model validation, both can be employed, whereas from a practical point of view, the cross-validation based on predicted torque is more convincing to verify the model suitability for different data. Accordingly, two possible calculations of the past torque in (2.5) lead to two

corresponding predicted output forms — $\hat{y}_m(t)$ and $\hat{y}_p(t)$, which are computed as a function of past measured eEMG, past measured torque or past predicted torque in this way :

$$\hat{y}_m(t|t-1) = f(u(t-i), y_m(t-i), \theta) \quad (2.6)$$

$$\hat{y}_p(t|t-1) = f(u(t-i), \hat{y}_p(t-i), \theta) \quad (2.7)$$

The second approach shown in (2.7) only uses measured eEMG signals to predict future torque, which implies the use of eEMG as a synthetic torque sensor for torque estimation when torque measurement is not available [Erfanian et al., 1998]. In this case, the predicted torque can be initialized at zero, $\hat{y}_p(0) = 0$, when no stimulation is delivered to the muscle.

2.2.2 Model Identification

Model identification — a process to determine model order and identify model parameters — and model validation are two operations of a model. The model order determines the model complexity, and then the number of model parameters which need to be identified. For a black-box model, if the model order is large enough, it can represent most system behaviors, but the resultant huge parameters are difficult to identify. Thus, a tradeoff between model complexity and accuracy should be taken into account when identifying the model order. In contrast, model parameter identification is to determine a set of coefficients from input output data sets. The performance of model predictability depends on various factors, such as model accuracy, prediction horizon, uncertainty level and identification method. In this chapter, the accuracy of the eEMG-to-torque model is evaluated based on the Ordinary Least Squares (OLS) method, and the next chapter will go into an adaptive identification method.

Model Parameter Identification

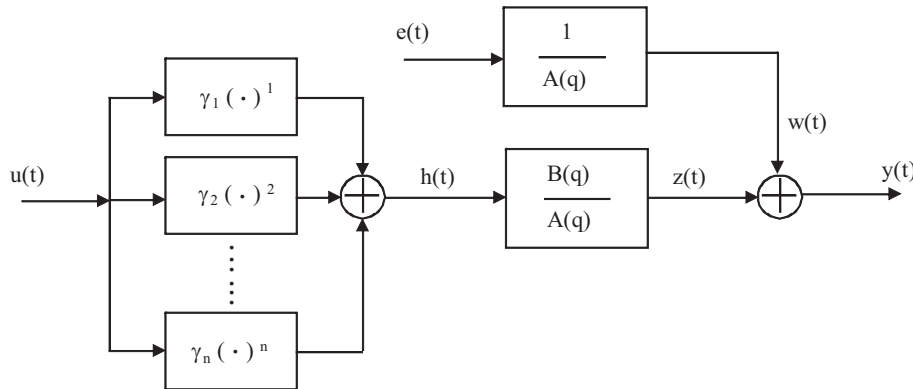


FIGURE 2.2 – Multi-Hammerstein model structure.

In the PHM, the nonlinear polynomial function enables us to transform a single-input single-output model into a multi-input single-output linear model. This is achieved by treating each polynomial term as a separate input to the filter. The configuration is shown in Fig. 2.2, where the $(\cdot)^i$ denotes $(u(t))^i$. Then the nonlinear identification problem is transformed to resolve a multi-input single-output linear identification problem. The model (2.5) can be rewritten as a

linear equation,

$$y(t) = \begin{bmatrix} a_1 \cdots a_l \mu_{11} \cdots \mu_{mn} \end{bmatrix} \underbrace{\begin{bmatrix} y(t-1) \\ \vdots \\ y(t-l) \\ u(t-1) \\ \vdots \\ u(t-m)^n \end{bmatrix}}_{\mathbf{X}(t)} = \boldsymbol{\theta} \mathbf{X}(t) \quad (2.8)$$

where $\mathbf{X}(t) \in \mathbb{R}^{(l+m*n) \times 1}$ contains modified multi-inputs.

To determine various unknown model parameters in $\boldsymbol{\theta}$, the known model input and measurable output data are filtered. Although it is not possible to find exact model parameters, a cost function permits optimal parameters to be found by resolving an optimization problem. For example, the Least Squares (LS) method, which aims to minimize the residuals between the experimental output and the predicted output, is widely used to achieve approximately optimal model parameters. Consider a system like (2.8), the residual is defined by $\epsilon(t) = y(t) - \hat{y}(t)$, where $y(t)$ is the output of measurement and $\hat{y}(t)$ is the predicted output from the model.

The collected data after sampling consist of N samples of modified input, $\mathbf{X}(k)$, and N samples of output measurement, $y(k)$, where $k = 1, 2, \dots, N$. The observation data sets $[(\mathbf{X}(1), y(1)), \dots, (\mathbf{X}(N), y(N))]$ are formed for model identification. The best parameter estimate $\hat{\boldsymbol{\theta}}(k)$ is computed by minimizing the prediction error $\epsilon(k)$ between $y(k)$ and $\hat{y}(k|k-1)$ at instant k ,

$$\begin{aligned} \hat{\boldsymbol{\theta}}(k) &= \arg \min_{\boldsymbol{\theta}} \sum_{k=1}^N \|\epsilon(k)\|^2 \\ &= \arg \min_{\boldsymbol{\theta}} \sum_{k=1}^N \|\hat{y}(k|k-1) - y(k)\|^2 \end{aligned}$$

where $\|\cdot\|$ denotes the Euclidean or ℓ_2 norm. The identification procedure is illustrated in Fig. 2.3.

For resolving the optimization problem, the OLS method is carried out. Once the model parameters are obtained, they are applied to predict system output through (2.5) or (2.8), and yield output estimates. In order to evaluate the performance of the prediction, Normalized Root Mean Squares (NRMS) error, which is a frequently-used measure of the differences between model prediction and real sensor measurement, is calculated simultaneously. It is defined as :

$$NRMS(\hat{y}(k)) = \frac{\sqrt{E[(\hat{y}(k|k-1) - y(k))^2]}}{y_{max} - y_{min}} = \frac{\sqrt{\frac{1}{N} \sum_{k=1}^N (\hat{y}(k|k-1) - y(k))^2}}{y_{max} - y_{min}}$$

Model Complexity Identification

The size of parameter vector $\boldsymbol{\theta}$ in (2.5), depending on model complexity, needs to be identified. Increasing model complexity will decrease systematic error but increase the system varia-

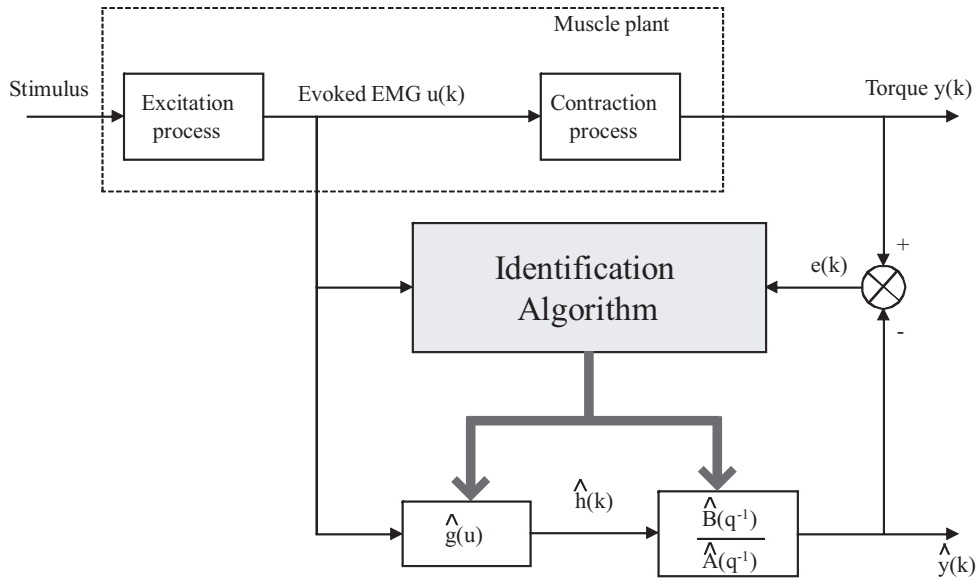


FIGURE 2.3 – Identification scheme of muscle contraction model.

bility [Ljung, 1999]. Therefore, the selection of model order (l,m,n) is a key step in the identification of the unknown parameters in θ . The nonlinearity — that is, the recruitment curve of the muscle — is modeled as a 3rd-order polynomial of instantaneous eEMG; that is, (n=3), as suggested in [Chia et al., 1991]. Linear model order is determined by comparing the Rissanen's Minimum Description Length (MDL) [Rissanen, 1978] obtained for different model order options, since the MDL principle provides a criterion for tradeoff between the simplicity of the model and the model's applicability to the data. The MDL is defined by the following equation under the hypothesis of Gaussian disturbances.

$$MDL = V * (1 + d * \frac{\ln(N)}{N}) \quad (2.9)$$

where $d = \dim(\theta)$ is the number of identified parameters, N is the length of data samples for this identification, and V is the loss function given by

$$V = \frac{1}{2} \epsilon^T(\hat{\theta}(k), k) \epsilon(\hat{\theta}(k), k)$$

where ϵ is a N-by-1 vector of the residuals between measurements and model estimates and $\hat{\theta}(k)$ is the identified model parameter at instant k. Using MDL to perform a relative comparison of the different model complexities, the smaller value of MDL indicates a better model.

Next, the eEMG-to-torque model is identified and cross-validated by experimental data. Two experiments were performed on SCI patients with a fatigue-inducing test. The experiments and relevant data processing are described in the next section. The fatigue properties and model identification for torque prediction are presented further on.

2.3 Experimental Description and Signal Processing

As we know, intermittent stimulation is useful to reduce muscle fatigue in FES, but the muscle recovery complicates the fatigue behavior. Previous works [Erfanian et al., 1998] have

focused on percutaneous intramuscular FES and a continuous stimulation protocol, and the method they proposed did not involve torque prediction during different fatigue states. In this work, two types of FES are carried out to investigate the fatigue properties and torque prediction method via the eEMG signal. The experiment of surface FES is described here and another experiment of a special case—implanted FES—can be found in Appendix A. To help understand the description of the FES experiments, some fundamental concepts are also given in Appendix A.



FIGURE 2.4 – Experimental set-up for electrical stimulation and EMG, torque acquisition.

The experiments of surface FES were conducted on five SCI subjects in the Propara Rehabilitation Center, Montpellier, France. All subjects were classified as ASIA A at different injury levels (see TABLE 2.1). The experimental set-up is depicted in Fig. 2.4. This study was approved by the ethical committee for person's protection of N mes, and all subjects signed informed consent forms.

TABLE 2.1 – Patient configurations

subject	Age (years)	Weight (kg)	Height (cm)	Level of injury	Months post injury
S1(M)	39	50	169	T6	3
S2	22	54	172	C7	30
S3	26	64	192	T6	36
S4	32	61.5	177	C5	8
S5	48	76	177	T6	18

2.3.1 Experiment Design

The subjects were seated on the chair with the ankle at 90° , while the joint center was aligned with the axis of a calibrated dynamometer (Biodex 3, Shirley Corp., NY, USA). The shank

was adjusted to be horizontal to the ground with the knee joint at approximately 40° . The foot was strapped to the pedal to transmit ankle torque to the dynamometer, and to allow the optimal recording of isometric ankle torque. Electrical current pulses were delivered to the right Triceps Surae muscle group via surface electrodes ($10\text{ cm} \times 3\text{ cm}$) to induce muscle contractions and to plantarflex the ankle joint as a result. One electrode was placed 5 cm beneath the popliteal cavity and the other beneath the insertion point of the Medial and Lateral Gastrocnemius on the Achilles tendon. The muscle group was stimulated with amplitude modulation at a constant frequency (30 Hz) and constant PW ($450\ \mu\text{s}$), under isometric condition, by a portable stimulator (Cefar physio 4, Cefar Medical, Lund, Sweden).

TABLE 2.2 – Stimulation parameters (FS = 30Hz, PW = $450\ \mu\text{s}$)

Subject	S1	S2	S3	S4	S5
I_{max}	65mA	85mA	80mA	60mA	100mA

2.3.2 Data Collection

Evoked EMG activity of the soleus in the Triceps Surae muscle group was collected, amplified (gain 1000) by a bipolar differential amplifier (Biopac MP 100, common mode rejection ratio (CMRR) $> 110\text{ dB}$ (50/60 Hz), Biopac Systems Inc., Santa Barbara, CA, USA), and sampled at 4 kHz, with a band-pass filter between 10-500 Hz and Signal to Noise Ratio (SNR) around 37 dB. EMG signals were then directed through a 12-bit analog-to-digital converter (Biopac MP 100) and stored on a laptop. In order to reduce the impedance between the skin and EMG electrodes, the skin under the electrodes was shaved, rubbed with sandpaper, cleaned with alcohol, and all the electrodes were firmly adhered and fastened. The bipolar Ag/AgCl EMG electrodes were positioned over the muscle belly in the direction of the muscle fiber with 20 mm interelectrode spacing. The reference electrode was placed on the patella of the other leg. Isometric ankle plantarflexion torque was measured using the dynamometer (Biodex 3), sampled at 2 kHz, and interfaced with the acquisition system (Biopac MP 100).

2.3.3 Experimental Protocol

The maximum stimulation amplitude (I_{max}) was found for each subject at the beginning (TABLE 2.2), by gradually increasing stimulation amplitude until torque arrived at saturation. For each subject, the experiment consisted of three test sessions, as shown in Fig. 2.5.

1. The fatigue-inducing session consists of several sequences (called fatigue1-fatigue5). Each sequence contains five trapezoidal trains with each trapezoidal train consisting of 4 s of stimulation (1-s ramp-up, 2-s plateau and 1-s ramp-down) and 2 s of rest. The stimulation amplitude during the plateau is chosen at 50% of the I_{max} with 30 Hz, $450\ \mu\text{s}$. In order to induce muscle fatigue, three such stimulation sequences are applied to subjects S1 and S2, four sequences to S3, and five sequences to S4 and S5.

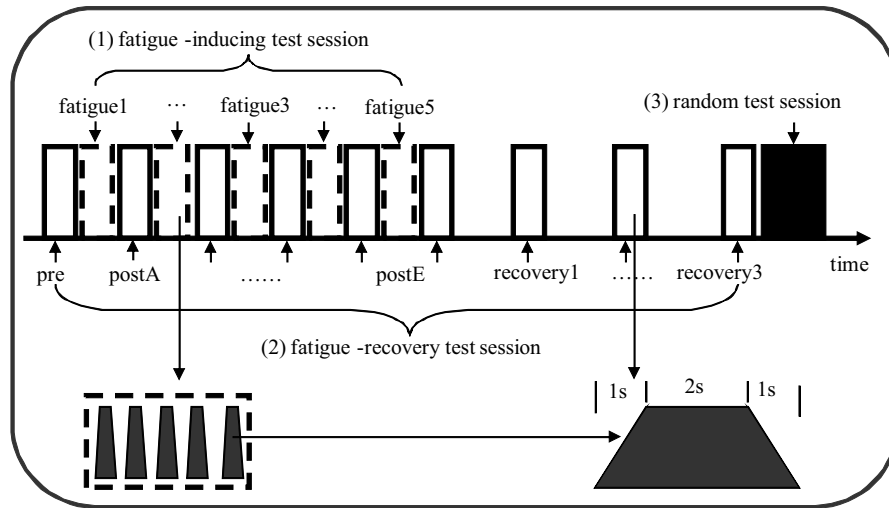


FIGURE 2.5 – Schematic representation of the experimental sessions.

2. The fatigue-recovery session consists of one trapezoidal train at I_{max} , which is delivered to the muscle just before and after each fatigue-inducing sequence. After the stimulation train postE, the same stimulation train is applied every 5 minutes, up to 15 minutes.
3. The random session delivered one stimulation sequence including several trapezoidal trains to the muscle. In this case, the stimulation amplitude in each train is increased from zero to a randomly determined value ($\leq I_{max}$) and is then symmetrically decreased over two minutes in total.

2.3.4 Signal Processing

Unlike in voluntary muscle contraction, artificially recruited motor units depolarize synchronously. Consequently, the eEMG is a synchronous summation of the recruited MUAPs, the so-called Mwave. Moreover, the surface eEMG signals are contaminated by stimulation artifacts which have quite larger magnitude than eEMG signals. Several works have proposed to remove the stimulation artifacts by software method [Sennels et al., 1997] [O’Keeffe et al., 2001], hardware method [Erfanian et al., 1998] or both [Chesler and Durfee, 1997]. The blanking window or blanking circuit is useful as long as the Mwave is not overlapped with stimulation artifacts, based on the assumption that the early T_{arf} from the onset of stimulation is the duration that contains the stimulation artifacts. This duration of the stimulation artifacts is usually variant with changes in the electrode location and stimulation PW in the same subjects, and differs among subjects. Fortunately, once the experimental setup is fixed for one subject, the duration of the stimulation artifacts is almost constant. Thus, we can estimate the duration of artifacts T_{arf} by pre-experiment.

The hardware blanking method removes the artifacts by switching the stimulation circuit off at the start of sending each stimulation pulse over a period of T_{arf} . Similarly, the software blanking window suppresses the stimulation artifacts by making the recording signal zero during T_{arf} . As the hardware method is not available to implement in the existing experimental system, the software method is adopted to remove stimulation artifacts from eEMG recording.

The removal of artifacts by zeroing the samples during T_{arf} probably generates some high frequency signals artificially, so the Fast Fourier Transform (FFT) is used to show the underlying frequency components of the eEMG signals. A cutoff frequency is selected accordingly to filter the high frequency components of the eEMG signals. Likewise, a cutoff frequency is determined for lowpass filtering of the torque signals.

$$MAV = \frac{1}{T} \int_0^T |x(t)| dt \quad (2.10)$$

Various EMG variables can be used to represent EMG characteristics. MAV, a "moving average" of full-wave rectified EMG, is chosen in this work. MAV is computed by (2.10), where $x(t)$ is the eEMG signal at time t , and T is the length of data being used for calculation. It is easy for determining the muscle contraction level and convenient for real-time calculation. As the EMG and torque levels are usually quite different among subjects, they are usually normalized by their maximum or initial value for comparison among subjects. Briefly, the collected eEMG and torque data were processed off-line in five steps as follows.

1. The stimulation artifact is removed from the raw eEMG signals by the blanking window method [Frigo et al., 2000], and the Mwave is consequently extracted.
2. The measured torque is offset with respect to the torque baseline to obtain the torque level. The torque baseline is the torque measurement when the muscle is at rest.
3. A lowpass filter is applied to the measured ankle torque (6th-order, cutoff frequency 100 Hz) and the measured eEMG (6th-order, cutoff frequency 300 Hz).
4. The filtered eEMG signals are divided into epochs with each epoch containing one Mwave, and the MAV of eEMG is calculated within five epochs. The average torque is calculated within the same time window.
5. The MAV and average torque are normalized with respect to their maximum values.

An example of the processed results is illustrated in Fig. 2.6, where $T_{arf} = 3$ ms. Note that the normalized MAV of eEMG and normalized torque are prepared as system input and output. An example of the relationship between eEMG and torque in a random session is shown in Fig. 2.7.

2.4 Results in Surface FES

The muscle fatigue characteristics in this intermittent stimulation protocol is investigated first. After identifying model parameters, the capacity of model prediction is verified. Finally, a comparative study is conducted in order to find a solution to improve model prediction quality.

2.4.1 Muscle Fatigue and Recovery Characteristics

In intermittent FES, the rest period is important to reduce muscle fatigue, and more practical in tasks when continuous stimulation is not necessary for a single muscle, such as in walking. The muscle fatigue is represented as torque decline with the same stimulation. For example, the torque decrease over time in subject S3 is demonstrated in Fig. 2.8. Joint torque declines 19% of initial torque with 151 s of stimulation within 191 s of intermittent stimulation.

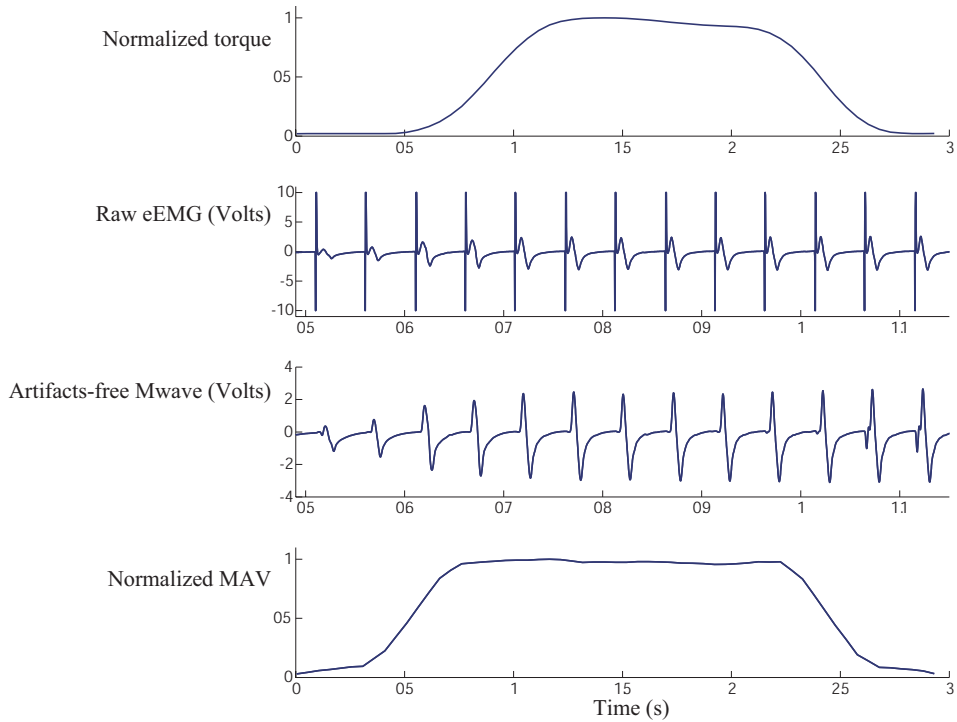


FIGURE 2.6 – An example of processed eEMG and torque. The raw eEMG signal and Mwave are zoomed in (0.5 s ~ 1.15 s) to show the details during stimulation increase. The raw eEMG was contaminated by stimulation artifacts. The blanking window is applied to remove artifacts so that the Mwave is effectively extracted. Note that the magnitudes of raw EMG and Mwave are quite different.

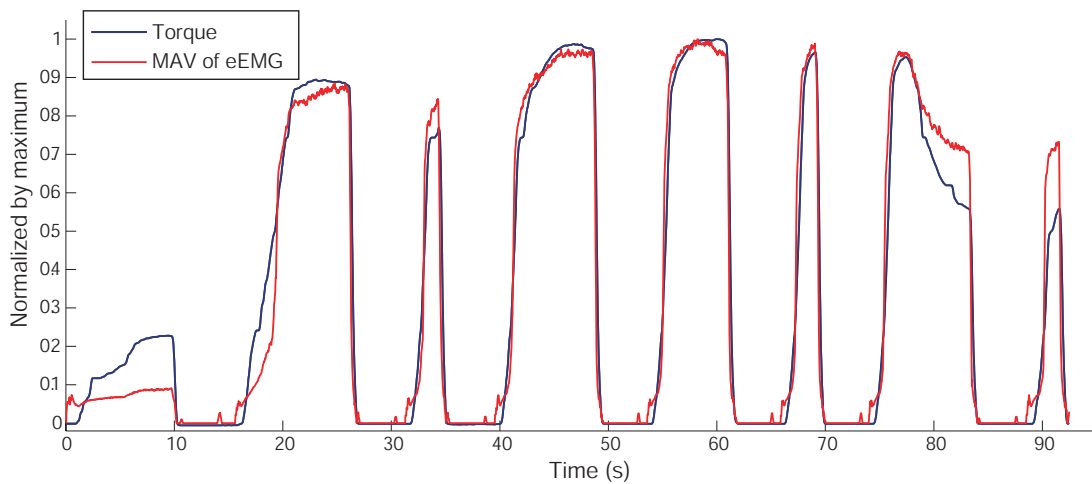


FIGURE 2.7 – An example of the relationship of eEMG and torque in intermittent stimulation. The maximum stimulation intensity during the plateau and the stimulation duration of each train is randomly determined. The MAV of eEMG is highly correlated with torque in the primary course.

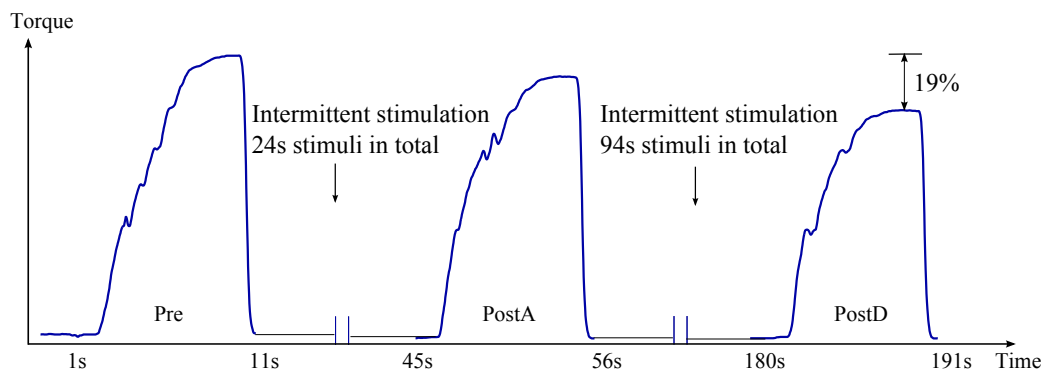


FIGURE 2.8 – Demonstration of FES-induced muscle fatigue in subject S3. Joint torque declines 19% of initial torque with 151 s of stimulation within 191 s of intermittent stimulation.

In order to observe the variations in torque and eEMG during this stimulation condition, the experimental data of the stimulation-recovery session are processed for this purpose. To keep a consistent comparison situation, the data during the plateau in each stimulation train are picked out for the analysis due to the same stimulation intensity during this period. The data are first treated as the processing step (1) (2) described in Section 2.3.4. Then the average torque, MAV and standard deviations are computed simultaneously and are depicted in Fig. 2.9. The torque of ankle plantarflexion gradually declines after each fatigue-inducing sequence, until around 90% (81% for S3) of initial torque in all subjects. After 5 minutes of rest, the average torque recovers less than 5% and then remains at the same level in all subjects, except in subject S1, in whom the torque recovers after 10 minutes of rest. As a whole, torque transition in fatigue generally shows a similar tendency in all subjects. As to the MAVs of eEMG, they represent different transitions among these subjects as depicted in Fig. 2.9 (b). Although the same tendency can be found in subjects S3 and S5, different tendencies are found among the five subjects. The results in S3 and S5 show a simple decline of MAV due to fatigue, S4 shows potentiation phenomenon within the first 2 s due to high frequency stimulation resulting in extreme muscle contraction, while S1 and S2 present somewhat combined characteristics of potentiation and fatigue.

Here, although we do not intend to interpret the fatigue characteristics, we confirm that the different fatigue behaviors of the subjects match the assumption that fatigue dynamics are subject-specific. Even for the same subject, the eEMG-to-torque relationship gradually varies over time, rather than remaining constant, as most prior works assumed in such intermittent fatigue protocol.

2.4.2 Model Identification and Prediction

Before model identification, the model order is determined as described in Section 2.2.2. The nonlinear model order is fixed at 3, and the model order of the linear ARX model is identified using processed eEMG and torque data by comparing MDL values at different model-order options. Model order ranging from $2 \leq l \leq 6$, and from $2 \leq m \leq 6$ are considered. The MDL values for all five subjects in the fatigue-inducing test are shown in Fig. 2.10. Ultimately, model order ($l = 3, m = 4$) was chosen with relatively less MDL value and a simpler model, and this choice is used for all subsequent analysis relating to this experiment.

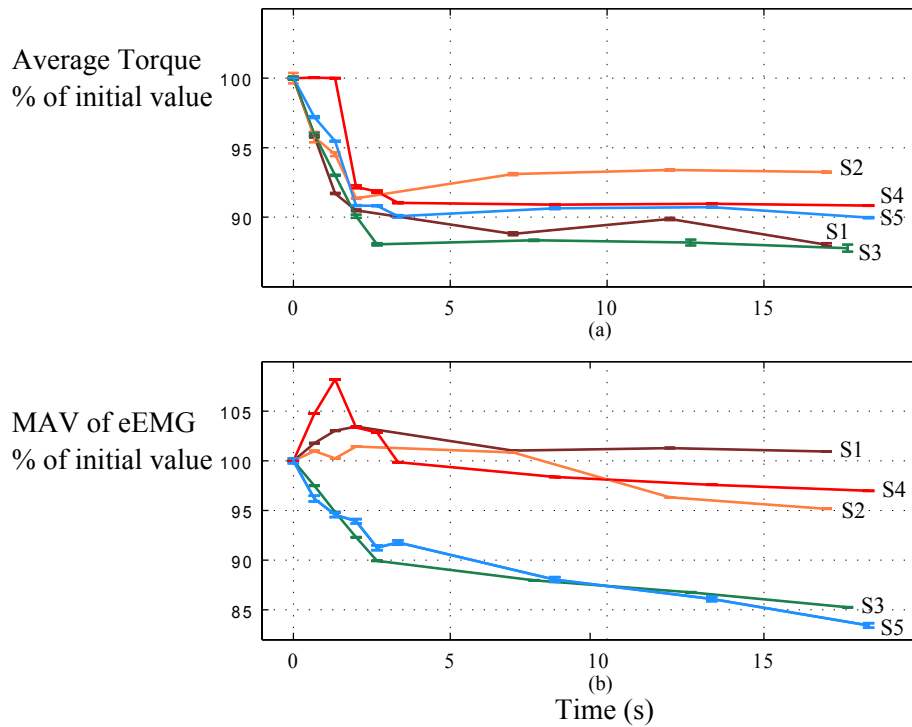


FIGURE 2.9 – The changes in torque and eEMG in surface intermittent FES. (a) Average torque and (b) MAV of eEMG in all subjects during the fatigue-recovery process. The results were represented as mean±standard deviation.

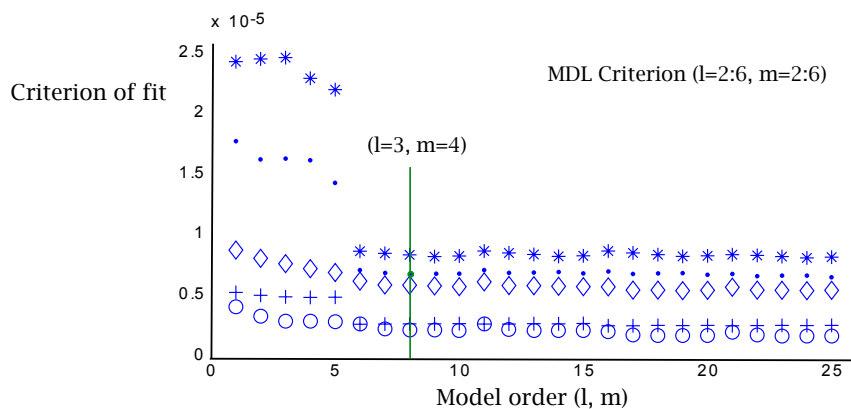


FIGURE 2.10 – Criterion of fit for determining appropriate model complexity. '*'--- S1, '*-'--- S2, 'o'--- S3, '◇'--- S4, '+'--- S5. The vertical line indicates the selected model order (3, 4).

To validate whether the model represents muscle electrical-mechanical behavior, the model parameters are identified by the OLS method first. Then the model prediction is driven by eEMG and the identified model. The experimental data in the random test are used for identification and prediction. Fig. 2.7 illustrates the relationship between eEMG and torque in this random test. The model parameters in θ are identified using the data before 68 s as (2.6), and the predicted torque is calculated for all the 98-s data. The difference is that the first 68-s torque prediction is calculated according to (2.6), whereas the next 30-s torque prediction is driven by the eEMG information and previously identified model parameters, without using torque measurement according to (2.7).

Fig. 2.11 illustrates the prediction result in subject S5. The corresponding prediction errors, NRMS errors, are shown in this figure. The randomly modulated stimulation PW results in random muscle response, which is more realistic when performing some complex movements. Furthermore, the random FES protocol has never been investigated for fatigue analysis in previous works. Therefore, it is vital to predict torque levels from the eEMG signal for fatigue tracking. In Fig. 2.11, the torque reproduction before 68 s has high quality with available eEMG and torque measurements, and the prediction is still good (7.13% NRMS error) in the last 30 s prediction without using torque measurement. At the end, the prediction has some higher error probably due to an increased fatigue level over prolonged stimulation.

The result in this random stimulation test represents the feasibility of model identification and its prediction performance. The good prediction in Fig. 2.11 benefits from enough data for identification and the assumption of similar muscle states for short-term stimulation durations (for example, 30 s in this test). However, as shown in Fig. 2.9, when muscle is stimulated intermittently, muscle fatigues and recovers alternately, resulting in complicated fatigue characteristics. Whether the model and identification methods can remedy this problem for prolonged intermittent application will be investigated in the next section.

2.4.3 Comparative Analysis to Improve Torque Prediction

In this section, the experimental data from the fatigue-inducing test session are used to compare the prediction quality of two different methods : the fixed-parameter model and adapted-parameter model. The fixed-parameter model is processed the same as above : the model parameters are identified with the data of the first sequence (fatigue1) and then cross-validated for all the remaining sequences (fatigue2-fatigue5). The prediction errors for all five subjects are shown in TABLE 2.3. Assuming a fixed eEMG-to-torque relationship, the prediction errors become higher as the muscle states vary through the entire stimulation in all subjects.

We then assume that if the model is identified again with the data in the latest sequence, the prediction will be improved. Therefore, the second method, the adapted-parameter model, is proposed. This time, the latest data are used to re-identify the model ; that is, the torque prediction of fatigue3 is based on the model parameters obtained from fatigue2, and so on. The prediction errors with the adapted-parameter model in all subjects are compared in TABLE 2.3. For example, for fatigue3 of subject S3, the NRMS error with the adapted model is 0.0345 (3.45% error), as compared with 0.0639 (6.39% error) with the fixed model. The average prediction of the adapted model was superior by 16.7-50.8% compared with the fixed model in all subjects.

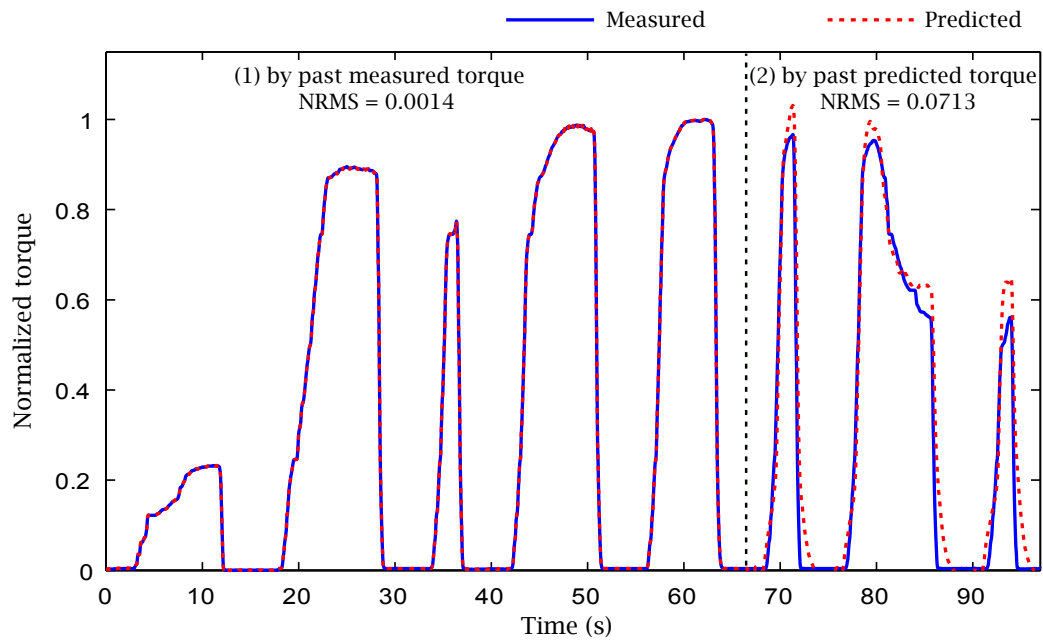


FIGURE 2.11 – The measured and predicted torque obtained by the eEMG-to-torque model in the random test of subject S5. The vertical dotted line is shown to separate the data into two parts. The model is identified by the OLS method using the data in the left part. (1) The torque is predicted based on the past measured MAV of eEMG and past measured torque. (2) The torque is predicted based on the past measured MAV of eEMG and past predicted torque, with initial predicted torque at zero.

Fig. 2.12 illustrates the predictions with the two methods (fixed model and adapted model) under different fatigue conditions in subject S3. Fatigue3 is not plotted in this figure, as there is only a small difference between fatigue3 and fatigue4. Apparently, FES-induced torque declines with the same stimulation as a result of muscle fatigue. The fixed model can still be used for torque prediction, as shown by the dotted red lines. In comparison with fatigue1 and fatigue2, the prediction of fatigue4 becomes less accurate based on the fixed model. For enhancing the prediction quality, the adapted model shows superior performance, as the dashdotted black line shows. Regarding the torque predictions in the intermittent experiment, when the torque mea-

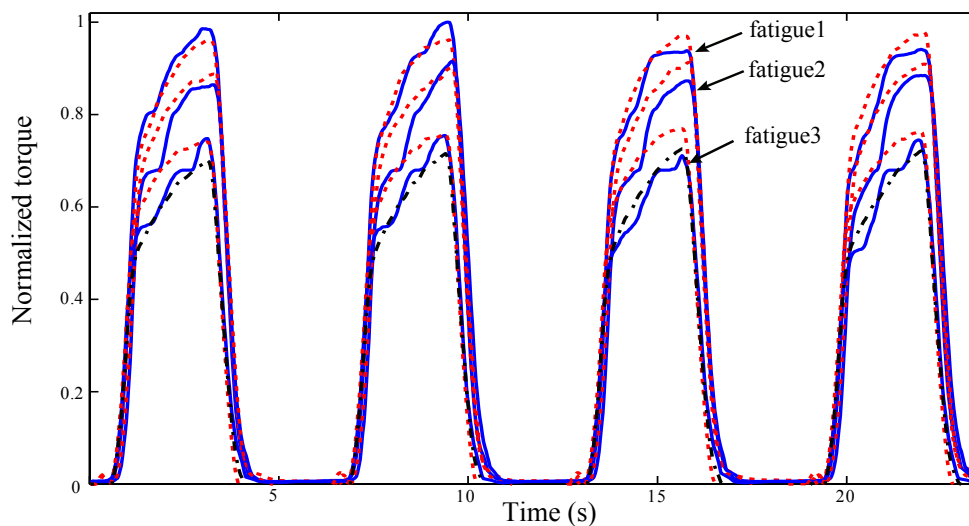


FIGURE 2.12 – The measured and predicted torque obtained by the eEMG-to-torque model in the fatigue-inducing protocol of subject S3. The solid blue lines indicate the measured torques. The dotted red lines represent the corresponding predicted torques based on the fixed model, which was identified using the data of fatigue1. The dashdotted black line represents the torque prediction of fatigue4 based on the adapted model, which was identified using the data of fatigue3. All the torques are normalized by the maximum measured torque in fatigue1.

surement is available, the model has high predictability probably due to similar muscle states and the autoregressive feature of the model. When torque measurements are suspended, the model is able to catch most mechanical behavior during finite stimulation duration. With prolonged or repetitive stimulations, the muscle fatigue levels change over the course of time, resulting in degraded prediction accuracy with fixed model parameters. The adapted-parameter model is assumed to improve prediction quality in this scenario. This improvement implies that, even though the relationship between eEMG and torque represents a time-varying property, it varies slowly in such a stimulation condition. Therefore, in order to achieve accurate torque prediction regardless of the fatigue levels, an online model identification and prediction is proposed in the next chapter.

TABLE 2.3 – Summary of the prediction error obtained with fixed or adapted eEMG-to-torque model

Subject	Model	NRMS Error				
		Fatigue1	Fatigue2	Fatigue3	Fatigue4	Fatigue5
S1	Fixed	0.0381	0.1009	0.2037	/	/
	Adapted	/	/	0.1272	/	/
S2	Fixed	0.0642	0.0767	0.1559	/	/
	Adapted	/	/	0.1298	/	/
S3	Fixed	0.0253	0.0467	0.0639	0.0572	/
	Adapted	/	/	0.0345	0.0254	/
S4	Fixed	0.0511	0.0520	0.0575	0.0702	0.0631
	Adapted	/	/	0.0480	0.0447	0.0438
S5	Fixed	0.0594	0.0641	0.0591	0.0597	0.0715
	Adapted	/	/	0.0457	0.0447	0.0476

2.5 Model Validation in Implanted FES

Apart from the validation of surface FES on SCI patients, we were fortunate to be able to perform an experiment on an implanted patient in order to investigate the mechanism of muscle fatigue in this special condition, as well as the feasibility of eEMG-based torque prediction. This work was conducted as part of a European project, Stand Up And Walk (SUAW), which our team participates in. The implantation was successfully carried out in 1999 and 2000 on a completely paraplegic subject (ASIA A, T8 level) [Guiraud et al., 2001]. For this patient, the stimulation electrodes were placed on the epimysium of the Gluteus Maximus and Medius, the Hamstrings and the Iliacus muscle groups, and around the appropriate nerve for the Quadriceps (femoral nerve) and the TA muscle (peroneal branch of the sciatic nerve). After implantation, the patient achieved standing and assisted walking until muscle fatigue occurred. The feasibility of gait restoration without using the withdrawal reflex was also demonstrated. In [Guiraud et al., 2006], the results of a 5-year patient follow-up after implantation were reported. In the 12-channel FES implantable system, the peroneal branch of the sciatic and femoral nerves was directly stimulated along the nerve axis by bipolar half-cuff electrodes. It was thus possible to perform an accurate, physiological ankle dorsiflexion owing to TA activation during the swing phase without using the unstable triple reflex employed by most other works [Kobetic et al., 1997]. The quadriceps, a key muscle group for the lower limbs, was also clearly and efficiently activated. The sequential stimulation command was transmitted to the implanted module through an Radio Frequency (RF) transmitter and computed on a portable microcontroller-based system. Neural stimulation has proved to be more efficient and stable over time than epimysial stimulation. In addition, this mode requires less energy supply and provides more selective stimulation. When

an EMG sensor is used in the case of neural stimulation, the eEMG signals are much less contaminated by stimulation artifacts.

2.5.1 Muscle Fatigue in Implanted FES

Although implanted stimulation is considered promising and superior to surface stimulation in terms of reliability, accuracy and selectivity, few works have reported lower limb movement restoration using implanted neural stimulation. Moreover, the muscle electrical behavior and its correlation with mechanical behavior during muscle fatigue have never been reported due to the limited number of available subjects. The experiment of this implanted FES is described in Appendix A.

With implanted neural stimulation, there is no typical stimulation artifact because the locations of the target muscle and neural stimulation site are far enough apart. Besides, the stimulus is at low intensity ($I_{max} = 3.15$ mA) and localized due to the use of bipolar electrodes. Instead, the RF signal could contaminate the EMG signal. Particularly during the stimulation, RF has high power to provide energy transfer for the battery of the implanted system, as well as to trigger each stimulus pulse while the implanted wires are both electrically connected to the cuff electrodes and the implanted electronics.

As only TA muscle is stimulated, by activating merely the corresponding peroneal branch of sciatic nerve to provide ankle dorsiflexion, the eEMG signals recorded from quadriceps provide only stimulation artifacts. They are thus used to detect the stimulation onset and remove artifacts from the TA eEMG signals. The recorded eEMG from TA and ankle torque are processed in Section 2.3.4 to retrieve artifact-free Mwave. The time-domain EMG parameter, MAV, is then calculated by (2.10), and the frequency-domain EMG parameter, MDF, is calculated by (2.11). MDF is the frequency at which the power spectrum is divided into two parts of equal power

$$\int_0^{MDF} P(\omega)d\omega = \int_{MDF}^{\infty} P(\omega)d\omega = \frac{1}{2} \int_0^{\infty} P(\omega)d\omega \quad (2.11)$$

where $P(\omega)$ is the power spectrum density of the EMG signal and ω is the frequency variable.

The relationship between measured torque and MAV, and MDF variations over time, are plotted in Fig. 2.13 and Fig. 2.14. In these two fatigue tests, the same stimulation pattern ($I=3.15$ mA, $PW = 600 \mu s$, $FS = 30$ Hz) is applied. In the first 50-s continuous stimulation (Fig. 2.13), before 17 s, the torque represents potentiation, then it maintains for around 10 s and starts decaying until 24.1% of the maximum torque. The MAV of eEMG presents the same tendency with the change of torque with fatigue progress, except during the initial potentiation, where the eEMG increases slowly before arriving at the maximum and then decreases with fatigue. MDF shifts to the lower frequency with increasing muscle fatigue, as fast muscle fibers drop out and slow muscle fibers contribute dominantly to the muscle contraction. Polynomial approximations (fifth order) of MDF are plotted to show the global tendency of the frequency components of eEMG. From the frequency domain of the eEMG signal, the TA muscle proves to be fatigued in the course of stimulation and this can be observed in the measured eEMG using the classical fatigue index of MDF.

In the second fatigue test (Fig. 2.14), the torque and MAV of eEMG are normalized by the maximum value of the first fatigue sequence. The torque varies wildly during the first 4 s, then maintains at 42.8% of the maximum, and gradually decreases to 14.3%. The MAV varies

similarly to torque, but more mildly during initial potentiation. Comparing the torque level variations in Fig. 2.13 and Fig. 2.14, even though the muscle is stimulated continuously except for a short pause for switching programs, the joint torque still recovers from 24.1% (47 s ~ 50 s in Fig. 2.13) to 42.8% (after 4s in Fig. 2.14). This phenomenon indicates the fast fatigue and fast recovery features in the continuous stimulation protocol. Several factors may contribute to this fast fatigue. First, this subject has been damaged for ten years and thus suffer from severe muscle atrophy. In addition, TA muscle is a fast contraction muscle and it is more fatigable after paralysis due to the variations in muscle fiber components. Second, the continuous fatigue protocol allows the muscle to rest. Even though eEMG changes differently compared with torque variations during intermittent FES (Section 2.4.1), the findings in this implanted experiment support the use of eEMG to indicate muscle fatigue and to predict torque decline with fatigue in implanted stimulation condition.

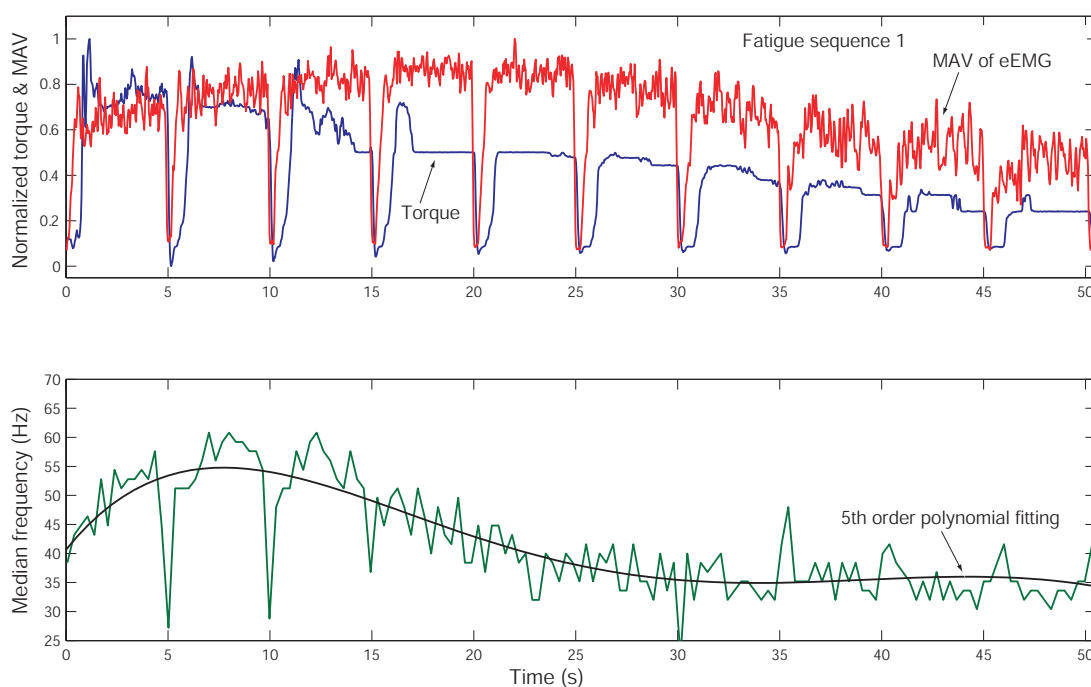


FIGURE 2.13 – Top : Normalized measured torque and MAV of eEMG in fatigue sequence 1. The measured torque becomes negative after the strong contraction, due to the reaction force generated when the muscle relaxes suddenly. Bottom : MDF transition in the same test fit by a fifth-order polynomial function.

2.5.2 Muscle Model Validation in Implanted FES

With the experimental data collected from the implanted SCI patient, the muscle fatigue behavior is investigated, and the feasibility of torque prediction based on eEMG signals is further verified using the identification method described above.

The two approaches to eEMG-to-torque model prediction (2.6) and (2.7) were carried out to predict joint torque in two fatigue tests. The model identification is processed using data from the first recruitment test and the first fatigue test, respectively. Fig. 2.15 illustrates the prediction results for two 50-s fatigue sequences. The blue solid line indicates the measured torque. The

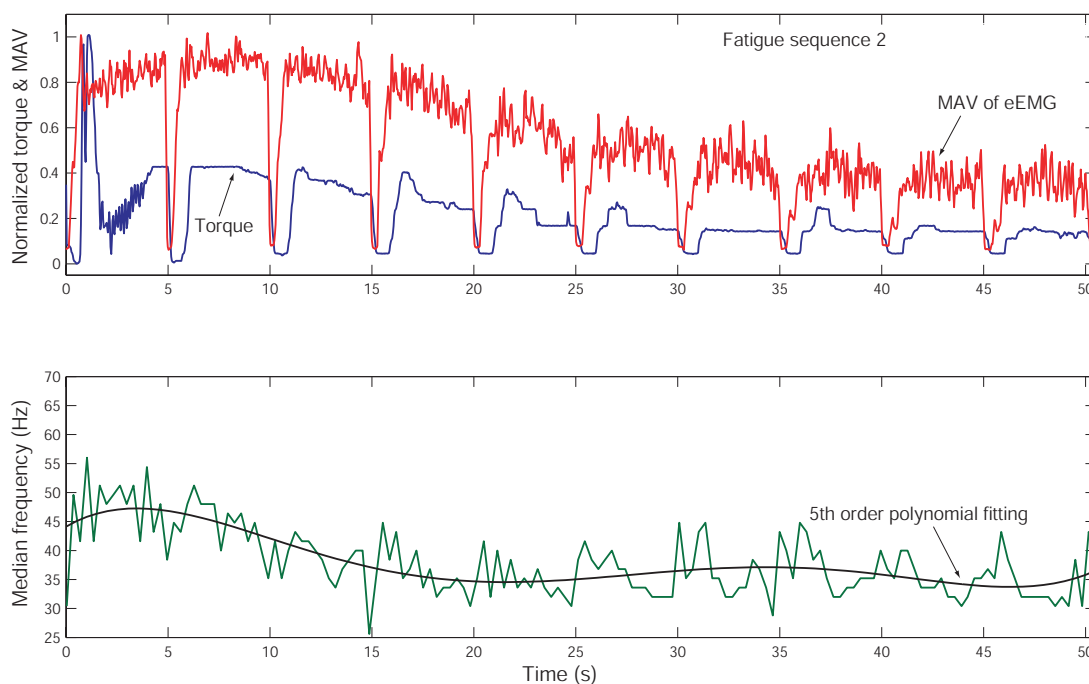


FIGURE 2.14 – Top : Normalized measured torque and MAV of eEMG in fatigue sequence 2. Bottom : Median frequency transition in the same test fit by a fifth-order polynomial function.

dashdotted black line represents Prediction1, which corresponds to a torque prediction based only on eEMG signals, and the dotted red line represents Prediction2, which is the predicted torque based on the torque and eEMG measurements. Note that the output scale is the absolute value of the ankle torque in Nm.

In fatigue sequence 1, the NRMS error is 0.145 for Prediction1 and 0.00884 for Prediction2 within the entire measured data. As in practice the potentiation can be avoided by warming up the muscle in advance, we also calculate the NRMS error after the potentiation period. The prediction performance is higher exclusive of potentiation, with the NRMS error 0.0725 for Prediction1 and 0.0047 for Prediction2. In fatigue sequence 2, the potentiation is localized, and the NRMS is 0.0876 for Prediction1 and 0.00822 for Prediction2 during the entire stimulation. However, we need to pay attention to the underestimation when muscle fatigue increases ; for instance, after 40 s in Fig. 2.15. These underestimates possibly result from constant model parameters unsuitable to catch the current muscle behaviors.

2.6 Discussion and Perspectives

This thesis focuses on the design of a model-based controller with muscle fatigue compensation in FES. A suitable model is important to achieve accurate prediction for enhancing control performance. In previous works, most researchers assumed that eEMG could be used directly for monitoring muscle fatigue or predicting force. Other researchers found that the relationship between the variations in eEMG and force could change in severe muscle fatigue or during the recovery process [Yu and Chang, 2009]. The complex features of fatigue, sensitive

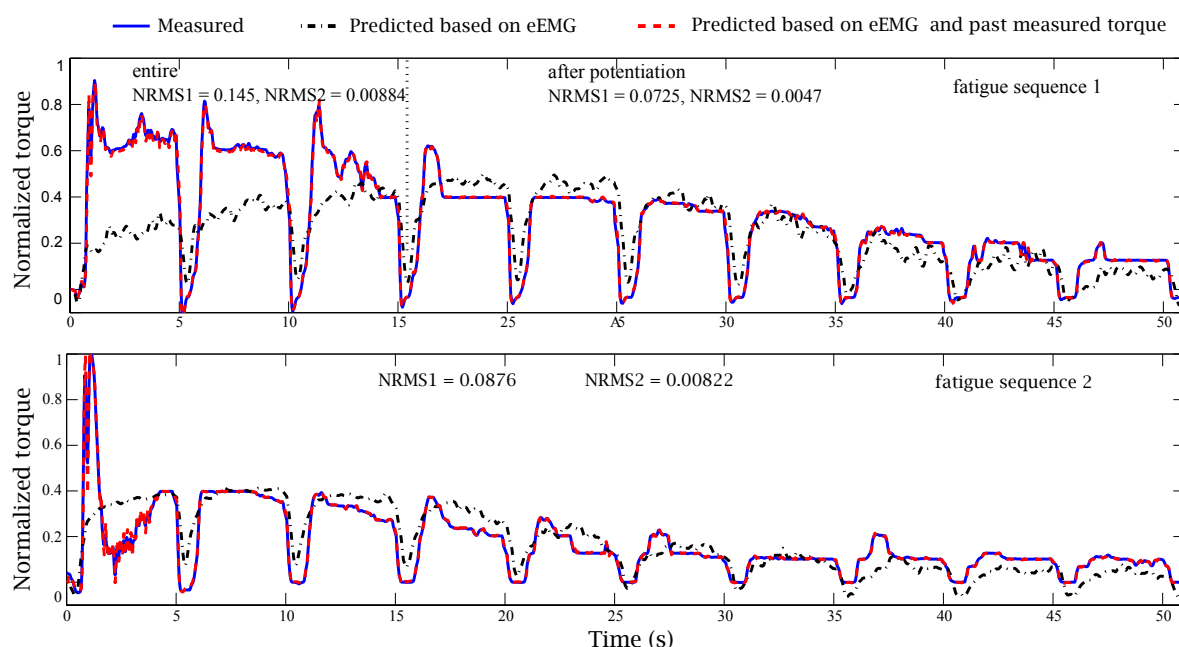


FIGURE 2.15 – The measured and predicted torque obtained with the eEMG-to-torque model during implanted continuous fatigue protocol. The torque prediction when both eEMG and torque measurement are used matches the torque measurement quite well. Interestingly, the torque prediction only based on eEMG signal and previously identified model is acceptable, with NRMS error around 7.25% and 8.76% in two fatigue tests.

sensor recording and insufficient clinical experiments have restricted its practical development. Two experimental protocols on SCI patients are conducted in this work to look for solutions for model-based FES control in the presence of muscle fatigue. The FES-evoked EMG signal from stimulated muscle was correlated with the induced joint torque under isometric condition.

The stimulation artifacts in EMG recording were rejected by the blanking window method. Note that, in order to ensure artifact removal without eliminating useful muscle response information, the recording electrodes should be located as far away as possible from the stimulation electrodes. Another problem in EMG recording is muscle cross-talk, which occurs when the muscle of interest is not easily separated from neighboring muscles. To overcome these recording problems, suitable filters, careful placement of the electrodes, and preparation of the skin are required. Besides, implanted EMG recording is quite interesting and possibly provides more reliable recording. In addition, although this work did not investigate the day-to-day variations in data acquisition, they are probably noticeable in practice.

The muscle fatigue properties were explored with two different FES systems. In intermittent stimulation on triceps surae muscle, with a stimulation intensity of I_{max} , the torque decreases slowly to around 90% (81% for S3) of the initial torque and recovers slowly during a 15-min rest (Fig. 2.9) in all subjects. The eEMG signals vary progressively during stimulation, but in different trends compared with torque among all the subjects. The fatigue-inducing stimulation with an intensity of $I_{max} * 50\%$ was delivered just after each fatigue-recovery train. Assuming the same muscle states during neighboring sessions, and comparing the torque decrease rate in postC of the fatigue-recovery session and that in fatigue4 of the fatigue-inducing session in S3, the lower

stimulation intensity in the fatigue-inducing session generates more fatigue, representing more decrease in torque (76%). A possible explanation is that high stimulation intensity activates both the slow and fast muscle fibers, whereas low stimulation intensity activates more fast muscle fibers and fewer slow muscle fibers. Thus, due to the fatigability of fast muscle fiber, lower stimulation intensity generates more fatigue than higher stimulation intensity. In comparison with the intermittent condition, in implanted continuous stimulation on TA muscle, the torque decreases faster and recovers faster, as described in section 2.5.1. The amplitude parameter (MAV) and frequency parameter (MDF) both vary with fatigue, indicating the feasibility of using these eEMG variables for fatigue monitoring.

In order to predict torque in fatiguing muscle, an eEMG-to-torque model has been adopted with the OLS method being applied to identify model parameters. First, when the muscle state does not change significantly in a short time, the fixed-parameter model is able to provide good prediction, as shown in Fig. 2.11 and 2.15. Prolonged stimulation likely leads to severe fatigue at a high rate, and the rest process leads to different recovery rates in muscle electrical and mechanical activities. As a result, the torque prediction gets worse in these situations, indicating that the fixed-parameter model is no longer suitable to predict muscle behavior. Fortunately, when the model was identified again with the latest experimental data, the torque prediction performance could be improved, as shown in Fig. 2.12. This finding indicates that muscle fatigues with gradual stimulation, the relationship between eEMG and torque is time-variant, and the parameters of the eEMG-to-torque model should be updated accordingly when eEMG is used to predict torque.

2.7 Conclusion

This chapter has investigated the feasibility of torque prediction based on eEMG signals in two different stimulation conditions. The muscle fatigue properties, muscle contraction modeling and torque prediction using eEMG have been explored. The results demonstrate some clues and also challenges when using the eEMG signal for torque prediction. First, both eEMG and torque change with fatigue, but the varying tendencies are different in some conditions (such as potentiation and recovery) and among subjects. Second, the eEMG-to-torque model is validated with the experimental data in surface FES and implanted FES. A fixed-parameter model is able to track most of the force decline with the development of fatigue. However, the quality of torque prediction degrades when potentiation occurs or when the fatigue level increases. The potentiation problem can usually be resolved by warming up the muscle in advance. Still, the improvement of torque prediction during different fatigue levels should be taken into account. Last, an adapted-parameter model is proposed and presents higher accuracy in predicting torque. This improvement implies that the relationship between eEMG and torque is time-varying, but probably slow. Thus, the adaptively updated model is able to catch the time-varying information for more accurate prediction.

If the muscle fatigue cannot be detected or fed back when FES proceeds, it is not possible to adjust stimulation accordingly. As a result, the patients cannot achieve the desired motion, and probably collapse. Therefore, accurate torque estimation that can be implemented in real-time is vital for designing a model-based controller reacting to muscle state changes. To achieve this purpose, an adaptive estimation method will be developed in the next chapter.

CHAPTER 3

Adaptive Torque Prediction and Fatigue Tracking from FES-Evoked EMG

Contents

3.1	Introduction	52
3.2	Previous Works	52
3.3	Online Torque Prediction during Muscle Fatigue	54
3.3.1	State-Space Representation and Filter Configuration	54
3.3.2	Kalman Filter with Forgetting Factor	56
3.3.3	Filter Configuration	58
3.4	Results of Time-Variant Torque Prediction	59
3.4.1	Time-Variant Parameter Tracking in Simulation	59
3.4.2	Fatigue Tracking Based on Experimental Data	62
3.4.3	Robust Fatigue Tracking	70
3.4.4	Discussion	74
3.5	Conclusion	75

3.1 Introduction

The goal of this chapter is to develop an adaptive torque estimation method that takes into account different fatigue states and subject-specific factors for the design of an advanced model-based FES controller. When FES is applied in a rehabilitation system, motor function is achieved by muscle contraction triggered by electrical current. The mechanical output level depends not only on the stimulation level but also on the muscle excitation and contraction abilities under isometric condition. Muscle fatigue, which results from the failure of the muscle excitation, excitation-contraction coupling or muscle contraction mechanism, is one of the main factors directly affecting muscle mechanical production. The idea of this work is to predict joint torque from muscle activity for fatigue tracking and compensation.

In Chapter 2, the muscle fatigue features during various stimulation conditions are displayed. Muscle activity—that is, eEMG signals recorded from activated muscle—drives a predictive model for estimating FES-induced torque. The prediction is accurate, assuming similar muscle states over a short prediction horizon. In the meantime, we found that the prediction accuracy degraded during prolonged stimulation or recovery. Thus, although valuable information extracted from eEMG signals can be applied for torque estimation, a suitable estimation method to compensate time-variant muscle responses is important to improve the accuracy and robustness of fatigue tracking during FES. The prediction improvement through an adaptive eEMG-to-torque model motivates us to develop an adaptive estimation method to track time-varying fatigue for advanced FES control. This method should also adapt to different stimulation situations and subject-specific differences. In addition, when motor nerve is activated by surface FES, it transforms into muscle activation via direct (efferent) and indirect (afferent) pathway—the so-called reflex. As a result, the reflex produces additional muscle forces which are difficult to model and predict, while a changing environment distorts the torque measurement. This probably occurs during walking and, therefore, the robustness of this method with regard to sensing failure, reflexes and environmental contacts is important.

This chapter is organized as follows. First, a probabilistic framework based on KF with forgetting factor is proposed to estimate the time-variant muscle contraction dynamics. Second, a simulation study and experimental assessment are conducted to present the performance and improvement of the proposed prediction method. The torque prediction method integrated into a fatigue tracking problem allows for the estimation of the temporary torque based only on eEMG information. The performance of the tracking robustness is evaluated and discussed.

3.2 Previous Works

In classic studies in FES, many researchers assumed that the muscle dynamics remain the same as the stimulation proceeds. However, in practice, the dynamics change during muscle contraction. In order to adapt the stimulation parameters to various uncertainties (e.g., fatigue), the prediction of muscle output is vital. Although several fatigue models have been proposed through mathematical or experimental statistical analysis, various factors limit the range of their applications, as described in section 2.1.2. In addition, as most works have been assessed in simulation and specific stimulation situations or tasks, further research is required to verify whether these methods can work in real applications or be extended to other conditions.

Evoked EMG is a potential approach to indicate fatigue and predict force or torque. Most of the previous works reported a high correlation between this muscle electrical behavior and muscle mechanical behavior. For example, when muscle force decreased with stimulation, Peak-to-Peak (PTP), RMS or MAV decreased [Tepavac and Schwirtlich, 1997], Second Phase Area (SPA) increased [Zhang et al., 2009], and frequency shifted to the lower component [Mizrahi et al., 1997a]. However, other works showed that this correlation was time-variant at different muscle fatigue levels [Mizrahi and Isakov, 1994] and during the recovery process [Yu and Chang, 2009]. Our experiments on SCI patients also found different variation tendencies in eEMG and torque during an intermittent protocol and different fatigue rates in an implanted continuous protocol, as presented in Chapter 2. Such evidence indicates the limitations of previous force/torque prediction strategies based on fixed-parameter models. Although an adaptive tuning of the parameters of eEMG was suggested for predicting the stimulated force in [Yu and Chang, 2009], they did not propose a feasible and effective method to do this. Furthermore, the reliability of the eEMG signals suffered from pickup variations and complex signal processing, which suggests other challenges for employing eEMG for muscle force/torque prediction. The first two problems may be resolved by implanting the EMG electrodes, which has been explored by several groups [Lowery et al., 2006] [Farnsworth et al., 2008].

Time-variant fatigue dynamics complicate the design of the FES controller. Even though the estimation of muscle output has been deemed as an active work for more advanced FES control, it has not been extensively studied in terms of different fatigue levels, compensating reflexes and day-to-day variations. The estimation method is related to the muscle model being employed and the facility for implementation. In the application of feedback control to physiological systems, a compromise between model complexity and control performance must be taken into account.

In [Ziai and Menon, 2011], although OLS was considered to be superior to several commonly used regression models for estimating isometric joint torque based on eEMG signals, retraining the model was suggested to regain high estimation quality due to degraded estimation accuracy over time. Therefore, the online estimation method proposed in this work is preferable to characterize the muscle contraction dynamics for real-time FES control. In the scenario of biomechanics, several works estimated nonlinear time-varying muscle dynamics through the recursive least squares (RLS) method or KF, which are especially effective for estimating slowly time-variant systems. In [Chia et al., 1991], the authors proposed an RLS method with time-varying parameter constraints in order to enhance the accuracy of parameter identification. The constraints were determined from available *a priori* knowledge about recruitment nonlinearity. A Hammerstein model, which was constructed by a polynomial and ARX function, was identified via the standard weighted LS method [Erfanian et al., 1998]. However, these authors did not consider the effects of different muscle fatigue states and subject-specific differences. In [Schauer et al., 2005], a modified KF, the extended Kalman filter (EKF), was adopted to estimate the joint angle for FES control. Another modified KF, the sigma point Kalman filter (SPKF), was proposed to online estimate nonlinear muscle force induced by FES in [Hayashibe et al., 2008]. For tremor suppression with FES, both EKF and SPKF were assessed to estimate joint motion and tremor motion in [Bó et al., 2011].

In this work, a KF is therefore proposed to online estimate muscle contraction dynamics, with a forgetting factor for tracking time-variant muscle fatigue. As long as the updated model provides sufficient torque predictions, the stimulation parameters are adaptively adjusted before

being delivered to the muscle. As a result, perturbations such as muscle fatigue can be compensated. KF is a recursive estimation method that is useful when parameter estimates are required in real-time, such as when the information is used in adaptive control or real-time diagnosis. This formulation explicitly takes into account the uncertainties related to the model, the measurement and the parameters. Moreover, the implementation can be easily extended to multi-input multi-output models, as long as additional sensors are introduced.

3.3 Online Torque Prediction during Muscle Fatigue

In the proposed formulation, KF is used for the online parameter identification of the muscle contraction model. KF is efficient for estimating the internal states and parameters of a discrete-time system from a series of noisy measurements. The PHM described in Chapter 2 is employed here.

3.3.1 State-Space Representation and Filter Configuration

State-space representation is basically required to implement the recursive algorithm for model estimation. It provides a convenient and compact way for estimation and control problems with its notational expression. The state-space form relates a set of input, output, and state variables by first-order differential equations, and permits us to track the internal state variables from input-output data sets, whether they are measurable or not.

Considering a time-variant PHM (l,m,n) as described in (2.5),

$$f(u(k-i), y(k-i), \theta(k)) = \sum_{i=1}^l a_i(k)y(k-i) + \sum_{i=1}^m \sum_{j=1}^n \mu_{ij}(k)(u(k-i))^j, \quad (3.1)$$

$\theta(k)$ is the vector containing the time-variant model parameters :

$$\theta(k) = [a_1(k), \dots, a_l(k), \mu_{11}(k), \dots, \mu_{1n}(k), \dots, \mu_{m1}(k), \dots, \mu_{mn}(k)]^T. \quad (3.2)$$

Consequently, a PHM (l,m,n) has (l+m*n) parameters. At a given time instant t, the computation of future joint torque estimates using (3.1) is straightforward, assuming a stationary or slowly varying system within the prediction horizon. Next, we will describe the chosen parameter model, the state space representation, and the measurement model.

Parameter model

In a time-varying muscle contraction model, if indicative information about the evolution in muscle fatigue is available—for instance, the fatigue rate is indicated by eEMG amplitude or frequency components—the model parameters can be easily modeled by incorporating into (3.3). Otherwise, the changes in model parameters are considered absolutely random, and the parameters are represented by a random walk process,

$$\theta(k) = \theta(k-1) + \varepsilon(k) \quad (3.3)$$

where k indicates the current time step and $\theta(k)$ is the kth-step parameters. The parameter transition is assumed to be Gaussian white noise ε , $\varepsilon \sim N(0, \sigma^2)$. This implies that the mean of

the parameter process is constant, but its variance is not constant. Thus, the parameter model is non-stationary, and the variance is variant with time. In practice, this model structure makes the prediction process very simple since all the future values of $\theta(k+s)$ for $s > 0$ are assumed to be equal to $\theta(k)$ and the variance is set according to the system dynamics. For example, if the variation in torque is considered higher in comparison with the variation in eEMG with an increase in muscle fatigue level, the coefficients of past torque $a_i(k)$ should be set relatively higher than the coefficients of past eEMG $\mu_{ij}(k)$. In other words, we assume more uncertainty concerning muscle mechanical behavior than muscle electrical behavior with increasing fatigue.

Process and measurement models

A state-space model consists of a measurement model relating the observations to the state vector, and a Markovian transition equation describing the evolution in the state vector over time. The detailed process to obtain the state-space model of a PHM is described in Appendix B.1. For a PHM (l,m,n), the state vector, which consists of $q=\max(l,m)$ variables, is given by

$$\mathbf{x}(k) = \begin{bmatrix} x_1(k) & x_2(k) & \cdots & x_q(k) \end{bmatrix}^T \quad (3.4)$$

The previous state $\mathbf{x}(k-1)$ is transferred to the current state $\mathbf{x}(k)$ by a transfer matrix $\mathbf{A}(k) \in \mathbb{R}^{q \times q}$, such that

$$\mathbf{x}(k) = \underbrace{\mathbf{A}(k)\mathbf{x}(k-1) + \mathbf{B}(k)\mathbf{u}(k-1)}_{\mathbf{f}(\mathbf{x}(k-1), \mathbf{u}(k-1), \mathbf{w}(k))} + \mathbf{w}(k) \quad (3.5)$$

$$\mathbf{u}(k-1) = \begin{bmatrix} u(k-1) \\ u(k-1)^2 \\ \vdots \\ u(k-1)^n \end{bmatrix} \quad (3.6)$$

where $\mathbf{u}(k-1) \in \mathbb{R}^{n \times 1}$ contains the exponents of previous model inputs, which are known at each current step. Vector $\mathbf{w}(k)$ is Gaussian white noise of the system model. $\mathbf{B}(k) \in \mathbb{R}^{q \times n}$ relates the previous model input $\mathbf{u}(k-1)$ to the current state $\mathbf{x}(k)$. The state process has a linear feature

with matrix $\mathbf{A}(k)$ and matrix $\mathbf{B}(k)$, which are represented as follows :

$$\mathbf{A}(k) = \begin{bmatrix} a_1(k) & 1 & 0 & \cdots & 0 & 0 \\ a_2(k) & 0 & 1 & \cdots & 0 & 0 \\ \vdots & \vdots & \vdots & \ddots & \vdots & \vdots \\ a_{l-1}(k) & 0 & 0 & \cdots & 0 & 1 \\ a_l(k) & 0 & 0 & \cdots & 0 & 0 \\ 0 & 0 & 0 & \cdots & 0 & 0 \\ \vdots & \vdots & \vdots & \ddots & \vdots & \vdots \\ 0 & 0 & 0 & \cdots & 0 & 0 \end{bmatrix}, \quad \mathbf{B}(k) = \begin{bmatrix} \mu_{11}(k) & \mu_{12}(k) & \cdots & \mu_{1l}(k) \\ \mu_{21}(k) & \mu_{22}(k) & \cdots & \mu_{2l}(k) \\ \vdots & \vdots & \vdots & \vdots \\ \mu_{m1}(k) & \mu_{m2}(k) & \cdots & \mu_{ml}(k) \end{bmatrix}, \quad \text{when } l < m,$$

$$\mathbf{A}(k) = \begin{bmatrix} a_1(k) & 1 & 0 & \cdots & 0 & 0 \\ a_2(k) & 0 & 1 & \cdots & 0 & 0 \\ \vdots & \vdots & \vdots & \ddots & \vdots & \vdots \\ a_{l-1}(k) & 0 & 0 & \cdots & 0 & 1 \\ a_l(k) & 0 & 0 & \cdots & 0 & 0 \end{bmatrix}, \quad \mathbf{B}(k) = \begin{bmatrix} \mu_{11}(k) & \mu_{12}(k) & \cdots & \mu_{1l}(k) \\ \mu_{21}(k) & \mu_{22}(k) & \cdots & \mu_{2l}(k) \\ \vdots & \vdots & \vdots & \vdots \\ \mu_{m1}(k) & \mu_{m2}(k) & \cdots & \mu_{ml}(k) \\ 0 & 0 & \cdots & 0 \\ \vdots & \vdots & \vdots & \vdots \\ 0 & 0 & \cdots & 0 \end{bmatrix}, \quad \text{when } l \geq m.$$
(3.7)

As for the measurement model, it relies only on the first state element $x_1(k)$, being written in vector expression as

$$y(k) = \mathbf{C}\mathbf{x}(k) + v(k), \quad (3.8)$$

where $v(k)$ is Gaussian white noise of the measurement sensor. When the system has a single output, the observer is scalar variable y ; otherwise, it is a vector and the corresponding noise element is also with vector expression. The current state $\mathbf{x}(k)$ is correlated with the current system output $y(k)$ by measurement matrix $\mathbf{C} \in \mathbb{R}^{1 \times q}$

$$\mathbf{C} = \begin{bmatrix} 1 & 0 & \cdots & 0 & 0 \end{bmatrix}.$$

In the prediction phase of KF, the evolution in the model states is given by (3.5), while the evolution in the model parameters is given by (3.3). In the correction phase, the measurement from output sensor, $y(k)$, will be applied to update the estimates of model states and model parameters.

3.3.2 Kalman Filter with Forgetting Factor

In order to identify the time-variant model states in $\mathbf{x}(k)$ and the parameters in $\theta(k)$, even though a dual KF is a solution to identify them in two parallel KF, as described in [Aboy et al., 2005], another treatment is more direct and convenient for this purpose and is used in this work. The main idea is to identify the model states and the model parameters concurrently by regarding the unknown model parameters as elements of the state vector. In this way, the basic KF algorithm does not need to be modified, except that the state vector $\mathbf{x}(k)$ will be augmented with the unknown parameters in $\theta(k)$. That is, the meta-state vector $\Theta(k)$ is

given by

$$\Theta(k) = \begin{bmatrix} \mathbf{x}(k) \\ \theta(k) \end{bmatrix}_{[(q+l+m \times n) \times 1]} \quad (3.9)$$

Accordingly, from equation (3.3) (3.5) and (3.8), the augmented system is rewritten by

$$\Theta(k) = \underbrace{\begin{bmatrix} \mathbf{f}(\mathbf{x}(k-1), \mathbf{u}(k-1), \mathbf{w}(k)) \\ \theta(k-1) + \varepsilon(k) \end{bmatrix}}_{\mathbf{F}(\Theta(k-1), \mathbf{u}(k-1), \mathbf{v}(k))} \quad (3.10)$$

$$y(k) = \underbrace{\begin{bmatrix} \mathbf{C} & \mathbf{0}_{1 \times (l+m \times n)} \end{bmatrix} \Theta(k)}_{\mathbf{G}(\Theta(k), v(k))} + v(k) \quad (3.11)$$

where the process noise $\mathbf{w}(k)$, the parameter noise $\varepsilon(k)$ and the measurement noise $v(k)$ are the same as shown in (3.3) (3.5) and (3.8). They are assumed to be independent, white and normally distributed,

$$\mathbf{v}(k) = \begin{bmatrix} \mathbf{w}(k) \\ \varepsilon(k) \end{bmatrix} \quad (3.12)$$

$$p(\mathbf{v}) \sim (0, \mathbf{Q}) \quad (3.12)$$

$$p(v) \sim (0, R) \quad (3.13)$$

The recursive algorithm of KF is a mature technique that consists of two phases, prediction and correction. In the prediction phase, the system is assumed to be stationary, which implies the *a priori* estimate of the state at instant k, $\hat{\Theta}^-(k)$, is equal to the *a posteriori* state at the previous instant k-1, $\hat{\Theta}(k-1)$,

$$\hat{\Theta}^-(k) = \mathbf{F}(\hat{\Theta}(k-1), \mathbf{u}(k-1), 0) \quad (3.14)$$

The estimate error covariance $\mathbf{P}(k)$ is propagated according to (3.15) :

$$\mathbf{P}^-(k) = \mathbf{D}(k)\mathbf{P}(k-1)\mathbf{D}^T(k) + \mathbf{Q}(k-1) \quad (3.15)$$

where $\mathbf{Q}(k-1)$ is a diagonal matrix containing the process noise covariance, and $\mathbf{D}(k)$ is the Jacobian matrix of partial derivations of process transfer function \mathbf{F} with respect to the variables involved in Θ , with each element D_{ij} being computed by :

$$D_{ij}(k) = \frac{\partial F_i}{\partial \Theta_j}(\hat{\Theta}(k-1), \mathbf{u}(k-1), 0) \quad (3.16)$$

In the correction phase, $\mathbf{K}(k)$ in (3.17) is called a KF gain that minimizes the *a posteriori* error covariance,

$$\mathbf{K}(k) = \mathbf{P}^-(k)\mathbf{H}^T(k)(\mathbf{H}(k)\mathbf{P}^-(k)\mathbf{H}^T(k) + R(k))^{-1} \quad (3.17)$$

where $R(k)$ is a scalar measurement noise covariance (for a single output system). $\mathbf{H}(k)$ is the Jacobian matrix of partial derivations of sensor transfer function \mathbf{G} with respect to Θ , with each element H_{ij} being computed by :

$$H_{ij}(k) = \frac{\partial G_i}{\partial \Theta_j}(\hat{\Theta}^-(k), 0) \quad (3.18)$$

incorporating to (3.11), $\mathbf{H}(k) = \begin{bmatrix} \mathbf{C} & \mathbf{0}_{1 \times (l+m \times n)} \end{bmatrix}$.

When actual measurement $y(k)$ is available, an *a posteriori* state estimate is generated by incorporating measurement as in (3.19). An *a posteriori* error covariance estimate is obtained via equation (3.20).

$$\hat{\Theta}(k) = \hat{\Theta}^-(k) + \mathbf{K}(k)(y(k) - \mathbf{G}(k)(\hat{\Theta}^-(k), 0)) \quad (3.19)$$

$$\mathbf{P}(k) = (\mathbf{I} - \mathbf{K}(k)\mathbf{H}(k))\mathbf{P}^-(k) \quad (3.20)$$

Although the KF is an effective way of estimating the state and parameters of a discrete time-controlled process, its performance in estimating the time-varying parameters is degraded by the fact that it refers to the entire history of past measurements [Mack and Jain, 1983]. This is particularly troublesome when it is used to estimate the muscle contraction system, since the activity of stimulated muscles tends to vary, with prolonged or repetitive stimulation leading to variant muscle states. In order to track the time-varying muscle condition, a forgetting factor λ is deliberately introduced to forget the old measurements when muscle fatigue increases. Consequently, (3.15) and (3.17) can be rewritten as,

$$\mathbf{P}^-(k) = \mathbf{D}(k)\mathbf{P}(k-1)\mathbf{D}^T(k)/\lambda \quad (3.21)$$

$$\mathbf{K}(k) = \mathbf{P}^-(k)\mathbf{H}^T(k)(\mathbf{H}(k)\mathbf{P}^-(k)\mathbf{H}^T(k) + \lambda)^{-1} \quad (3.22)$$

Choosing the forgetting factor $\lambda \in [0, 1]$ depends on how much of the old measurements we expect the filter to forget. If the forgetting factor is smaller, the filter will forget more past measurements that are farther away from the present instant. A smaller forgetting factor enables us to track changes in the system quickly, but it requires a longer time to arrive at convergence, which may lead to more fluctuations. Whereas if a forgetting factor is close to 1, it assures fast convergence but is not sensitive to the system variations. Consequently, a tradeoff between the smoothness of tracking and the lag in detecting system changes should be considered when a forgetting factor is introduced to a KF. Generally, $\lambda \in [0.9, 1]$ is suitable for most applications. Moreover, if a system changes slowly over time, one can select a forgetting factor close to 1. Otherwise, a smaller forgetting factor is usually preferred. In summary, the implementation of the KF with forgetting factor is listed as follows.

3.3.3 Filter Configuration

In classic KF, the tuning parameters are the process covariance matrix \mathbf{Q} and measurement covariance matrix \mathbf{R} . Generally, they are empirically chosen depending on our confidence in the model and the measurements. In this work, the tuning problem is reduced to only one parameter—forgetting factor λ , in accordance with the muscle fatigue level. In other words, the forgetting factor should be farther away from 1 with the increase in muscle fatigue severity.

Algorithm The algorithm of KF with forgetting factor

1. $k \leftarrow 0$
 2. initialize states of the filter $\hat{\Theta}(0)$, corresponding covariance $\mathbf{P}(0)$, initial measurement $y(0)$, observation matrix \mathbf{H} using equation (3.18), and forgetting factor λ
 3. **while** system is running **do**
 4. $k \leftarrow k + 1$
 // prediction phase
 5. compute *a priori* state estimates $\hat{\Theta}^-(k)$ using equation (3.14)
 6. compute *a priori* observation estimate considering $\hat{y}^-(k) = \mathbf{H}\hat{\Theta}^-(k)$
 7. compute the Jacobian matrix $\mathbf{D}(k)$ using equation (3.16)
 8. compute *a priori* error covariance estimates $\mathbf{P}^-(k)$ using equation (3.21)
 // correction phase
 9. update Kalman gain $\mathbf{K}(k)$ using equation (3.22)
 10. compute *a posteriori* state estimates $\hat{\Theta}(k)$ using equation (3.19)
 11. compute *a posteriori* covariance estimates $\mathbf{P}(k)$ using equation (3.20)
 12. **end**
-

For a PHM (l,m,n), a $\max(l, m) + (l + m \times n)$ dimensional meta-state will be estimated. The $\max(l, m)$ parameters are the internal states of the filter and the rest are the parameters of the muscle model. The elements of the meta-state vector are initialized as $\hat{\Theta}(0) = 0$. The initial output estimate $y(0)$ is set at zero whenever the muscle is at rest. The estimate error covariance is initialized as $\mathbf{P}(0) = \mathbf{I}$, where \mathbf{I} is an identity matrix.

3.4 Results of Time-Variant Torque Prediction

The elements of θ , as well as the eEMG-to-torque features, are time-varying in nature due to the effects of fatigue and the associated biochemistry. At a given time k , the future torque is predicted using (3.1) by assuming the system is stationary, or slowly time-varying, during the prediction horizon. In this section, the time-varying parameter estimation performed by the KF is evaluated in simulations and with experimental data. The outlines of the muscle model and KF were described previously. NRMS error is used to quantify the performance of estimation accuracy and parameter convergence during a period of interest.

3.4.1 Time-Variant Parameter Tracking in Simulation

In simulation, invariant parameter tracking is evaluated first with the KF to investigate the convergence of the muscle model. Second, in order to investigate the filter's adaptivity to the time-varying fatigue phenomenon, the model parameters are slowly changed at different instants to simulate changes in muscle condition. The advantage of simulation is that the true

parameters are known to be compared with the estimated ones. The simulation model order is chosen as ($l=2, m=2, n=1$) to reduce model complexity, as it is difficult to know how the model output changes when too many parameters change. Thus, four parameters, $a_1, a_2, \mu_{11}, \mu_{21}$, are estimated via the KF algorithm in simulation. In the beginning, all the parameters are kept constant. After 33 s or 50 s, they are changed linearly (a_1 and μ_{21}) or in steps (a_2 and μ_{11}). As the variation rates of the parameters are designed high, a KF with forgetting factor 0.97 is selected to identify the model. The pseudorandom binary sequence (PRBS), which is commonly used in muscle identification [Farahat and Herr, 2005], is chosen as the model input. The output is corrupted with zero mean white noise with SNR of 25 dB and 50 dB. The two SNR levels are selected, as experimental SNR is approximately 37 dB. The SNR is defined as

$$SNR = 10 * \log_{10} \left(\frac{\sum_{k=0}^N y^2(k)}{\sum_{k=0}^N v^2(k)} \right)$$

where $y(k)$ is a clean signal and $v(k)$ is the measurement noise at time k , and N is sample length. The real model input, output and the *a posteriori* estimate of the output (SNR = 50 dB) are shown in Fig. 3.1.

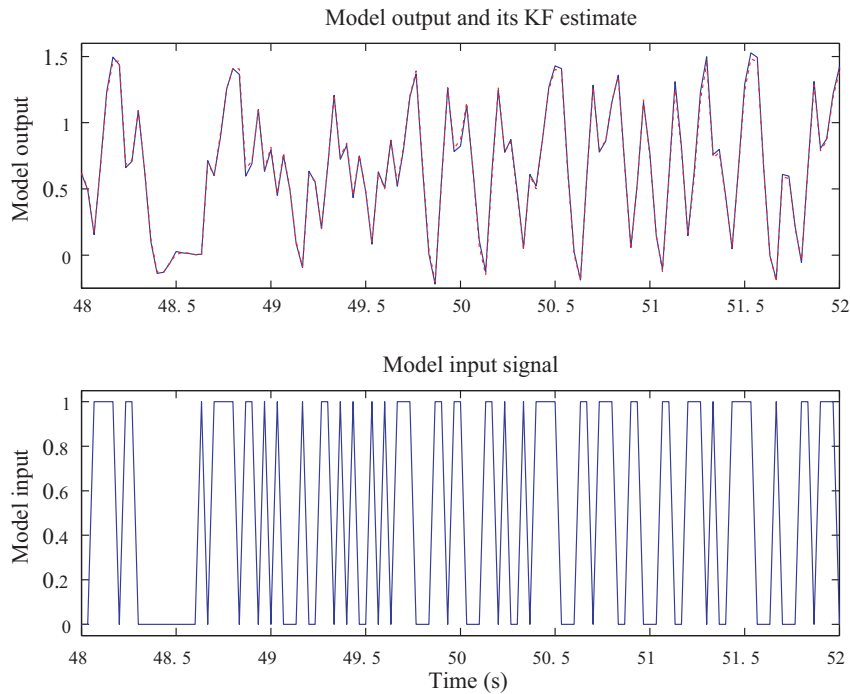


FIGURE 3.1 – Top : The model output (blue) and its estimate (red) by KF with forgetting factor. Outputs are generated by simulation using a PHM (2,2,1) and corrupted by noises with SNR = 50 dB. Bottom : Model input (PRBS signals).

The corresponding parameter estimates of the model (SNR = 50 dB) are depicted in Fig. 3.2. The solid lines indicate the true parameters, while the dotted lines indicate parameter estimates. All the parameters converge steadily after 5 s when the parameters are static. After

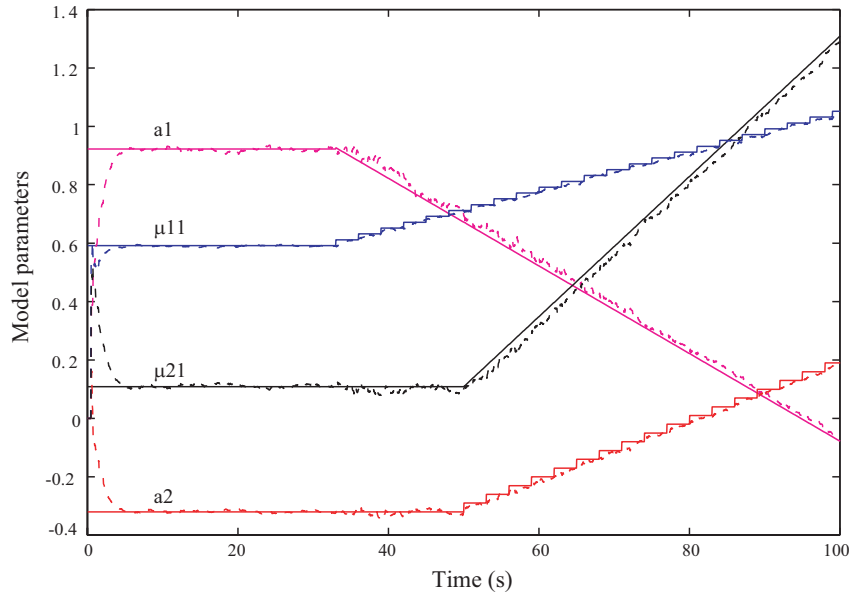


FIGURE 3.2 – Convergence and tracking of both static and time-variant parameters. Solid lines indicate true parameters. Dotted lines indicate parameter estimates. All the initial estimates are set at zero.

33 s or 50 s, the model parameters gradually vary, and the estimates track the changes well, which implies that the estimation method is suitable for time-variant parameter tracking with a PHM.

A statistical average error, for estimates of system output and parameters at various SNR (25 dB and 50 dB), is given in TABLE 3.1. It demonstrates that the accuracy and convergence of the estimation are both better with higher SNR. However, when SNR is low (25 dB), the estimation error is not wild, which implies that the estimation method can still work even when the signal is quite noisy.

TABLE 3.1 – NRMS error of estimation

Estimate	Signal-to-Noise Ratio (SNR)	
	25 dB	50 dB
output	0.0773	0.0306
a_1	0.0821	0.0743
a_2	0.0421	0.0363
μ_{11}	0.0396	0.0373
μ_{21}	0.0561	0.0422

3.4.2 Fatigue Tracking Based on Experimental Data

In this section, the estimation of time-varying parameters and the torque prediction for fatigue tracking are performed based on experimental data using the KF with forgetting factor. The robustness of the KF-based estimator is also investigated. The experimental data from surface and implanted stimulation are used for this study. Moreover, the data from successive series of fatigue-inducing tests in surface FES are concatenated to have sufficient data and obvious fatigue states. The model order is chosen at (3,4,3) and the KF is configured as described in 3.3.3. Apart from the NRMS error over the entire period of interest, the identification error and prediction error are calculated and displayed. The identification error, reflecting the accuracy of parameter estimation, is calculated as the absolute difference between measured and estimated torque at each evolution. The prediction error, measuring the prediction ability of the identified model, is calculated as the NRMS error and Normalized Peak Error (NPE) between the measured and predicted torque within a given prediction horizon.

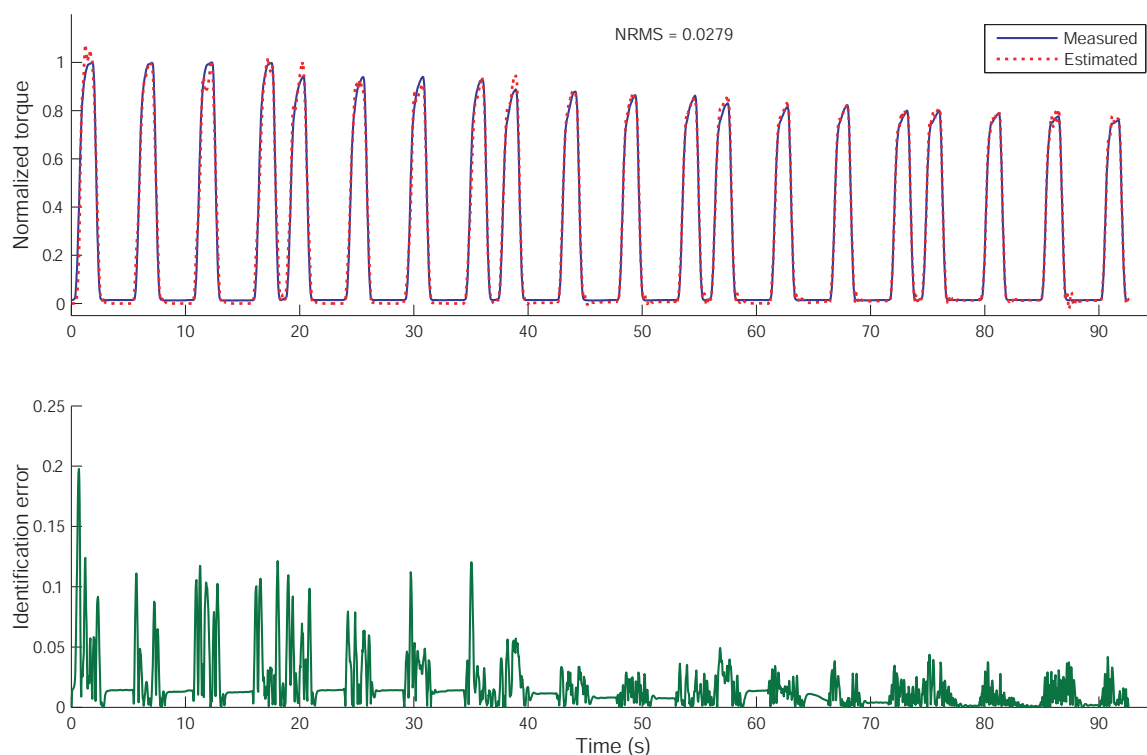


FIGURE 3.3 – The estimated torque and identification error in subject S5. At each instant, the eEMG-to-torque model parameters are updated adaptively by KF with forgetting factor 0.997. The identification error of each evolution is plotted at the bottom. The identification takes approximately 1 s to converge.

First, to illustrate the evolution in the model parameters, the torque estimates and identification error in both FES systems are plotted. One result is shown in Fig. 3.3 for subject S5, where the torque declines 21%, and the estimator updates the model parameters adaptively and accurately tracks the fatigue effect. The estimation takes approximately 1 s to converge and then the identification error maintains almost less than 0.1 (corresponding to 10% of the measured

torque). Notably, after a 40-s evolution, the model arrives at a steadier state, representing less than 5% identification errors. Similarly, Fig. 3.4 is plotted for the implanted subject in fatigue sequence 1, where the torque decreases to around 24.1% of the maximum torque. Except for the first 17-s potentiation, the identified parameters afterward are suitable to estimate the torque. Large errors at the sharp corner between two adjacent trains probably arise from a quickly altered muscle response but sparse data for the estimator to find the optimal parameters. This can hopefully be avoided by designing a suitable rising and falling period during each train, and allowing a period of rest between two adjacent trains. More results are shown in Appendix C to demonstrate the torque estimates and parameter evolutions (see Fig. B.1, Fig. B.2 and Fig. B.3). Apparently, the model parameters vary over time and generally with a low varying rate, which makes it possible to obtain good torque prediction in a given prediction horizon.

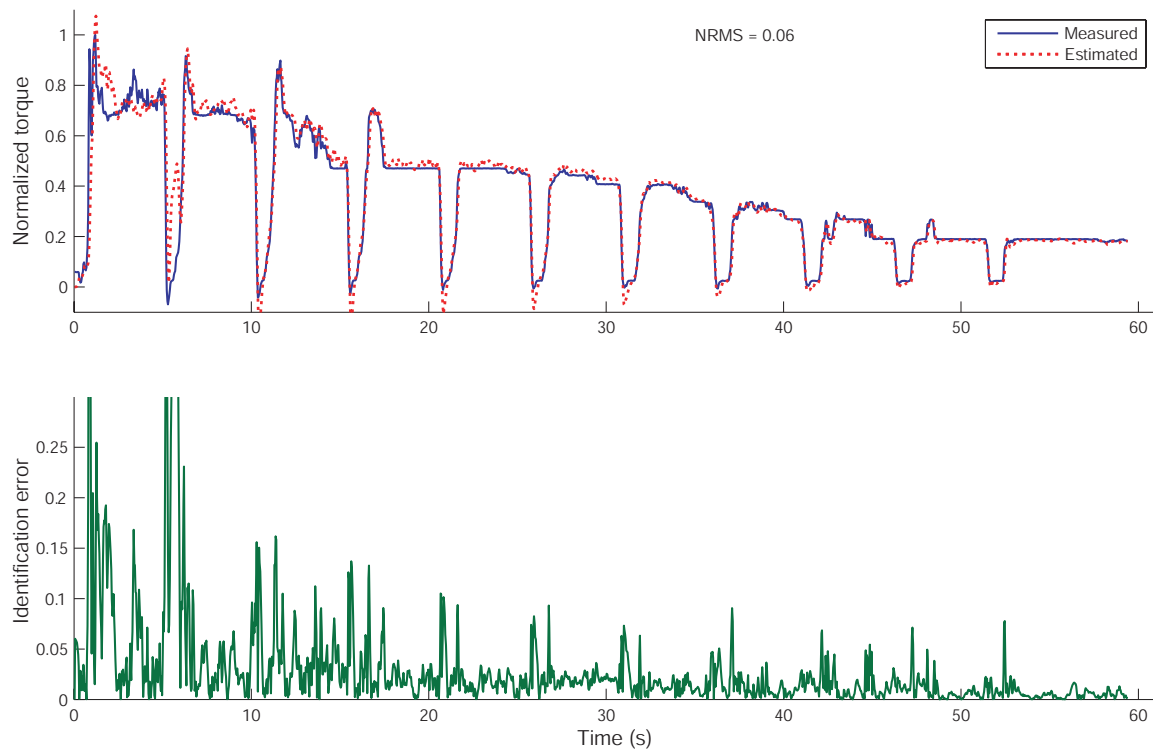


FIGURE 3.4 – The estimated torque and identification error in the implanted subject. At each instant, the eEMG-to-torque model parameters are updated adaptively by KF with forgetting factor 0.997. The identification error of each evolution is plotted at the bottom. The high identification error during the initial potentiation indicates dissociation between eEMG and torque during this period.

3.4.2.1 Fatigue Dynamics

The estimation of the muscle contraction process is used to explore the dynamics of fatigue phenomena. The parameter estimates in $\hat{\theta}(k)$ are used to compute the poles of the muscle contraction system by making $A(q)$ in (2.4) equal to 0. At each evolution, a PHM (l,m,n) has 1

poles, and the solution is to solve a polynomial function as

$$q^l + a_1q^{l-1} + \dots + a_{l-1}q + a_l = 0$$

The locations of these poles in subjects S1 and S3 are indicated in Fig. 3.5. The unit circles are also plotted in this figure. All the poles are located within the unit circles, which is of significance in ensuring the model stability under such a stimulation protocol. The arrows denote the direction of movement of the z-plane poles. The time-varying property of the poles may also interpret the muscle dynamics. Moreover, the locations and movements of the z-plane poles in all subjects present similar characteristics, suggesting that it is possible to assess muscle fatigue dynamics from such information. In general, the damping ratio increases when the muscle is highly fatigued. This matches our intuition concerning the effect of muscle fatigue.

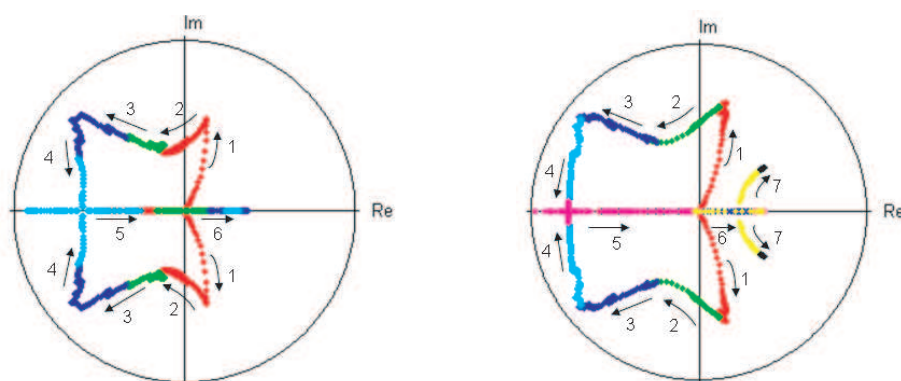


FIGURE 3.5 – The changes of the muscle contraction dynamics of muscle behavior due to fatigue during surface FES in subjects S1 (left) and S3 (right). The arrows denote the direction of "movement" of the z-plane pole. The plot color is changed every 16s to show the time transition.

3.4.2.2 Torque Prediction Performance

To investigate the torque prediction performance in time, t_1 , t_2 and t_3 , corresponding to 6-s, 18-s and 30-s ahead predictions, are evaluated. The idea is illustrated in Fig. 3.6, which features the estimated model at time instant t_0 . The torque predictions are computed using (3.1) and are only driven by the eEMG signals and identified model at t_0 , assuming a stationary system within the prediction horizon. At each instant, the NRMS error and NPE during a given prediction horizon are computed. NRMS has been defined before, and NPE is the peak error during the prediction horizon at each evolution. The prediction errors in all subjects in surface FES are quantified in TABLE 3.2. Eighteen seconds is considered to be appropriate, as it provides a tradeoff between a sufficient interval for measurement update in KF and satisfactory prediction performance. The prediction errors for the 6-s, 18-s and 30-s prediction horizons in subject S3 are plotted in Fig. 3.7. The solid blue line indicates the NRMS error, while the dotted black line indicates peak error. The identification error at each instant is also displayed in the bottom plot.

Since the estimation algorithm is intended for online implementation in real-time FES control, the computational time is important to guarantee the adaptive response of the controller. The elapsed time taken to perform torque prediction of different prediction horizons is listed

TABLE 3.2 – Prediction performance with experimental data

Subject	Average error	Prediction horizon		
		6s	18s	30s
S1	NRMS	0.0638	0.0974	0.1282
	NPE	0.1616	0.2990	0.3414
S2	NRMS	0.0763	0.0925	0.1110
	NPE	0.2466	0.3402	0.4230
S3	NRMS	0.0278	0.0314	0.0366
	NPE	0.0743	0.0962	0.1146
S4	NRMS	0.0524	0.0534	0.0556
	NPE	0.1208	0.1523	0.1697
S5	NRMS	0.0387	0.0418	0.0437
	NPE	0.1036	0.1360	0.1510

in TABLE 3.3 for one subject, S3. A laptop with Core 2 Duo CPU P8400 @ 2.226 GHz 2.27 GHz and 4.00 GB memory, was used for computation.

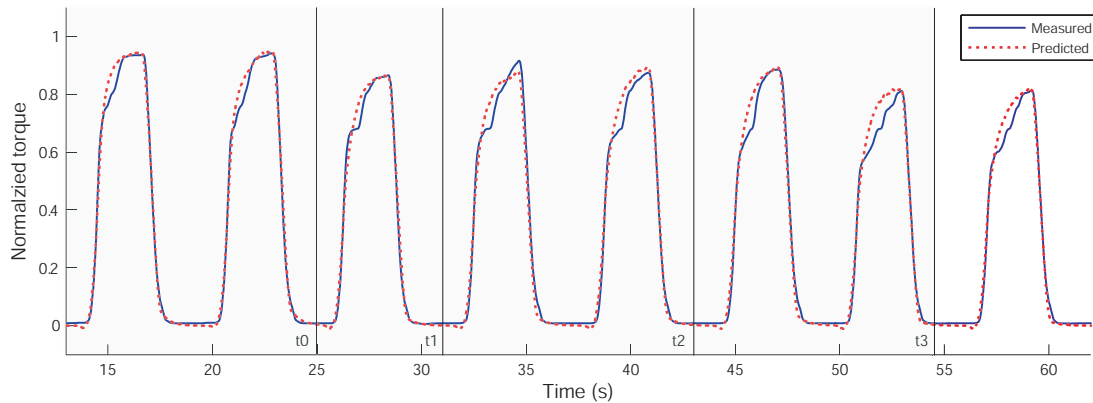


FIGURE 3.6 – Illustration of torque estimation based on eEMG information. For evaluating prediction performance at t_0 , the prediction errors for prediction horizons t_1 , t_2 , and t_3 (6 s, 18 s and 30 s, respectively) are measured. A KF with forgetting factor 0.997 is used to estimate the model.

3.4.2.3 Adaptive Performance for Internal and External Disturbances

The prediction filter must be robust for the internal and external changes in muscle response. For instance, when joint motion suffers from sudden torque variations, such as a resistant effect from environmental contact, the torque measurement is affected unexpectedly. Without knowledge of the muscle activity, the control is likely to be unstable. On the contrary, when muscle activity is taken into account, if the prediction is accurate enough, the controller can

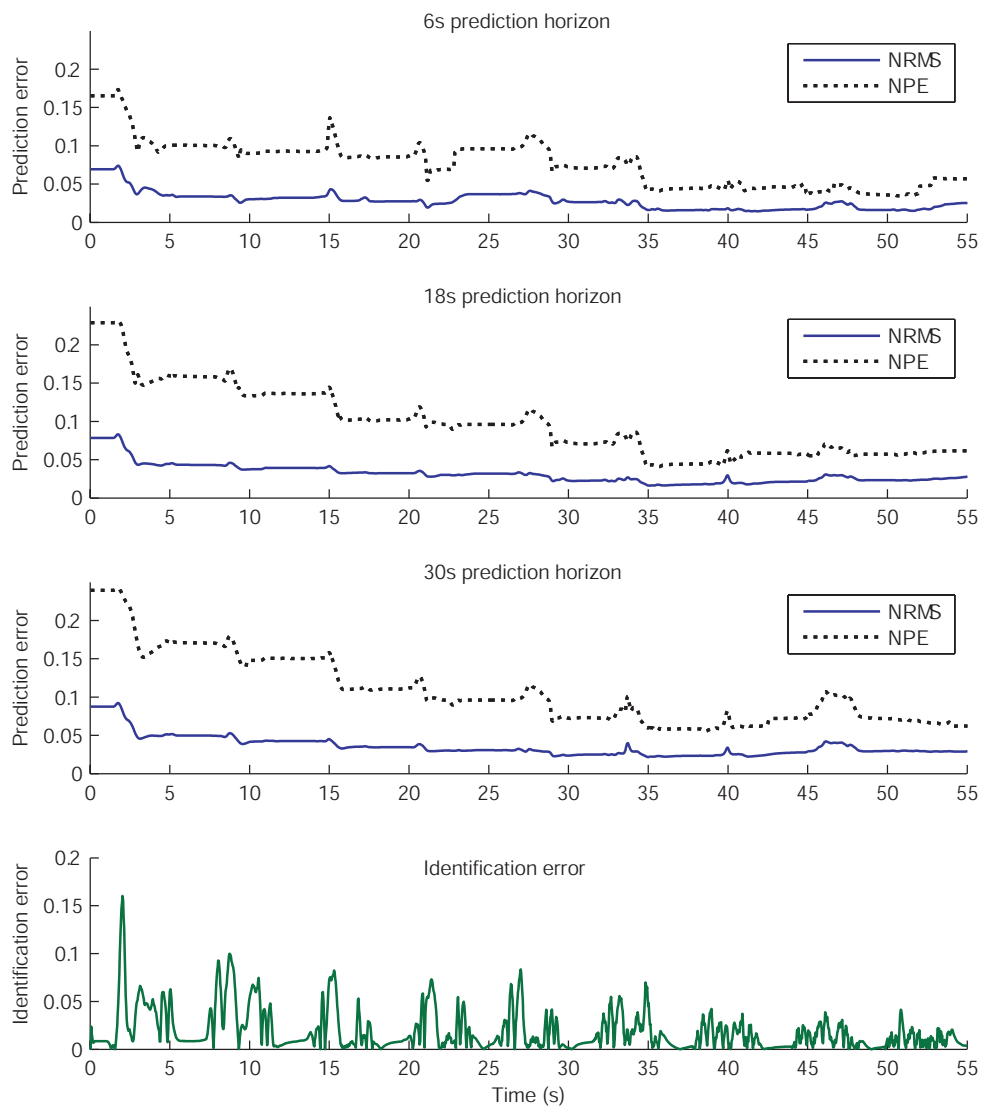


FIGURE 3.7 – Prediction errors in subject S3 - From top to bottom, the NRMS and NPE error for a 6-s, 18-s, and 30-s prediction horizon and estimation error, respectively.

TABLE 3.3 – Computational time of different prediction horizons

Prediction horizon	Elapsed time (ms)
2s	0.264
6s	0.275
18s	0.349
30s	0.488

provide suitable stimulation for compensating such sudden change. Otherwise, the controller will wait for reestablishment of prediction quality. In order to investigate the filter's behavior in response to such sudden torque changes, a resistive torque is simulated in an arbitrarily selected period. For subject S3, the amplitude of torque is decreased to 85% of the original value from instant 19 s to 24.8 s. For the implanted subject, the amplitude of torque is decreased to 80% of the original value from instant 25.9 s to 31 s. The behavior of the filter and the evolution in the prediction errors for a prediction horizon of 6 s are analyzed and plotted in Fig. 3.8 and Fig. 3.9.

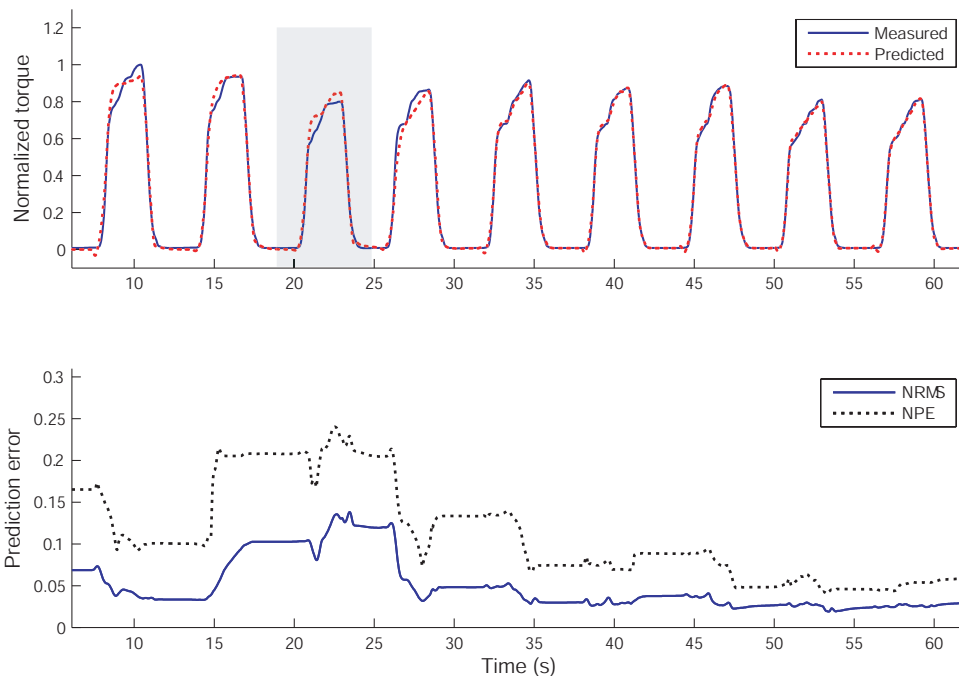


FIGURE 3.8 – (Top) The original torque is decreased from 19 s to 24.8 s to 85% of its original value in subject S3. (Bottom) The prediction errors of the 6 s horizon indicate a big prediction error against such an event. Nevertheless, the estimator reestablishes the prediction quality in 12 s.

As the reflex that occurs during stimulation of motor point in surface FES certainly affects muscle response, the adaption of the filter to such an event is also investigated. For subject S3,

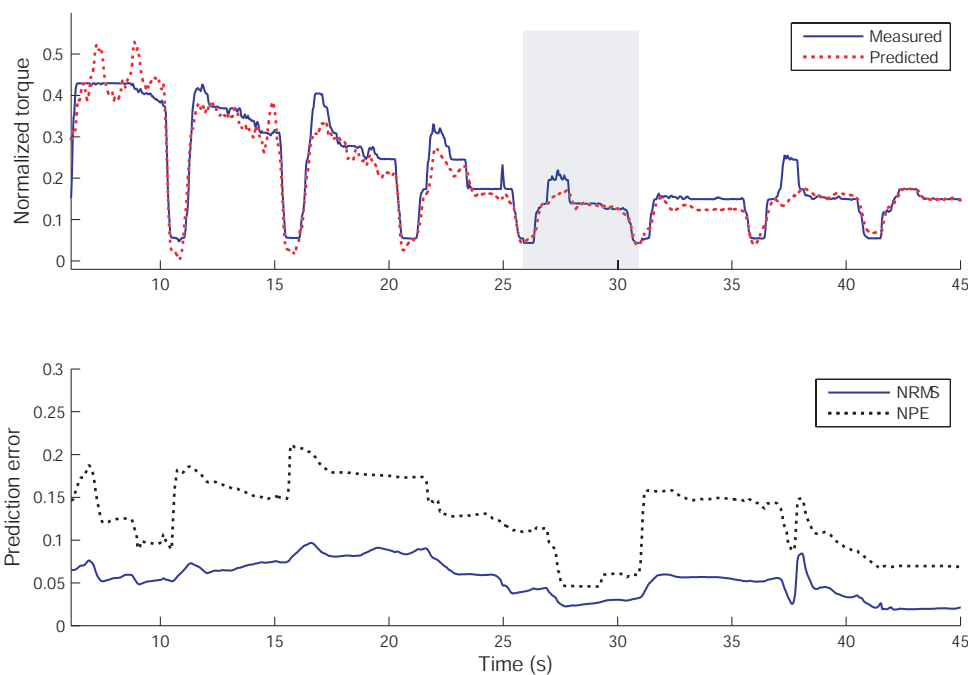


FIGURE 3.9 – (Top) The original torque is decreased from 25.9 s to 31 s to 80% of its original value in the implanted subject (fatigue sequence 2). (Bottom) The prediction error of a 6-s prediction horizon indicates fast filter adaptation to such sudden change.

additional torque with a value equal to 10% of the original value is induced from 30.8 s to 37 s. For the implanted subject, additional torque with a value equal to 20% of the original value is induced from 20.8 s to 25.9 s to simulate any other source resulting in additive torque. The prediction results and prediction errors of the 6-s prediction horizon are plotted in Fig. 3.10 and Fig. 3.11.

3.4.2.4 Discussion on Filter Predictive Performance

Given the identification accuracy as shown in Fig. 3.3 and Fig. 3.4, the identification errors are large at the corner between adjacent trains and during initial potentiation (Fig. 3.4). However, except for these cases, the small estimation errors indicate suitable identification of the model. Although increasing the model order of the PHM may improve prediction quality, the improvement is not significant. Therefore, the model order is kept small to avoid possible instabilities and aggressive computational cost.

The prediction results presented in Fig. 3.7 reveal good performance of the predictive filter, which successively acquires the mechanical behavior of the muscle under FES. In addition, the error values given in TABLE 3.2 indicate that neither NRMS error nor NPE increases significantly when the prediction horizon is extended. This indicates that the proposed eEMG-to-torque model properly fits muscle behavior. If the prediction quality degrades when an expanded prediction horizon is selected, this is probably due to the variations in severe internal or external disturbances during the horizon. For instance, continuous stimulation may result in severe muscle fatigue over a short time. In this case, a possible solution is to select a smaller forgetting factor

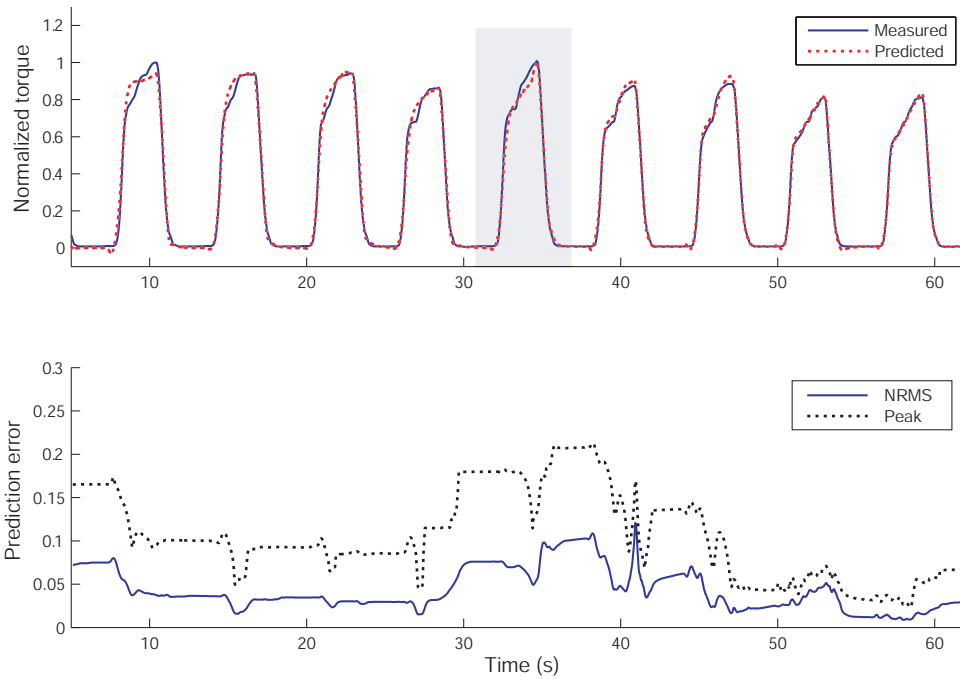


FIGURE 3.10 – (Top) Additional torque disturbances with a value equal to 10% of the original value for simulating reflex is induced from 30.8 s to 37 s in subject S3. (Bottom) The prediction quality of the 6-s horizon is quickly reestablished after the disturbances.

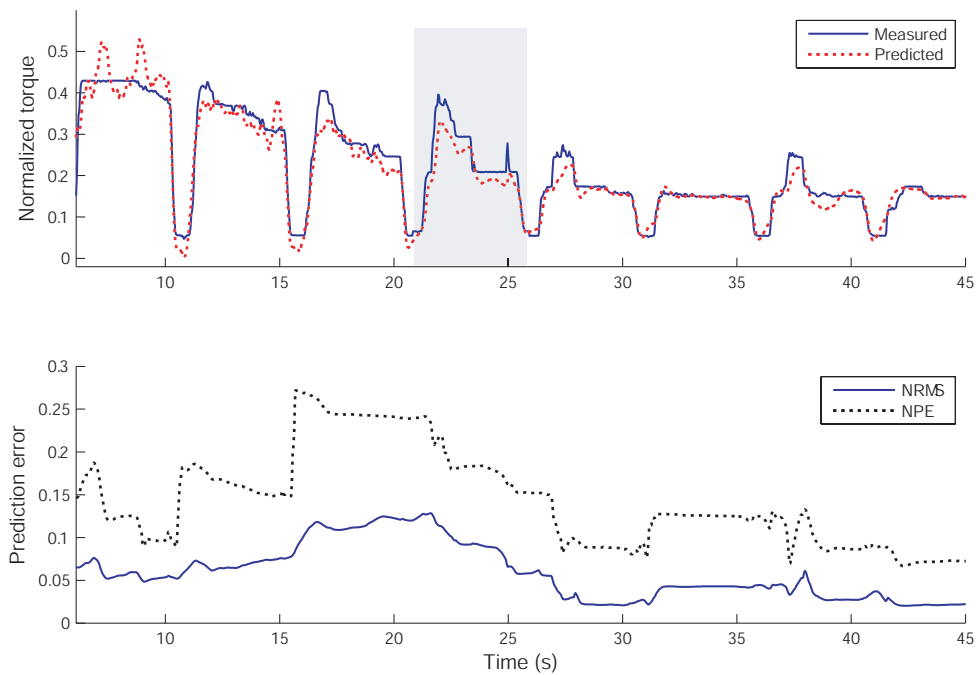


FIGURE 3.11 – (Top) Additional torque with a value equal to 20% of the original is induced from 20.8 s to 25.9 s in the implanted subject (fatigue sequence 2). (Bottom) The prediction error of a 6-s prediction horizon indicates fast filter adaptation to such an event.

that allows the forgetting of more previous information. Furthermore, the computational power with various prediction horizons is high enough to be implemented in real-time identification.

The adaptive capability of the filter to torque variations due to unexpected torque changes is presented in Fig. 3.8 and Fig.3.9. Observing the prediction error, the filter takes approximately twice as much time to re-adapt the torque changes and then stabilizes at a low level. Reflex is another challenging physiological phenomenon in the FES system, such as correcting drop foot via the withdrawal reflex in surface FES. The prediction performance reacting to additive torque variations (such as reflex) is shown in Fig. 3.10. Another example of reacting to additional torque in the implanted FES is shown in Fig. 3.11. The filter in both conditions reestablishes the prediction quickly after the disturbances.

3.4.3 Robust Fatigue Tracking

The fatigue tracking method described above assumes torque measurement is always available, and the model parameters are updated immediately when new measurements are obtained. Then the identified parameters are applied to predict torque in a prediction horizon. As a result, tracking is not robust to disturbances caused by sensing failure. In order to resolve this problem, torque prediction is integrated into a fatigue tracking task. The objective is to use joint torque estimated by KF to bridge the period of disturbances or the absence of torque sensing.

Any event such as interrupted or unreliable torque measurement is assumed to result in such tracking failure. If the prediction tracks the measured torque well, this suggests that when torque measurement is unavailable or unreliable, the predicted torque based on eEMG can be used to bridge such gaps to perform the model-based FES control. Otherwise, they are just used for bridging the unexpected events, and the controller will wait for sufficient tracking quality. This procedure can be explicitly accomplished in a predictive controller by specifying suitable output and/or input constraints, which can be obtained for each subject in a pre-experiment.

The idea for verifying the robustness of the filter is that, assuming measurement is unavailable or unreliable from time instant t_0 to t_1 , the identified model at t_0 can be used to predict the torque induced by stimulation until instant t_1 , as shown in Fig. 3.12. When prediction is executed, the model is only driven by the eEMG and identified model at t_0 , while model updating is suspended. To evaluate the prediction performance in different muscle fatigue states, this process is repeated until the end of stimulation, where the measurement update in KF is switched off for 18 s.

Fig. 3.12 and Fig. 3.13 illustrate fatigue tracking performance in subjects S3 and S1 for surface FES. The predicted torque is calculated either with identification on or with identification off as indicated in the figure. The parameter evolutions have been partly plotted in these figures. As a whole, the model changes over time representing variant muscle systems, as seen from the variant model parameters. When identification is suspended, the model parameters maintain stationary, while the torque can still be well tracked. More results on other subjects are shown in Appendix C. The forgetting factor is still fixed at 0.997 for these subjects in surface FES. The high tracking quality may result from two factors. One is that the Hammerstein model is suitable to catch the muscle electrical mechanical behavior under isometric condition. The other is that the intermittent stimulation protocol causes a slow fatigue rate, which yields a time-variant but

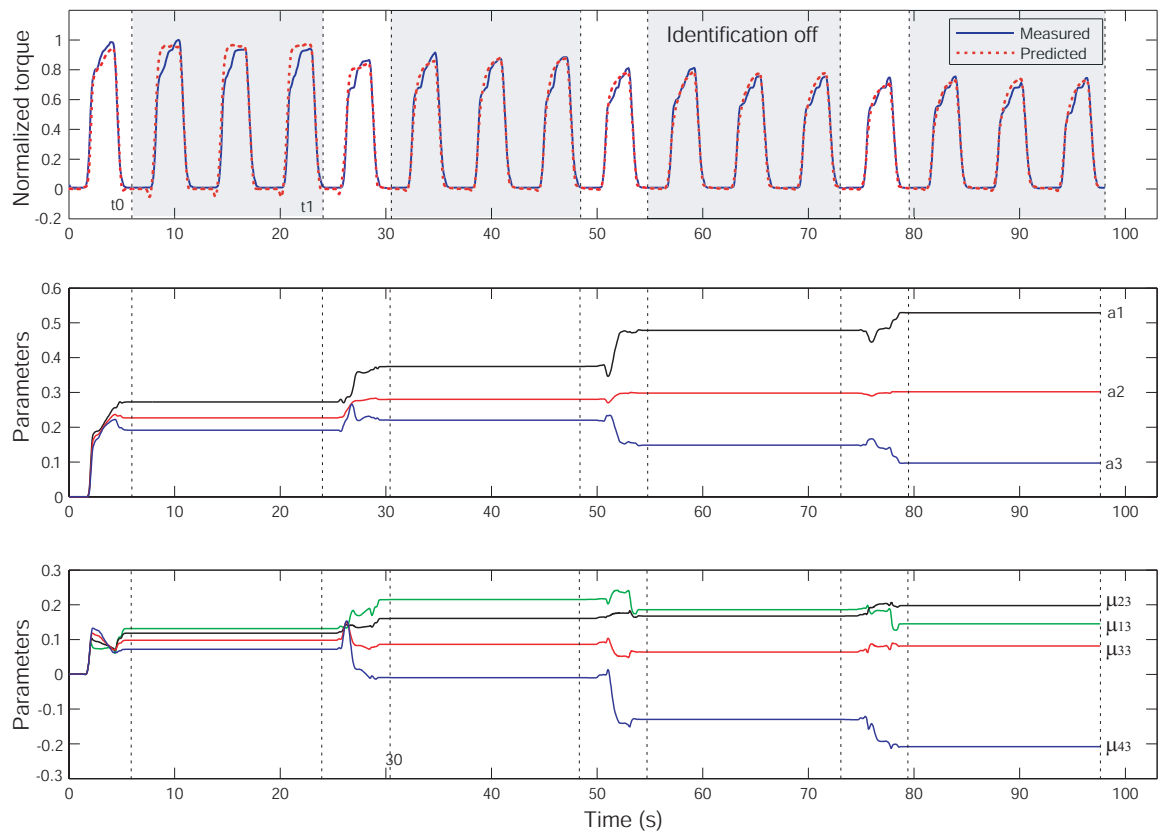


FIGURE 3.12 – Robust fatigue tracking based on the eEMG-to-torque model and KF in subject S3. The model identified at t_0 is used to predict the torque from t_0 to t_1 , while the online identification is switched off for 18 s (with background color in the upper plot). The predicted torque is accurate enough for use in a model-based controller. Middle : The identified model parameters of the past torque. Lower : The identified model parameters of the 3rd power of the past eEMG. The identified model parameters are maintained stationary during identification off.

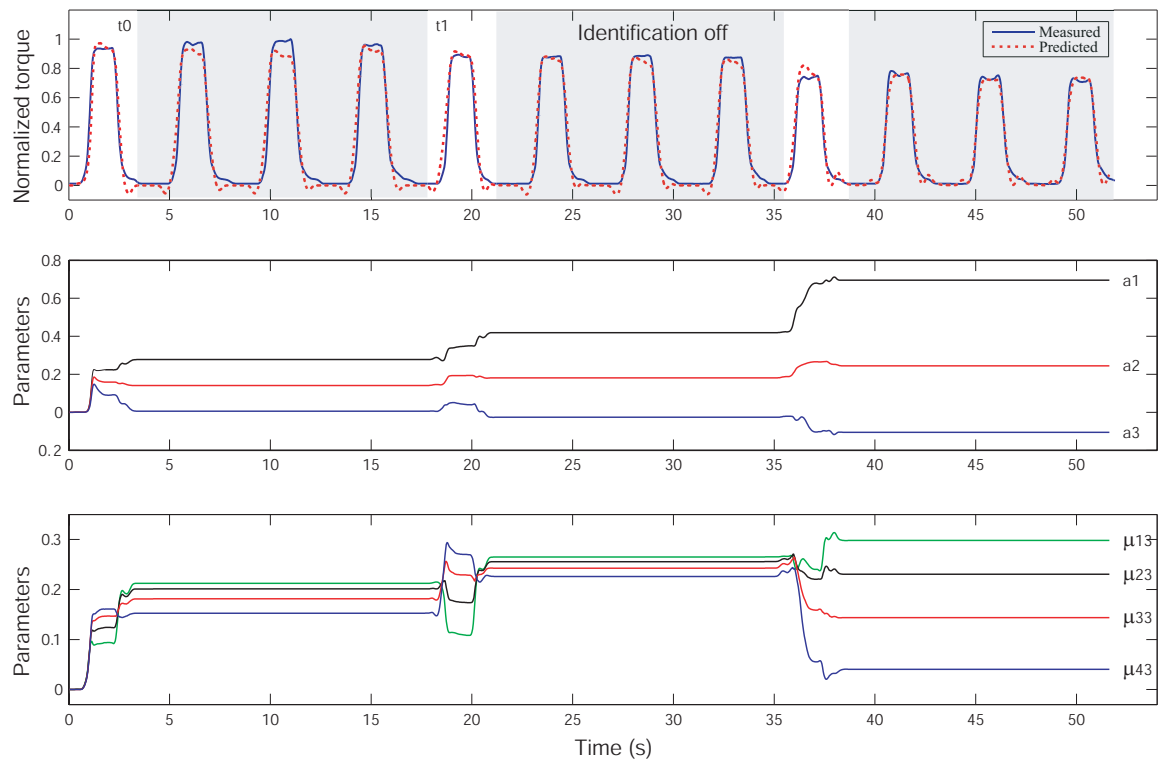


FIGURE 3.13 – Robust fatigue tracking based on the eEMG-to-torque model and Kalman filter in subject S1. The model identified at t_0 is used to predict the torque from t_0 to t_1 , while the online identification is switched off for 15 s (with background color in the upper plot). The identified model parameters are maintained stationary during identification off.

stable muscle system as shown in Fig. 3.5. Consequently, the KF is suitable to track the gradually time-varying fatigue by adaptively identifying the model.

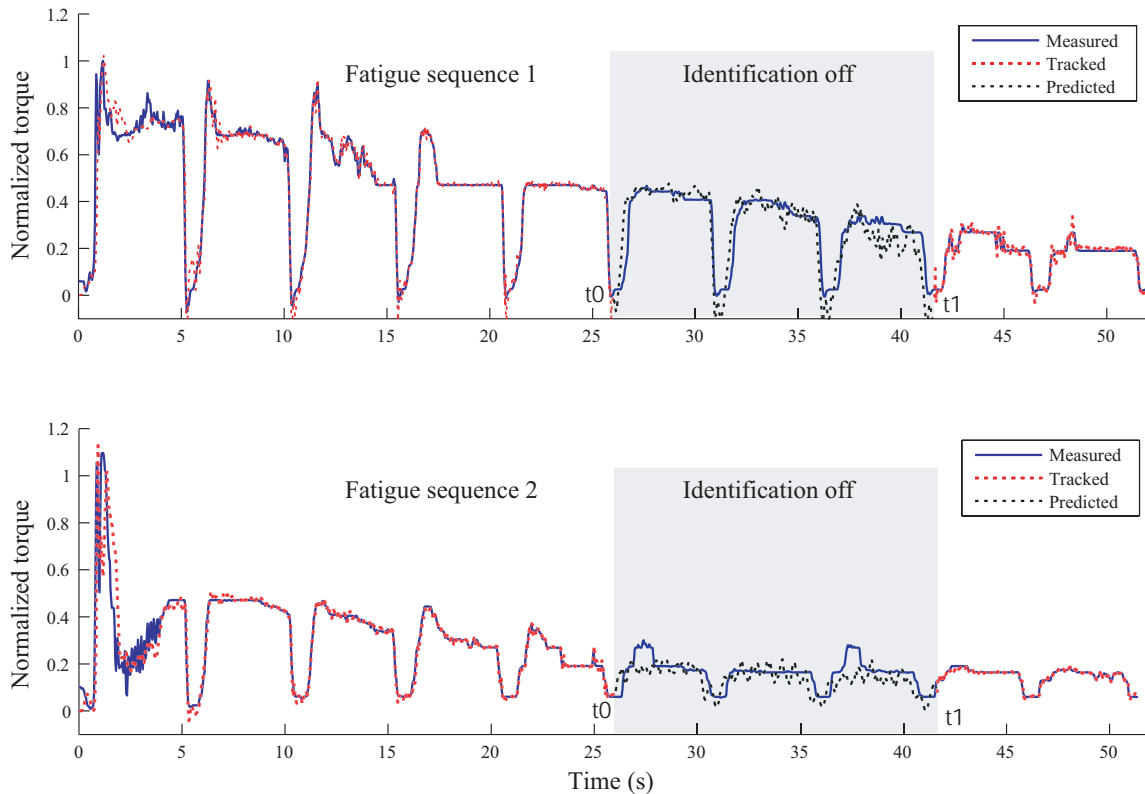


FIGURE 3.14 – Robust fatigue tracking based on the eEMG-to-torque model and Kalman filter in implanted FES. The model identified at t_0 is used to predict the torque from t_0 to t_1 , where the online identification is suspended for 15 s. The forgetting factor is chosen at 0.97 to react to the fast fatigue under continuous stimulation condition.

As continuous stimulation produces a higher fatigue rate in comparison with the intermittent pattern, when assessing the robustness of the filter to track fatigue in such conditions, the forgetting factor is preferably lower to react to muscle changes quickly. The measurement failure is simulated by suspending the prediction phase of KF at an arbitrary instant t_0 . To reestablish the tracking of muscle fatigue, the identified model at t_0 is used for the prediction of torque generation for 15 s. To reveal the accuracy of the predicted torque, the measured torque is also shown for comparison. The results of two fatigue sequences in the implanted subject are illus-

trated in Fig. 3.14. Note that the torque and MAV of eEMG in both sequences are normalized by the maximum values in fatigue sequence 1.

3.4.4 Discussion

Stimulus-evoked EMG has been previously proposed to predict the mechanical behavior of muscles in FES rehabilitation systems [Tepavac and Schwirtlich, 1997] [Erfanian et al., 1998]. These prediction methods were investigated on the hypothesis of a fixed eEMG-to-torque model during stimulation. Other researchers found that this relationship is time-variant under different muscle conditions [Mizrahi and Isakov, 1994] [Yu and Chang, 2009]. However, they did not propose a feasible, effective method to resolve the torque prediction problem in a systematic way. In this work, we also found the time-varying property of myoelectrical and mechanical muscle behavior from experiments on SCI subjects. This implies the limitations of the torque prediction method based on the fixed eEMG-to-torque model, and increases the difficulties of torque estimation when muscle response is time-variant. The present work proposes the use of the PHM to represent muscle contraction dynamics with the MAV of eEMG as input, with an adaptive identification method performed by a KF with forgetting factor.

In the simulation study, both stationary and extremely time-variant systems are simulated. As the SNR of the experimental data is approximately 37 dB, additional noises with SNR of 25 dB and 50 dB were added to corrupt the system output, respectively. The KF adaptively identified the model and tracked the real parameters well even when the simulated output was quite noisy. The forgetting factor was chosen at 0.97 as the parameters all change fast; for example, parameter μ_{21} increased eleven times from 0.1 to 1.2 within 50 s. If the model varies slowly, a bigger forgetting factor is preferred to improve the tracking performance and avoid divergence.

With the experimental data, the plots of z-poles display a slow time-variant but stable muscle contraction system in such a stimulation situation. The adaptive performance of the filter is verified by simulating internal and external perturbations. Unexpected torque reduction due to environmental contact is simulated; the filter presents sufficiently fast adaptivity to such torque amplitude changes. The filter also adapts to external force or reflex phenomena in a short time compared with the duration of the events. The robustness of the torque prediction method is verified in terms of torque sensing failure. From the results of the surface intermittent FES system, Fig. 3.12 and Fig. 3.13, the torque predictions during the suspended model updating are still accurate, and they can thus be used in a model-based controller. Although the torque prediction has some oscillations in the implanted continuous FES system, the torque does not deviate extremely. Moreover, we find that the torque tracking in all these results is accurate and converges quickly after the failure event. This phenomenon means the predicted torque successfully bridges the gap resulting from sensing failure. Therefore, although the controller does not use the predicted torque to adaptively modulate the stimulation pattern, it can wait for the ending of the event and retrieve high tracking performance.

The muscle contraction dynamics model were described in a previous work [Erfanian et al., 1998], where the recursive least squares method was used for identification in percutaneous continuous stimulation. However, there was no consideration of different fatigue states, or subject-specific and protocol-specific differences. In this study, the proposed identification method is validated for ankle torque prediction and fatigue tracking using processed

eEMG signals under isometric condition. A promising next step would be to verify this in dynamic conditions by introducing a torque-joint angle model combined with the proposed muscle model, as proposed in [Farahat and Herr, 2005].

Even though the forgetting factor is empirically chosen, $\lambda = 0.97 \sim 0.997$ is considered suitable in these experiments. As an improper forgetting factor may lead to divergence or misestimation, an adaptive forgetting factor can hopefully improve the prediction adaptation and accuracy. A simple solution is using a big forgetting factor at the beginning of the recursion, when the muscle state is relatively stable, and using a smaller one later, when the muscle response tends to be time-variant with prolonged or repetitive stimulation.

In this work, we did not consider the effect of day-to-day changes, but the online identification is able to identify parameters for different subjects. Therefore, as long as we do not intend to research how the parameters change depending on the experimental set-up—for example, electrode position—this method itself can work even if there are day-to-day changes. Of course, it is important to investigate the effect of different experimental set-ups. In this case, we may introduce a tuning function to offset the day-to-day variances, and to assess the underlying relationship between these variances and the corresponding conditions.

3.5 Conclusion

The objective of this work is to develop a model-based FES controller for muscle fatigue compensation. As FES induces fast fatigue and unexpected disturbances, whereas the patients cannot perceive the muscle fatigue, accurate torque estimation is essential to feedback muscle output for adaptive adjustment of the stimulation. In this work, we confirm that muscle contraction dynamics are time-varying with FES. A time-varying eEMG-to-torque model was employed to represent the electrical and mechanical behaviors of stimulated muscle, with the model parameters identified by a KF with forgetting factor. The predictive performance of the adaptive identification method has been validated in simulation and with experimental data. The results demonstrate sufficient adaptivity to internal muscle changes or external disturbances in a systematic way.

In terms of improvements in fatigue tracking, when the measurement of the torque sensor suffers from recording interruption or distortion, the proposed method could bridge these problems and provide sufficiently accurate fatigue tracking only on eEMG measurement. The success of torque prediction only based on eEMG is significant in FES. In addition, we may have good torque estimation ability both in surface and implanted FES. On the basis of predicted torque, the torque can be used in a model-based predictive controller aiming at torque control. In the classic FES system, the actual muscle activation is never explicitly taken into consideration. However, since the muscle response is time-variant, it is essential to improve and even break the limitations of the current FES control paradigm. The next chapter focuses on the novel FES control strategy with EMG-feedback function.

CHAPTER 4

EMG Feedback Predictive Torque Control in FES

Contents

4.1 Control System for Movement Induced by FES	78
4.2 Previous Works	80
4.3 Muscle Excitation and Contraction Model	81
4.4 Controller Design	83
4.4.1 Nonlinear Generalized Predictive Control	83
4.4.2 Closed-Loop Implementation of the Dual Predictive Controller	85
4.5 Evaluation of Predictive Performance for Drop Foot Correction	87
4.5.1 Experimental Validation of Predictive Torque Control	88
4.5.2 Simulation Results on Predictive Control Performance	96
4.6 Discussion	97
4.7 Conclusions	100

In this chapter, an EMG-based feedback system for predictive control of FES is proposed, rather than conventional position control, in order to achieve closed-loop torque control for a more accurate, safe and robust FES system. An FES system delivers electrical charges that are determined by a control unit to excitable motor neurons, in order to contract target muscle. The intended movement is achieved by the correct stimulation pattern, which depends on the specific applications and stimulation interface. The challenge in the present FES system starts with the problem of how to process the high nonlinearity and complexity of musculoskeletal systems, which complicate the model identification process. Another challenge arises from time-varying muscle dynamics due to physiological and biochemical factors (such as fatigue, reflex), as these need to be compensated in order to augment the applications of FES. In addition, as most patients who would benefit from FES have lost both motor function and sensory function, safe and natural stimulation pattern is particularly important. Therefore, in this work, eEMG feedback, which represents muscle activity, contributes by taking the muscle state into account in the FES control system. The predictive nature facilitates the prediction of the muscle response and therefore the system can respond to the time-variant muscle state changes in advance. The following section presents the experimental data collected from healthy subjects in an FES-induced drop foot correction protocol. The control performance, robustness, and fatigue compensation ability are evaluated and discussed on the basis of experimental and simulation studies.

4.1 Control System for Movement Induced by FES

The conventional control systems for FES are illustrated in Fig. 4.1. Most current FES systems work in an open-loop paradigm (Fig. 4.1 (a)), where predefined stimulation patterns are delivered to the muscle without feedback on the real response. When the actual trajectory is not suitable for performing the desired task, the stimulation pattern cannot be accordingly adjusted. The application of an open-loop FES system is thus limited due to the degradation in performance caused by muscle state changes or other disturbances. The currently used manual FES modulation (such as a hand switch) tends to cause distraction and is thus suboptimal. Compared with open-loop control, a closed-loop controller is superior as it feeds back useful information on the current state of the system for regulating system input in accordance with the desired output. A sensor-based closed-loop control scheme is shown in Fig. 4.1 (b). It is driven by the errors between the actual trajectory and the desired trajectory. The integration of more available sensors would be beneficial to provide more useful information, but mounting, calibrating and computing the time of signal processing are complicated in implementation. In this context, the standard Proportional Integral Derivative (PID) controller and extended PID controller have been investigated. However, tuning the PID parameters to produce satisfactory tracking performance and robustness is difficult. The model-based closed-loop controller shown in Fig. 4.1 (c) is a promising means to deal with the nonlinear and time-varying characteristics of the musculoskeletal system. Model-based control techniques, such as feed-forward and predictive control strategies, require sensors and dynamic models of the system, as well. The FES control performance would thus be enhanced by a model-based controller if sufficient knowledge of the system were available.

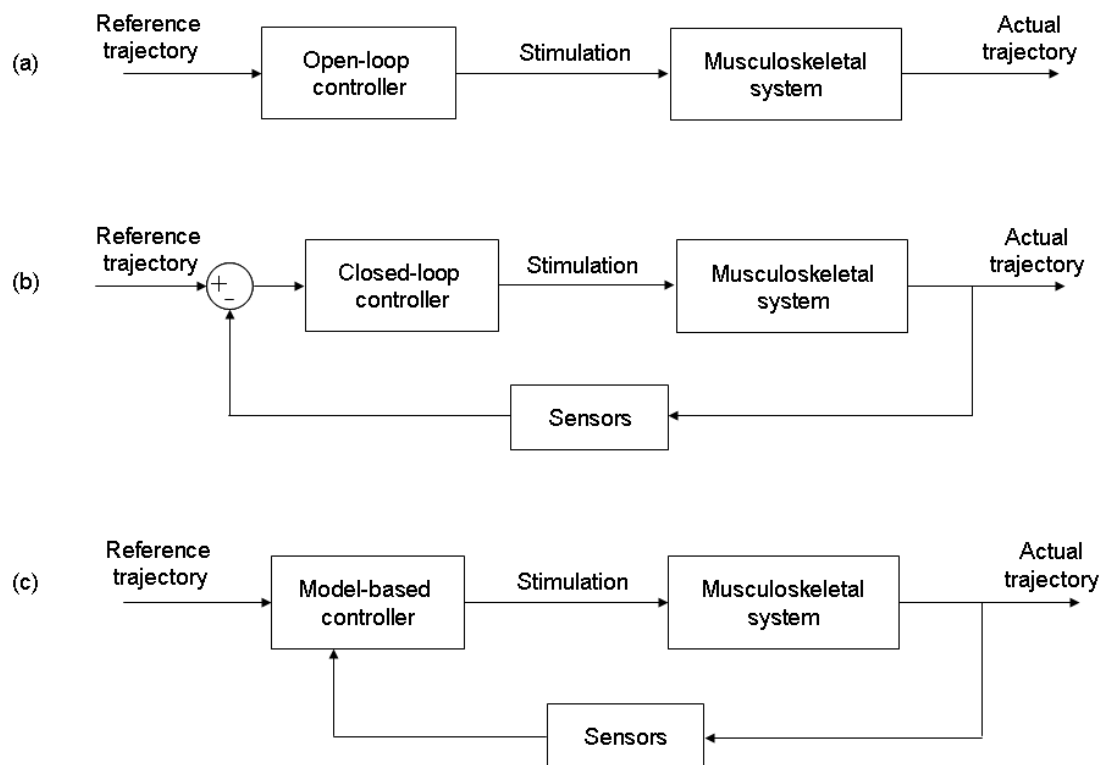


FIGURE 4.1 – Organization of traditional functional electrical stimulation control systems : open-loop (a), closed-loop (b) and model-based control scheme (c) [Popović and Sinkjær, 2000].

4.2 Previous Works

In the current FES systems, closed-loop control has been investigated in the lab but has not been widely applied in practice. Regarding the scenario of lower limb FES closed-loop control, one goal has been to adaptively modulate the stimulation onset according to effects, such as walking speed, gait rhythm, or the intentions of users. For example, when the movement event was detected through physical sensors such as force-sensing resistor [Liberson et al., 1961], accelerometer and gyroscope [Williamson and Andrews, 2001], the stimulation was triggered when necessary to accomplish a task. In [Chen et al., 2001], a closed-loop FES system controlled by position sensors and triggered by a foot-switch was proposed. A micro-controller dynamically adjusting the FES intensity through a built-in algorithm was presented in [Breen et al., 2006], which was able to generate a stimulation envelope with any shape, reflecting walking speed changes. By taking advantage of EMG signals, an eEMG-triggered FES control system was presented through a pattern recognition approach, and the eEMG signals were collected from upper trunk above-lesion sites [Kordylewski and Graupe, 2001]. In another work [Dutta et al., 2008], the FES system was triggered by the recognition of the patient's intention from eEMG signals from incompletely paralyzed muscles. Natural sensory feedback provided another solution for closed-loop FES control [Haugland and Sinkjaer, 1995] [Djilas, 2008], when a recording implant was available. These works contributed to the adaptive adjustment of the stimulation onset with regard to walking speed or walking surface. However, they did not compensate muscle property changes, nor did they provide a reliable stimulation pattern for the desired complex movement (such as stepping up/down stairs with different stair heights, or various sports movements).

To achieve a reliable stimulation pattern and compensate muscle property changes during FES, the ideas have varied from a sensor-based approach to a model-based approach. All these works investigated knee joint angle control in FES and have been reviewed in section 1.4.3. For example, in [Ferrarin et al., 2001], the authors suggested using model-based approaches to achieve an efficient and robust FES system. In [Jezernik et al., 2004], a sliding model closed-loop control method was proposed to control shank movement. Another work [Ajoudani and Erfanian, 2009] combined the classic sliding model control and a neural network to control FES to track the desired knee joint trajectory. In these works, the feedback signal was based on joint motion recording. However, as muscle contraction is induced by artificial stimulation in FES, the drawback of closed-loop control of joint motion is that the resultant motion may not only derive from stimulation but also from external forces (such as environmental contact). A stimulation pattern based only on motion sensors is likely to be unsafe and unreliable in this case.

By using eEMG signals, the stimulation was adjusted according to the intended motion functions, which were obtained from EMG-based pattern recognition in [Graupe et al., 1989]. In another work [Winslow et al., 2003], the authors proposed a method to indicate when to add stimulation signals for fatigue compensation, via two artificial neural network modules. Their control purpose was to maintain the joint angle at a constant level. However, neither group considered how to compensate the torque changes arising from various fatigue levels or the subject-specific variations. In this work, eEMG is used as the feedback of actual muscle activation information, which is useful to predict torque and then to achieve torque control

rather than position control. This chapter aims at developing an FES control strategy based on FES-evoked EMG feedback from stimulated muscle to induce the desired torque trajectory.

Furthermore, the stimulation pattern of FES should be reliable to avoid over-stimulation, for the safety of patients. Smooth and natural muscle activation is desired due to the limitation of muscle response rate. That is, even if the stimulation should be suddenly changed, muscle cannot respond to such input due to the limitations from physiological natures. Therefore, assuming that the muscle response is predictable, by using a predictive control method, we can regulate the stimulation pattern before they are delivered. From these considerations and assumption, a model-based predictive control strategy taking the eEMG signal as feedback is proposed in this work. Predictive control has been widely applied in chemical or biomechanical situations with a variety of interesting benefits, such as conceptually simple treatment of control constraints and the cost function in the optimization [Camacho and Bordons, 1999]. In the domain of FES, several simulation studies can be found in [Mohammed et al., 2007] and [Esfanjani and Towhidkhah, 2005] for different purposes.

This chapter first introduces the muscle excitation and contraction model and their state-space representation briefly. Next, an EFPC consisting of two Nonlinear Generalized Predictive Control (NGPC) is addressed. Experimental data from FES-supported drop foot correction are used to validate the control scheme and some simulation studies are conducted. Finally, discussion on this control strategy and future perspectives are given.

4.3 Muscle Excitation and Contraction Model

In FES, external electrical currents are used to excite the peripheral motor nerves via surface or implanted electrodes ; action potentials are subsequently generated and propagate toward the muscle. When the action potentials reach the target muscle, the muscle contracts and produces joint torque and then joint movement. Joint torque control is carried out by adjusting stimulation parameters, either stimulation frequency, stimulation amplitude or PW. By introducing an additional EMG sensor to accompany the torque sensor, the muscle excitation and contraction dynamics are respectively modeled. Just as the muscle contraction dynamics are modeled by a PHM model, a PHM is also applied to describe the muscle excitation responding to the stimulation impulses. This model structure is able to represent a time-varying nonlinear process, as described in Chapter 2 and Chapter 3.

For complete and subsequent usage, the model structure of a PHM is recalled and reformulated in order to separately identify the parameters of the linear and nonlinear terms in PHM. This separation is useful to employ a predictive controller without approximating the nonlinear model. Although two PHM models are involved to resolve the control problem of both the excitation and contraction processes, a generic PHM structure and its state-space form are introduced here for simplification as they have the same structure. By modeling the linear and nonlinear parts of the Hammerstein cascade with an ARX and a polynomial basis function, respectively, the PHM at a given time k is parameterized as :

$$f(u(k-i), y(k-i), \theta) = \sum_{i=1}^l a_i y(k-i) + \sum_{i=1}^m \sum_{j=0}^n b_i \gamma_j [u(k-i)]^j \quad (4.1)$$

Note that the MAV of the eEMG is the input u of the contraction dynamics, but for simplification,

the abbreviation of eEMG is used instead of the MAV of eEMG in the following description. The weights of inputs are separated for linear and nonlinear terms, rather than being coupled as in (3.1).

The delivered stimulus, the collected eEMG, and the torque signals are provided to identify both the muscle excitation and contraction models, as shown in Fig. 4.2. Apparently, the eEMG acts as the output of the excitation model with stimulation as the input, as well as the input of the contraction model with joint torque as the output. To indicate the two distinct statuses of eEMG in these two models, different notations are used for eEMG, with u as input and y as output. Furthermore, the model input u , the unmeasurable internal variable h , and the model output y in the above-mentioned generic formulation are substituted by u_s, h_s, y_m in the excitation model and u_m, h_m, y_t in the contraction model, as shown in Fig. 4.2.

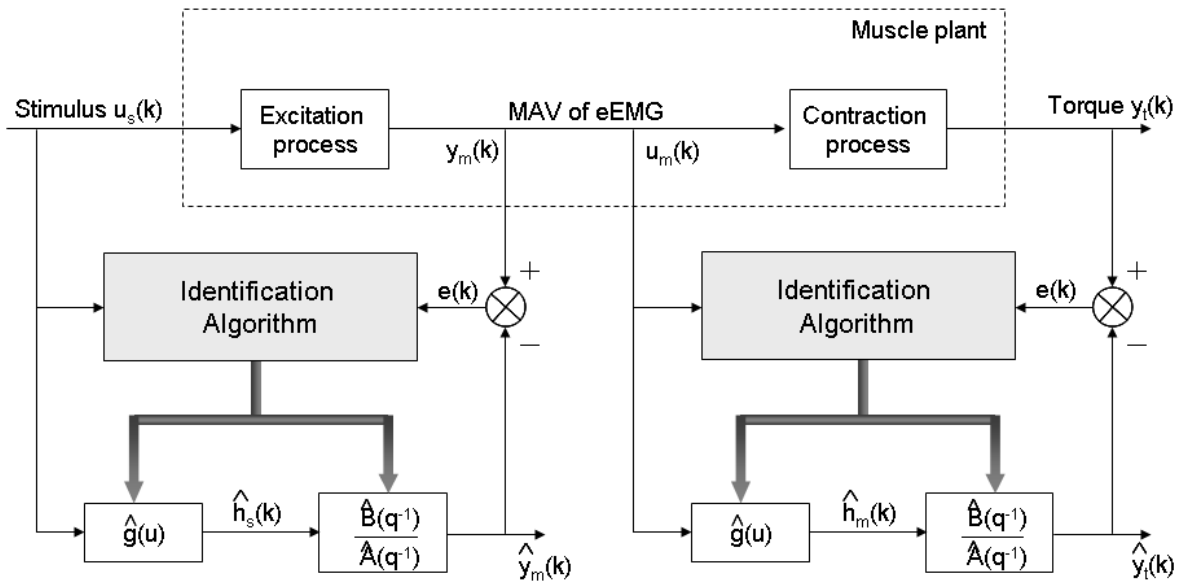


FIGURE 4.2 – Model structure of stimulated muscle for model identification. The contraction dynamics model relates eEMG to torque. The excitation dynamics model relates stimulation to eEMG.

With the same model structure representing the muscle excitation and contraction dynamics, the identifications of both models are processed in the same way. The only difference is that data sets $(u_s(i), y_m(i))$ are prepared to identify the stimulation-to-eEMG model, while data sets $(u_m(i), y_t(i))$ are prepared to identify the eEMG-to-torque model. When constructing the state-space form of the generic PHM (l,m,n) model, the following process equation is used instead of the equation (3.5) in Chapter 3 :

$$\mathbf{x}(k) = \underbrace{\mathbf{A}\mathbf{x}(k-1) + \mathbf{B}\Psi\mathbf{u}(k-1)}_{\mathbf{f}(\mathbf{x}(k-1), \mathbf{u}(k-1), \mathbf{w}(k))} + \mathbf{w}(k) \quad (4.2)$$

where $\mathbf{u}(k-1)$ is the previous model input as (3.6) and subscript k denotes the current time step. The current state vector $\mathbf{x}(k) = [x_1(k) \ x_2(k) \ \cdots \ x_q(k)]^T$, $q = \max(l, m)$. Matrix $\mathbf{A} \in$

$\mathbb{R}^{q \times q}$ correlates the previous states with the current states as (3.7). Vector \mathbf{B} and Ψ contain linear and nonlinear weights of eEMG,

$$\mathbf{B} = [b_1 \ b_2 \ \cdots \ b_m]^T \quad (4.3)$$

$$\Psi = [\gamma_0 \ \gamma_1 \ \cdots \ \gamma_n] \quad (4.4)$$

Thus, the linear and nonlinear parameter vectors can be written as

$$\theta_l = [a_1 \ a_2 \ \cdots \ a_l \ b_1 \ b_2 \ \cdots \ b_m]^T \quad (4.5)$$

$$\theta_n = [\gamma_0 \ \gamma_1 \ \cdots \ \gamma_n] \quad (4.6)$$

This improvement is meaningful for the direct application of the predictive control scheme with the linear part of the PHM model. Next, all the time-varying states and parameters involved are identified concurrently by KF with forgetting factor, as proposed in Section 3.3.2.

4.4 Controller Design

This work aims at developing an EMG feedback closed-loop control strategy which can adaptively modulate the stimulation pattern to obtain the desired torque trajectory. This control scheme is developed based on the two internal PHM models described above. Accordingly, the controller consists of two NGPC in series, as shown in Fig. 4.3. The control target is to generate an optimal stimulation signal u_s to produce the desired isometric joint torque y_d . The main idea is to use the eEMG signal for a dual purpose resulting in EFPC, which involves an activation controller and a stimulation controller. The activation controller takes eEMG as the control signal m_d to drive the predicted torque y_p , close to the desired torque trajectory y_d , based on the contraction dynamics model. The stimulation controller takes m_d obtained from the activation controller as the desired eEMG trajectory, so that the control signal, stimulation PW u_s , is computed to drive the predicted eEMG m_p close to m_d , based on the excitation dynamics model. In both the activation controller and the stimulation controller, the same model structure — a generic PHM model — is used for process prediction and optimization. Therefore, the overall control problem can be reduced to resolve two single NGPC problems. The link between these two NGPC controllers lies in that, at each sample time, the output of the activation controller is used as the input of the stimulation controller. Therefore, in the next section, the control solution based on a single generic PHM model is discussed. The notations are kept consistent, as described in section 4.3.

4.4.1 Nonlinear Generalized Predictive Control

As a whole, the solution of a single NGPC consists of two parts : a linear part and a nonlinear part, as shown in Fig. 4.4. The control problem of the linear part is first resolved by the Generalized Predictive Control (GPC) algorithm, which has been described in a number of publications such as [Camacho and Bordons, 1999] and [Zhu et al., 1991]. Although different methods can be used to obtain the control law of GPC, the general idea is to minimize a multistage cost

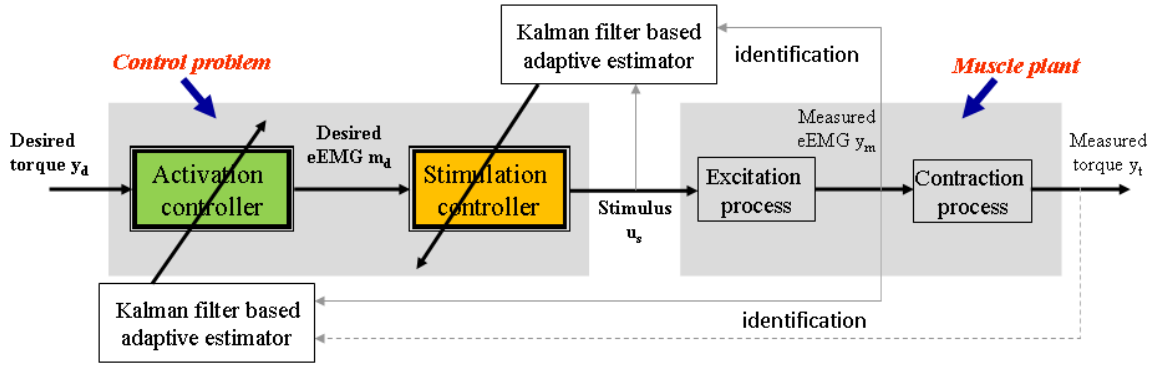


FIGURE 4.3 – Diagram illustrating the EMG-feedback predictive control strategy. The control signal obtained from the activation controller is used as the desired reference of the stimulation controller. In each controller, a nonlinear generalized predictive control algorithm is applied based on a PHM model. The torque measurement y_m and eEMG measurement m_m are only used for model identification, as shown by the dashed lines.

function given by

$$J = \sum_{j=1}^{N_p} \xi_j [\hat{y}_{k+j|k} - v_{k+j}]^2 + \sum_{j=1}^{N_u} \delta_j [\Delta h_{k+j-1}]^2 \quad (4.7)$$

where $\hat{y}_{k+j|k}$ is an optimum j -step ahead prediction of the controlled variable using data up to time instant k , v_{k+j} is the future reference trajectory, and $\Delta h_{k+j-1} = h_{k+j|k} - h_k$ is the increment of control action. Weighting coefficients ξ_j , δ_j respectively penalize the tracking performance regarding $\hat{y}_{k+j|k}$ and the smoothness of the control signal regarding Δh_{k+j-1} . N_p is known as the prediction horizon and the control horizon is N_u ; $1 \leq N_u \leq N_p$ implies that all the increments of the control effort are assumed to be zero for $j > N_u$.

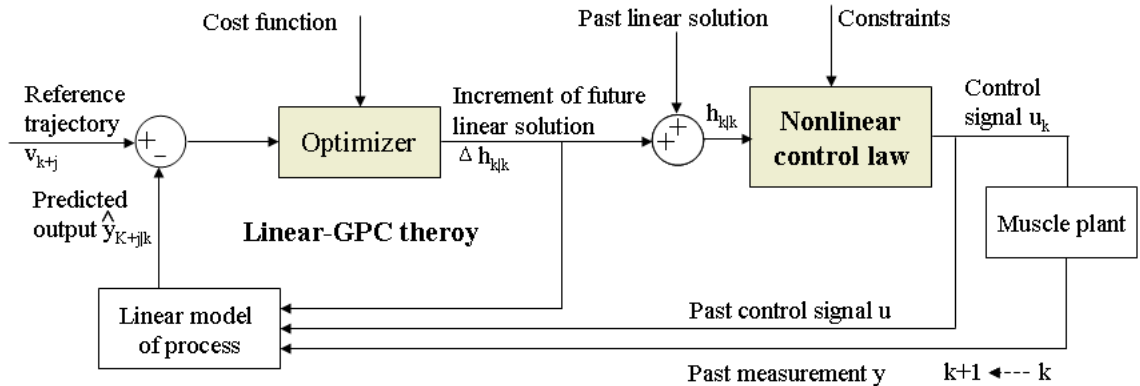


FIGURE 4.4 – A single nonlinear generalized predictive controller based on a PHM model. The linear solution is provided by the linear generalized predictive control law. The nonlinear solution is obtained by resolving a polynomial function.

In this work, a simpler formulation of GPC is applied to resolve the linear control problem, instead of solving recursive Diophantine equations [Albertos and Ortega, 1989], with the main

idea described in Appendix C.1. In short, the optimization problem is computed online and in real-time in terms of the control action sequence $[h_{k|k}, h_{k+1|k}, \dots, h_{k+N_u-1|k}]$, so that the predicted controlled variables $[\hat{y}_{k+1|k}, \hat{y}_{k+2|k}, \dots, \hat{y}_{k+N_p|k}]$ follow a desired reference trajectory $[v_{k+1}, v_{k+2}, \dots, v_{k+N_p}]$.

The control signal $h_{i|k}$, $i = k \sim k + N_u - 1$ computed by GPC is a solution of the linear predictive control problem at step k , which is required to be applied to the linear part of the system. It is also provided to generate the plant input u_k on the basis of function (2.1). The nonlinear problem can be stated such that, at each time step, the signal $h_{i|k}$ is obtained as described above, the nonlinear model coefficients $\gamma_0, \dots, \gamma_n$ are known by model identification, and the nonlinear problem is to find the control input signal $u_{i|k}$, $i = k \sim k + N_u - 1$. It can be resolved as finding zeros of the following function

$$p(u_{i|k}) = \gamma_0 + \gamma_1 u_{i|k} + \gamma_2 u_{i|k}^2 + \dots + \gamma_n u_{i|k}^n - h_{i|k}. \quad (4.8)$$

In this work, $u_{i|k}$ is calculated by finding eigenvalues using the Frobenius companion matrix [Malek and Vaillancourt, 1995]. Until now, the control problem of a nonlinear generalized predictive controller was solved in two steps, first a linear solution and then a nonlinear solution. Usually, only the first element of the control sequence $u_{k|k}, u_{k+1|k}, \dots, u_{k+N_u-1|k}$ is actually implemented during time interval $[k, k+1]$; that is, $u_k = u_{k|k}$. The procedure is repeated at the next sampling time. However, the control signals in this sequence can be delivered to the plant, if it is unnecessary to update the control signal calculation at every sample update. This can happen when the system changes slowly or the implementation is not accomplished at one sample time.

In this way, an NGPC has four tuning parameters : N_p , N_u , ξ and δ . The tuning processes of these parameters are not independent from one another but are interactive. Usually, the selection of prediction horizon N_p relies on the sampling time. The selection of control horizon N_u depends on a trade-off between reducing the amount of computation and achieving global optimization [Henson, 1998]. A large N_u may avoid a violation of constraints before they are arrived at, but it may also result in a substantial amount of computation [Camacho and Bordons, 1999]. The effect of δ is related to suppressing aggressive control action, while ξ allows the assignment of weight to reduce the prediction error for trajectory tracking. The tuning of δ and ξ can be simplified by fixing one of them as a constant and tuning the other one.

4.4.2 Closed-Loop Implementation of the Dual Predictive Controller

As described above, the proposed dual predictive controller consists of two NGPC controllers that work successively. Each of them works as described in section 4.4.1. The entire control scheme is illustrated in Fig. 4.5. However, as opposed to the single NGPC, where the first element in the control signal sequence is usually sent to the plant, in this dual NGPC, the control signal sequence (black dots) obtained in the activation controller is treated as the reference trajectory (black dots) for the stimulation controller. In the stimulation controller, only the first control signal is sent to the stimulator at each sample time. The closed-loop implementation of the EFPC consists of the following steps periodically :

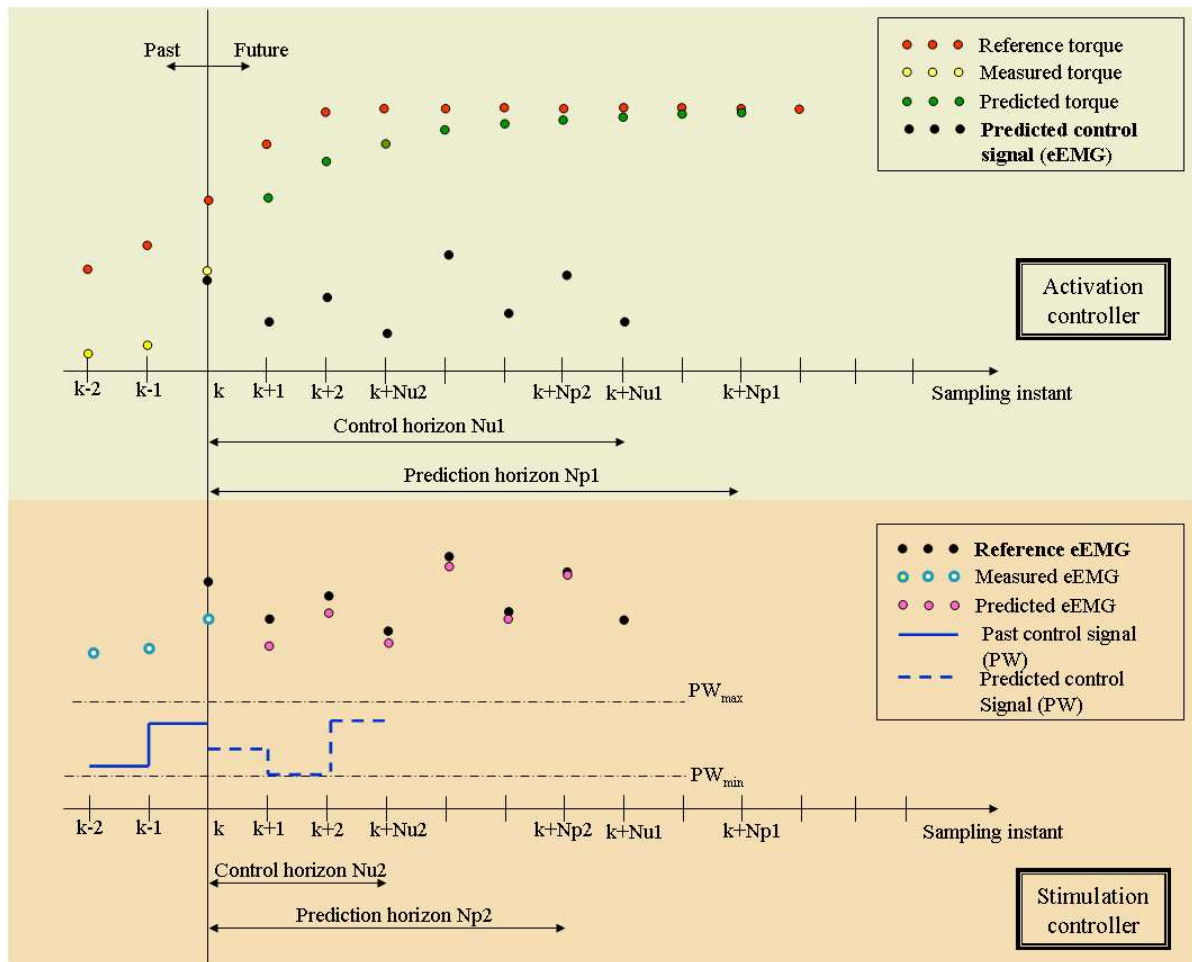


FIGURE 4.5 – Diagram illustrating the dual predictive control strategy. The output (predicted control signal) of the activation controller is used as input (reference eEMG) for the stimulation controller. In each controller, a nonlinear generalized predictive control algorithm is applied based on an internal PHM model.

Algorithm Closed-Loop Implementation of the Dual Predictive Controller

1. $k \leftarrow 0$
 2. Initialize the KF, and the control parameters for the activation and stimulation controllers : prediction horizon N_{p1} , N_{p2} , control horizon N_{u1} , N_{u2} , and weighting factors ξ_1 , δ_1 , ξ_2 , δ_2 .
 - 3 **while** system is running **do**
 4. $k \leftarrow k + 1$
 5. Collect the eEMG and torque signals (at current instant k)
 6. Update the model parameter estimates by KF for both the muscle excitation model and the contraction model. Note that, both the linear parameters in θ_l (4.5) and the nonlinear parameters in θ_n (4.6) are simultaneously identified
//activation controller
 7. Calculate linear solution sequence h_m by GPC (see Fig. 4.4)
 8. Calculate control signal sequence m_d using (4.8), and then these are used as the desired reference for the stimulation controller
//stimulation controller
 9. Calculate the intermediate signal h_s by GPC (see Fig. 4.4)
 10. The control signal u_s is calculated using (4.8)
 11. Apply u_s to the stimulator
 12. **end**
-

4.5 Evaluation of Predictive Performance for Drop Foot Correction

Drop foot is a condition in which an individual is not able to adequately dorsiflex or lift the foot. It is associated with a variety of conditions such as stroke, head injury, spinal cord injury, multiple sclerosis, and cerebral palsy [Lyons et al., 2002]. Regardless of the mechanism of injury, the drop foot condition can be improved by different techniques, which are typically referred to as drop foot correction. FES is one of the solutions, and it was put forward for lower limb rehabilitation in 1961 [Liberson et al., 1961]. In this context, most interest is focused on methods for detecting gait events [Azevedo and Héliot, 2005] and the development of an optimal stimulation system and optimal stimulation patterns [O’Keeffe et al., 2003]. However, closed-loop FES control for drop foot correction has not yet attracted a lot of attention.

To assess the performance of the proposed EFPC, preliminary experiments for drop foot correction are conducted on three healthy subjects. Surface stimuli are applied with stimulation PW modulation and constant amplitude and frequency. The common peroneal nerve and the TA are both activated as usual to induce dorsiflexion. Isometric ankle torque and eEMG signals are collected for off-line analysis. For each subject, recruitment, random and fatigue stimulation protocols are alternatingly carried out. The stimulation parameters are listed in TABLE 4.1, and

TABLE 4.1 – Stimulation parameters for drop foot correction (Stimulation frequency $FS = 40$ Hz, maximum stimulation PW $PW_{max} = 450\mu s$)

Subject	OR	HG	ZQ
Stimulation amplitude	35 mA	26 mA	52 mA

a detailed experimental description can be found in [Hayashibe et al., 2011a]. After signal processing as described in section 2.3.4, the relationship between stimulation, MAV of eEMG, and torque in 45-s recruitment and random stimulation sessions are respectively plotted in Fig. 4.6. In random test sessions, the stimulation PW at a plateau of each train is randomly determined from 20% ~ 100% of maximum PW. This protocol is important to verify more realistic and complex gait events and is rarely investigated.

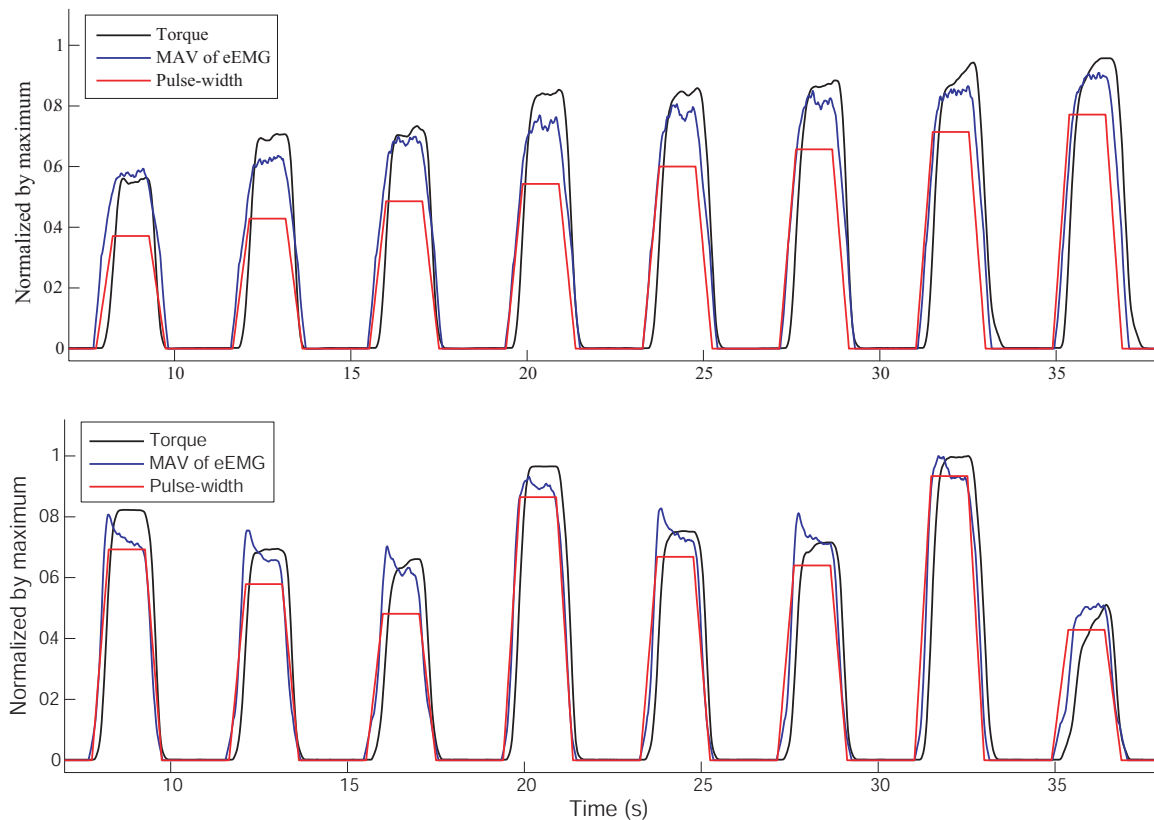


FIGURE 4.6 – Relationship among stimulation pulse width, MAV of eEMG, and torque in recruitment (top) and random (bottom) tests. All variables are normalized by their maximum value.

4.5.1 Experimental Validation of Predictive Torque Control

First, the control performance is evaluated by comparing the obtained control signal with the actual experimental stimulation PW. The measured torque is considered as the desired torque reference, where the control signal is computed by the EFPC, as described in section

TABLE 4.2 – Coefficient initialization for online identification of the muscle excitation and contraction models

Parameters	a_1	a_2	a_3	b_1	b_2	b_3	b_4	γ_0	γ_1	γ_2	γ_3
Initial values	0.2	0.2	0.2	0.1	0.1	0.1	0.1	0.01	1.0	1.0	1.0

4.4.2. As we use experimental data for this study, the actual stimulation input corresponding to the generated torque is known. Here, we try to verify whether the input solution from the EFPC controller is appropriate in comparison with the true stimulation input. If they match well, this implies that the model identification and controller work correctly. The forgetting factor of the Kalman filter is fixed at 0.999 as the muscle fatigue rate is lower in healthy subjects than in patients with SCI. The initial model parameters (for both the excitation and contraction models) are listed in Table 4.2. The sampling time is 0.025 s, consistent with a 40-Hz stimulation frequency. The control signal u_s , the normalized MAV of eEMG, is constrained within [0,1], representing respectively, non-fiber recruitment and maximal fiber recruitment. For convenience, in each NGPC, the weighting coefficient of the controlled variables is set at $\xi = 1$, while the weighting coefficient of the control signal is adjustable. Therefore, the tuning problem is reduced to tuning one weighting parameter δ_1 in the activation controller and one δ_2 in the stimulation controller. The RMS errors of torque tracking and PW matching in a random test in subject OR are shown in TABLE 4.3. After comparing these RMS errors among three subjects, $\delta_1 = 1.5$, $\delta_2 = 0.01$ was selected for all the control problem in this work. Some other parameters are chosen to take into account the tradeoff between tracking accuracy and the amount of computation as presented in TABLE. 4.4.

Three examples of the obtained results are shown in Fig. 4.7 ~ Fig. 4.9 and more results can be found in Appendix D. The reproduced torque through the EFPC shows good fidelity with the desired trajectory. The control signals show acceptable accuracy with an RMS error of 7.2% ~ 9.1% of PW_{max} . Moreover, the muscle fatigue that results from repetitive stimulation and the effect of withdrawal reflex in this stimulation protocol are unavoidable, so the control performance also indicates the ability of this control strategy to compensate muscle fatigue and reflex to some extent. Hopefully, the mismatch between the control signal and the actual PW will be improved by the increasing prediction quality.

Torque control only based on the eEMG signal

In order to assess the robustness of the proposed controller in the scenario where a torque sensor is not available or controllability is based only on eEMG information, the identification of the muscle contraction model is switched off at an arbitrary time instant t . This scenario is quite useful for FES control in the presence of sensor failure or control based only on eEMG feedback while torque control quality is maintained. The results in two subjects are illustrated in Fig. 4.10 and Fig. 4.11. The performance is not extremely degraded compared with Fig. 4.7 and Fig. 4.8. This indicates that control without a torque update is feasible in the identification process, especially when muscle fatigue develops slowly, which may occur in some subjects. The RMS errors of controlled torque, intermediate state — the MAV of eEMG and the control signal — stimulation PW, are averaged in several tests in each subject and summarized in TABLE 4.5.

TABLE 4.3 – The selection of penalty weights in a dual NGPC controller

penalty weights (δ_1, δ_2)	RMS error of torque tracking (Nm)	RMS error of PW matching (μs)
(5, 0.01)	2.23	34.2
(3, 0.01)	1.88	32.3
(2, 0.01)	1.68	32.1
(1.5, 0.01)	1.58	32.4
(1, 0.01)	1.48	33.1
(0.5, 0.01)	1.39	34.6
(0.1, 0.01)	1.44	37
(1.5, 1)	3.64	35.8
(1.5, 0.5)	2.91	34.1
(1.5, 0.1)	1.97	32.6
(1.5, 0.05)	1.78	32.5
(1.5, 0.01)	1.58	32.4
(1.5, 0.005)	1.53	32.4
(1.5, 0.001)	1.47	32.5
(0.5, 0.001)	1.29	34.5
(1, 0.001)	1.37	33.1
(5, 0.001)	2.12	35

TABLE 4.4 – Configuration of dual predictive controller (Weighting factor $\xi = 1$)

	Prediction horizon N_p	Control horizon N_u	Weighting factor δ
Activation controller	40	30	1.5
Stimulation controller	20	10	0.01

TABLE 4.5 – Summary of the control errors while eEMG-to-torque model identification is switched on/off

Subject (Number of tests)	Variable	Averaged RMS Error	
		ON	OFF
OR (N=6)	Torque (Nm)	2.28	2.16
	PW (μs)	39.8	40.47
HG (N=9)	Torque (Nm)	1.77	1.78
	PW (μs)	45.5	46.9
ZQ (N=2)	Torque (Nm)	0.895	0.915
	PW (μs)	49	50.4

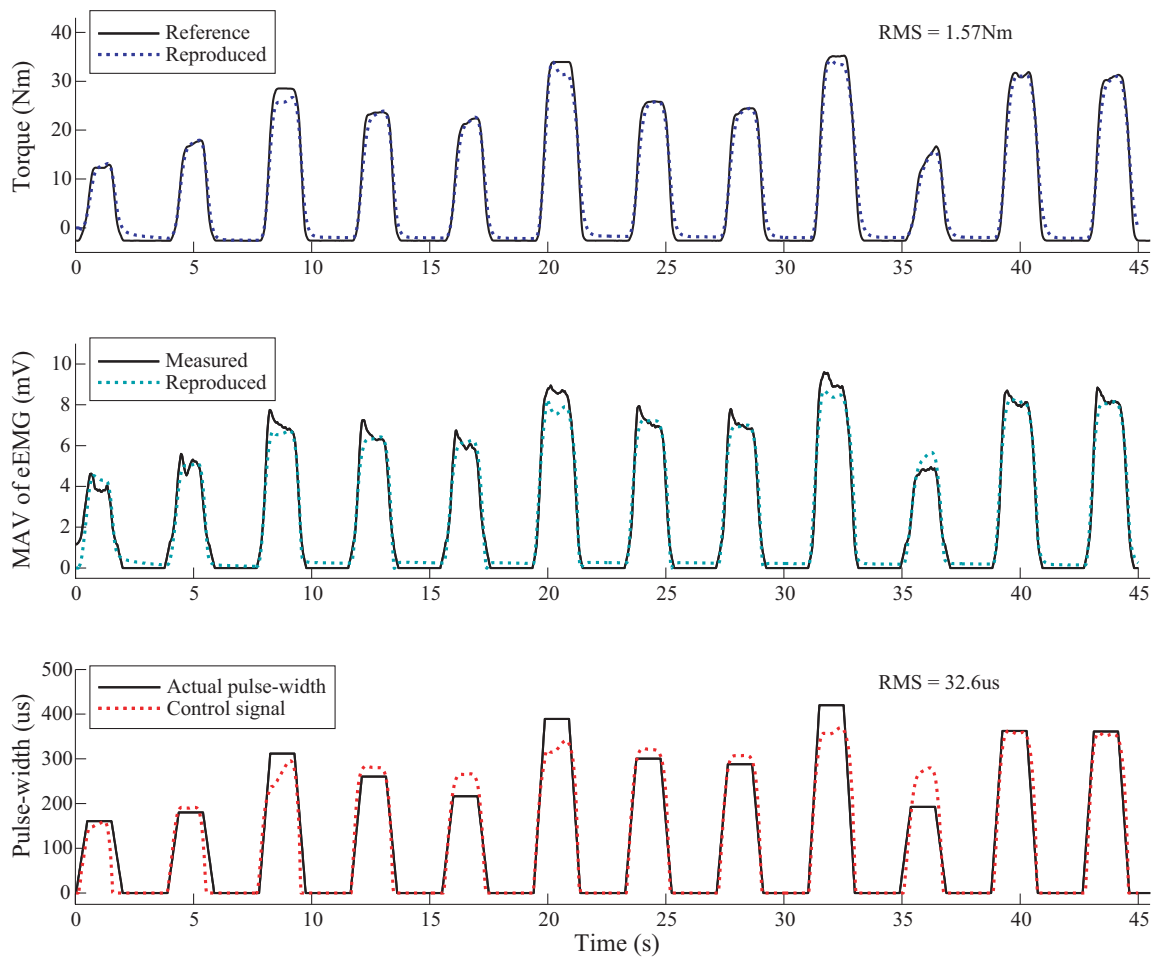


FIGURE 4.7 – Evaluation of EFPC to obtain randomly changed torque in subject OR. Upper : Reproduced torque from the muscle model (dashed blue) tracks the desired torque (solid black) well. Middle : The actual eEMG and the reproduced eEMG through the excitation model are shown. Bottom : The control signal matches the actual stimulation input well, indicating the controllability and fatigue compensation ability of the proposed EFPC.

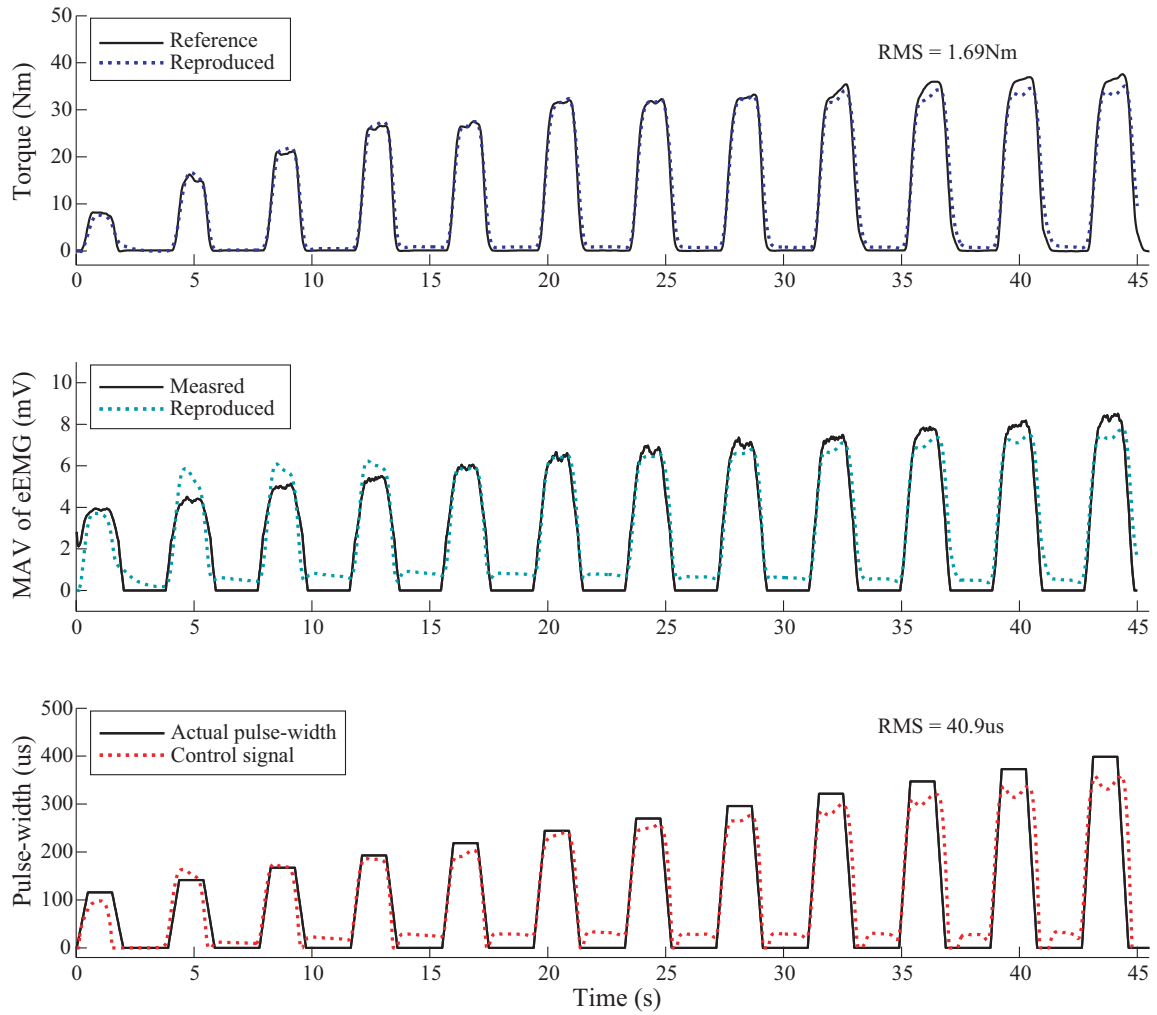


FIGURE 4.8 – Evaluation of EFPC to obtain gradually increased torque in subject HG.

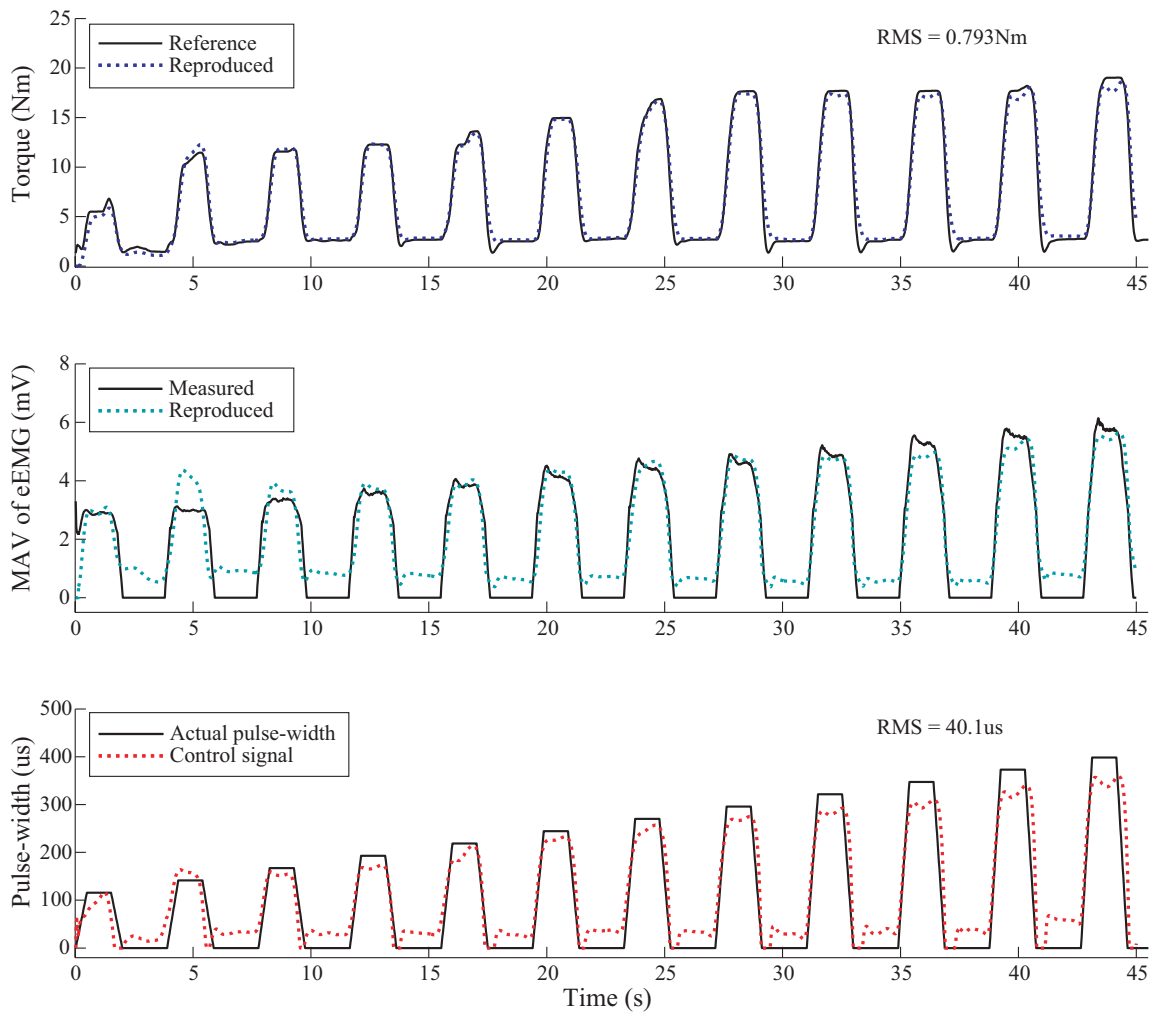


FIGURE 4.9 – Evaluation of EFPC to obtain gradually increased torque in subject ZQ. The torque baseline shift is apparent, which probably leads to degraded prediction quality and thus a mismatch in the control signal.

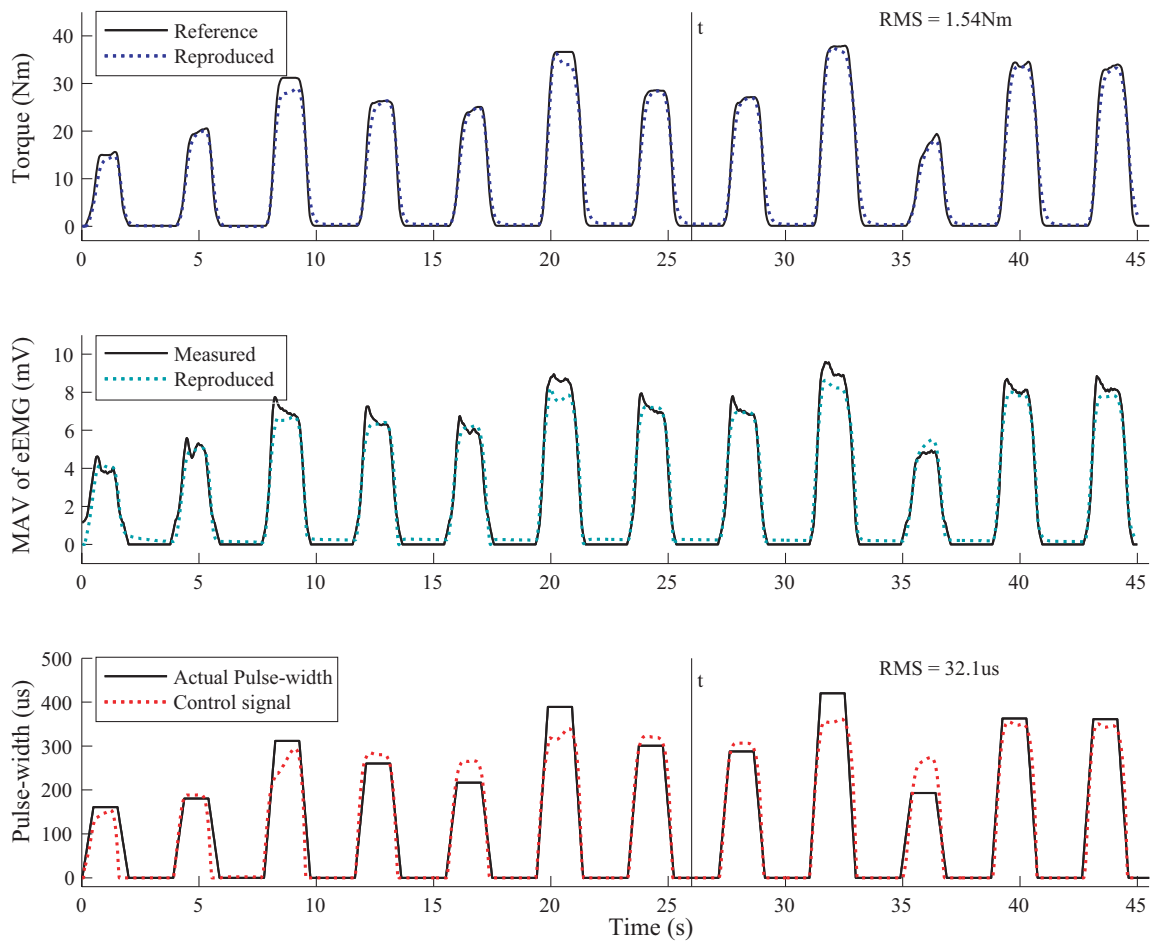


FIGURE 4.10 – Evaluation of the robustness of the proposed EFPC to obtain randomly changed torque in subject OR. Top : The reproduced torque tracks the desired torque well. Bottom : The control signal still matches the actual stimulation PW well, even when eEMG-to-torque model identification is switched off from instant t , simulating unreliable torque measurement.

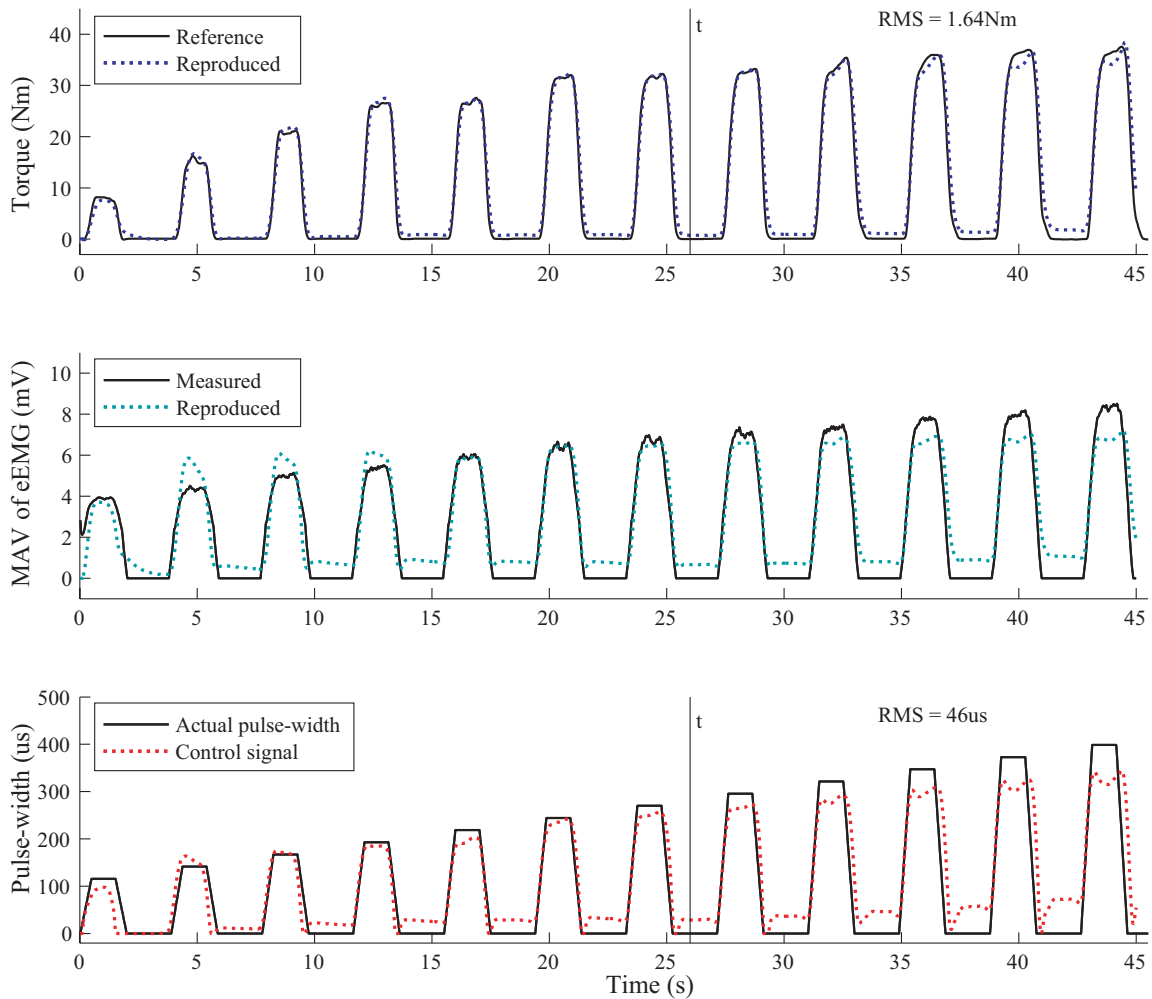


FIGURE 4.11 – Evaluation of the robustness of the proposed EFPC to obtain randomly changed torque in subject HG. Top : The reproduced torque tracks the desired torque well. Bottom : The control signal does not deteriorate extremely, even when eEMG-to-torque model identification is switched off from instant t .

4.5.2 Simulation Results on Predictive Control Performance

In this preliminary work, the fatigue compensation approach is not incorporated into real-time FES control. Therefore, simulation studies are carried out to evaluate the performance of the EFPC in generating an appropriate stimulation pattern for an arbitrary torque envelope and compensating fatigue. Virtual subjects are constructed with the model identified by the experimental data. From the successful experimental results in section 4.5.1, we expect that the identified model reflects the actual muscle properties quite well. The effects of the weighting factor and input constraints in guaranteeing patient safety are assessed. Next, the versatility of the proposed EFPC is evaluated in terms of muscle fatigue compensation and the generation of the stimulation pattern.

Effects of weighting factors

The torque reference consists of a sequence with a square train and a trapezoidal train. The tracking performance of the desired torque is shown in the left plot of Fig. 4.12. Three sets of weighting coefficients are tested, respectively referred to as EFPC1 ($\delta_1 = 0.1, \delta_2 = 20$), EFPC2 ($\delta_1 = 0.5, \delta_2 = 5$) and EFPC3 ($\delta_1 = 20, \delta_2 = 2$). It is found that, on the one hand, different weighting coefficients lead to different converging times to the desired torque and, on the other hand, even though different weighting coefficients are selected, the controlled torque is able to track the torque reference in a limited time and the transient processes are smooth in both torque tracking and control input, which is important for muscle to gradually respond to the stimulation. It also matches the intuitive requirements of muscle response during electrical stimulation.

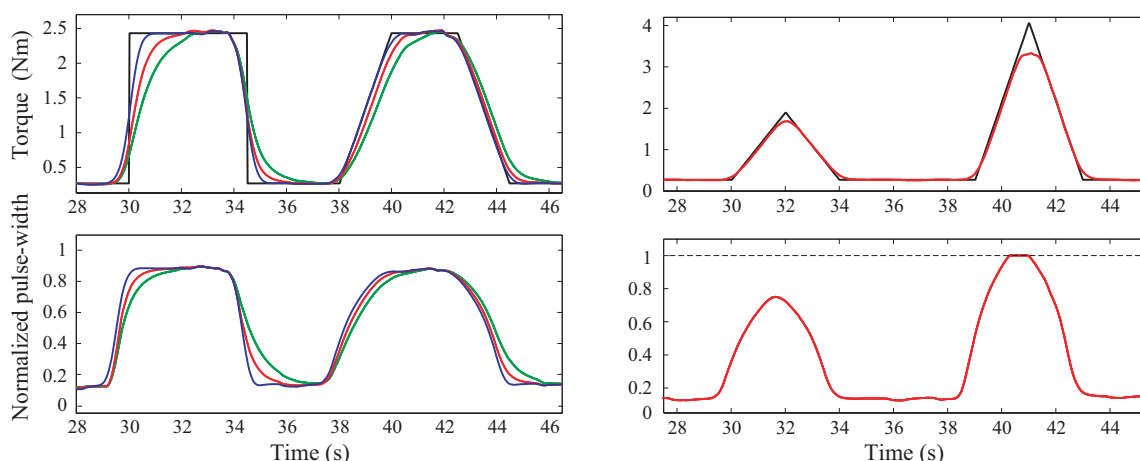


FIGURE 4.12 – Left : To track the torque reference (black), three sets of weighting factors are tested, EFPC1 (green), EFPC2 (red), and EFPC3 (blue). Right : Torque reference (black) and reproduced torque (red) are shown in the top plot. The normalized control signal is constrained in $[0,1]$ to guarantee stimulation safety of subjects (bottom).

In particular, when these two torque types are compared, the trapezoidal ramp-up period is important to reduce the spasticity resulting from sudden stimulation and the ramp-down period is important to avoid foot-flap or foot-slap [Lyons et al., 2002]. Thus, the trapezoidal profile is more realistic than the square profile in practice. The tracking performance of trapezoidal torque

is better than the tracking of square torque. This implies that a realistic torque trajectory ensures better controller performance. Moreover, even if an unrealistic torque trajectory is designed by mistake, the controller can generate a more realistic stimulation signal by adjusting the weighting coefficients. This feature is important since the muscle reactive rate is limited, whereas the controller has the ability to ensure practical input transition.

Effects of control constraints

The desired torque reference consists of a sequence of two triangular trains, where different maximum peaks are set. The simulation result is shown in the right plot of Fig. 4.12. The proposed EFPC is used to generate the stimulation PW to drive the predicted torque as close as possible to the desired torque. The stimulation pulse width represents saturation when the stimulation arrives at the maximum value within the predefined stimulation range. This property is important so that the FES controller ensures the safety of patients, rather than damaging them with overstimulation.

Muscle fatigue compensation

The goal of this study is to assess the ability of the EFPC to compensate fatigue effects. A torque trajectory with the same torque level is assumed as the torque reference, and the virtual subject is used as above. The EFPC works to generate suitable stimulation PW in order to maintain the torque level. Fig. 4.13 and Fig. C.4 depict the results for a desired trapezoidal torque trajectory. The averages of the RMS errors are approximately 2.18 Nm and 2.31 Nm for the two virtual subjects. The torque trajectories converge to obtain constant maximum torque, and the stimulation has to be increased gradually, as the virtual models are identified by experimental data representing real muscle states. Even though these results were obtained in simulation, the virtual model was identified with experimental data. Thus, this result is significant for advanced FES control that allows torque control with automatic muscle fatigue compensation.

Complex stimulation pattern generation

The proposed EFPC is also able to track the torque trajectory with any shape in order to perform a complex task. In Fig. 4.14, the envelope of torque reference is simulated according to muscle activity during natural gait [O’Keeffe et al., 2003]. The control framework yields the stimulation PW that is required to produce the desired trajectory. This is important and convenient to generate the required stimulation pattern for the intended trajectory, which is superior to the empirically defined stimulation pattern. Fig. 4.15 shows another torque trajectory with different levels of torque. The torque level changes frequently from 0.7 Nm to 9.05 Nm, and the EFPC calculates the required stimulation pattern, and reproduces the torque through the virtual model with small RMS error (0.194 Nm).

4.6 Discussion

Open-loop control of FES delivers a predefined stimulation pattern to target muscle. It does not provide feedback on the real muscle response. Closed-loop control is preferred in order to adaptively adjust the stimulation in reaction to unexpected variations in the muscle properties, thereby improving FES performance in terms of robustness. In the context of gait restoration by FES, some research has attempted to develop the optimal stimulation pattern to produce natural gait for open-loop control of FES, which is still useful when the muscle state does not change much, as we see from the performance of existing commercial FES systems. But if we

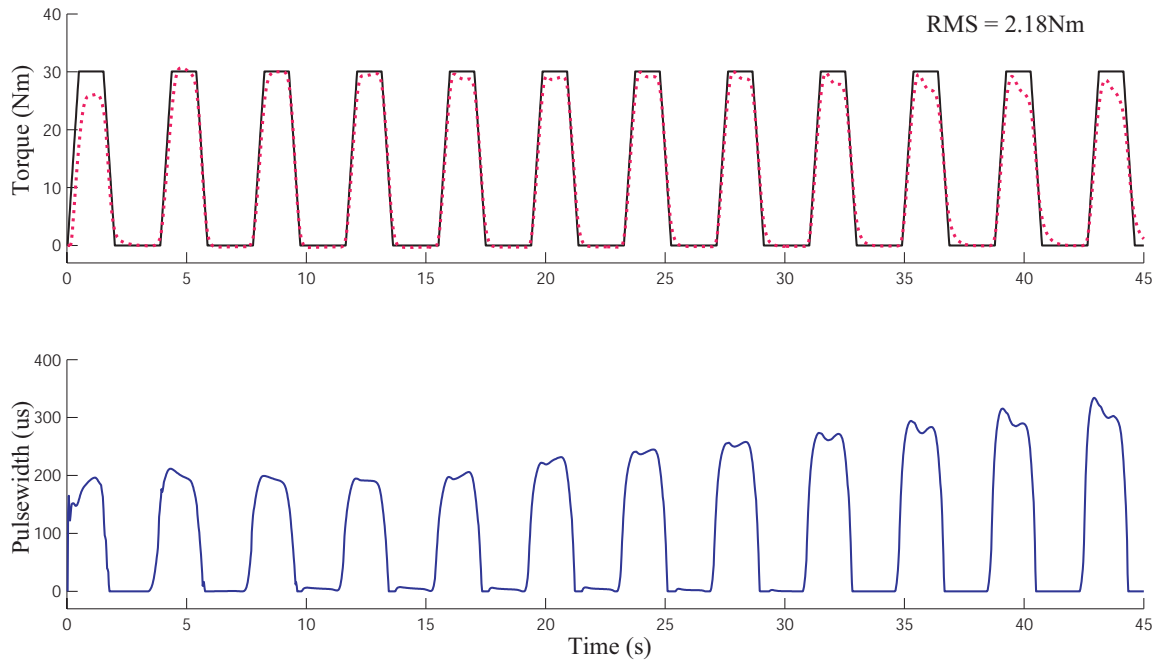


FIGURE 4.13 – The torque is desired to be maintained with constant maximum level. The PW required to obtain this torque trajectory is calculated by the proposed EFPC and represents the compensation effect against fatigue.

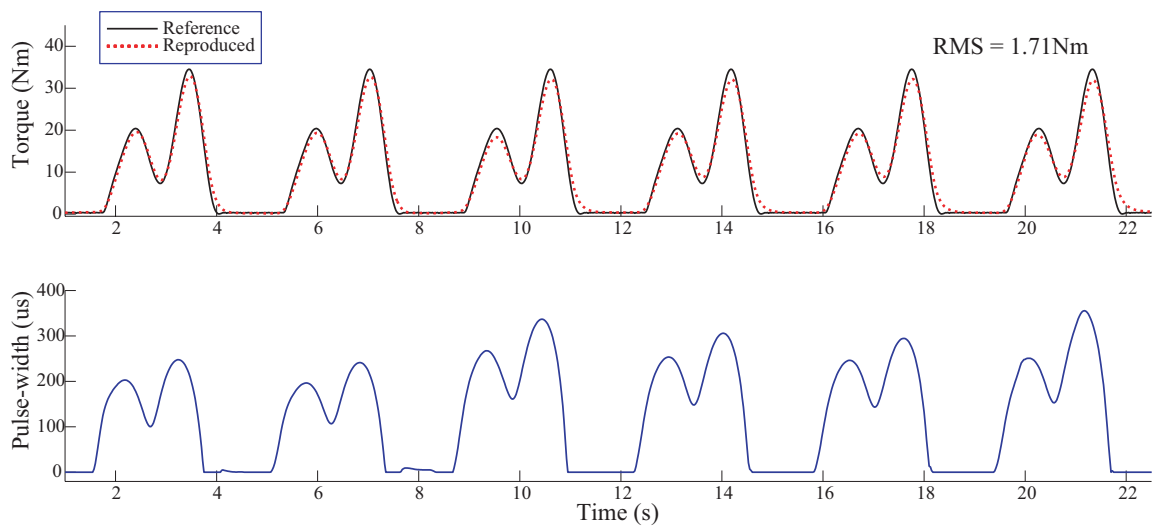


FIGURE 4.14 – The top plot traces the torque trajectory (black) and the reproduced torque from the muscle model. The bottom plot traces the stimulation pattern that was created by EFPC for the designed gait torque trajectory.

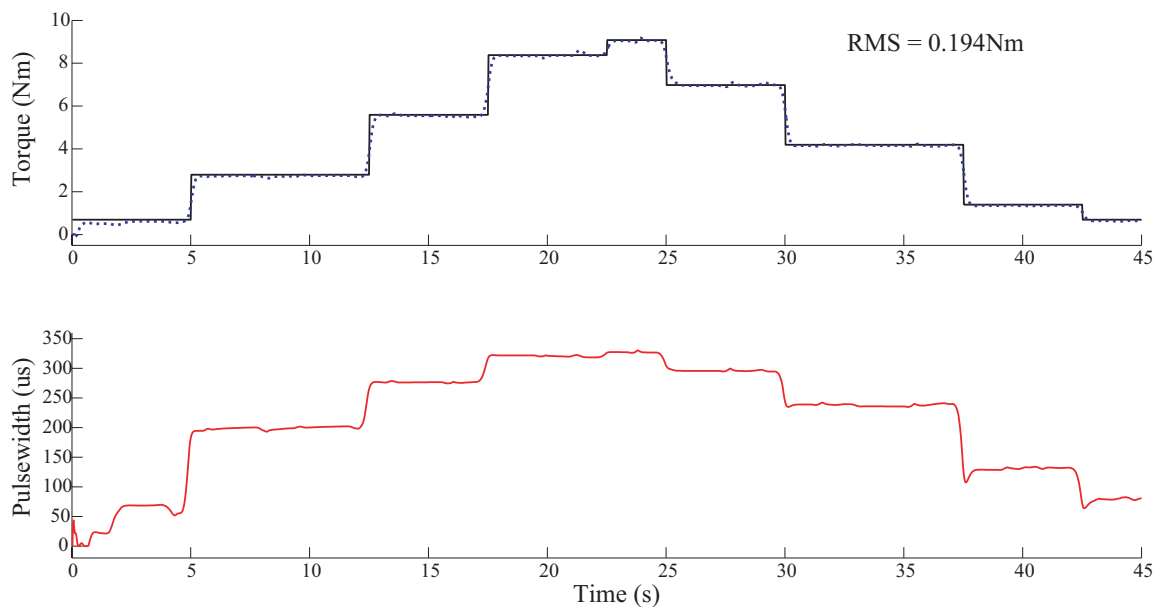


FIGURE 4.15 – The desired torque has different levels from 0.7Nm to 9.05Nm (top), and the instantaneous stimulation PW is shown in the bottom.

need to specify the exact torque trajectory for a certain desired motion, the appropriate stimulation pattern is still unknown for complex gait events. Thus, it is also important to find a way to generate an optimal stimulation pattern, even for open-loop control, while minimizing muscle fatigue. For this purpose, an optimal stimulation pattern was proposed in [O’Keeffe et al., 2003] by time-consuming optimization. In another work [Johnson and Fuglevand, 2011], a transfer function converting eEMG signals into an appropriate pattern of electrical stimulation was proposed to generate the desired torque trajectory.

In this work, an EFPC framework for FES is developed. This framework provides control adaptability and torque control rather than classical position control. The eEMG signal recorded from stimulated muscle is used to feedback the actual muscle activity to achieve torque control, which has never been tried in the FES context, since an appropriate torque sensor has not been available for human joints, which differ from robotic joints. As muscle mechanical behavior always lags after muscle electrical behavior, it is feasible to use eEMG to predict torque generation before delivering a stimulus to the target muscle. In addition, the predictive feedforward property of the predictive controller contributes smooth input transition, taking into account the physiological muscle activation process in advance. This EFPC contributes to augmenting the FES system in several aspects. First, an appropriate and secure stimulation pattern can easily be generated to produce the desired torque for open-loop use. This is useful when muscle fatigue is not evident or tracking accuracy is not strictly required. Second, in this control strategy, the control signal can be explicitly constrained to guarantee stimulation safety. Last, this control strategy is capable of muscle fatigue or reflex compensation. Moreover, the solution of the EFPC mainly consists of a two-step solution with a simple NGPC structure, where only the linear system is considered in the cost function, while the nonlinear term is excluded. Consequently, the calculation of each control update takes less than 15 ms in the Matlab environment, which is

sufficient for real-time implementation of FES with the commonly used stimulation frequency of 20 Hz~50 Hz. The typical drawback of predictive control is that model inaccuracy may affect control performance. This issue is covered in this work by KF with forgetting factor for time-varying and subject-specific model identification.

The proposed controller is validated using experimental data for drop foot correction on three healthy individuals, where the dorsiflexion is elicited through surface FES in isometric condition. The evoked EMG signal and ankle torque are recorded for model identification and controller validation. The proposed EFPC enables the production of a stimulation PW profile to obtain the desired torque trajectory. It is also able to track the desired torque well even when only based on an eEMG signal in the absence of a torque measurement update, as shown in Fig. 4.10 and Fig. 4.11. This implies that it is feasible to use this control strategy without a torque sensor when the muscle condition does not significantly change. When the muscle state changes greatly over time, it is possible to use the estimated torque instead of the torque update, and this can be calculated by the inverse dynamics from motion sensors. The proposed control framework allows many types of applications, depending on the available sensors. Online identification of a stimulation-to-eEMG model may not be required in the scenario where the time-varying property is not significant.

With the proposed method, we can easily obtain the open-loop stimulation profile taking into account subject-specific characteristics. The results in Fig. 4.14 and Fig. 4.15 demonstrate that the proposed controller also provides a method to automatic FES pattern generation with a given complex shape of the joint torque profile. For instance, the desired joint torque trajectory from natural gait can be directly given to the controller and the appropriate stimulation pattern can be instantly generated for each subject. In this context, the advantages of our approach compared with that of [O’Keeffe et al., 2003] and [Johnson and Fuglevand, 2011] are that it yields good fidelity with explicit and easy implementation, and it can systematically deal with subject-specific differences and muscle condition differences by online identification.

Although only the constraint of the stimulation signal is considered in this work, in practice, the torque and eEMG can also be explicitly constrained, if necessary. Generally, the torque constraints depend on what the task requires, and the eEMG constraints relate to the physiological limitations allowing reasonable muscle activation speed.

4.7 Conclusions

The purpose of this work is to improve the performance of FES systems in terms of accurate, safe and robust control of stimulation. As eEMG has been validated for torque prediction in the last chapter, an EFPC strategy is developed. To obtain the desired joint torque while taking into account the time-varying muscle dynamics, the eEMG signal is used to feedback actual muscle states. The control problem of the EFPC is resolved as a solution of dual NGPC in series. In practical application, when torque tracking is successful, the controller simply sends a constant stimulation pattern, as it works in open-loop. Once the torque deviates from the desired trajectory due to the effects of variations in muscle states or unexpected disturbances, the controller will recalculate the appropriate stimulation pattern to achieve the desired torque as long as it does not conflict with stimulation constraints. This control framework provides satisfactory control accuracy and notable robustness for sensing failure, according to the experimental and

simulation investigations. In addition, the controller is able to generate a suitable stimulation pattern for a given torque trajectory, which is superior to the empirically predetermined one. This model-based control framework is useful for various applications in isometric FES conditions and also in dynamic motion control, if an appropriate joint model is introduced along with the proposed muscle modeling.

General Conclusion

Concluding remarks

This thesis is focused on the prediction and control of FES-induced joint torque based on eEMG feedback under isometric condition. The goal is to achieve more accurate, safe and robust torque control in FES rather than conventional position control. The time-varying muscle fatigue and subject-specific properties complicate the prediction of torque variations with fatigue and the subsequent control of joint torque. To resolve these problems, this thesis mainly contributed to two aspects as described below.

First, in order to predict the generated torque in FES, eEMG signals recorded from the activated muscle are used, as this reflects the actual muscle activity and can be easily incorporated as feedback information in the FES control system. Due to the highly nonlinear and time-varying properties of muscle dynamics, PHM is employed to describe muscle activation and myoelectrical and mechanical responses. PHM, which consists of a memoryless nonlinear subsystem followed by a linear dynamic subsystem, contributes to the identifiability and controllability of muscle excitation and contraction processes. In order to resolve the time-variant torque prediction problem, an adaptive estimation method based on KF with forgetting factor is proposed. Integration of the eEMG-based predictive torque model and KF-based adaptive identification significantly improves the tracking accuracy, the subject-specific and protocol-specific differences, and the robustness to external disturbances, internal variations (such as muscle fatigue) and sensing failure.

Next, we proposed a new type of FES control strategy based on eEMG feedback compared to conventional position control, which mainly modulates stimulation pattern corresponding to the desired joint position trajectory. Position control is not robust when the position is generated both by muscle contractions and contacts with external environment since the sensor information from different sources is not distinguishable. In this scenario, development of techniques such as feedback torque control is essential with confirmation of the actual time-variant muscle activity. In this thesis, an EFPC strategy has been proposed based on accurate torque prediction and fatigue tracking performance. The controller was able to drive the joint torque close to the predefined torque reference using eEMG feedback. In a closed-loop control scenario, if the torque tracking is successful, the proposed controller maintains the stimulation. When the torque tracking deteriorates, the controller recalculates the stimulation signals for systematically compensating the muscle property variations. In addition, the proposed controller was able to automatically generate appropriate stimulation pattern for desired torque trajectory in any shape.

In a robust controlled FES environment, the compensation process needs to be accomplished synchronously with sending the stimulation commands. It requires fast computational power to track the muscle state changes and their control. The proposed EFPC can be computed at frequencies up to 70 Hz, which is sufficient for real-time FES application on patients, since a stimulation frequency of 20 Hz \sim 50 Hz is commonly used in conventional FES systems.

Perspectives

In order to achieve a reliable EMG-feedback torque control system with compensation of muscle state changes, the following issues should be taken into account.

- Time-varying rate of muscle state changes - The proposed torque prediction method through KF with forgetting factor is developed based on the hypothesis that the system varying rate is low. Once the muscle system changes too fast, the prediction performance probably decreases. As a result, the proposed EFPC is likely to be unable to generate a suitable stimulation pattern to track torque trajectory. An adaptive forgetting factor is one solution to improve prediction adaptivity to different muscle fatigue rates. However, as the stimulation pattern is adjustable in a limited range, fast muscle fatigue probably drives the stimulation parameter to reach the maximum value quickly, which consequently leads to suboptimal improvement in FES. Therefore, an optimal stimulation protocol, such as intermittent or selective stimulation, is still important when designing a FES system to reduce the muscle fatigue rate.
- Fatigue level identification - Apart from an optimal stimulation protocol to delay fatigue or reduce the fatigue rate, an effective method for indicating the fatigue level could contribute to more adaptive and accurate FES control. For instance, if we could extract suitable information from eEMG (in frequency domain) to indicate the fatigue level, this process could be used along with the EFPC to adaptively adjust the forgetting factor. The results of the implanted continuous FES are promising with regard to achieving this purpose. For other stimulation conditions, more advanced signal processing techniques or sensing modalities are required.

To execute torque tracking with compensation of muscle changes in real time, a schematic overview of the FES system is depicted in Fig. 4.16. The acquisition of eEMG and torque is completed by an EMG block (Biopac EMG 100C) and dynamometer (Biodex 3), respectively. An acquisition card (NI DAQ 6036E, US) is chosen to accomplish A/D conversion. The stimulator (ProStim, MXM, France) is computer-controlled and important for realizing real-time processing and control of FES.

In a short-term perspective, this work will be validated in two aspects.

- Identifying a stimulation pattern for open-loop FES - This function allows us to conveniently generate a stimulation pattern for the intended trajectory in any shape. In this case, the PHM is identified by *a priori* experimental data collected from a given subject. EFPC is performed to generate the stimulation pattern for a desired torque trajectory as shown in Fig. 4.14 and Fig. 4.15. When we assume that the muscle fatigue is not significant, the FES system works in open-loop. The generated stimulation pattern is then delivered to the same subject with the same experimental set-up. The differences between the desired and real torque trajectories are used to evaluate the efficacy and accuracy of this method.
- Compensation in closed-loop FES - The stimulation pattern obtained above can also be used for torque control in a closed-loop FES system; that is, when the torque tracks the trajectory well, the stimulation pattern is maintained at a predefined level. When the real

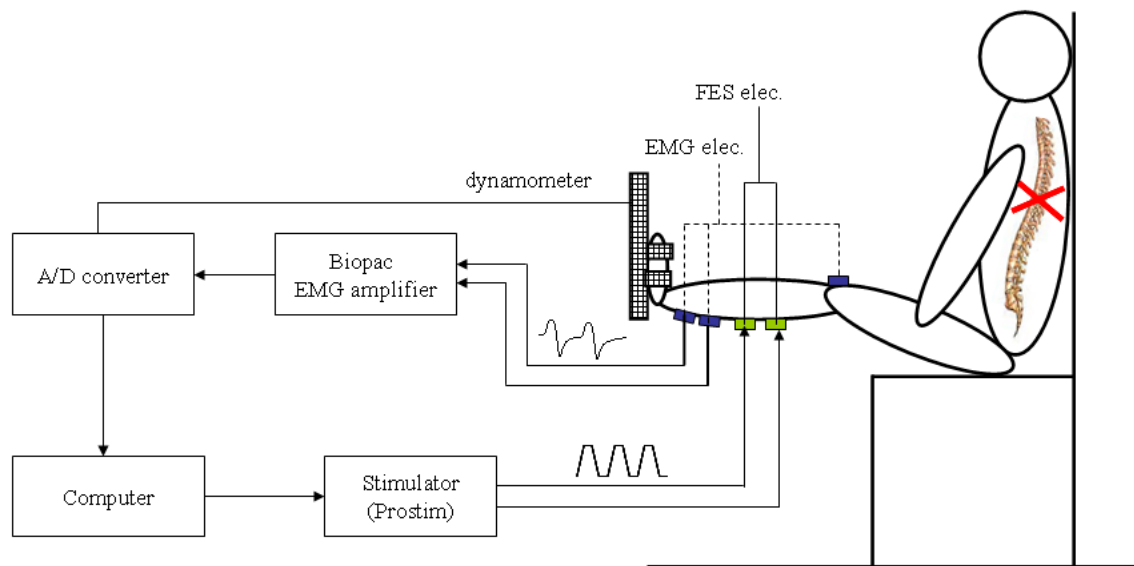


FIGURE 4.16 – FES system for real-time fatigue compensation and torque tracking. Torque and eEMG signals are recorded by an EMG block first. After A/D conversion with an acquisition card, the digital signals are processed to produce control signals with the method proposed in this thesis. The stimulator receives the commands for the stimulation parameters from the computer and then sends them to the stimulation electrodes to contract muscle — another control loop is followed.

torque deviates from the desired trajectory, closed-loop EFPC allows adaptive modulation of the stimulation pattern to compensate the time-variant muscle changes.

In a long-term perspective, an extensive work for dynamic motion control will probably be accomplished by estimating torque from other sensors, such as gyroscopes, accelerometers, electrogoniometers or multi-sensor integration, along with a joint dynamics model. In this case, torque control for dynamic motion would be achieved by introducing the joint dynamics model [Farahat and Herr, 2005] and without a torque sensor. In this scenario, as we do not need a dynamometer, this would provide mobility to patients during FES torque control that could be used in their daily lives.

APPENDIX A

FES Experiment Description

A.1 Fundamental Concepts in FES

Before explaining the experiment, we would like to introduce some fundamental concepts commonly used in FES, which may confuse some engineers who do not work on FES, but on other fields, such as mechanical, control or information. Different stimulators generate different stimulation impulse waveform to meet specific requirements as shown in Fig. A.1. In each stimulation pulse, three stimulation parameters — pulse amplitude (current I or voltage U), PW, and stimulation frequency $FS = 1/T$ — can be modulated as shown in Fig. A.2. Single stimulation pulse can only induce muscle twitch, while successive stimulation pulses are generally delivered to induce fused muscle force. The successive stimulation pulses compose a stimulation train (Fig. A.3). To obtain desired trajectory, suitable stimulation envelope should be designed with appropriate Choosing different stimulation parameters, different can be generated, which ultimately result in different force profiles. Two examples of stimulation envelopes are shown in Fig. A.3. Several stimulation trains designed according to the requirement of intended task, make up of a stimulation sequence. The rest time between neighboring trains can be zero or nonzero, respectively being called continuous or intermittent stimulation (Fig. A.3).

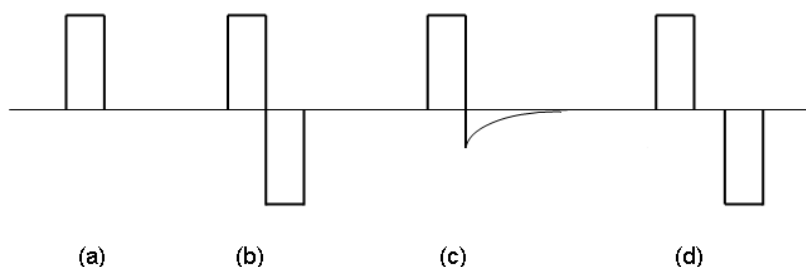


FIGURE A.1 – Common stimulus output waveform : (a) Monophasic (b) Symmetric biphasic (such as Cefar) (c) Asymmetric biphasic (such as ProStim) (d) Symmetric biphasic with interpulse interval.

A.2 Experiment Description of Implanted FES

A.2.1 Experimental design

The experiment was conducted with the implanted patient, a completely paraplegic subject (ASIA A, T8 level), 15 years post injury and 10 years post implantation. A fully implantable system was applied on this subjects as described in [Guiraud et al., 2006]. This study was approved by the ethical committee of N mes, France, 2008-2010 and the subject signed informed consent form. The implanted electrodes and experimental set-up are depicted in Fig. A.4. The subject was seated on a chair with the right foot being strapped on the pedal. The ankle oriented at 90° , while the joint center was aligned with the axis of a calibrated dynamometer (Biodex3). The

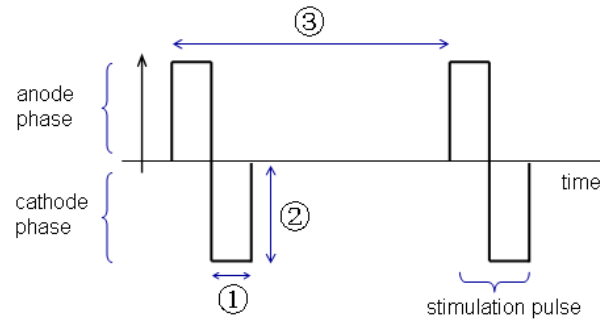


FIGURE A.2 – The stimulation parameters which can be modulated : (1) pulse width PW (μs) ; (2) pulse amplitude I (mA) or U (mV) ; (3) stimulation period T (ms).

shank was adjusted to be horizontal to the ground with the knee joint at 40° . During the experiments reported here, only TA muscle was stimulated, by activating merely the corresponding peroneal branch of sciatic nerve to provide ankle dorsiflexion.

TABLE A.1 – Stimulation parameters

	Thresholds	Maximum
Amplitude (I)	$400\mu A$	3.15mA
Pulse width (PW)	$300\mu s$	$816\mu s$
Stimulation frequency (FS)	25Hz	31.25Hz

A.2.2 Data collection

The EMG signals were collected using the same acquisition system (Biopac MP100) as in the first experiment. Two channels of EMG signals were recorded from TA and quadriceps muscle. On the TA muscle, the active electrodes were placed on the muscle belly and aligned along the muscle fiber direction, with 20 mm interelectrode spacing. Aluminum foil was used to cover the electrodes in order to reduce the effect of radio transmitting. The EMG recording from the quadriceps was just used for detecting the stimulation onset. The reference electrode was placed on the patella. The EMG signal was recorded, amplified (gain 1000) and sampled at 4 KHz by an acquisition system (Biopac MP100) synchronizing with torque measurement as described above. The isometric ankle dorsiflexion torque was recorded with the dynamometer (Biodex3), interfaced with the acquisition system.

A.2.3 Experimental protocol

The TA muscle was stimulated using stimulation amplitude modulation at constant stimulation frequency and constant pulse width in each session. The stimulation waveform is current-controlled, square pulse followed by a passive exponential recovery phase. The stimulation para-

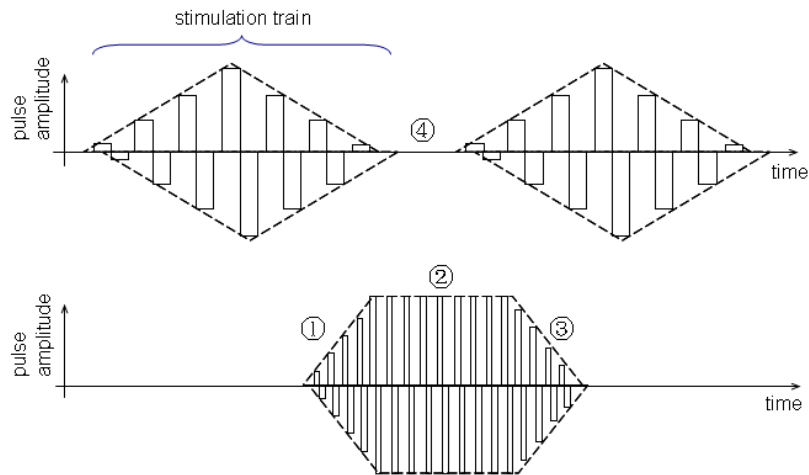


FIGURE A.3 – Top : One stimulation train is made up of successive stimulation pulses. One stimulation sequence is made up of several stimulation trains. Bottom : Various stimulation envelope is designed depending on desired movement. The phases that can be designed include : (1) ramp up (or rising) ; (2) plateau (or plateau) ; (3) ramp down (or falling) ; (4) rest. Continuous stimulation pattern has no rest between two adjacent trains. Otherwise, it is intermittent stimulation pattern.

meters are shown in TABLE A.1. In order to induce muscle fatigue, stimulation PW was chosen at $600 \mu\text{s}$, which generates maximum torque while amplitude at I_{max} . The stimulation frequency is selected a little lower than the available maximum frequency when all the channels are used at the same time according to [Guiraud et al., 2006]. The experiment consists of two test sessions, recruitment and fatigue, with no interval between them.

1. Recruitment test : The stimulation sequence consists of eight stimulation trains with duty cycle around 43% (0.5-s ramp-up, 1-s plateau and 2-s rest). The stimulation amplitude at stimulation plateau was gradually increased from 20 ~ 100% of I_{max} . The session was repeated three times, with stimulation frequency at 20Hz, 25Hz and 30Hz respectively.

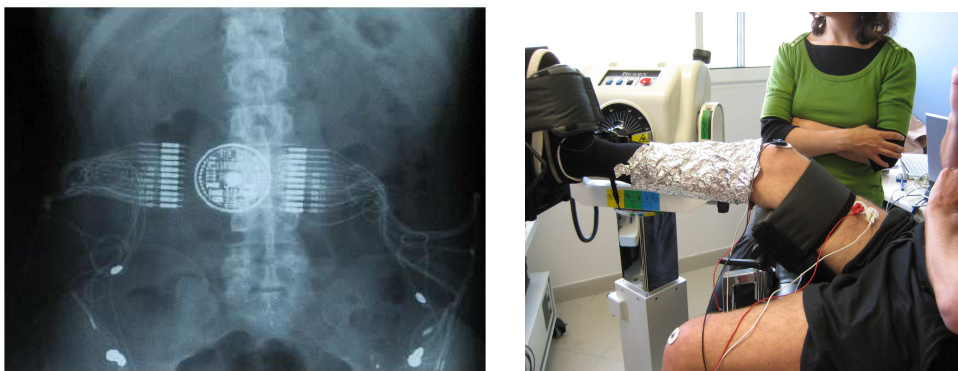


FIGURE A.4 – Implant position and experimental set-up illustration. The neural stimulation electrodes are located at the bottom right.

2. Fatigue test : The fatigue inducing pattern is a 50s sequence consisting of a 5s periodic ramp-and-hold signal (1s ramp-up and 4s plateau). No rest was set between two neighboring trains in order to induce a high level of fatigue to exhibit visible fatigue phenomenon. The practical stimulation scheme activates the TA with a duty cycle around 30% and with lower intensities. This test session was conducted after recruitment test and repeated twice.

A.2.4 Data Processing

In the case of implanted neural stimulation, there is no stimulation artifact effect because the locations of the target muscle and neural stimulation site are far enough apart. Besides, the stimulus is at low intensity and localized due to the use of bipolar electrodes. Instead, RF signal could contaminate the eEMG signals. As the quadriceps muscle was not stimulated, its eEMG signal contained only RF signal. The main phase of the RF signal occurs within the first 3 ms after the onset of stimulation in the captured EMG signal, and there is a time delay of about 20 ms from the onset of stimulation to the first Mwave spike. Thus, the eEMG signal on quadriceps was used to detect the stimulation onset at the beginning of each RF signal occurrence. The recorded eEMG and torque signals were processed as section. 2.3.4, with removal of the radio signals instead of the stimulation artifacts. An example of processed result is shown in Fig.A.5. The RF is efficiently removed and Mwave is retrieved simultaneously for the subsequent analysis. The MAV was calculated every three epoches, and $T_{arf} = 3ms$. As seen from three recruitment tests which performed successively at the beginning, the induced torque increases with increasing stimulation amplitude and increasing stimulation frequency. However, the MAV of eEMG changes slightly when frequency arrived at 30Hz (Fig. A.6), probably due to the occurrence of slight fatigue.

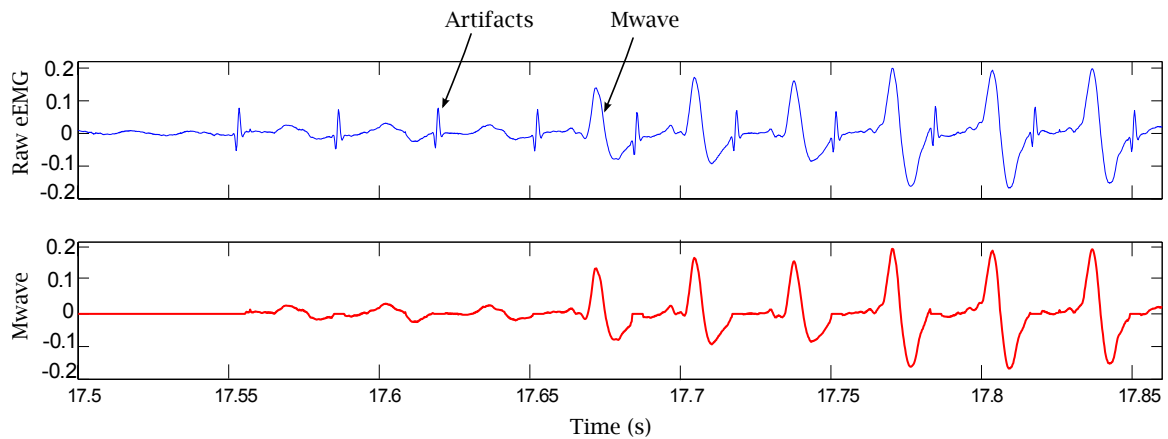


FIGURE A.5 – Removal of radio signal from the eEMG signal.

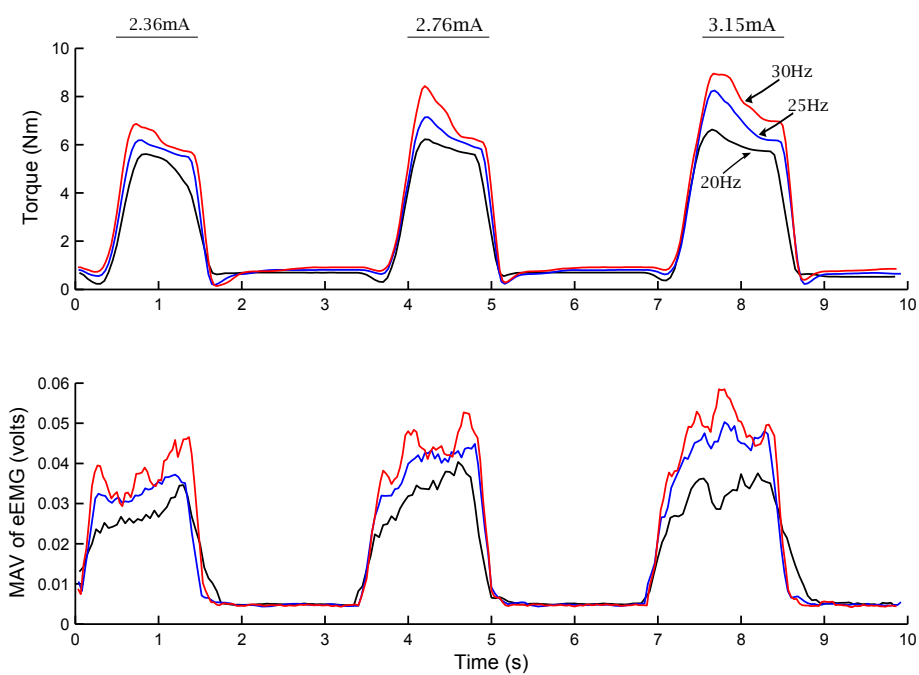


FIGURE A.6 – Torque and eEMG respond to variations of stimulation amplitude and stimulation frequency.

APPENDIX B

State-Space and Kalman Filter

B.1 State-Space of Polynomial Hammerstein Model

In order to derive the state-space form of a PHM, we consider a simple system and then obtain the generic form from the simple example. Considering a discrete PHM with model order (2,2,2), we treat the linear ARX model first and then the nonlinear polynomial part.

State-Space of ARX model

According to (2.2),

$$\begin{aligned} y(k) &= \sum_{i=1}^2 a_i y(k-i) + \sum_{i=1}^2 b_i h(k-i) \\ &= a_1 y(k-1) + a_2 y(k-2) + b_1 h(k-1) + b_2 h(k-2) \end{aligned} \quad (\text{B.1})$$

Its state variables can be expressed as :

$$x_2(k+1) = a_2 y(k) + b_2 h(k) \quad (\text{B.2})$$

$$x_1(k+1) = x_2(k) + a_1 y(k) + b_1 h(k) \quad (\text{B.3})$$

From (B.2),

$$x_2(k) = a_2 y(k-1) + b_2 h(k-1) \quad (\text{B.4})$$

Substitute (B.4) into (B.3),

$$x_1(k+1) = a_1 y(k) + a_2 y(k-1) + b_1 h(k) + b_2 h(k-1)$$

and then

$$x_1(k) = a_1 y(k-1) + a_2 y(k-2) + b_1 h(k-1) + b_2 h(k-2)$$

Comparing (B.1) and (B.5), we get

$$y(k) = x_1(k) \quad (\text{B.5})$$

Substitute (B.5) into (B.2) and (B.3),

$$x_2(k+1) = a_2 x_1(k) + b_2 h(k)$$

$$x_1(k+1) = a_1 x_1(k) + x_2(k) + b_1 h(k)$$

Therefore, the state-space model of a ARX (2,2) model can be written as :

$$\mathbf{x}(k) = \mathbf{A}\mathbf{x}(k-1) + \mathbf{B}h(k-1) \quad (\text{B.6})$$

$$y(k) = \mathbf{C}\mathbf{x}(k) \quad (\text{B.7})$$

where

$$\mathbf{x}(k) = \begin{bmatrix} x_1(k) \\ x_2(k) \end{bmatrix} \quad \mathbf{A} = \begin{bmatrix} a_1 & 1 \\ a_2 & 0 \end{bmatrix} \quad \mathbf{B} = \begin{bmatrix} b_1 \\ b_2 \end{bmatrix} \quad \mathbf{C} = \begin{bmatrix} 1 & 0 \end{bmatrix}$$

State-Space of PHM Model

When we think about the state-space model of an PHM (1,m,n) model, we can use the polynomial function (2.1) to substitute the $h(k)$ in (B.6). Still assuming a PHM (2,2,2) model, its state-space has a form as below,

$$\begin{aligned} y(k) &= \sum_{i=1}^2 a_i y(k-i) + \sum_{i=1}^2 \sum_{j=1}^2 b_i \gamma_j (u(k-i))^j \\ &= a_1 y(k-1) + a_2 y(k-2) + b_1 \gamma_1 u(k-1) + b_1 \gamma_2 (u(k-1))^2 \\ &\quad + b_2 \gamma_1 u(k-1) + b_2 \gamma_2 (u(k-1))^2 \\ &= a_1 y(k-1) + a_2 y(k-2) + \mu_{11} u(k-1) + \mu_{12} (u(k-1))^2 \\ &\quad + \mu_{21} u(k-1) + \mu_{22} (u(k-1))^2 \end{aligned} \quad (\text{B.8})$$

where, we write $\mu_{ij} = b_i \gamma_j$ to make it simple, when we do not care about the value of b_i and γ_j . Otherwise, we do not use this replacement. If we consider $(u(k))^j$ as a model input, the state variables of this PHM (2,2,2) can be derived as above,

$$\begin{aligned} x_1(k) &= a_1 x_1(k-1) + x_2(k-1) + \mu_{11} u(k-1) + \mu_{12} (u(k-1))^2 \\ x_2(k) &= a_2 x_1(k-1) + \mu_{21} u(k-1) + \mu_{22} (u(k-1))^2 \\ y(k) &= x_1(k) \end{aligned}$$

As a result, the state-space corresponding to (B.8) is

$$\begin{aligned} \mathbf{x}(k) &= \mathbf{A}\mathbf{x}(k-1) + \mathbf{B}\mathbf{u}(k-1) \\ y(k) &= \mathbf{C}\mathbf{x}(k) \end{aligned} \quad (\text{B.9})$$

where

$$\mathbf{u}(k-1) = \begin{bmatrix} u(k-1) \\ u(k-1)^2 \end{bmatrix} \quad \mathbf{x}(k) = \begin{bmatrix} x_1(k) \\ x_2(k) \end{bmatrix} \quad \mathbf{A} = \begin{bmatrix} a_1 & 1 \\ a_2 & 0 \end{bmatrix} \quad \mathbf{B} = \begin{bmatrix} \mu_{11} & \mu_{12} \\ \mu_{21} & \mu_{22} \end{bmatrix} \quad \mathbf{C} = \begin{bmatrix} 1 & 0 \end{bmatrix}$$

In addition, when we need individual linear and nonlinear coefficients b_i and γ_j in (B.8), the (B.9) in state space model is changed to

$$\begin{aligned} \mathbf{x}(k) &= \mathbf{A}\mathbf{x}(k-1) + \mathbf{B}\Psi\mathbf{u}(k-1) \\ y(k) &= \mathbf{C}\mathbf{x}(k) \end{aligned} \quad (\text{B.10})$$

where

$$\mathbf{B} = \begin{bmatrix} b_1 \\ b_2 \end{bmatrix} \quad \Psi = \begin{bmatrix} \gamma_1 & \gamma_2 \end{bmatrix}$$

When we identify the model state and parameters, the measurement is noisy, we do not need add a Gaussian white noise element in the model. But when we use the model for simulation, a noise model should be added to simulate the process and measurement noise in practice. For example, the state-space model in (B.9) is rewritten as,

$$\mathbf{x}(k) = \mathbf{A}\mathbf{x}(k-1) + \mathbf{B}\mathbf{u}(k-1) + \mathbf{w}(k) \quad (\text{B.11})$$

$$y(k) = \mathbf{C}\mathbf{x}(k) + v(k) \quad (\text{B.12})$$

where,

$$\mathbf{w}(k) = \begin{bmatrix} w_1(k) \\ w_2(k) \end{bmatrix} \quad (\text{B.13})$$

and $P(\mathbf{w}) \sim N(0, \mathbf{Q})$, $P(v) \sim N(0, R)$.

B.2 Results of Model Identification and Torque Prediction

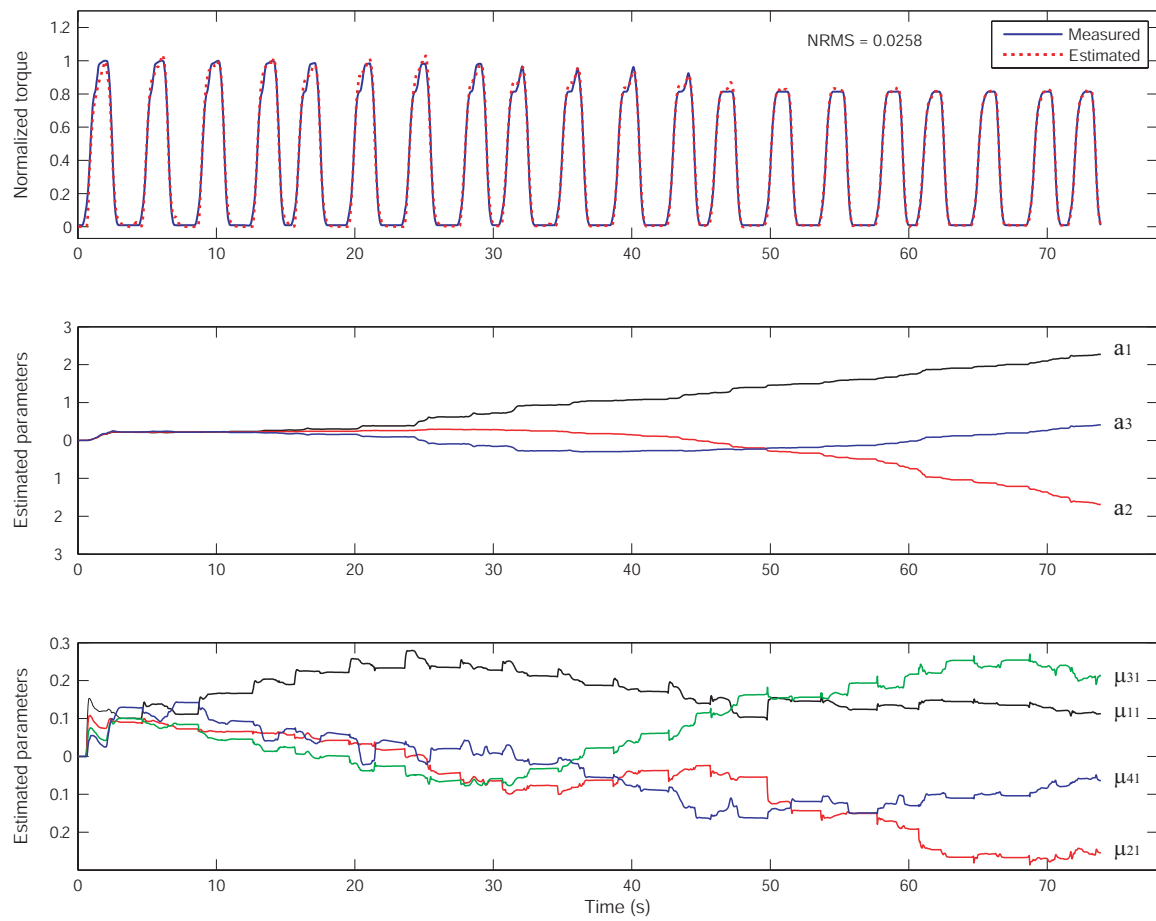


FIGURE B.1 – Estimated torque and model parameters in subject S4.

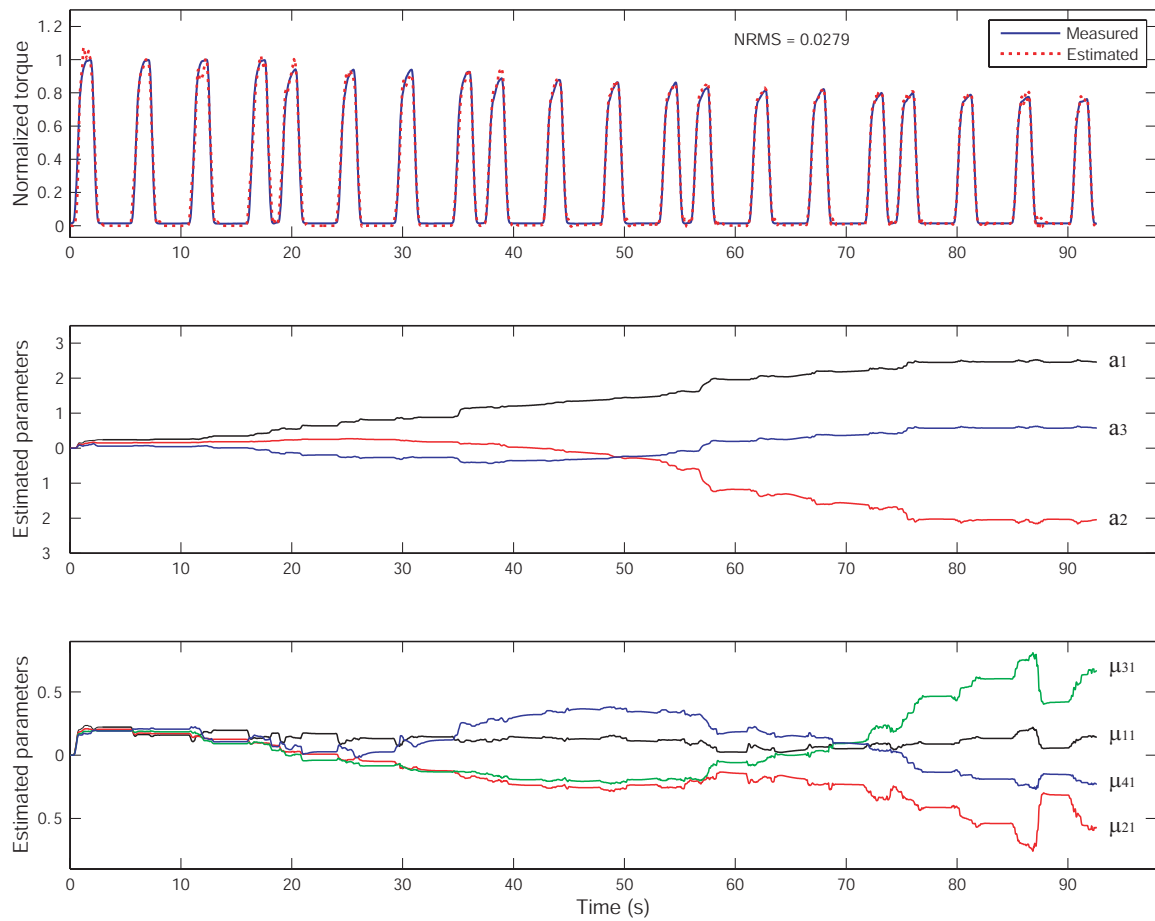


FIGURE B.2 – Estimated torque and model parameters in subject S5.

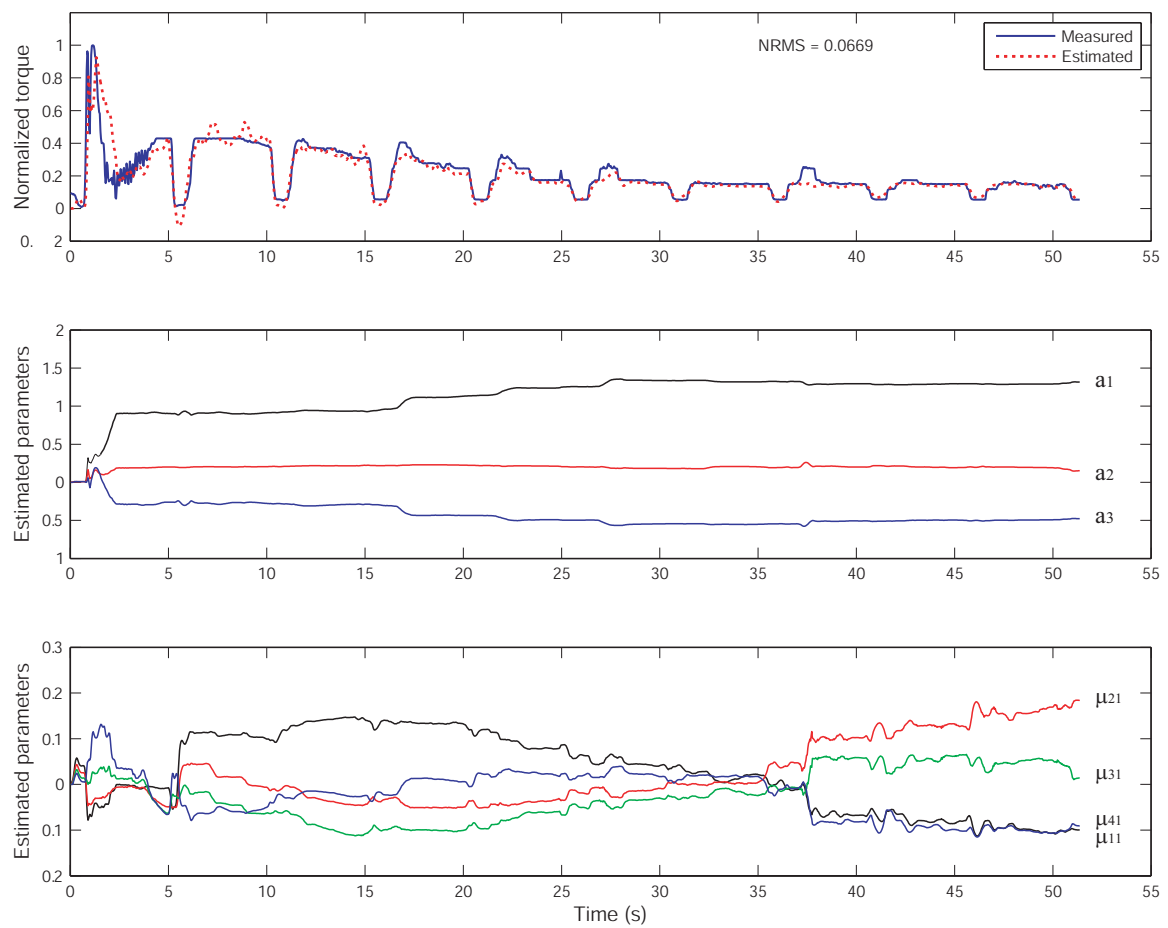


FIGURE B.3 – Estimated torque and model parameters in implanted subject.

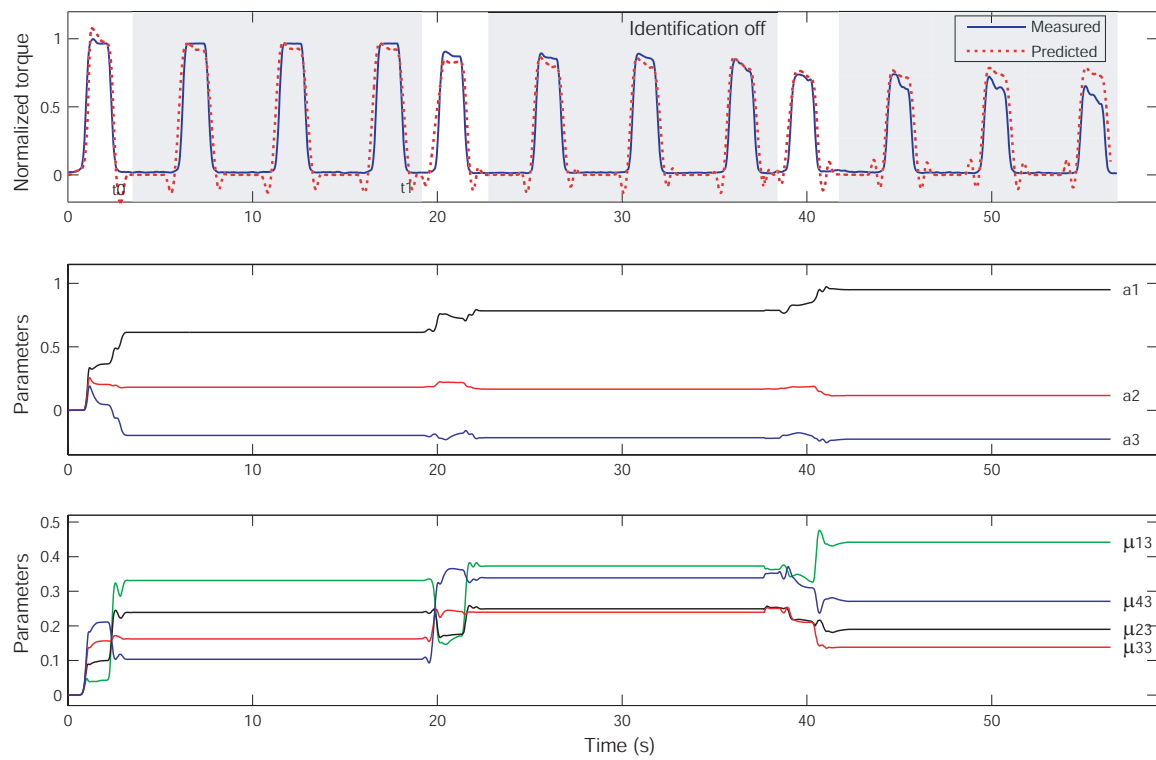


FIGURE B.4 – Fatigue tracking based on eEMG-to-torque model and KF in subject S2. The online identification in $[t_0, t_1]$ is suspended to simulate sensing failure. The model identified at t_0 is used to predict torque until t_1 , 15s later.

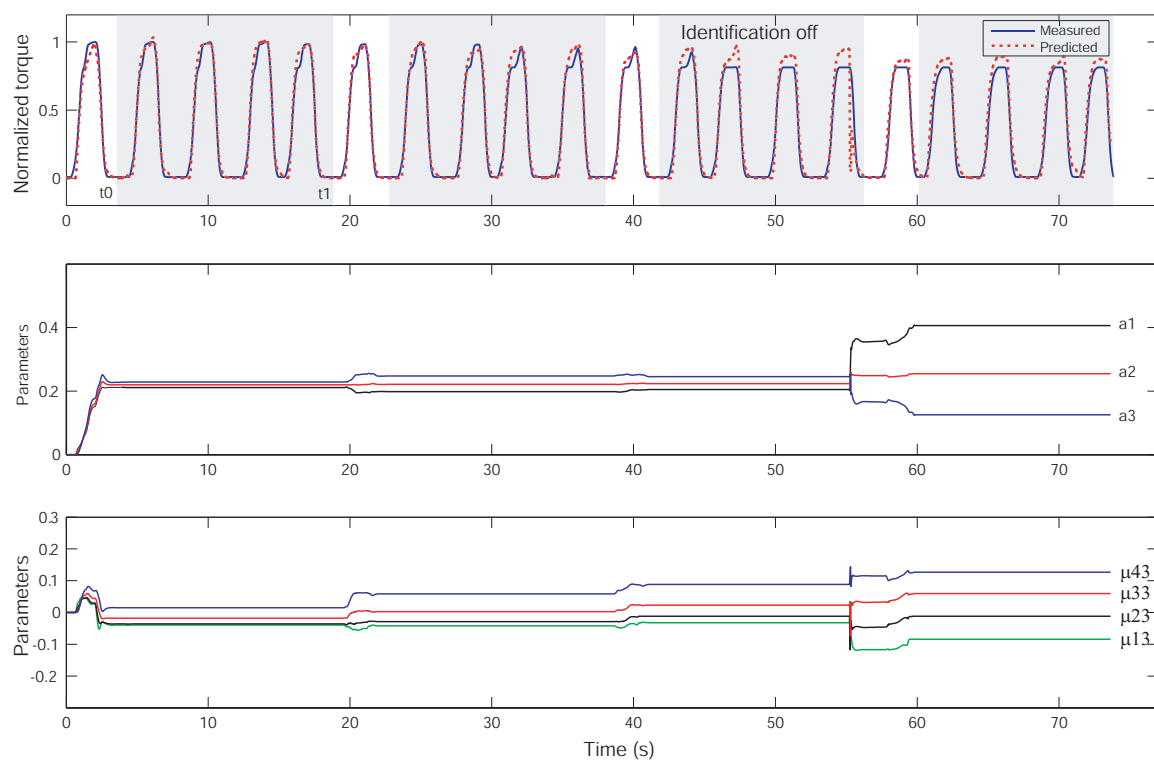


FIGURE B.5 – Fatigue tracking based on eEMG-to-torque model and KF in subject S4.

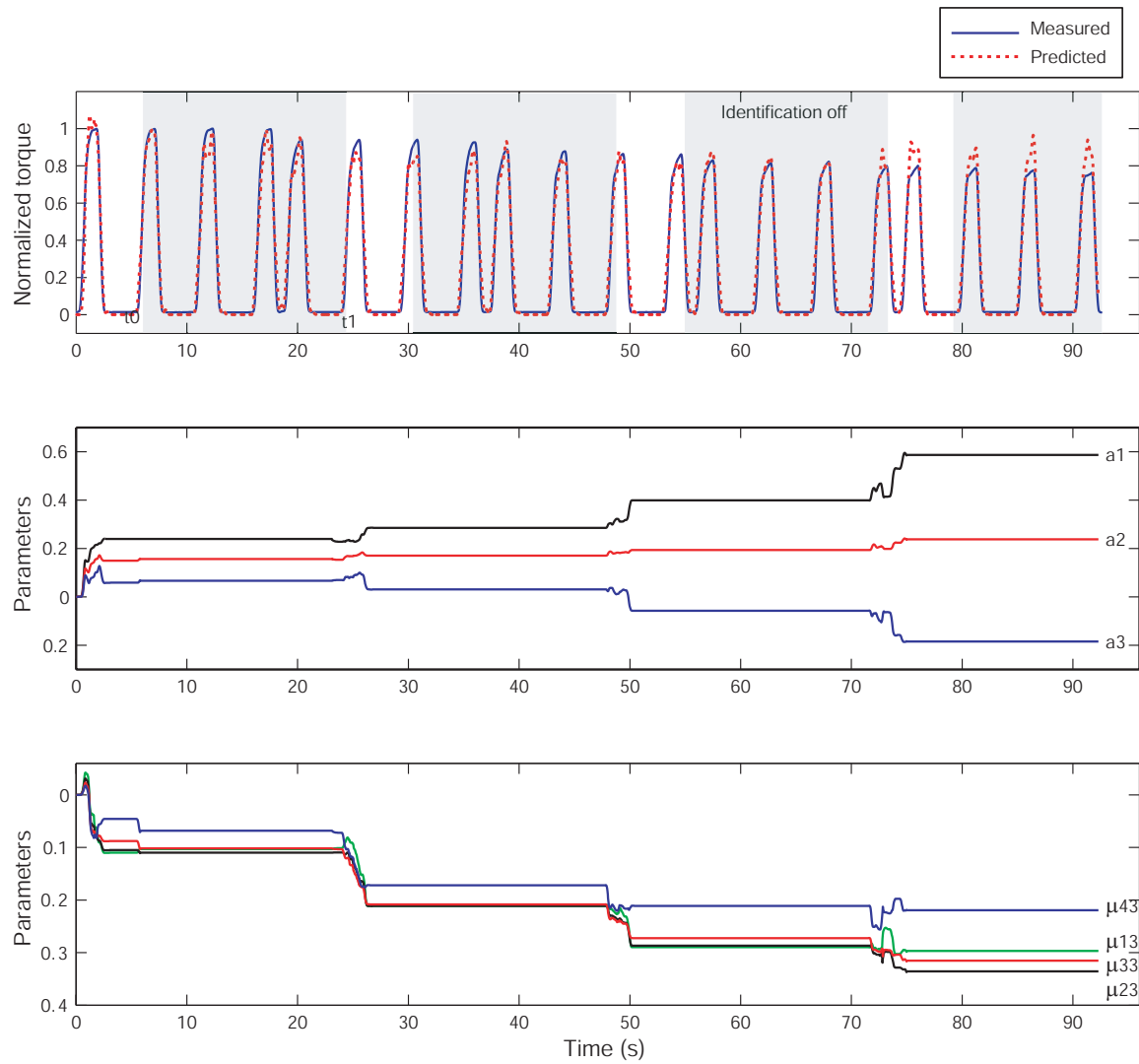


FIGURE B.6 – Fatigue tracking based on eEMG-to-torque model and KF in subject S5.

APPENDIX C

EMG Feedback Predictive Control

C.1 Generalized Predictive Control

In order to resolve a GPC control problem, a simpler formulation of GPC is used instead of solving recursive Diophantine equations [Albertos and Ortega, 1989]. Considering a discrete-time system in state-space form as (B.6) :

$$\begin{aligned} \mathbf{x}(k+1) &= \mathbf{A}\mathbf{x}(k) + \mathbf{B}h(k) \\ y(k) &= \mathbf{C}\mathbf{x}(k) \end{aligned} \quad (\text{C.1})$$

If the control increment Δh_k is considered as model input, and substitute $h(k) = h(k-1) + \Delta h(k)$ to the above system,

$$\begin{aligned} \begin{bmatrix} \mathbf{x}(k+1) \\ h(k) \end{bmatrix} &= \begin{bmatrix} \mathbf{A} & \mathbf{B} \\ \mathbf{0} & \mathbf{I} \end{bmatrix} \begin{bmatrix} \mathbf{x}(k) \\ h(k-1) \end{bmatrix} + \begin{bmatrix} \mathbf{B} \\ \mathbf{I} \end{bmatrix} \Delta h(k) \\ y(k) &= \begin{bmatrix} \mathbf{C} & 0 \end{bmatrix} \begin{bmatrix} \mathbf{x}(k) \\ h(k-1) \end{bmatrix} \end{aligned} \quad (\text{C.2})$$

By introducing $\mathbf{w}_k = [\mathbf{x}(k) \quad h(k-1)]^T$, the system can be rewritten as

$$\begin{aligned} \mathbf{w}(k+1) &= \mathbf{M}\mathbf{w}(k) + \mathbf{N}\Delta h(k) \\ y(k) &= \mathbf{Q}\mathbf{w}(k) \end{aligned} \quad (\text{C.3})$$

where

$$\mathbf{M} = \begin{bmatrix} \mathbf{A} & \mathbf{B} \\ \mathbf{0} & \mathbf{I} \end{bmatrix}, \quad \mathbf{N} = \begin{bmatrix} \mathbf{B} \\ \mathbf{I} \end{bmatrix}, \quad \mathbf{Q} = [\mathbf{C} \quad 0]$$

The output prediction can be obtained recursively from (C.3) :

$$\hat{y}(k+j|k) = \mathbf{Q}\mathbf{M}^j \hat{\mathbf{w}}(k) + \sum_{i=0}^{j-1} \mathbf{Q}\mathbf{M}^{j-1-i} \mathbf{N} \Delta h(k+i)$$

In the form of vector, the optimal j -step ahead output predictions along the prediction horizon are given by :

$$\mathbf{y} = \mathbf{F}\hat{\mathbf{w}}(k) + \mathbf{H}\Delta \mathbf{h} \quad (\text{C.4})$$

where

$$\mathbf{y} = \begin{bmatrix} \hat{y}(k+1|k) \\ \hat{y}(k+2|k) \\ \vdots \\ \hat{y}(k+N_p|k) \end{bmatrix} \quad \Delta \mathbf{h} = \begin{bmatrix} \Delta h(k|k) \\ \Delta h(k+1|k) \\ \vdots \\ \Delta h(k+N_u-1|k) \end{bmatrix} \quad \mathbf{F} = \begin{bmatrix} \mathbf{Q}\mathbf{M} \\ \mathbf{Q}\mathbf{M}^2 \\ \vdots \\ \mathbf{Q}\mathbf{M}^{N_p} \end{bmatrix}$$

and \mathbf{H} is a $N_p \times N_u$ block lower triangular matrix with its non-null elements defined by $H_{ij} = \mathbf{Q}\mathbf{M}^{i-j}\mathbf{N}$.

As the control objective is to obtain a vector $\Delta\mathbf{h}$ of future control sequence, which will minimize the cost function (4.7), the cost function can be rewritten as following by substituting (C.4) to (4.7) :

$$J = (\mathbf{H}\Delta\mathbf{h} + \mathbf{F}\hat{\mathbf{w}}(k) - \mathbf{v})^T \bar{\mathbf{R}}(\mathbf{H}\Delta\mathbf{h} + \mathbf{F}\hat{\mathbf{w}}(k) - \mathbf{v}) + \Delta\mathbf{h}^T \bar{\mathbf{Q}}\Delta\mathbf{h} \quad (\text{C.5})$$

in which $\bar{\mathbf{R}}$ and $\bar{\mathbf{Q}}$ are diagonal weighting matrices whose diagonal elements are $[\xi_1, \dots, \xi_{N_p}]$ and $[\delta_1, \dots, \delta_{N_u}]$, respectively. Assuming there are no constraints on the control signals, the minimum of J , can be computed by making differential of J with respect to $\Delta\mathbf{h}^T$ equal to zero, which leads to :

$$\Delta\mathbf{h} = \mathbf{K}(\mathbf{v} - \mathbf{F}\hat{\mathbf{w}}(k)) \quad (\text{C.6})$$

where \mathbf{K} is known as predictive controller gain matrix. It is determined by the dynamic matrix, and the weight matrices $\bar{\mathbf{R}}$ and $\bar{\mathbf{Q}}$.

$$\mathbf{K} = (\mathbf{H}^T \bar{\mathbf{R}} \mathbf{H} + \bar{\mathbf{Q}})^{-1} \mathbf{H}^T \bar{\mathbf{R}} \quad (\text{C.7})$$

As a receding horizon strategy is used, only the first element of the control sequence, $\Delta h(k|k)$ is sent to the plant during time interval $[k, k+1]$, and the procedure is repeated at the next sampling time. In this case,

$$\Delta h(k|k) = \mathbf{K}\mathbf{K}(\mathbf{v} - \mathbf{F}\hat{\mathbf{w}}(k)) \quad (\text{C.8})$$

where $\mathbf{K}\mathbf{K}$ is the first row of \mathbf{K} , such that the future control input applied to the plant is

$$h(k) = h(k-1) + \mathbf{K}\mathbf{K}(\mathbf{v} - \mathbf{F}\hat{\mathbf{w}}(k)) \quad (\text{C.9})$$

C.2 Results of Control Performance

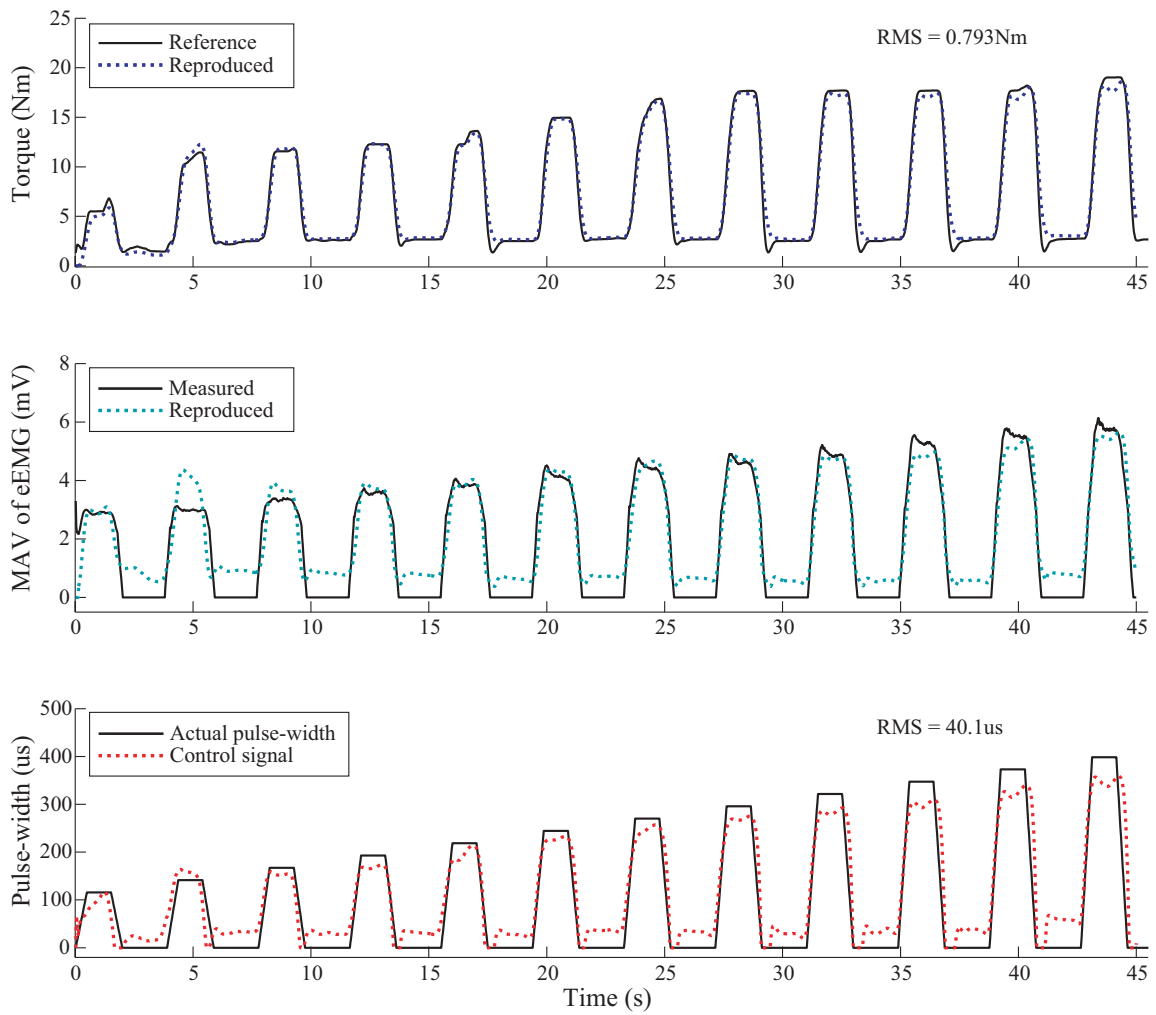


FIGURE C.1 – Control performance of the EFPC with gradually increased stimulation in subject S3.

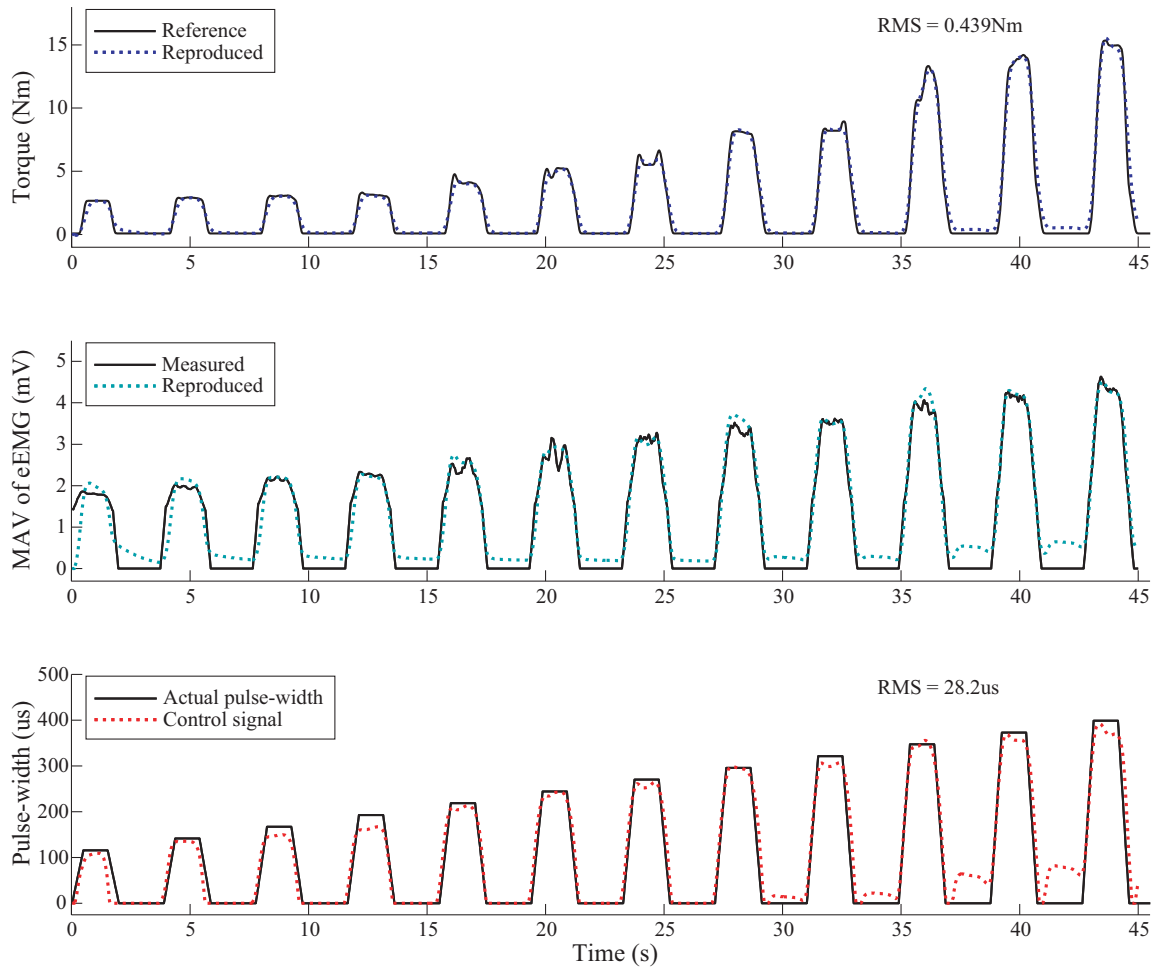


FIGURE C.2 – Control performance of the EFPC with gradually increased stimulation in subject S1.

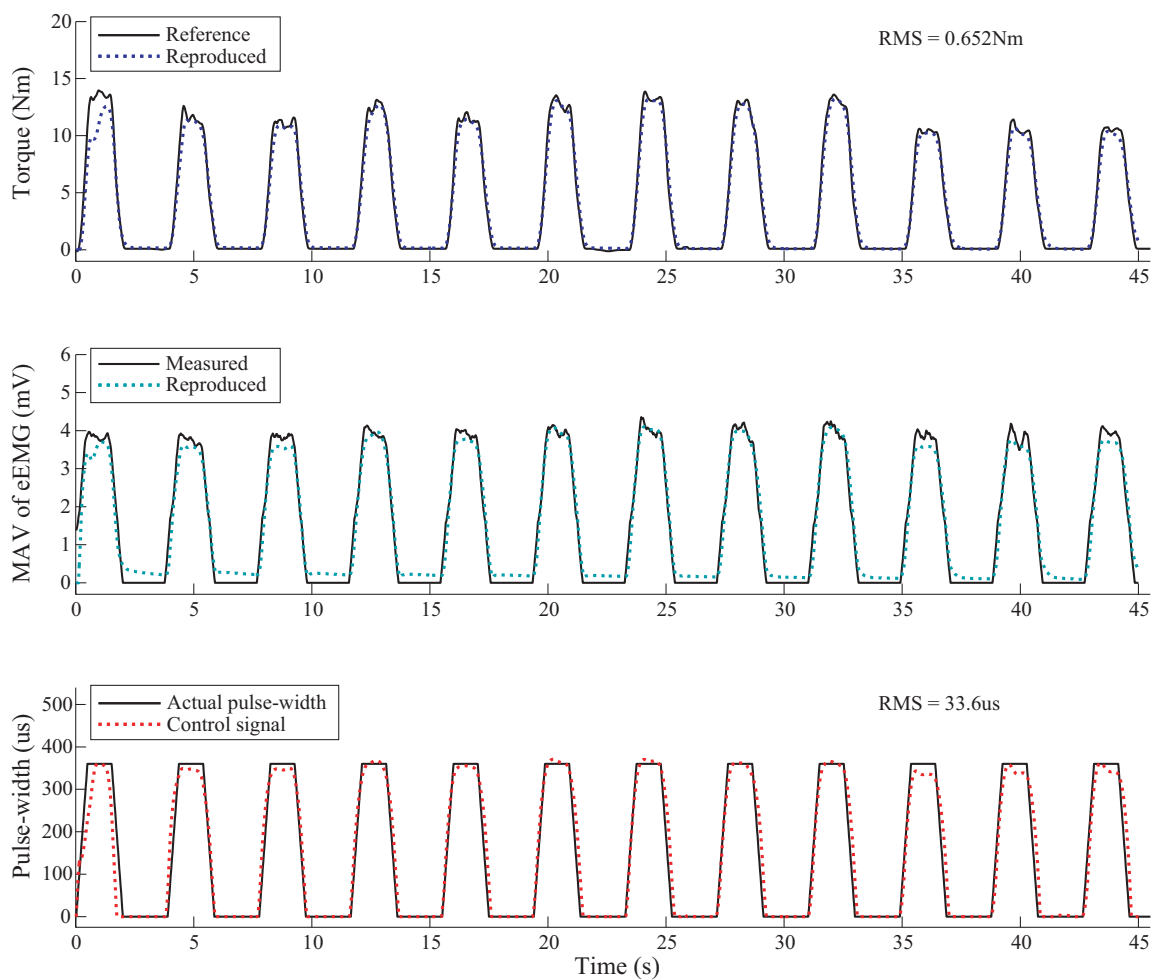


FIGURE C.3 – Control performance of the EFPC with constant stimulation strategy in subject S1.

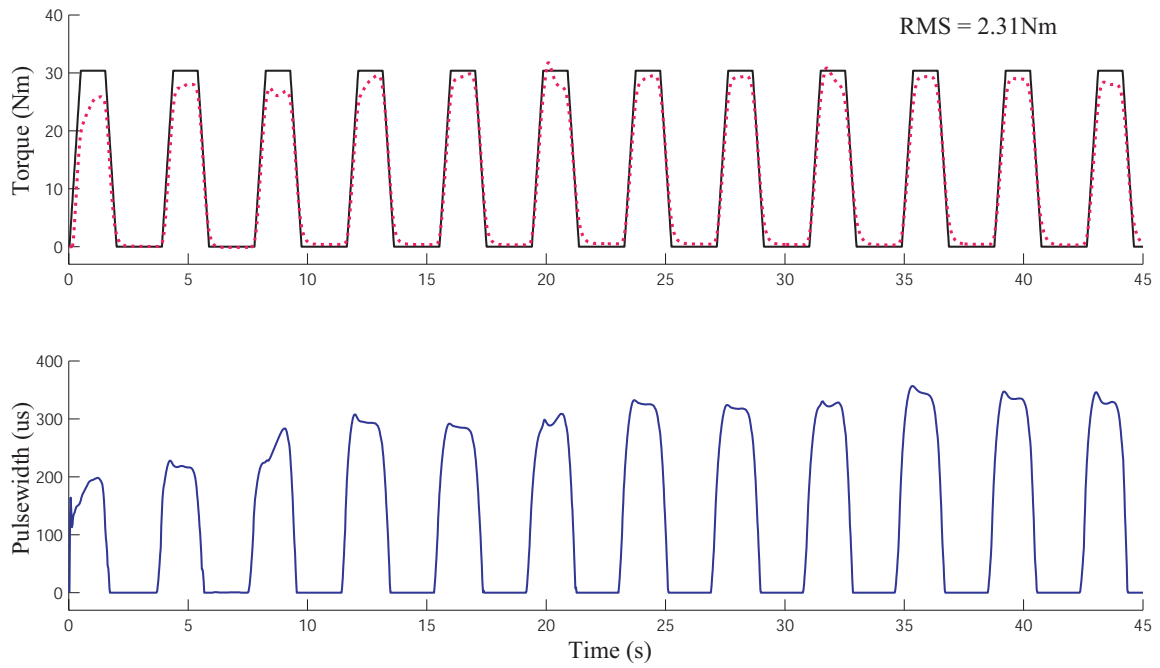


FIGURE C.4 – Simulation of fatigue compensation performance of the EFPC.

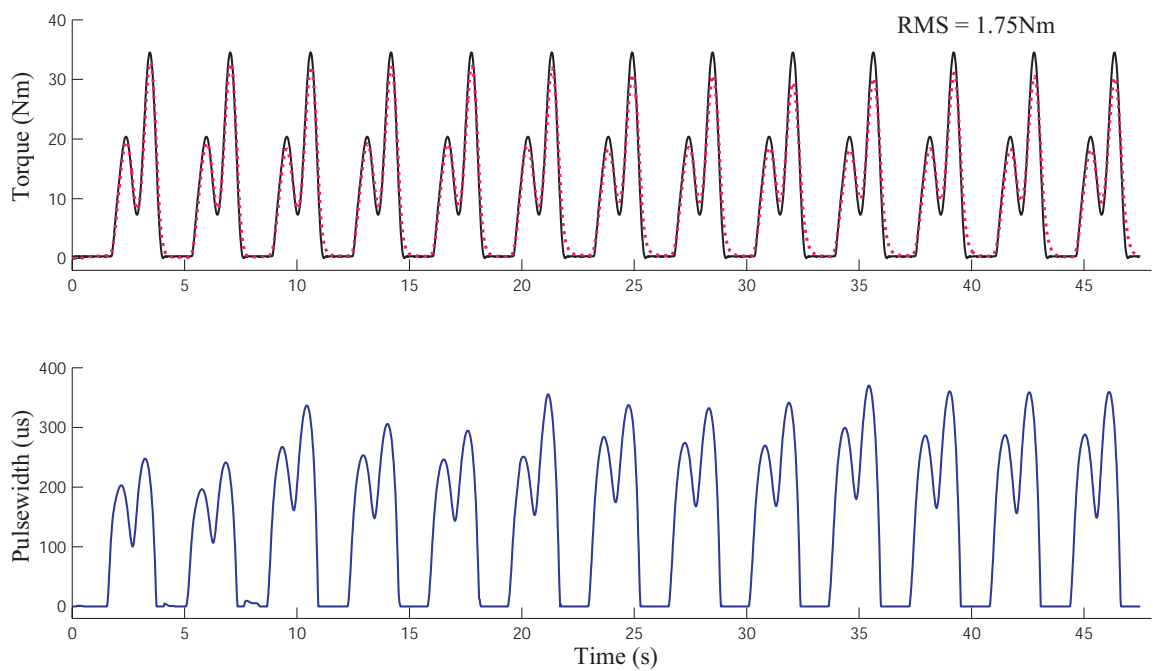


FIGURE C.5 – The performance of the EFPC in generating stimulation pattern for natural trajectory.

List of Publications

- Journals
 - Zhang, Q., Hayashibe M., Fraise, P., and Guiraud, D., "FES-induced Torque Prediction with Evoked EMG Sensing for Muscle Fatigue Tracking", IEEE/ASME Transactions on Mechatronics (focused section on Sensing Technologies for Biomechatronics), Vol. 16 (5), pp. 816-826, 2011.
 - Hayashibe M., Zhang, Q., Guiraud, D., and Fattal, C., "Evoked EMG based Torque Prediction under Muscle Fatigue in Implanted Neural Stimulation", Journal of Neural Engineering, 8 (6), 2011.
- Peer-reviewed international conference papers
 - Zhang, Q., Hayashibe M., and Guiraud, D., "Muscle Fatigue Tracking based on Stimulus Evoked EMG and Adaptive Torque Prediction", presented at International Conference on Robotics and Automation, Shanghai, China, pp. 1433-1438, 2011.
 - Hayashibe M., Zhang, Q. and Azevedo-Coste, C., "Dual Predictive Control of Electrically Stimulated Muscle using Biofeedback for Drop Foot Correction", at IEEE/RSJ International Conference on Intelligent Robots and Systems, San Francisco, USA, pp. 1731-1736, 2011.
 - Zhang, Q., Hayashibe M., Papaiordanidou, M., Fraise, P., Fattal, C. and Guiraud, D., "Torque Prediction Using Stimulus Evoked EMG and its Identification for Different Muscle Fatigue States in SCI Subjects", presented at International Conference of the IEEE Engineering in Medicine and Biology Society, Buenos Aires, Argentina, pp. 3523-3526, 2010.
 - Zhang, Q., Hayashibe M., Sablayrolles, B., and Azevedo-Coste, C., "Torque Prediction Based on Evoked EMG in Fatiguing Muscle Toward Advanced Drop Foot Correction", presented at International Functional Electrical Stimulation Society Conference, Vienna, Austria, pp. 105-107, 2010.
 - Zhang, Q., Hayashibe M., Papaiordanidou, M., Fraise, P., Fattal, C. and Guiraud, D., "Torque assessment based on evoked EMG for FES-induced muscle contractions in SCI patients", presented at International Functional Electrical Stimulation Society Conference, Seoul, South Korea, pp. 51-53, 2009.
- Abstracts selected in journals
 - Q. Zhang, M. Hayashibe, B. Sablayrolles, C. Azevedo-Coste, "Torque Prediction Based on Evoked EMG in Fatiguing Muscle Toward Advanced Drop Foot Correction", Artificial Organs, A42-87, vol. 34, 2010.
 - M. Hayashibe, Q. Zhang, D. Guiraud, C. Fattal, P. Fraise, "Modeling and Experimental Identification for Muscular force Estimation Based on Evoked EMG in FES", Journal of Biomechanics, vol.43, sup.1, S66, 2010.

BIBLIOGRAPHY

- [Aboy et al., 2005] Aboy, M., Marquez, O. W., McNames, J., Hornero, R., Trong, T., and Goldstein, B. (2005). Adaptive modeling and spectral estimation of nonstationary biomedical signals based on kalman filtering. *IEEE Transactions on Biomedical Engineering*, 52 :1485–1489.
- [Ajoudani and Erfanian, 2009] Ajoudani, A. . and Erfanian, A. (2009). A neuro-sliding-mode control with adaptive modeling of uncertainty for control of movement in paralyzed limbs using functional electrical stimulation. *IEEE Transactions on Biomedical Engineering*, 56(7) :1771–1780.
- [Albertos and Ortega, 1989] Albertos, P. and Ortega, R. (1989). On generalized predictive control : two alternative formulations. *Automatica*, 25(5) :753–755.
- [Azevedo and Héliot, 2005] Azevedo, C. and Héliot, R. (2005). Rehabilitation of functional posture and walking : coordination of healthy and impaired limbs. *Journal of Automatic Control*, 15(Supplement) :11–14.
- [Bernotas et al., 1986] Bernotas, L. A., Crago, P. E., and Chizeck, H. J. (1986). A discrete-time model of electrically stimulated muscle. *IEEE Transactions on Biomedical Engineering*, BME-33 :829–838.
- [Bhadra and Kilgore, 2004] Bhadra, N. and Kilgore, K. (2004). Direct current electrical conduction block of peripheral nerve. *IEEE Transactions on Neural Systems and Rehabilitation Engineering*, 12 :313–324.
- [Binder-Macleod and Snyder-Mackler, 1993] Binder-Macleod, S. and Snyder-Mackler, L. (1993). Muscle fatigue : clinical implications for fatigue assessment and neuromuscular electrical stimulation. *Physical Therapy*, 73(12) :902–910.
- [Bó et al., 2011] Bó, A. P. L., Poignet, P., and Geny, C. (2011). Pathological tremor and voluntary motion modeling and online estimation for active compensation. *IEEE Transactions on Neural Systems and Rehabilitation Engineering*, 19(2) :177–185.
- [Bó and Poignet, 2010] Bó, A., P. L. and Poignet, P. (2010). Tremor attenuation using fes-based joint stiffness control. In *Proceedings of IEEE International Conference on Robotics and Automation (ICRA 2010)*, pages 2928–2933.
- [Breen et al., 2006] Breen, P., O’Keeffe, D., Conway, R., and Lyons, G. (2006). A system for the delivery of programmable, adaptive stimulation intensity envelopes for drop foot correction applications. *Medical Engineering and Physics*, 28 :177–186.
- [Brodal, 2010] Brodal, P. (2010). *The central nervous system : structure and function (fourth edition)*. Oxford university press.
- [Cai et al., 2010] Cai, Z. J., Bai, E.-w., and Shields, R. K. (2010). Fatigue and non-fatigue mathematical muscle models during functional electrical stimulation of paralyzed muscle. *Biomedical Signal Processing and Control*, 5 :87–93.
- [Camacho and Bordons, 1999] Camacho, E. F. and Bordons, C. (1999). *Model Predictive Control*. Springer.
- [Chen and Yu, 1997] Chen, J. J. and Yu, N. Y. (1997). The validity of stimulus-evoked emg for studying muscle fatigue characteristics of paraplegic subjects during dynamic cycling movement. *IEEE Transactions on Rehabilitation Engineering*, 5(2) :170–178.

- [Chen et al., 2001] Chen, Y. L., Li, Y. C., Kuo, T. S., and Lai, J. S. (2001). The development of a closed-loop controlled functional electrical stimulation (FES) in gait training. *Journal of Medical Engineering Technology*, 25(2) :41–48.
- [Chesler and Durfee, 1997] Chesler, N. C. and Durfee, W. K. (1997). Surface EMG as a fatigue indicator during FES-induced isometric muscle contractions. *Journal of Electromyography and Kinesiology*, 7(1) :27 – 37.
- [Chia et al., 1991] Chia, T. L., Chow, P. C., and Chizeck, H. J. (1991). Recursive parameters identification of constrained systems : an application to electrically stimulated muscle. *IEEE Transactions on Biomedical Engineering*, 38 :429–442.
- [Chou et al., 2008] Chou, L.-W., Lee, S. C., and Therese E. Johnston, Stuart A. Binder-Macleod, P. (2008). The effectiveness of progressively increasing stimulation frequency and intensity to maintain paralyzed muscle force during repetitive activation in persons with spinal cord injury. *Archives of Physical Medicine and Rehabilitation*, 89 :856–864.
- [Cifrek et al., 2009] Cifrek, M., Medved, V., Tonkovic, S., and Ostojic, S. (2009). Surface EMG based muscle fatigue evaluation in biomechanics. *Clinical Biomechanics*, 24 :327–340.
- [Colombo, 2000] Colombo, Gery, a. J. M. a. S. R. (2000). Treadmill training of paraplegic patients using a robotic orthosis. *Journal of Rehabilitation Research and Development*, 37 :693–700.
- [Davoodi and Andrews, 1998] Davoodi, R. and Andrews, B. J. (1998). Computer simulation of fes standing up in paraplegia : a self-adaptive fuzzy controller with reinforcement learning. *IEEE Transactions on Rehabilitation Engineering*, 6 :151–161.
- [Dempsey and Westwick, 2004] Dempsey, E. J. and Westwick, D. T. (2004). Identification of hammerstein models with cubic spline nonlinearities. *IEEE Transactions on Biomedical Engineering*, 51 :237–245.
- [Ding et al., 2000] Ding, J., Wexler, A. S., and Binder-macleod, S. A. (2000). A predictive model of fatigue in human skeletal muscles. *Journal of Applied Physiology*, 89 :1322–1332.
- [Djilas, 2008] Djilas, M. (2008). *Interpretation des informations sensorielles des recepteurs du muscle squelettique pour controle externe*. PhD thesis, University of Montpellier II.
- [Dosen and Popovic, 2006] Dosen, S. and Popovic, D. B. (2006). Functional electrical stimulation : a matlab based tool for designing stimulation patterns. *Proceedings of IEEE International Conference on Medicine and Biology, NY, USA*, 1 :5404–5407.
- [Duan et al., 1999] Duan, C. P., TRUMBLE, D. R., SCALISE, D., and MAGOVERN, J. A. (1999). Intermittent stimulation enhances function of conditioned muscle. *American Journal of Physiology - Regulatory, Integrative and Comparative Physiology*, 276 :1534–1540.
- [Dutta et al., 2008] Dutta, A., Kobetic, R., and Triolo, R. J. (2008). Ambulation after incomplete spinal cord injury with EMG-triggered functional electrical stimulation. *IEEE Transactions on Biomedical Engineering*, 55(2) :791–794.
- [Edwards, 1981] Edwards, R. H. (1981). Human muscle function and fatigue. *Ciba Foundation symposium*, 82 :1–18.

- [Erfanian et al., 1994] Erfanian, A., Chizeck, H. J., and Hashemi, R. M. (1994). A characterization of changes in the dynamics of muscle contraction during prolonged electrical stimulation. *Proceedings of the 16th Annual International Conference of the IEEE Engineering in Medicine and Biology Society (EMBC94), Baltimore, MD*, pages 343–344.
- [Erfanian et al., 1996] Erfanian, A., Chizeck, H. J., and Hashemi, R. M. (1996). Excitation-contraction fatigue during sustained electrical stimulation of paralyzed muscle. *Proceedings of the 18th Annual International Conference of the IEEE Engineering in Medicine and Biology Society (EMBC96), Amsterdam, Netherlands*, 4 :1460–1461.
- [Erfanian et al., 1998] Erfanian, A., Chizeck, H. J., and Hashemi, R. M. (1998). Using evoked EMG as a synthetic force sensor of isometric electrically stimulated muscle. *IEEE Transactions on Biomedical Engineering*, 45(2) :188–202.
- [Esfanjani and Towhidkhah, 2005] Esfanjani, R. M. and Towhidkhah, F. (2005). Application of nonlinear model predictive controller for FES-assisted standing up in paraplegia. In *Proceedings of the 27th Annual Conference of the IEEE Engineering in Medicine and Biology Society (EMBC05), Shanghai, China*.
- [Farahat and Herr, 2005] Farahat, W. and Herr, H. (2005). A method for identification of electrically stimulated muscle. In *Proceedings of the 27th Annual Conference of the IEEE Engineering in Medicine and Biology Society (EMBC05), Shanghai, China*.
- [Farina et al., 2010] Farina, D., Lorrain, T., Negro, F., and Jiang, N. (2010). High-density emg e-textile systems for the control of active prostheses. *32nd Annual International Conference of the IEEE EMBS Buenos Aires, Argentina*, pages 3591–3593.
- [Farina and Merletti, 2000] Farina, D. and Merletti, R. (2000). Comparison of algorithms for estimation of EMG variables during voluntary isometric contractions. *Journal of Electromyography and Kinesiology*, 10(5) :337–349.
- [Farnsworth et al., 2008] Farnsworth, B. D., Triolo, R. J., and Young, D. J. (2008). Wireless implantable EMG sensing microsystem. *Proceedings of the 7th IEEE Conference on Sensors, Lecce, Italy*, pages 1245 – 1248.
- [Ferrarin et al., 2001] Ferrarin, M., Palazzo, F., Riener, R., and Quintern, J. (2001). Model-based control of FES induced single joint movements. *IEEE Transactions on Neural Systems and Rehabilitation Engineering*, 9(3) :245–257.
- [Frigo et al., 2000] Frigo, C., Ferrarin, M., Frasson, W., Pavan, E., and Thorsen, R. (2000). EMG signals detection and processing for on-line control of functional electrical stimulation. *Journal of Electromyography and Kinesiology*, 10(5) :351 – 360.
- [Gandevia et al., 1995] Gandevia, S., Enoka, R. M., McComas, A. J., Stuart, D. G., and Thomas, C. K., editors (1995). *Fatigue : neural and muscular mechanisms*. Plenum press, NY.
- [Graham et al., 2006] Graham, G. M., Thrasher, T. A., and Popovic, M. R. (2006). The effect of random modulation of functional electrical stimulation parameters on muscle fatigue. *IEEE Transactions on Neural Systems and Rehabilitation Engineering*, 14(1) :38–45.
- [Graupe et al., 1989] Graupe, D., Kohn, K. H., and Basseas, S. P. (1989). Control of electrically-stimulated walking of paraplegics via above- and below-lesion emg signature identification. *IEEE Transactions on Automatic Control*, 34(2) :130–138.

- [Graupe and Kordylewski, 1997] Graupe, D. and Kordylewski, H. (1997). Neural network control of neuromuscular stimulation in paraplegics for independent ambulation. *Proceedings of the 19th Annual International Conference of the IEEE Engineering in Medicine and Biology Society (EMBC96), Chicago, IL, USA*, 3 :1088–1091.
- [Grill, 1996] Grill, WM Jr, a. M. J. (1996). The effect of stimulus pulse duration on selectivity of neural stimulation. *IEEE Transactions on Biomedical Engineering*, 43(2) :161–166.
- [Guiraud et al., 2001] Guiraud, D., Pacetti, A., E., M., Divoux, J. L., and Rabischong, P. (2001). One year implanted patients follow up : SUAW project first results. *Proceedings of the 6th International Conference of Functional Electrical Stimulation, Cleveland, OH, USA*, 3 :268–275.
- [Guiraud et al., 2006] Guiraud, D., Stieglitz, T., P., K. K., Divoux, J. L., and Rabischong, P. (2006). An implantable neuroprosthesis for standing and walking in paraplegia : 5-year patient follow-up. *Journal of Neural Engineering*, 3 :268–275.
- [Hamada et al., 2004] Hamada, T., Kimura, T., and Moritani, T. (2004). Selective fatigue of fast motor units after electrically elicited muscle contractions. *Journal of Electromyography and Kinesiology*, 14 :531–538.
- [Hardin et al., 2007] Hardin, E., Kobetic, R., Lori Murray, P., and Michelle Corado-Ahmed, P. (2007). Walking after incomplete spinal cord injury using an implanted fes system : A case report. *Journal of rehabilitation research and development*, 44 :333–346.
- [Haugland and Sinkjaer, 1995] Haugland, M. K. and Sinkjaer, T. (1995). Cutaneous whole nerve recordings used for correction for footdrop in hemiplegic man. *IEEE Transactions on Biomedical Engineering*, 3 :307–317.
- [Hayashibe et al., 2008] Hayashibe, M., Poignet, P., Guiraud, D., and El Makssoud, H. (2008). Nonlinear identification of skeletal muscle dynamics with sigma-point kalman filter for model-based FES. *Proceeding of the IEEE International Conference on Robotics and Automation (ICRA2008), Pasadena, CA, USA*, pages 2049–2054.
- [Hayashibe et al., 2011a] Hayashibe, M., Zhang, Q., and Azevedo-Coste, C. (2011a). Dual predictive control of electrically stimulated muscle using biofeedback for drop foot correction. *Proceeding in IEEE/RSJ International Conference on Intelligent Robots and Systems, San Francisco, USA*, pages 1731–1736.
- [Hayashibe et al., 2011b] Hayashibe, M., Zhang, Q., Guiraud, D., and Fattal, C. (2011b). Evoked EMG based torque prediction under muscle fatigue in implanted neural stimulation. *Journal of Neural Engineering*, 8 (6).
- [He et al., 2009] He, H., Zhou, P., Li, G. l., and Kuiken, T. (2009). Spatial filtering improves EMG classification accuracy following targeted muscle reinnervation. *Annals of Biomedical Engineering*, 37 :1849–1857.
- [Heasman et al., 2000] Heasman, J. M., Scott, T. R. D., Vare, V. A., Flynn, R. Y., Gschwind, C. R., Middleton, J. W., and Butkowski, S. B. (2000). Detection of fatigue in the isometric electrical activation of paralyzed hand muscles of persons with tetraplegia. *IEEE Transactions on [see also IEEE Trans. on Neural Systems and Rehabilitation] Rehabilitation Engineering*, 8(3) :286–296.
- [Henson, 1998] Henson, M. A. (1998). Nonlinear model predictive control : Current status and future directions. *Computers and Chemical Engineering*, 23 :187–202.

- [Hoffer, 1988] Hoffer (1988). Closed-loop, implanted-sensor, functional electrical stimulation system for partial restoration of motor functions. *Patent*, United States :4,750,499.
- [Holobar et al., 2009] Holobar, A., Farina, D., Gazzoni, M., Merletti, R., and Zazula, D. (2009). Estimating motor unit discharge patterns from high-density surface electromyogram. *Clinical Neurophysiology*, 120 :551–562.
- [Huxley, 1957] Huxley, A. F. (1957). Muscle structure and theories of contraction. *Progress in Biophysics and Biophysical Chemistry*, 7 :255–318.
- [Ikharia and Westwick, 2006] Ikharia, B. I. and Westwick, D. T. (2006). Identification of time-varying Hammerstein systems using a basis expansion approach. *Proceeding of the Canadian Conference on Electrical and Computer Engineering, Ottawa, Ont.*, pages 1858–1861.
- [Jaeger, 1994] Jaeger, R. J. (1994). While FES remains a controversial alternative for SCI clients, researchers continue to study its potential. *Team Report, Pritzker institute of medical engineering, Illinois institute of technology*, pages 1–4.
- [Jezernik et al., 2004] Jezernik, S., Wassink, G. V., and Keller, T. (2004). Sliding mode closed-loop control of FES : controlling the shank movement. *IEEE Transactions on Biomedical Engineering*, 51(2) :263–272.
- [Johnson and Fuglevand, 2011] Johnson, L. A. and Fuglevand, A. J. (2011). Mimicking muscle activity with electrical stimulation. *Journal of Neural Engineering*, 8 :1–15.
- [Johnston et al., 2005] Johnston, T. E., Betz, R. R., Smith, B. T., Benda, B. J., Mulcahey, M. J., Davis, R., H. T. P. M. a., Kill, A., and Creasey, G. H. (2005). Implantable fes system for upright mobility and bladder and bowel function for individuals with spinal cord injury. *Spinal Cord*, 43 :713–723.
- [Johnston et al., 2003] Johnston, T. E., Betz, R. R., Smith, B. T., and Mulcahey, M. J. (2003). Implanted functional electrical stimulation : an alternative for standing and walking in pediatric spinal cord injury. *Spinal Cord*, 41 :144–152.
- [Kandel et al., 2000] Kandel, E. R., Schwartz, J. H., and Jessell, T. M. (2000). *Principles of neural science*. McGraw-Hill.
- [Karu et al., 1995] Karu, Z. Z., Durfee, W. K., and Barzilai, A. M. (1995). Reducing muscle fatigue in FES applications by stimulating with N-let pulse trains. *IEEE Transactions on Biomedical Engineering*, 42(8) :809–817.
- [Kern et al., 2010] Kern, H., Carraro, U., Adami, N., Biral, D., and Hofer, C. (2010). Home-based functional electrical stimulation rescues permanently denervated muscles in paraplegic patients with complete lower motor neuron lesion. *Neurorehabilitation and Neural Repair*, 24 :709–721.
- [Kesar and Binder-Macleod, 2006] Kesar, T. and Binder-Macleod, S. (2006). Effect of frequency and pulse duration on human muscle fatigue during repetitive electrical stimulation. *Experimental Physiology*, 91 :967–976.
- [Kesar et al., 2008] Kesar, T., W., C. L., and A., B.-M. S. (2008). Effects of stimulation frequency versus pulse duration modulation on muscle fatigue. *Journal of Electromyography and Kinesiology*, 18 :662–671.

- [Knutson et al., 2002] Knutson, J. S., Naples, G. G., Peckham, P. H., and Keith, M. W. (2002). Electrode fracture rates and occurrences of infection and granuloma associated with percutaneous intramuscular electrodes in upper-limb functional electrical stimulation applications. *Journal of Rehabilitation Research and Development*, 39(6) :671–683.
- [Kobetic et al., 2009] Kobetic, Rudi, C. S. T., Schnellenberger, J. R., and Audu, M. L. (2009). Development of hybrid orthosis for standing, walking, and stair climbing after spinal cord injury. *Journal of rehabilitation research and development*, 46 :447– 462.
- [Kobetic et al., 1997] Kobetic, R., Triolo, R. J., and Marsolais, E. B. (1997). Muscle selection and walking performance of multichannel FES systems for ambulation in paraplegia. *IEEE Transactions on Rehabilitation Engineering*, 5 :23–29.
- [Kordylewski and Graupe, 2001] Kordylewski, H. and Graupe, D. (2001). Control of neuromuscular stimulation for ambulation by complete paraplegics via artificial neural networks. *Neurological Research*, 23(5) :472–481.
- [Kralj, 1973] Kralj, A. (1973). Functional electrical stimulation - a new hope for paraplegic patient. *Bulletin of Prosthetics Research*, pages 75–102.
- [Lafor t et al., 2011] Lafor t, J., Guiraud, D., Andreu, D., Taillades, H., and Azevedo-Coste, C. (2011). Smooth muscle modeling and experimental identification : application to bladder isometric contraction. *Journal of Neural Engineering*, 8(3).
- [Le et al., 2010] Le, F., Markovsky, I., T. Freeman, C., and Rogers, E. (2010). Identification of electrically stimulated muscle models of stroke patients. *Control Engineering Practice*, 18 :396–407.
- [Levin and Mizrahi, 1999] Levin, O. and Mizrahi, J. (1999). EMG and metabolite-based prediction of force in paralyzed quadriceps muscle under interrupted stimulation. *IEEE Transactions on Rehabilitation Engineering*, 7(3) :301–314.
- [Liberson et al., 1961] Liberson, W., Holmquest, H., and Scott, M. (1961). Functional electrotherapy : stimulation of the common peroneal nerve synchronised with the swing phase of gait of hemiplegic subjects. *Archives of Physical Medicine and Rehabilitation*, 42 :202–205.
- [Lim et al., 2000] Lim, J. K., Nam, M. H., and Khang, G. (2000). Model of activation dynamics for FES-induced muscle fatigue. *Proceedings of the 22nd Annual International Conference of the IEEE Engineering in Medicine and Biology Society (EMBC00), Chicago, IL., USA*, pages 2251–2253.
- [Ljung, 1991] Ljung, L. (1991). Issues in system identification. *IEEE Control Systems*, pages 25–29.
- [Ljung, 1999] Ljung, L. (1999). *System identification : theory for the user (2nd edition)*. New Jersey, USA : Prentice-Hall.
- [Lowery et al., 2006] Lowery, M. M., Weir, R. f., and Kuiken, T. A. (2006). Simulation of intramuscular EMG signals detected using implantable myoelectric sensors (IMES). *IEEE Transactions on Biomedical Engineering*, 53(10) :1926–1933.
- [Lyons et al., 2002] Lyons, G. M., Sinkjær, T., Burridge, J. H., and Wilcox, D. J. (2002). A review of portable FES-based neural orthoses for the correction of drop foot. *IEEE Transactions on Neural systems and Rehabilitation Engineering*, 10(4) :260–279.

- [Mack and Jain, 1983] Mack, G. A. and Jain, V. K. (1983). Speech parameter estimation by time-weighted-error Kalman filter. *IEEE Transactions on Acoustics, Speech, and Signal Processing*, ASSP-31 :1300–1303.
- [Mackenzie, 2004] Mackenzie, B. (2004). Range of movement (ROM). In <http://www.brianmac.co.uk/musrom.htm>.
- [Madeleine et al., 2006] Madeleine, M. L., Richard, F. f. W., and Todd, A. K. (2006). Simulation of intramuscular EMG signals detected using implantable myoelectric sensors (IMES). *IEEE Transactions on Biomedical Engineering*, 53 :1926–1933.
- [Malek and Vaillancourt, 1995] Malek, F. and Vaillancourt, R. (1995). A composite polynomial zero-finding matrix algorithm. *Computers Mathematics Application*, 30 :37–47.
- [Mangold et al., 2005] Mangold, S., Keller, T., a. C. A., and Dietz, V. (2005). Transcutaneous functional electrical stimulation for grasping in subjects with cervical spinal cord injury. *Spinal Cord*, 43 :1–13.
- [Matsunaga et al., 1999] Matsunaga, T., Shimada, Y., and Sato, K. (1999). Muscle fatigue from intermittent stimulation with low and high frequency electrical pulses. *Archives of Physical Medicine and Rehabilitation*, 80(1) :48–53.
- [Merletti et al., 2008] Merletti, R., Holobar, A., and Farina, D. (2008). Analysis of motor units with high-density surface electromyography. *Journal of Electromyography and Kinesiology*, 18 :879–890.
- [Milos, 2001] Milos, R. Popovic ; Thierry, k. I. P. V. D. M. M. (2001). Surface-stimulation technology for grasping and walking neuroprostheses. *IEEE engineering in medicine and biology*, pages 82–93.
- [Mizrahi and Isakov, 1994] Mizrahi, J. and Isakov, E., a. S. Z. (1994). Myoelectric and force characteristics in transcutaneous isometric FES. *Basic and Applied Myology*, 4(2) :147–154.
- [Mizrahi et al., 1997a] Mizrahi, J., Levin, O., Aviram, A., Isakov, E., and Susak, Z. (1997a). Muscle fatigue in interrupted stimulation : effect of partial recovery on force and EMG dynamics. *Journal of Electromyography and Kinesiology*, 7(1) :51–65.
- [Mizrahi et al., 1994] Mizrahi, J., Levy, M., Ring, H., Isakov, E., and Liberson, A. (1994). EMG as an indicator of fatigue in isometrically FES-activated paralyzed muscles. *IEEE Transactions on Neural Systems and Rehabilitation*, 2(2) :57–65.
- [Mizrahi et al., 1997b] Mizrahi, J., Seelenfreund, D., Isakov, E., and Susak, Z. (1997b). Predicted and measured muscle forces after recoveries of differing durations following fatigue in functional electrical stimulation. *Artificial organs*, 21 :236–239.
- [Mohammed et al., 2007] Mohammed, S., Poignet, P., Fraise, P., and Guiraud, D. (2007). Lower limbs movement restoration using input-output feedback linearization and model predictive control. in *Proceeding of the 2007 IEEE International Conference on Intelligent Robots and Systems, San Diego, CA, USA,*, pages 1945–1950.
- [Nikitczuk et al., 2009] Nikitczuk, J., Weinberg, B., Canavan, P. K., and Mavroidis, C. (2009). Active knee rehabilitation orthotic device with variable damping characteristics implemented via an electrorheological fluid. *IEEE/ASME Transactions on Mechatronics*, 15 :952–960.

- [O'Halloran et al., 2003] O'Halloran, T., Haugland, M., Lyons, G., and Sinkjær, T. (2003). Modified implanted drop foot stimulator system with graphical user interface for customised stimulation pulse-width profiles. *Medical & Biological Engineering and Computing*, 41 :701–709.
- [O'Keeffe et al., 2003] O'Keeffe, D. T., Donnelly, A. E., and Lyons, G. M. (2003). The development of a potential optimized stimulation intensity envelope for drop foot applications. *IEEE Transactions on Neural Systems and Rehabilitation Engineering*, 11(3) :249–256.
- [O'Keeffe et al., 2001] O'Keeffe, D. T., Lyons, G. M., Donnelly, A. E., and Byrne, C. A. (2001). Stimulus artifact removal using a software-based two-stage peak detection algorithm. *Journal of Neuroscience Methods*, 109 :137–145.
- [Pelletier and Hicks, 2011] Pelletier, C. and Hicks, A. (2011). Muscle fatigue characteristics in paralyzed muscle after spinal cord injury. *Spinal Cord (2011)*, 49 :125–130.
- [Popović and Sinkjær, 2000] Popović, D. and Sinkjær, T. (2000). *Control of movement for the physically disabled (first edition)*. Springer.
- [Popović and Popović, 2009] Popović, D. B. and Popović, M. B. (2009). Automatic determination of the optimal shape of a surface electrode : selective stimulation. *Journal of Neuroscience Methods*, 178 :174–181.
- [Rabischong and Chavet, 1997] Rabischong, E. and Chavet, P. (1997). Regression-based indices of fatigue in paraplegics' electrically stimulated quadriceps. *Medical Engineering and Physics*, 19(8) :749–754.
- [Ragnarsdottir, 2001] Ragnarsdottir (2001). The treatment and cure of spinal injury motion for a recommendation. <http://assembly.coe.int/Main.asp?link=/Documents/WorkingDocs/Doc01/EDOC9154.htm>.
- [Riener, 1999] Riener, R. (1999). Model-based development of neuroprostheses for paraplegic patients. *Philosophical Transactions of the Royal Society of London B*, 354 :877–894.
- [Riener et al., 1996] Riener, R., Quintern, J., and Schmidt, G. (1996). Biomechanical model of the human knee evaluated by neuromuscular stimulation. *Journal of Biomechanics*, 29(9) :1157–1167.
- [Rissanen, 1978] Rissanen, J. (1978). Modeling by shortest data description. *Automatica*, 14 :465–471.
- [R.J. et al., 1996] R.J., T., C., B., J., U., R., K., A., S., and E.B., M. (1996). Implanted functional neuromuscular stimulation systems for individuals with cervical spinal cord injuries : clinical case reports. *Archives of Physical Medicine and Rehabilitation*, 77 :1119–1128.
- [Rosen and Arcan, 2001] Rosen, Jacob, B. M. B. F. M. and Arcan, M. (2001). A myosignal-based powered exoskeleton system. *IEEE Transactions on Systems, Man and Cybernetics - Part A : Systems and Humans*, 31 :210–222.
- [Routh and Durfee, 2003] Routh, G. R. and Durfee, W. K. (2003). Doublet stimulation to reduce fatigue in electrically stimulated muscle during controlled leg lifts. *Proceedings of the 25th Annual International Conference of the IEEE Engineering in Medicine and Biology Society, Cancun, Mexico*, pages 1531–1534.

- [Russ et al., 2002] Russ, D. W., Vandenborne, K., and Binder-Macleod, S. A. (2002). Factors in fatigue during intermittent electrical stimulation of human skeletal muscle. *Journal of Applied Physiology*, 93 :469–478.
- [Schauer et al., 2005] Schauer, T., Nergård, N.-O., Previdi, F., Hunt, K., Fraser, M., Ferchland, E., and Raisch, J. (2005). Online identification and nonlinear control of the electrically stimulated quadriceps muscle. *Control Engineering Practice*, 13 :1207–1219.
- [Sennels et al., 1997] Sennels, S., Biering-sorensen, F., Andersen, O. T., and Hansen, S. D. (1997). Functional neuromuscular stimulation controlled by surface electromyographic signals produced by volitional activation of the same muscle : adaptive removal of the muscle response from the recorded EMG-signal. *IEEE Transactions on Rehabilitation Engineering*, 5(2) :195–206.
- [Shimada et al., 2006] Shimada, Y., ITO, H., Matsunaga, T., M., A., Kawatani, M., and Itoi, E. (2006). Reduction of muscle fatigue by catchlike-inducing intermittent electrical stimulation in rat skeletal muscle. *Biomedical Research*, 27 :183–189.
- [Solomonow et al., 2000] Solomonow, M., Baratta, R., and D’Ambrosia, R. (2000). Standing and walking after spinal cord injury : experience with the reciprocating gait orthosis powered by electrical muscle stimulation. *Topics in Spinal Cord Injury Rehabilitation*, 5 :29–53.
- [Solomonow et al., 1995] Solomonow, M., Baratta, R., Zhou, B., Bernardi, M., and Acicmo, S. (1995). Analysis of EMG crosstalk in neighboring and antagonist cat muscles. *Proceeding of the 17th Annual Conference of IEEE Engineering in Medicine and Biology Society (EMBC95), Montreal, Que., Canada*, 2 :1353–1354.
- [Szlavik and de Bruin, 1999] Szlavik, R. B. and de Bruin, H. (1999). The effect of stimulus current pulse width on nerve fiber size recruitment patterns. *Medical Engineering and Physics*, 21 :507–515.
- [Tai et al., 2009] Tai, C. f., James, R. R., and William, C. d. G. (2009). Analysis of nerve conduction block induced by direct current. *Journal of Computational Neuroscience*, 27 :201–210.
- [Tepavac and Schwirtlich, 1997] Tepavac, D. and Schwirtlich, L. (1997). Detection and prediction of FES-induced fatigue. *Journal of Electromyography and Kinesiology*, 7(1) :39– 0.
- [Thomas and E.Butler, 2003] Thomas, Christine K. ; Lisa Griffin ; Sharlene Godfrey, E. R.-C. and E.Butler, J. (2003). Fatigue of paralysed and control thenar muscles induced by variable or constant frequency stimulation. *Journal of Neurophysiology*, 89 :2055–2064.
- [Tsukahara et al., 2011] Tsukahara, A., Hasegawa, Y., and Sankai, Y. (2011). Gait support for complete spinal cord injury patient by synchronized leg-swing with hal. In *2011 IEEE/RSJ International Conference on Intelligent Robots and Systems, San Francisco, CA, USA*.
- [Tyler and Dliran, 1995] Tyler, D. and Dliran, D. (1995). Combined modulation of pulse width and pulse amplitude to enhance functional selectivity of neural stimulation. *Proceeding of 17th Annual Conference of the IEEE Engineering in Medicine and Biology Society (EMBC95), Montreal, Que., Canada*, 2 :1109 – 1110.
- [Vallery, 2009] Vallery, H. (2009). Stable and user-controlled assistance of human motor function. *PhD thesis*.

- [Wang et al., 2008] Wang, J. c., Shen, B., James, R. R., William, C. d. G., and Changfeng, T. (2008). Influence of frequency and temperature on the mechanisms of nerve conduction block induced by high-frequency biphasic electrical current. *Journal of Computational Neuroscience*, 24 :195–206.
- [WHO, 2007] WHO (2007). Stroke statistics. In *World Health Report*.
- [Williamson and Andrews, 2001] Williamson, R. and Andrews, B. J. (2001). Detecting absolute human knee angle and angular velocity using accelerometers and rate gyroscopes. *Medical & Biological Engineering & Computing*, 39 :294–302.
- [Winslow et al., 2003] Winslow, J., Jacobs, P. L., and Tepavac, D. (2003). Fatigue compensation during fes using surface emg. *Journal of Electromyography and Kinesiology*, 13(6) :555 – 568.
- [Winters and Crago, 2000] Winters, J. M. and Crago, P. E. (2000). *Biomechanics and Neural Control of Posture and Movement*. Springer-Verlag.
- [Wise et al., 2001] Wise, A. K., Morgan, D. L., Gregory, J. E., and Proske, U. (2001). Fatigue in mammalian skeletal muscle stimulated under computer control. *Journal of Applied Physiology*, 90 :189–197.
- [Yoshida and Horch, 1996] Yoshida, K. and Horch, K. (1996). Closed-loop control of ankle position using muscle afferent feedback with functional neuromuscular stimulation. *IEEE Transactions on Biomedical and Engineering*, 43 :167–176.
- [Yu and Chang, 2009] Yu, a. and Chang, S. (2009). Mechanical and electromyographic response to stimulated contractions in paralyzed tibialis anterior post fatiguing stimulations. *13th International Conference on Biomedical Engineering (ICBME 2008)*, 23 :1667–1671.
- [Yu et al., 2002] Yu, W., Yamaguchi, H., Yokoi, H., Maruishi, M., Mano, Y., and Kakazu, Y. (2002). EMG automatic switch for FES control for hemiplegics using artificial neural network. *Robotics and Autonomous Systems*, 40(2-3) :213 – 224.
- [Yukawa et al., 1996] Yukawa, T., khalid, M., hl. Cchiyama, and Inooka, H. (1996). Modular hybrid functional electrical stimulation system. In *Proceedings of the 1996 IEEE International Conference on Robotics and Automation Minneapolis, Minnesota*.
- [Zhang et al., 2007] Zhang, D. G., Tan, H., Ferdinan, W., and Wei, T. A. (2007). Functional electrical stimulation in rehabilitation engineering : a survey. In *ACM New York, NY, USA*.
- [Zhang et al., 2011a] Zhang, Q., Hayashibe, M., Fraise, P., and Guiraud, D. (2011a). FES-induced torque prediction with evoked EMG sensing for muscle fatigue tracking. *IEEE/ASME Transactions on Mechatronics (focused section on Sensing Technologies for Biomechatronics)*, 16 (5) :816–826.
- [Zhang et al., 2011b] Zhang, Q., Hayashibe, M., and Guiraud, D. (2011b). Muscle fatigue tracking based on stimulus evoked EMG and adaptive torque prediction. *Proceeding of IEEE International Conference on Robotics and Automation (ICRA 2011), Shanghai, China*, pages 1433–1438.
- [Zhang et al., 2010] Zhang, Q., Hayashibe, M., Papaiordanidou, M., Fraise, P., Fattal, C., and Guiraud, D. (2010). Torque prediction using stimulus evoked EMG and its identification for different muscle fatigue states in SCI subjects. *Proceeding in the 32nd Annual International Conference of the IEEE Engineering in Medicine and Biology, Buenos Aires, Argentina*, pages 3523–3526.

- [Zhang et al., 2009] Zhang, Q., Hayashibe, M., Papaiordanidou, M., Fraise, P., and Guiraud, D. (2009). Torque assessment based on evoked emg for fes-induced muscle contractions in sci patients. *Proceeding of the 14th Annual International Conference on Functional Electrical Stimulation, Seoul, South Korea*, pages 51–53.
- [Zhou et al., 2011] Zhou, P., Nina, L. S., and William, Z. R. (2011). Surface electromyogram analysis of the direction of isometric torque generation by the first dorsal interosseous muscle. *Journal of Neural Engineering*, 8.
- [Zhu et al., 1991] Zhu, Q., Warwick, K., and Douce, J. L. (1991). Adaptive general predictive controller for nonlinear systems. *IEEE proceedings-D*, 138(1) :33–40.
- [Ziai and Menon, 2011] Ziai, A. and Menon, C. (2011). Comparison of regression models for estimation of isometric wrist joint torques using surface electromyography. *Journal of NeuroEngineering and Rehabilitation*, 8(1) :56.

Abstract

Functional electrical stimulation (FES) is a potential technique to provide active improvement to spinal cord injured (SCI) patients in terms of mobility, stability and side-effect prevention. FES-elicited muscle force is required to be appropriate and persistent to perform intended movement or maintain a posture balance. However, muscle state changes such as muscle fatigue degrade the performance of FES. In addition, most of complete SCI patients don't have sensory feedback to detect the fatigue and in-vivo joint torque sensor is not available yet. Conventional FES control systems are either in open-loop or not robust to muscle state changes. Therefore, this thesis aims at a development of joint torque prediction and feedback control method in order to enhance the joint torque control of FES in terms of accuracy, robustness, and safety to the patients.

In order to predict FES-induced joint torque, evoked-Electromyography (eEMG) has been applied to correlate the muscle electrical activity and mechanical activity. Although muscle fatigue represents time-variant, subject-specific and protocol-specific characteristics, the proposed Kalman filter-based adaptive identification is able to predict the torque generation systematically. The robustness of the torque prediction has been investigated in a fatigue tracking task through experiments in SCI subjects. The results demonstrate good tracking performance against muscle state variations and external disturbances.

Based on accurate predictive performance of the proposed method, a new control strategy, EMG-Feedback Predictive Control (EFPC), is proposed to adaptively adjust stimulation pattern to obtain the desired joint torque trajectory. This control strategy is not only able to explicitly avoid over-stimulation to the patients and conveniently generate appropriate stimulation pattern for the desired torque trajectory, but also able to track the desired torque trajectory compensating time-variant muscle state changes.

Résumé

La stimulation électrique fonctionnelle (SEF) peut améliorer de manière significative la mobilité des blessés médullaires ainsi que la stabilité et la prévention des effets secondaires. Dans le domaine de la SEF pour les membres inférieurs, le couple articulaire doit être fourni de façon appropriée pour effectuer le mouvement prévu afin de maintenir l'équilibre postural. Toutefois, les changements d'état du muscle telle que la fatigue musculaire est une cause majeure qui dégrade ses performances. En outre, la plupart des patients, dont la blessure médullaire est complète, n'ont pas le retour sensorielle qui permet de détecter la fatigue. De plus, et les capteurs de couples in-vivo ne sont pas disponibles à l'heure actuelle. Les systèmes conventionnels de commande SEF sont soit en boucle ouverte ou en boucle fermée mais cependant pas assez robustes aux changements d'état du muscle. L'objectif de cette thèse est le développement de la prédiction du couple articulaire et de la commande en boucle fermée afin d'améliorer les performances de la commande SEF en termes de précision, de robustesse et de sécurité pour les patients.

Afin de prédire le couple articulaire induit de la SEF, l'électromyographie (EMG) induit est utilisée pour corréler l'activité musculaire électrique et mécanique. Bien que la fatigue musculaire représente une variation dans le temps, une dépendance aux sujets et aux protocoles, la méthode proposée d'identification adaptative, basée sur le filtre de Kalman, est capable de prédire le couple articulaire variant dans le temps de manière systématique. La robustesse de la prédiction du couple articulaire a été évaluée lors d'une tâche de suivi de la fatigue en expérimentation chez des sujets blessés médullaires. Les résultats montrent une bonne performance de suivi des variations d'état des muscles en présence de fatigue et face à d'autres perturbations.

Basée sur les performances de précision de la méthode prédictive proposée, une nouvelle stratégie de commande utilisant le retour EMG, "EMG-Feedback Predictive Control (EFPC)", est proposée afin de contrôler de manière adaptative les séquences de stimulation en compensant la variation dans le temps de l'état du muscle. De plus, cette stratégie de commande permet explicitement d'éviter d'appliquer une stimulation excessive aux patients, et de générer les séquences de stimulation appropriées pour obtenir la trajectoire désirée des couples articulaires.